PART I: SYNTHESIS OF QUINOLONES FOR INHIBITION OF THE B-BARREL ASSEMBLY MACHINE IN GRAM NEGATIVE BACTERIA

PART II: SYNTHESIS OF AZO DYE SENSORS FOR DETECTION OF METAL IONS IN AQUEOUS ENVIRONMENTS

by

Katryna Williams

A Dissertation Submitted in

Partial Fulfillment of the

Requirements for the Degree of

Doctor of Philosophy

in Chemistry

at

The University of Wisconsin - Milwaukee

May 2022

ABSTRACT

PART I: SYNTHESIS OF QUINOLONES FOR INHIBITION OF THE B-BARREL ASSEMBLY MACHINE IN GRAM NEGATIVE BACTERIA
PART II: SYNTHESIS OF AZO DYE SENSORS FOR DETECTION OF METAL IONS IN AQUEOUS ENVIRONMENTS

by

Katryna Williams

The University of Wisconsin-Milwaukee, 2022
Under the Supervision of Professor Dr. Alan Schwabacher

Part I: Antibiotic resistance in Gram-negative bacteria is a growing cause of concern worldwide. Thousands of people die from antibiotic resistant bacteria every year. The β-Barrel Assembly Machine (BAM) in Gram-negative bacteria plays a role in antibiotic resistance as its porin, BamA, can regulate which molecules enter the cell, meaning it can prevent antibiotics from entering the bacterial cell.

BamA exists in an open and closed form and is only selective in its closed form. BamA opens and closes through the H-bonding of two intramolecular β-strands. It is theorized that the creation of a β-sheet mimetic, based on work done by James Nowick, would be able to H-bond with one of the β-strands involved in closing BamA, therefore locking it in the open conformation and allowing antibiotics into the cell, thus rejuvenating effectiveness of current antibiotics.

Part II: There are metals present in all drinking water, most of which are of minimal health concern. However, across the world there are many instances of harmful metals being found in drinking water. Flint, Michigan is one of these places: their recent lead crisis was only

one of many. This is a problem worldwide, and there are currently no regenerable, real-time, and/or consumer-friendly methods of testing drinking water. As such, there is a need for a device that can detect and report small amounts of toxic metals in drinking water in real-time. No device like this currently exists on the market.

Azo-dyes function as wonderful metal sensors as evidenced by the Schwabacher group's previous small metal sensing project. Using this previous project as a general framework, multiple families of azo dyes were designed to meet the goal of detecting low ppb heavy metals in drinking water. These sensors have been tested for their ability to detect lead in aqueous solution as free dyes and have shown a lot of promise in preliminary testing. These sensors are able to enter the next stage of development which is placement onto a polymer and further testing.

DEDICATION

For myself: past, present, and future.

You did it!

"I say that there is no role for women – there is, instead, a role for each woman, and she must make it for herself." – Jasnah Kholin

TABLE OF CONTENTS

LIST OF FIGURES

LIST OF TABLES

LIST OF SCHEMES

LIST OF ABBREVIATIONS

Abs - Absorbance

AcOH - Acetic Acid

BAM - Beta Barrel Assembly Machine

Boc - *tert*. Butoxycarbonyl

BSA - N,O-bistrimetylsilylacetamide

DA – dialkylated

DAR – dialkylation reaction

DMSO -dimethyl sulfoxide

DMSS - dimethyl succinylsuccinate

EDTA - Ethylenediaminetetraacetic acid

EDC/EDAC - 1-Ethyl-3-(3-dimethylaminopropyl)carbodiimide

EPA – Environmental Protection Agency

EtOH – ethanol

EtOAc – ethyl acetate

HBTU - hexafluorophosphate benzotriazole tetramethyluronium

IR - Infrared Spectroscopy

J - Coupling constant (NMR)

JQ – Janus Quinolone

K_d – Dissociation Constant

LCMS - Liquid Chromatography Mass Spectrometry

LPS – Lipopolysaccharide

MA – Meldrum's Acid

MAD – Meldrum's Acid Derivative

MAR – monoalkylation reaction

MeOH - methanol

MOPS - 3-(N-morpholino)propanesulfonic acid

MS - mass spectrometry

MsCl - Mesyl chloride

NMP - N-Methyl-2-pyrrolidone

NMR - nuclear magnetic spectroscopy

PbSF1 – Lead sensor family 1

PbSF2 – Lead sensor family 2

PbSF3 – Lead sensor family 3

Pd/C – Palladium on carbon

Ph – Phenyl

pH - $-\log[H^+]$, acidity

pK_a - $-\log(K_a)$

Ppm – part per million

Ppb – part per billion

Rf - retention factor

RT - room temperature

tBuBA – tert. Butyl bromoacetate

tBuOH – tert. Butanol

TFA - trifluoroacetic acid

THF – tetrahydrofuran

TLC - thin layer chromatography

TMOF – trimethyl orthoformate

TMS – trimethylsilyl

TsCl – tosyl chloride

UV – Ultraviolet

WHO – World Health Organization

ACKNOWLEDGMENTS

Thank you to my puppy, Neutron, for sabotaging me as I write this thesis and for always providing me with good vibes and an excuse to take a break from work. Thank you to my cat, Pumpkin, for supervising me while I work from home throughout the years and being my cheese buddy.

I owe a massive thank you to my best friend, Caitlin, who has been there through all the highs and lows of this journey. I am so glad to have such an amazing friend in my life! Your support, advice, and perspective have helped me more than you know.

I am, of course, endlessly grateful to Trevor Hagemann for being a source of advice and a voice of reason throughout these four years, both in the program and out.

Thank you all for helping me to become my best self!

Chapter I. Introduction

Guest-Host Chemistry and the Schwabacher Group

Guest-Host chemistry is a type of supramolecular chemistry and is described as the process of a small "guest" interacting with a larger "host" molecule through a series of intermolecular reactions, such as hydrogen bonding interactions [1]. These intermolecular reactions facilitate association into a complex [2]. Guest-Host chemistry is what the Schwabacher group at the University of Wisconsin-Milwaukee (UWM) focuses on, as all projects undertaken by the Schwabacher group fall under this type of chemistry.

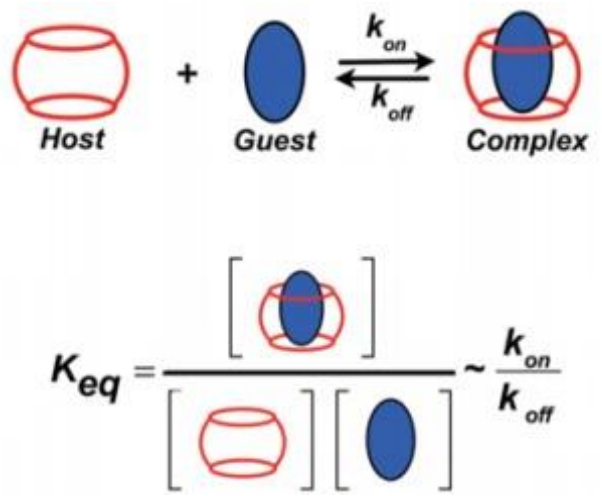

Figure 1: Guest Host Chemistry Complex, Equilibrium, and Energy [2]

As shown above in *figure 1*, the host encloses the guest in Guest-Host, facilitating intermolecular reactions to either stop or start a reaction process. Some hosts are active until guest is bound while others are active *only* when guest is bound [3]. An example of this is in the enzyme diastase, a host, which binds to a molecule of starch, a guest, and causes reaction to occur. In this case, the reaction produces a molecule of maltose[3,83].

Many enzymes in the body work in a similar fashion and are activated by the presence of a guest. Guest-Host interactions are found everywhere in chemistry and have many practical uses.

Guest-Host complexes associate and dissociate based on equilibria [3,4] as demonstrated above in *figure 1*. The complex is in equilibrium with the free guest and free host and the association and dissociation rate of these complexes can be changed by altering properties in solution. Changing the equilibrium between host and guest allows for regulation of binding. For example, in the case of diastase an excess of starch shifts this enzyme toward forming the complex. In contrast, an excess of maltose would shift the equilibrium toward "off" or toward dissociation. Alteration of concentration in solution allows for regulation of Guest-Host complex and regulation of action of the host. These properties can be utilized in both biological and synthetic environments.

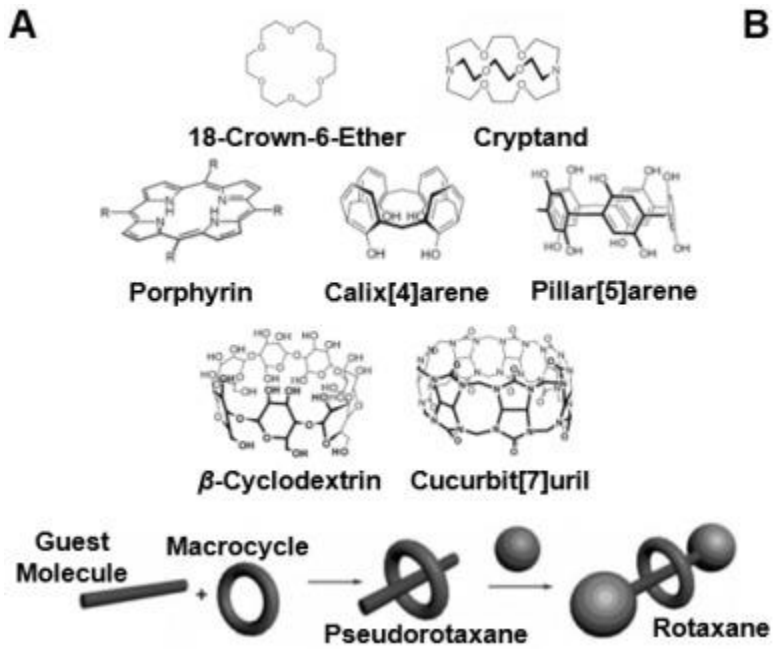

Figure 2: Common types of hosts [2]

There are many types of host structures, though they generally have a pocket to enclose guest. Many synthetic hosts are crown ethers or similar circular structures such as calixarenes or cyclodextrins[3,5].

Guest-Host systems are a fundamental part of chemistry, synthetic and biological [5,6,7]. As shown in *figure 3*, guest-host chemistry can be a metal interacting with a compound to alter fluorescence or absorbance. This is the foundation for Part II, or Chapter III, of this thesis.

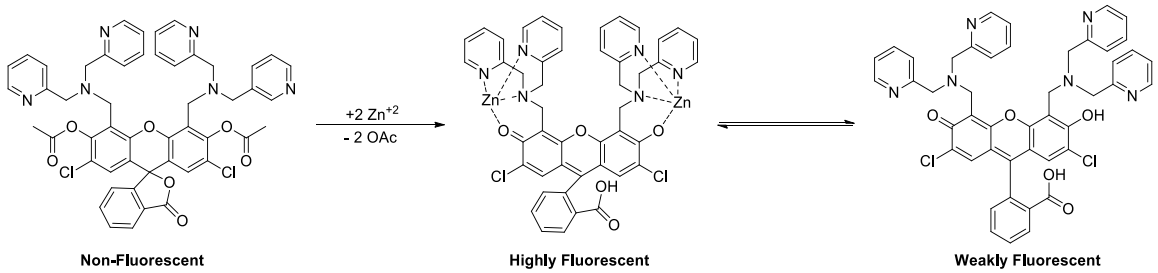

Figure 3: How guest-host chemistry can change spectral properties of compounds

Guest-host chemistry encompasses most of biochemistry, bio-organic, and synthetic organic chemistry. Many chemists synthesize molecules intended to interact with other molecules, which could be considered "guest-host."

Host-guest chemistry has many important applications in fields such as pharmaceuticals, one example of this being the modification of cyclodextrins as solubilizers for various drug molecules[81]. These cyclodextrin structures encapsulate drug molecules and facilitate their solubilization and travel through the body to reach their target receptors. Drugs that interact with enzymes or receptors undergo a guest-host sort of interaction[82,83]. As such, many pharmaceutical drugs themselves count as guest molecules and utilize the principles of guest-host chemistry.

Guest-host chemistry can also be used for industrial purposes, such as removal of a polluting molecule from a body of water. This has been demonstrated by the invention of host molecules that can facilitate the removal of aromatic amines from water. This provides a way to clean carcinogenic compounds from various water supplies[81,82].

These examples show how vast the applications of guest-host chemistry can be. Guest-host chemistry can be utilized to solve many different problems worldwide in different industries such as pharmaceuticals or water purification.

All projects undertaken by the Schwabacher group use the principles of guest-host chemistry. The Schwabacher group's quinolone project, part I or chapter II, uses the principles of guest-host chemistry to synthesize a molecule with the ability to act as a guest. This synthesized guest is intended to rejuvenate effectiveness of antibiotics in antibiotic resistant bacteria.

The metal sensing project undertaken by the Schwabacher group, part II or chapter III, uses these concepts to synthesize sensors that can act as hosts and can hydrogen bond metals in solution, changing the absorbance of the sensor molecule and signaling the presence of these metals.

Chapter II. Janus Quinolone Project

Introduction

A growing problem in the global health community is the rise of antibiotic resistant bacteria. In the United States alone, there are approximately 3 million cases of antibiotic resistant infection every year and 35,000 related deaths[8]. The World Health Organization (WHO) has declared antimicrobial resistance (AMR) is one of the top ten global health threats facing humanity [6,8].

The bacteria responsible for this rising problem are Gram-negative bacteria. In contrast to Gram-positive bacteria, Gram-negative bacteria are enclosed in a protective outer layer that makes it more difficult for white blood cells or antibiotics to combat them. This outer membrane (OM) is composed of lipopolysaccharides (LPSs) as well as outer membrane proteins (OMPs) and phospholipids[9]. This LPS layer is specific to Gram-negative bacteria and benefits the cell by making it harder to permeate and increasing its virulence factor. *Figure 4* shows the structure of this cell and demonstrates that between the LPS and the inside of the cell is the cell's outer membrane (OM). This OM is composed primarily of β-barrel proteins, which are composed of β-sheets [10,11]. These OM β-barrel proteins are synthesized by the β-barrel assembly machine (BAM) and these proteins are crucial to the bacterial cell's antibiotic resistance[9,12].

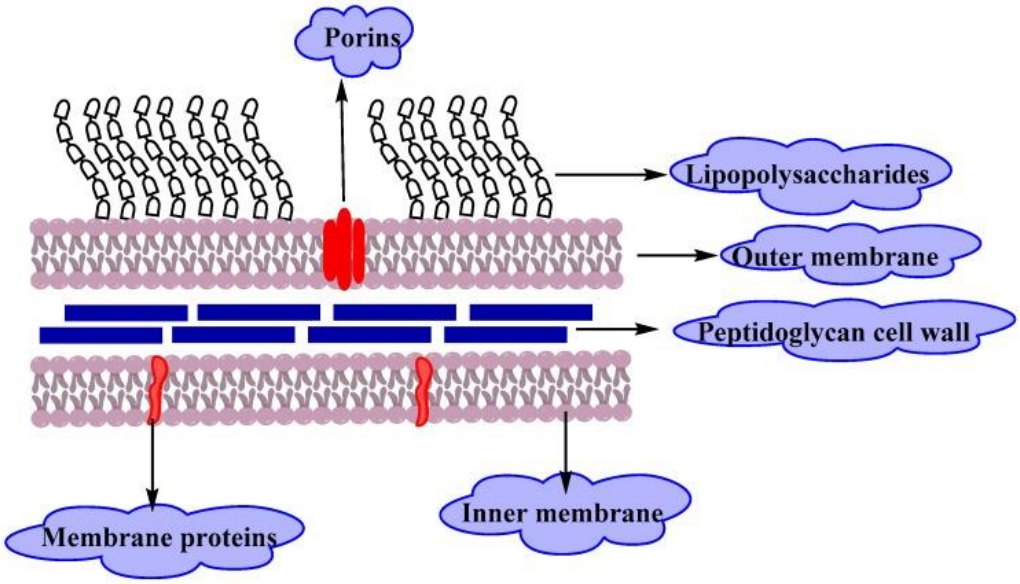

Figure 4: Membranes of Gram-Negative Bacteria [9]

This OM is largely composed of β-sheet proteins. β-sheets are a type of secondary structure and are an essential component to all life. β-sheets have a hydrogen bonding pattern that consists of alternating donors and acceptors, and these interactions are critical to maintaining shape and function of a β-sheet [10]. β-sheets are composed of multiple β-strands which can run parallel or antiparallel to one another. Regardless of the direction of the β-strands, the H-bonding pattern is always alternating donor and acceptor between the side chains of the amino acids in adjacent β-strands [9, 83], as shown in *figure 5*.

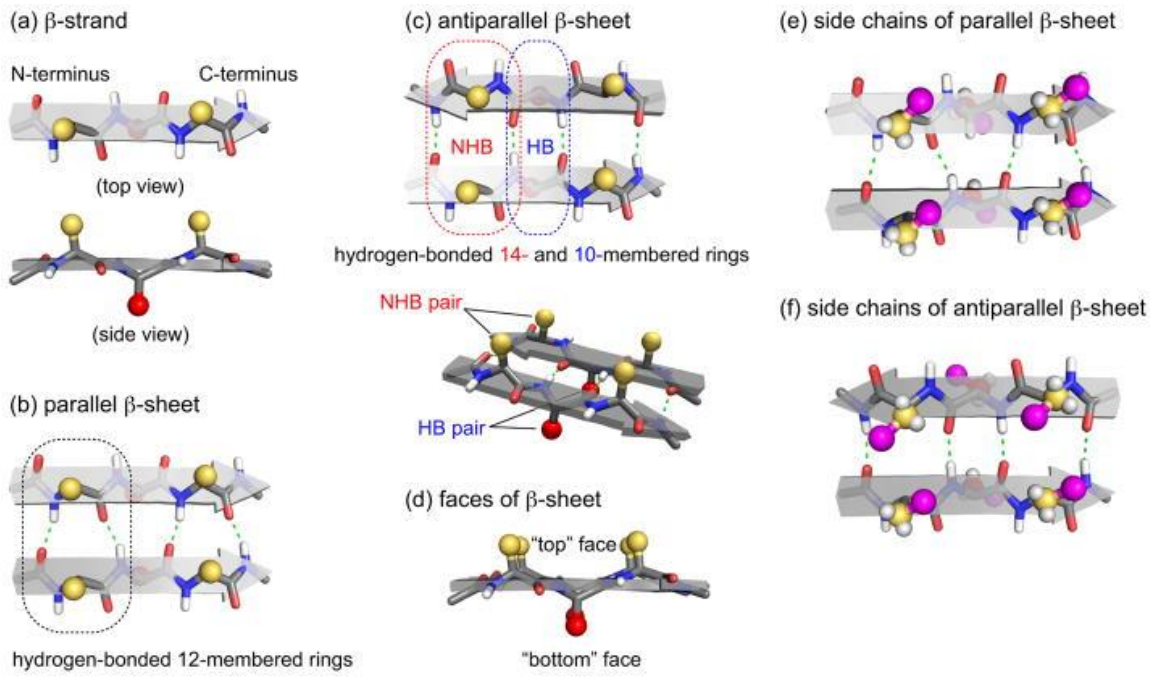

Figure 5: Beta Sheet Orientation and Hydrogen Bonding Pattern[83]

The β-barrel assembly machine (BAM) is responsible for folding the β-barrel membrane proteins found in the OM of gram-negative bacteria, including itself[8,10]. BAM is a membrane protein and is composed of five separate pieces[13]. These five pieces include a β-barrel protein called BamA and four accessory lipoproteins BamB, BamC, BamD, and BamE. Only two of these five pieces are conserved: BamA and BamD, which are essential for function and viability of BAM [9,12]. Ideal targets for inhibition must be highly conserved for maximal effect with different types of bacteria. As such, BamA and BamD are the most viable targets. Since BamD is an accessory lipoprotein, it is not ideal as a target. Instead, BamA, the β-barrel protein portion of BAM, is the preferred target.

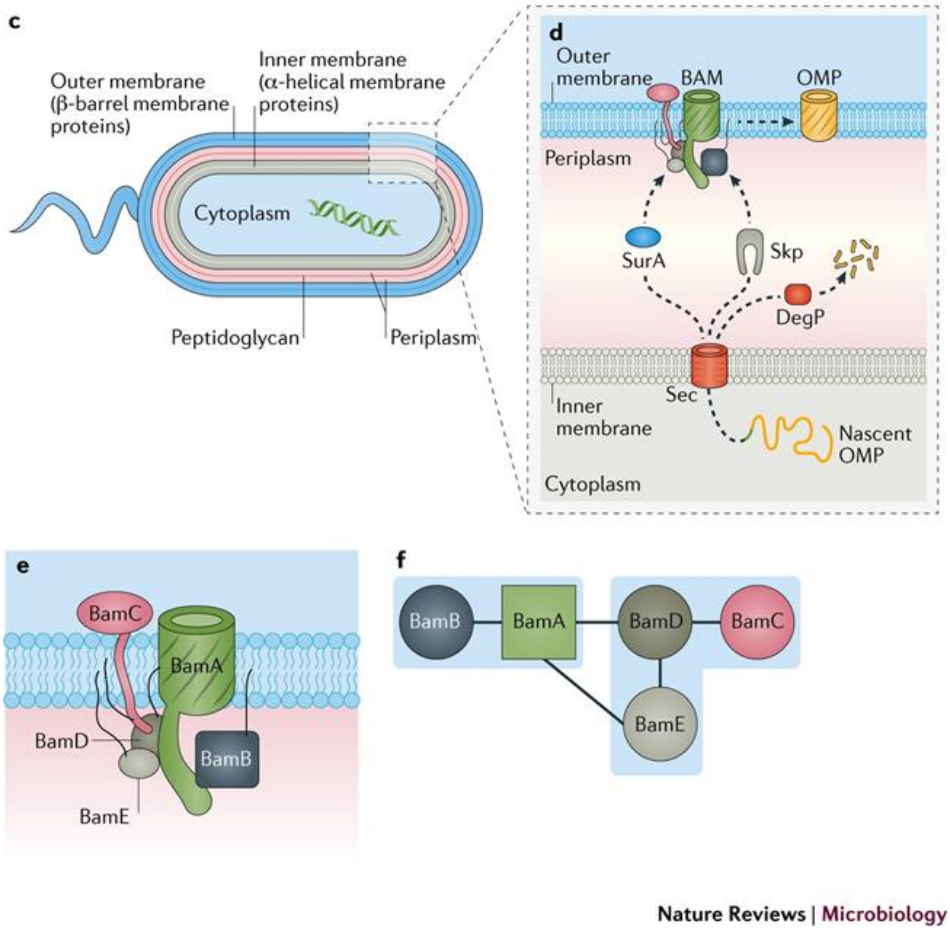

Figure 6: BAM and its components in the membrane[11]

BamA is a regulated pore capable of self-assembly, as shown in *figure 6*. The function of the pore is to transport molecules between the inside and outside of the cell membrane, and in Gram-negative bacteria this is the only functional way in or out of the cell for antibiotics or other large molecules. This means that antibiotics must go through BamA to get to their target, and thus that BAM is a desirable target for combating antibiotic resistance [3,5].

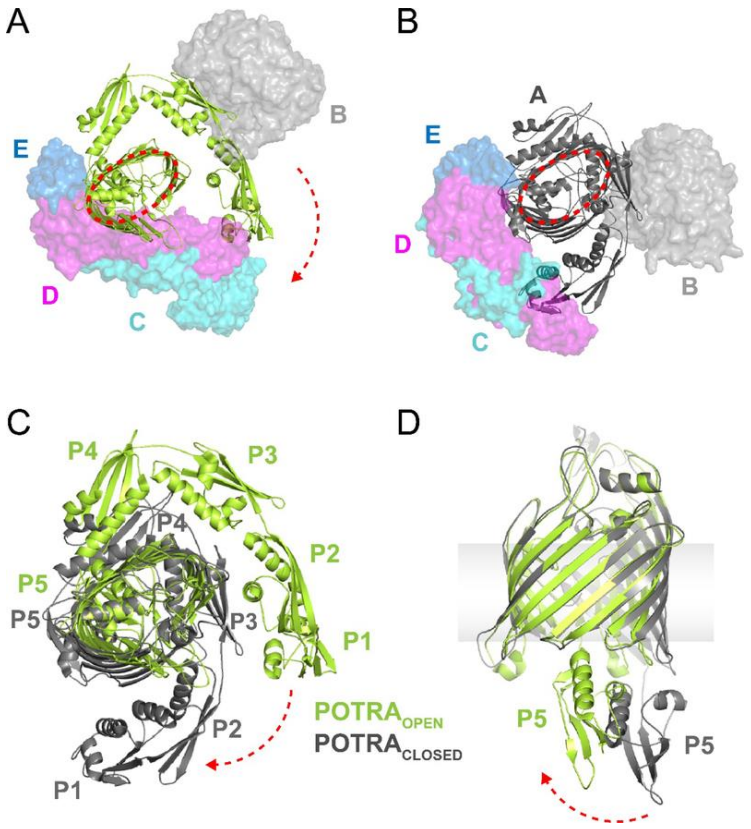

Figure 7: BAM structure in open and closed pore forms [16]

BamA is highly conserved across bacteria and is somewhat exposed on the outside of the cell. This makes it a good target for inhibition of the BAM complex. BamA functions by β-strands 1 and 16 folding themselves over, flipping between an open and closed form of BAM[14,16]. In the unfolded or open state, the BamA pore appears to be mostly unregulated, allowing molecules such as antibiotics through indiscriminately[11,16]. As such, targeting BamA in a manner that would lock it in an open conformation could rejuvenate the effectiveness of currently available antibiotics by allowing them into the cell [12,15,17].

The concept of inhibiting BAM to combat antibiotic resistance could likely be achieved in multiple ways, however the method currently being developed by the Schwabacher group uses

work done by James Nowick as a model for synthesizing small molecules to interact with BAM by insertion into a peptide [11,14].

Nowick demonstrated a method of synthesizing a β-sheet initiator. This was done by synthesizing a β-sheet mimetic which displayed the H-bonding pattern of a β-sheet with alternating acceptors and donors. This β-sheet initiator could be inserted into a peptide which would go into a cell and interact with various β-sheets [19,23].

BAM is, as discussed earlier, composed of many β-sheets and β-strands, some more critical than others. BamA, the pore, is the major target as interaction with an initiator could lock BamA in the open conformation therefore allowing antibiotics through and inhibiting BAM. β-strands 1 and 16 are what allows BAM to lock itself in the closed conformation. By interfering with the ability of these β-strands to associate, BAM can be prevented from closing. The design of a molecule that can H-bond to one of these β-strands was designed with the goal of inhibiting BAM's ability to close BamA.

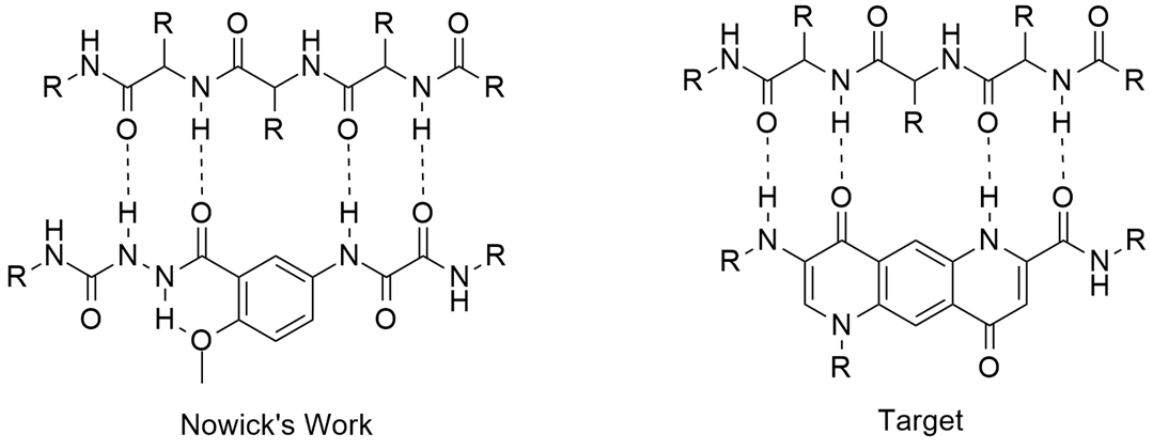

Figure 8: Nowick's Beta Sheet Mimetic and the Schwabacher Group Target

A fused quinolone target molecule was designed with Nowick's work in mind, as shown in *figure 8*. This target molecule is an asymmetric, three ringed quinolone with a β-sheet H-

bonding pattern on one face, and side chains on either end that allow for insertion into a peptide [23].

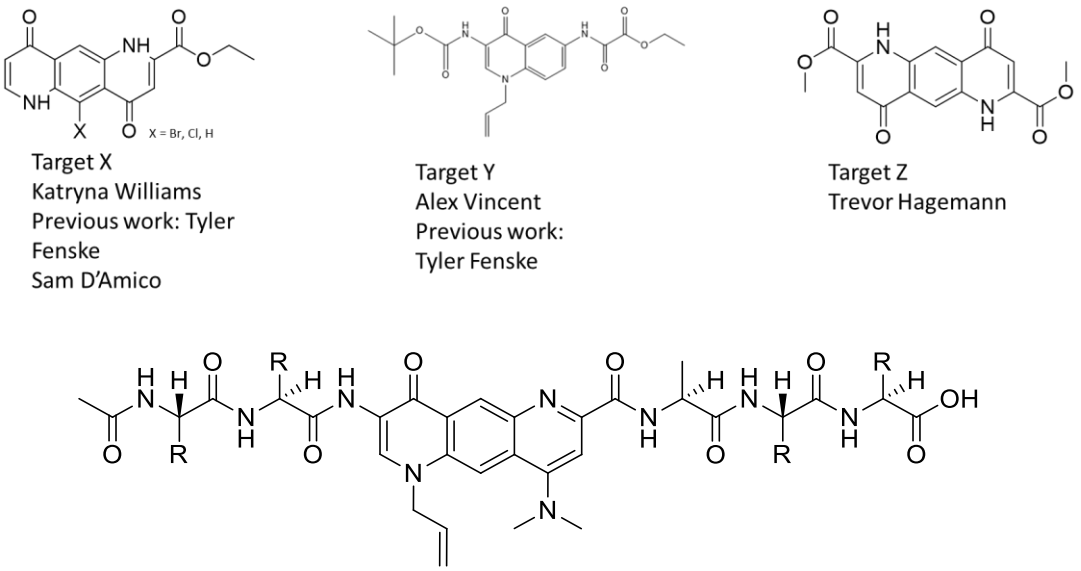

Figure 9: Interim targets X-Z and functionalized end-goal quinolone target

As shown above in *figure 9*, the ultimate target is a three ringed fused quinolone with asymmetric R groups on either end of the molecule, and an alternating H bonding pattern on one face. Instead of trying to synthesize this target, interim targets were designed for proof of concept and ease of synthesis. There were initially two interim targets, X and Y. Later, Trevor Hagemann made interim target Z, which caused a shift in project direction and caused target X to be scrapped as it was never successfully synthesized.

Initial Scheme

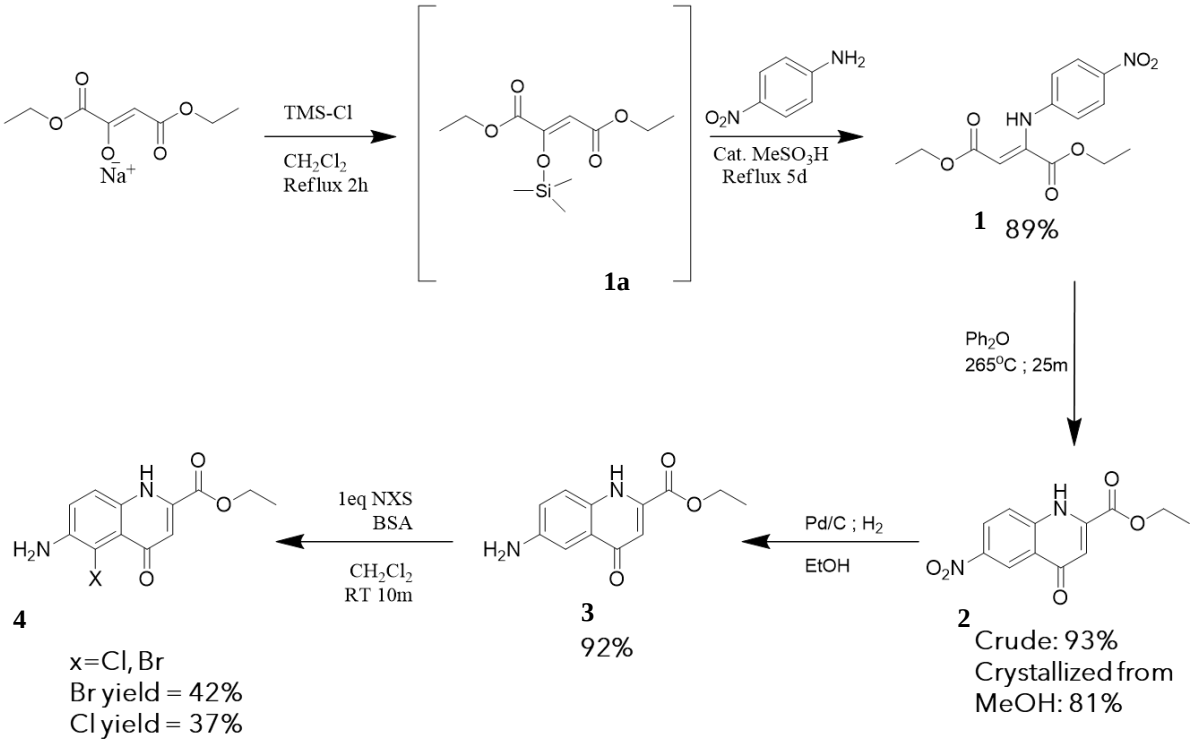

Scheme 1: Initial route to target quinolone

The primary route studied in this work was the route to interim Target X. This fused three-ringed quinolone proved difficult to synthesize.

This scheme started with the silylation of diethyl oxaloacetate with TMS-Cl to increase the solubility of diethyl oxaloacetate in dichloromethane. This silylation also increases the reactivity of the starting material, as it shifts the equilibrium of the reaction toward the products. Upon silylation, the -OTMS is primed as a leaving group. Without the TMS this oxygen is able to reform into the ketone and which causes reversal of reaction. This is why TMS-Cl is needed to keep this reaction moving in the forward direction.

Once solubilized, a catalytic amount of methane sulfonic acid and p-nitroaniline were added to form compound 1 in high yield (93%) after 5 days at reflux. This intermediate was then isolated and thermally cyclized to form a quinolone via reflux in diphenyl ether.

Initially the crystallization method for this quinolone, compound 2, involved ethanol and toluene, but the crystallization yields from this system were low and ranged from 32% to 39%. This was likely due to low solubility of the quinolone in ethanol. After solubility studies were performed, the crystallization system was switched to only methanol. This new system gave an average 82% yield of compound 2.

The quinolone was then moved on to hydrogenation, using 5% Pd/C as is standard. This step had a consistently high yield between 84-92% and was clean enough by NMR to move on without crystallization. Since it was an amine, compound 3 was kept under vacuum or moved on immediately as it was not highly stable in air.

Prior research performed by Tyler Fenske had focused on trying to cyclize the quinolone at this stage to form the desired product, target X, from this amine. Unfortunately, multiple attempts and conditions showed cyclization on the wrong carbon, creating a kinked structure shown below in *scheme 2*, as it is more energetically favorable.

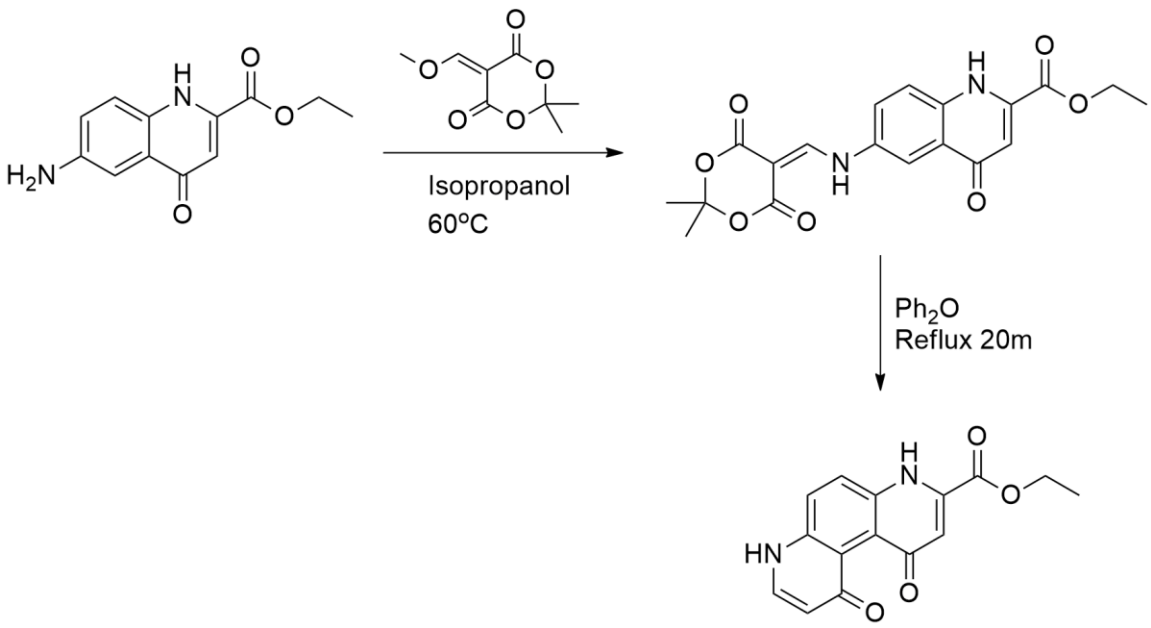

Scheme 2: Incorrect cyclization causing formation of a "kinked" quinolone

This is much more kinetically favorable than the desired product, so it was decided that a group needed to be placed on the carbon alpha to the amine to prevent cyclization from occurring on this carbon.

One simple method of putting a group on that carbon was halogenation using N-bromosuccinimide or N-chlorosuccinimide and BSA. This reaction did synthesize the desired halogenated product (compound 4b with Br and 4c with Cl), but was unpredictable, inconsistent, and low yielding.

The BSA was primarily for solubilization, and after multiple trials it was determined that the amount of BSA added did not increase or decrease yield. This reaction was largely just dumping BSA, halogenation agent, and starting material in a pot with dichloromethane and stirring for 10m. Stoichiometry had to be calculated to avoid over-halogenation, so a 1:1 ratio of compound 3 and NBS or NCS was used.

Unfortunately, each attempt at halogenation produced different results by NMR and TLC which can be seen in *figure 10*. Due to the unpredictability of reaction, some parameters were changed to increase yield or consistency.

This reaction had previously been performed by both Tyler Fenske and Sam D'Amico, both of which noted different results. Fenske's method required stirring at RT for ten minutes and then diluting with water and putting into the fridge. After multiple attempts, this method did not work. D'Amico's method was different in that the reaction stirred at RT for 48-72h before diluting with water and refrigerating.

Experiment Number	Halogen	Modification	Yield
KDW-1-25	Chlorine	None	7% crude
KDW-1-37	Bromine	None	9% crude
KDW-1-52	Bromine	24h rxn time	38% crude
KDW-1-53	Chlorine	24h rxn time	33%
KDW-1-60	Bromine	Excess NBS; 5% thiosulfate quench; 10m rxn time	42%
KDW-1-61	Bromine	Excess NBS; 5% thiosulfate quench; 10m rxn time	36%
KDW-1-68	Bromine	Excess NBS; 5% thiosulfate quench; 30m rxn time	28% crude
KDW-1-69	Chlorine	72h rxn time	37% crude

Table 1: Halogenation conditions and results

As shown in *table 1*, the halogenation agent, reaction time, and quenching were varied. The longer reaction time was inspired by the results D'Amico wrote about, while the 10m reaction time was modeled after Fenske's attempts. The best yield came from a 2x excess of NBS and a reaction time of 10m, followed by quenching with a 5% sodium thiosulfate solution and crystallization. This produced a 42% yield of **4b** and was closer to Fenske's conditions with

the addition of excess halogenating agent and quenching with thiosulfate. It did appear that longer reaction times also were successful, but the results from the longer reactions were more difficult to purify and product was often lost during workup.

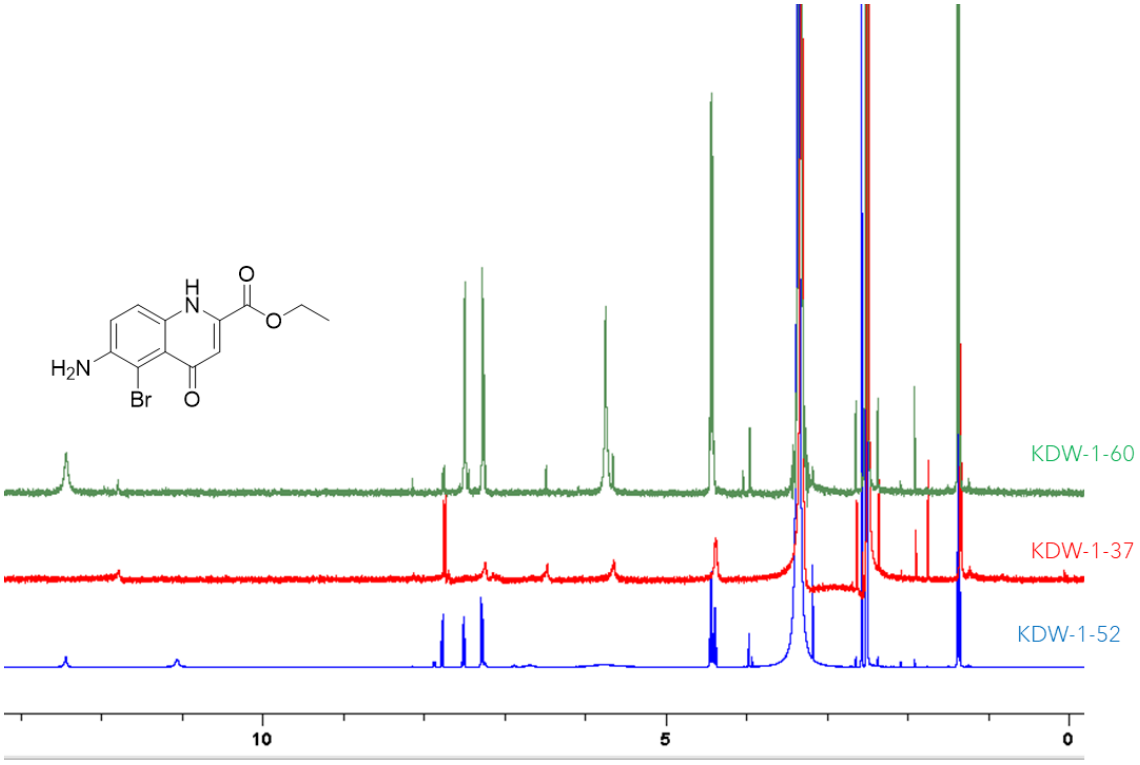

Figure 10: HNMR of different reactions to form 4b

Unfortunately, the HNMR for these products was incredibly inconsistent, demonstrating that this reaction was not giving replicable or reliable results. *Figure 12* shows three attempts at forming 4b using similar conditions and workups with wildly different spectral results. There are different numbers of peaks, different peak placement, and different contaminants in each new HNMR. Even upon repeating the conditions exactly, the results were not reliably replicable.

Method of Cyclization

While continuing to work with the halogenation, the method of cyclization was investigated using a series of model reactions seen below in *scheme 3.*

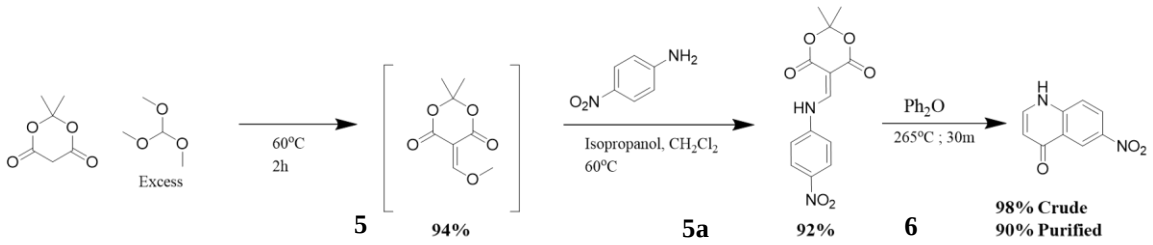

Scheme 3: Meldrum's Acid Model Scheme

This scheme shows the model reaction performed using trimethyl orthoformate and Meldrum's acid to make a Meldrum's acid derivative (MAD), compound 5. This MAD was then reacted with p-nitroaniline to form an enamine 5a which was then cyclized through thermal cyclization with diphenyl ether.

Initially, 5 was isolated in a 94% yield. However, it is incredibly hygroscopic and cannot be handled easily without liquification of the product, and it was found that performing the formation of the enamine is possible without workup of the enol ether. After heating for approximately 2 hours at 60ºC and verifying enol ether formation is complete by TLC, the aniline is added in solvent and heated until starting material is gone by TLC.

The literature used isopropanol at 60ºC for approximately four days, which is a long reaction time. Upon investigation it was found that other solvents can be used for faster reaction time, as seen in *table 2.*

Experiment Number	Meldrum's Acid Eq: Trimethyl Orthoformate Eq	Aniline (Eq)	Solvent for enamine formation?	Temp	Yield (enamine)	Time
KDW-1-26	1:1.6	p-nitroaniline (.92)	Isopropanol	Reflux	89%	4d
KDW-1-33	1:3.8	p-nitroaniline (1)	Isopropanol	60	95%	4d
KDW-1-41	1:5.25	4c	Isopropanol	60	58%	4d
KDW-1-43	1:6	4b	Isopropanol	60	82%	5d
KDW-1-64a	1:1.6	p-nitroaniline (.95)	Methanol	Reflux	90%	18h
KDW-1-64b	1:1.6	p-nitroaniline (1)	Toluene	Reflux	84%	12h
KDW-1-64c	1:1.6	p-nitroaniline (.98)	Acetonitrile	Reflux	88%	22h

Table 2: Meldrum's Acid reaction conditions

With how slow this reaction was, the first thing tried to decrease reaction time was increase of temperature. Instead of heating to 60ºC, reflux of IPA was tried. This did not decrease reaction time but it *did* lower yield slightly which was not the desired result.

Next, a polar protic, polar aprotic, and nonpolar solvent were each tried to determine effect on the reaction. Each solvent formed the desired product within 10% yield of the literature value, with the lowest yield belonging to toluene. Toluene had the fastest reaction time at 12h, but MeOH only took 18h and gave a higher yield by 4% and thus was used from this point forward in enamine formation. The hypothesis is that the higher the bp the faster the enamine formation, but this does not guarantee a higher yield. It appears isopropanol does give the highest yield of compound 6 with a yield of 95% in 4 days, but MeOH gives a 90% yield in 18h and the loss in yield is minor.

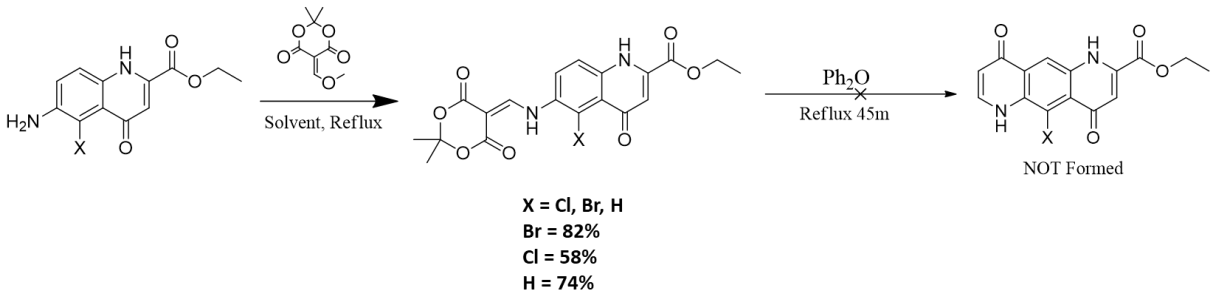

Scheme 4: Meldrum's Acid scheme applied to initial work to form

This scheme was then applied to compound 4 from *scheme 1*. Enamine formation did occur in reasonable yields ranging from 58-82% forming compounds 5b,c,d as shown in *scheme 4*, however cyclization did not occur. Cyclization conditions were varied through longer reaction time as well as addition of a solubilizing solvent, but no cyclized product was obtained in any of the eleven trials. Target X was unable to be formed through this route.

This could be due in part to solubility of starting material in diphenyl ether, but when cosolvents were added to increase solubility there was still no desired product for. It appears that thermal cyclization using a MAD form of compound 4 is not enough to overcome the energy barrier to formation of interim target X.

At this time, a new method needed to be planned to reach target X. During the research phase, Trevor Hagemann synthesized the Janus Quinolone, or interim target Z, allowing for an entirely new synthetic route and target to become the focus of this project. *Scheme 1* and interim target X were scrapped moving forward in favor of target Z.

The Janus Quinolone

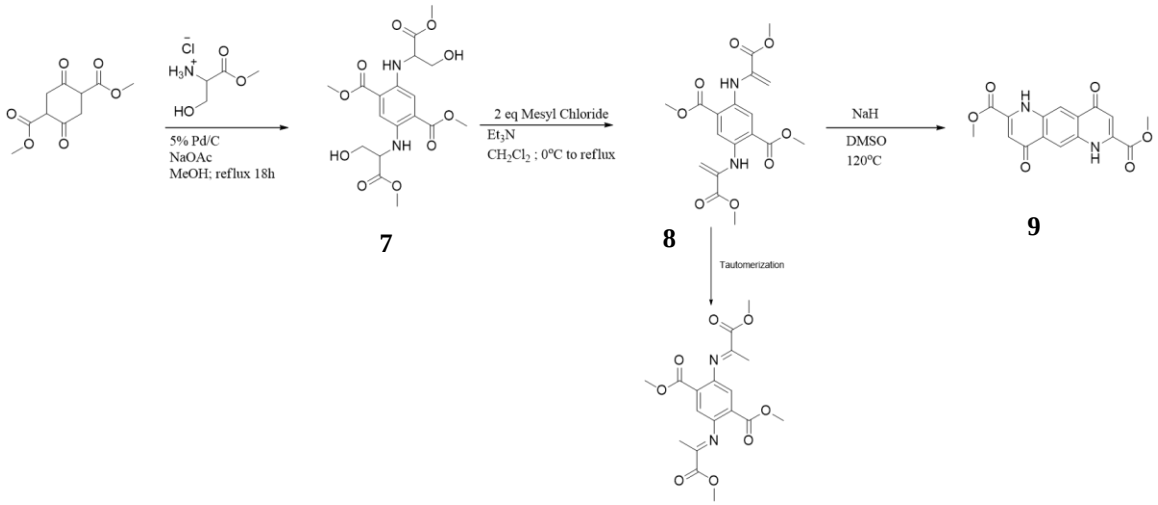

Scheme 5: The synthesis of the Janus Quinolone

At this point in time, a synthesis to form the Janus Quinolone (JQ) or interim target Z, was discovered by Trevor Hagemann. This scheme begins with the reaction of DMSS with Serine methyl ester HCl in MeOH with acetate and a staggered addition of Pd/C after 2h. This gave Hagemann a yield of 90%. This intermediate 7 was then mesylated and dehydrated to form compound 8, which formed in 98% yield. This can tautomerize over time to 8a, but both tautomers have been shown to lead to the JQ, 9, in high yield (97%) upon cyclization using NaH in DMSO.

The first question about this scheme was regarding the addition of Pd/C to the reaction after 2h. This was investigated by performing reactions where the Pd/C was in the reaction from the start. This method gave a slightly lower yield by 4%, but was still viable. With continued experimentation, Seresa McDowell showed evidence that adding Pd/C in the beginning of reaction may lead to faster degradation of product 7 and therefore decrease yield if not worked up on time. There also seem to be different side products produced when the reaction is started

with Pd/C in solution. This means that the addition of Pd/C after the reaction has already begun is important to achieve optimal results.

The second question was regarding the base used for cyclization to form the JQ. NaH is a very strong base that is not pleasant to work with and provides some safety concerns. For this reason, potassium t-butoxide was tried as a base in place of NaH. In this case, the highest yield obtained was 3% despite various attempts at temperatures ranging from 60-120 degrees and experiment lengths ranging from 12-72h. As such, this was scrapped in favor of continuing to use NaH due to the incredibly high success.

Desymmetrization

After the discovery of the JQ, the problem became desymmetrization. The JQ is symmetric, and the Schwabacher group's target molecule is asymmetric. As such, Trevor Hagemann took up trying various nitration methods with no success.

Instead, a method of nitrosation followed by oxidation was attempted. This was first done through a model reaction, as seen in *scheme 6*.

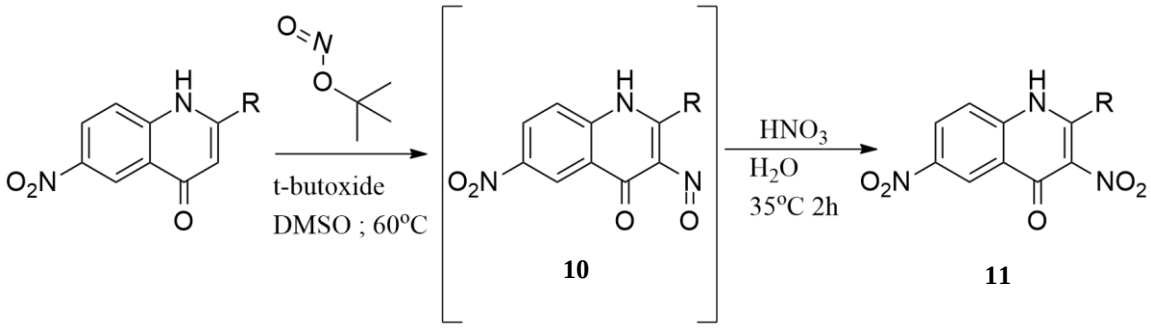

Scheme 6: Model nitrosation-oxidation reactions for testing new method of nitration

The reaction began with compound 6, previously synthesized from the Meldrum's acid model experiments from *scheme 3*, with t-butyl nitrite in DMSO with t-butoxide at 60ºC. DMSO and t-butoxide were used because these conditions were the only conditions known to dissolve the JQ, which this was a model for. Once nitrosation occurred by TLC, the product, 10, was moved on immediately to oxidation with nitric acid in water with gentle heat to form 11. Even

though the nitrosation product was moved on directly, a sample was still taken for NMR purposes.

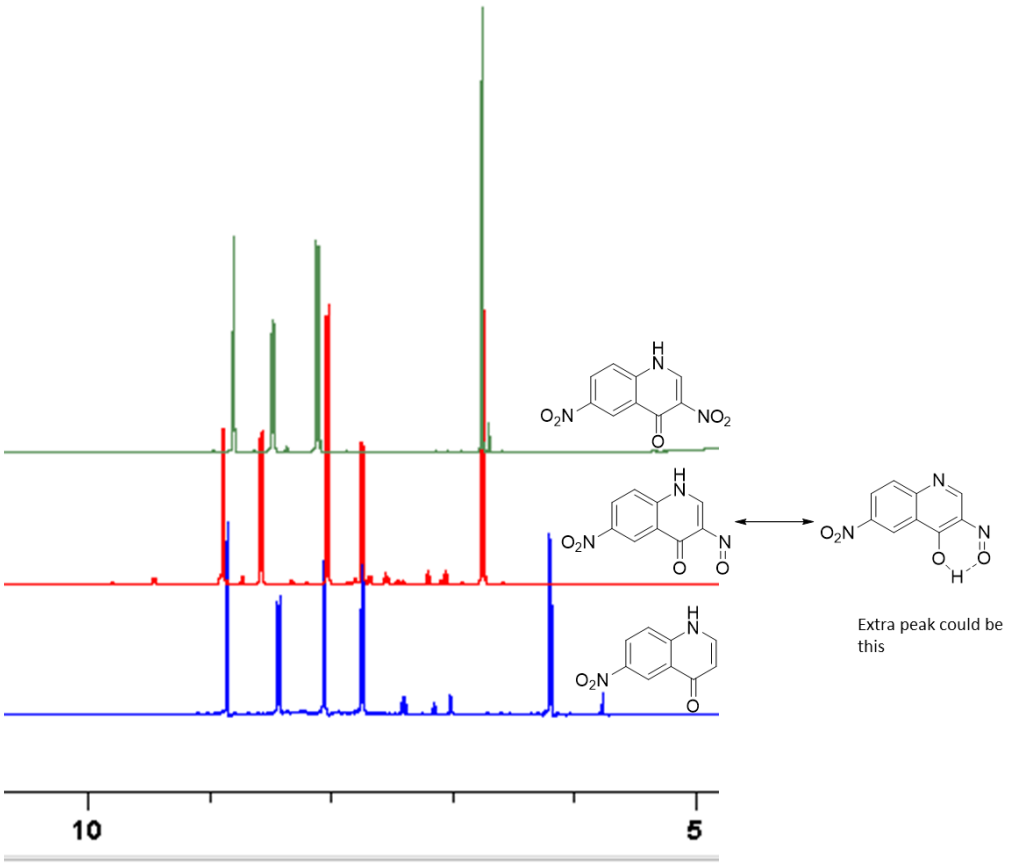

Figure 11: Compound 6 to 10a to 11a

In *figure 11* the HNMR of compound 6 is shown in blue, with five peaks each integrating to one, three aromatic and two vinyl protons. The HNMR above it in red shows compound 10a, the unstable nitroso intermediate. This HNMR appears to show that no nitrosation has occurred. However, when comparing this intermediate HNMR to the initial HNMR, some of the peaks have shifted. This intermediate is also different by TLC. This could be due to an intermolecular

hydrogen bond, which would aromatize the ring with the nitrogen and turn the carbonyl into a hydroxyl, as shown in *figure 11*. This would explain the changes and the extra peak present.

The top spectrum shows the final product after oxidation, compound 11a. This compound has the expected number of peaks in the HNMR, which is four. By TLC, HNMR, CNMR, and mass spectrometry this compound was confirmed to be synthesized, meaning this method of nitrosation followed by oxidation in *scheme 6* does work, and forms the desired product in a 64% yield.

This reaction was also done on compound 2 from *scheme 1*, as shown in *scheme 6*. This set of reactions was shown to work on compound 2 as well with a yield of 51%. The presence of the ethyl ester does seem to decrease yield of desired dinitro product, but still allows for the formation of this product.

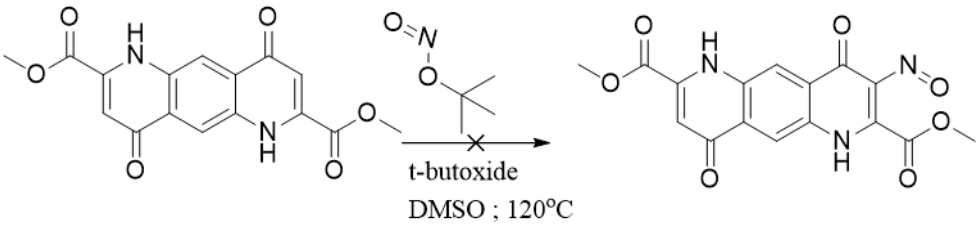

Scheme 7: Scheme for nitrosation of the JQ

Unfortunately, when this was tried on the JQ as shown in *scheme 7*, no product was formed. It appeared that no reaction was occurring by TLC, as no change was noted in the starting material.

Since the nitrosation-oxidation did not work to form an asymmetric JQ, Hagemann ended up trying new methods with different molecules to reach an asymmetric, three ring fused quinolone. *Figure 12* shows some of the scheme that Hagemann used to reach this asymmetric three ringed quinolone. This reaction scheme was successful and fulfills the purpose of the collaboration with the Kahne group at Harvard.

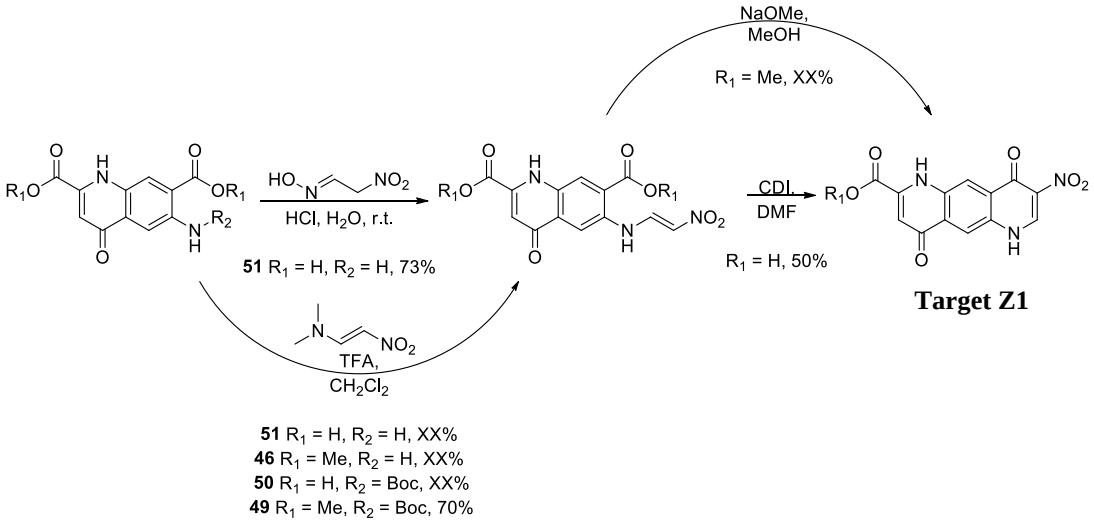

Figure 12: Trevor Hagemann's three ringed asymmetric quinolone, target Z1

This compound, target Z1, is a three-ringed fused quinolone with a nitro on one end and a carboxylic acid on the other. This allows for insertion into a peptide as was the goal of the quinolones shown in *figure 9.*

With this compound synthesized in a relatively high yield by Hagemann, different methods to reach an asymmetric three ringed quinolone were no longer needed, as other methods tried were generally less efficient than his syntheses. As such, aspects of this project have been

stepped away from to allow focus to fall on the successful syntheses that have been discovered and allow for the desired end-stage product to be formed.

Preliminary testing has been done on some of the Schwabacher group's compounds, particularly Alex Vincent and Tyler Fenske's two ringed quinolone, *figure 13*, below. The testing done by the Kahne group has been promising and appears to indicate that there is inhibition of the BAM by the compounds designed using the β-sheet mimetic concept inspired by Nowick's work.

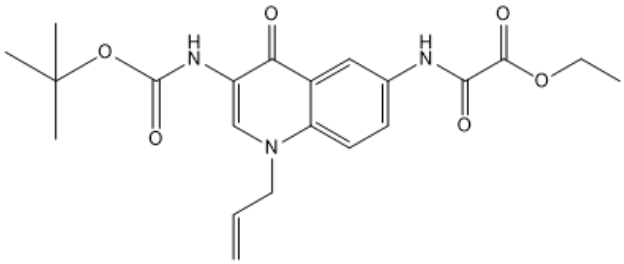

Figure 13: Compound synthesized by Tyler Fenske and Alex Vincent that has undergone preliminary testing by the Kahne group

This Fenske/Vincent quinolone has shown promise in the tests done so far. This quinolone, in contrast to Hagemann's quinolone and the initial three-ringed target, only has two fused rings and has an amide on either end. The Fenske/Vincent quinolone also contains an allyl group that could allow for further derivatization of the molecule, though synthetic attempts at making different derivatives by Vincent have been largely unsuccessful so far.

It is anticipated that the three-ringed quinolone synthesized by Hagemann will be more ideal for the inhibition of BamA. Testing has yet to be done, but the H-bonding pattern in Hagemann's quinolone appears to be more ideal and may give a stronger result when testing is performed.

Proposed Future Directions

The future of this project is bright, as the results so far have been promising and multiple target compounds have been synthesized. This project's goals moving forward will be dependent on results from the Kahne group. Modifications to quinolone structures may need to be made to optimize H-bonding between BamA and the quinolone.

These quinolones will be made into small peptides and tested for association and interaction with BamA by the Kahne group. Vincent can make modifications to his quinolone as needed to increase properties such as solubility or H-bonding ability. One proposed way to make this quinolone more soluble is to change the allyl group to an ester, which are generally much more soluble in aqueous solution and an aqueous solution is likely to be needed if these molecules were to make it to a drug-development phase.

Hagemann's quinolones can be tested for their interaction with BamA. Various modifications can be made to the structures to allow for increase in solubility or fluorescent properties. These fluorescent properties are very helpful for determining activity of these compounds upon interacting with BamA.

If these molecules are shown to work for the desired purpose and are able to enter into drug development they would fulfill a great need that is felt worldwide. Antibiotic resistance is an issue that needs to be solved or it will continue to grow and affect more people. If these quinolones can be shown to inhibit BamA this could lead to the bacterial cell being open for antibiotics to get in and perform their desired function. These molecules, if they are shown to inhibit BamA, would need to be tested for bioavailability, cytotoxicity, and many other factors as is common when taking a molecule on to the drug development phase. These tests would not be

undertaken by the Schwabacher group and instead would likely be done by the Kahne group at Harvard or perhaps outsourced to another group entirely.

Should these molecules become a drug and make it to a place where they can be marketed to consumers, they could be life-changing for many people and could prevent many deaths and severe illnesses by Gram-negative bacteria.

Experimental

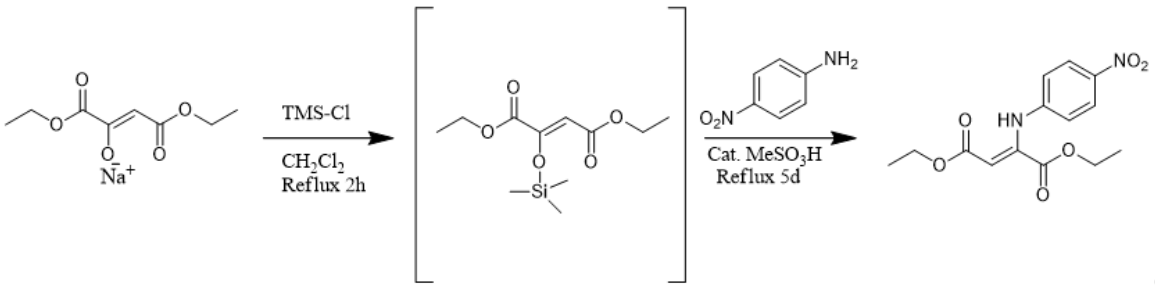

diethyl 2-((4-nitrophenyl)amino)fumarate, compound 1

6.003g of diethyl oxaloacetate sodium salt (28.6mmol) was combined with 3.7mL of TMS-Cl (29.2mmol) in 100mL of CH_2Cl_2 and set to reflux. The diethyl oxaloacetate is slowly solubilized upon reaction with TMS-Cl, and NaCl precipitates out. After diethyl oxaloacetate was solubilized, 2.096g (15.2mmol) of para-nitroaniline and 0.1mL (1.54mmol) $MeSO_3H$ were added, and the reaction was returned to reflux.

This reaction was followed by TLC using a 1:1:1 EtOAc, Et_3N, CH_2Cl_2 eluent.

Once complete by TLC, the reaction was removed from reflux and filtered to remove NaCl. The organic was then washed 3x75mL tribasic phosphate and 1x75mL brine. The organic layer was then dried over magnesium sulfate, filtered, concentrated down and left under vacuum overnight to yield a yellow solid (84% yield).

1H NMR (500 MHz, CDCl3) δ 9.82 (s, 1H), 8.16 (d, J = 9.1 Hz, 3H), 6.90 (d, J = 9.1 Hz, 3H), 5.69 (s, 1H), 4.26 (q, J = 7.1 Hz, 6H), 4.23 (q, J = 7.1 Hz, 6H), 1.32 (t, J = 7.1 Hz, 5H), 1.22 (t, J = 7.1 Hz, 5H).

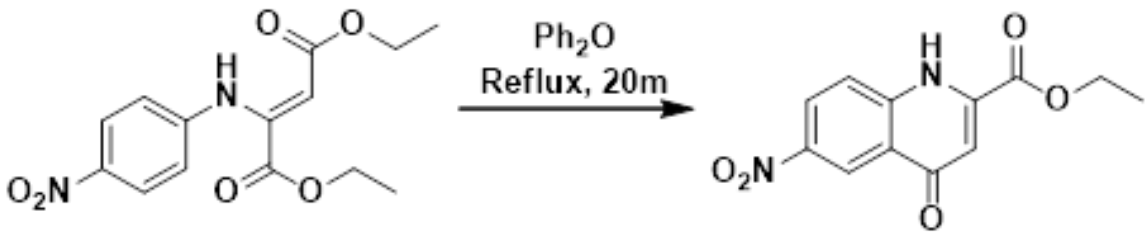

Reaction to form ethyl 2-carboxy-6-nitroquinol-4-one, compound 2

Diethyl 2-((4-nitrophenyl)amino)fumarate (4.14g, 13.4mmol) was combined with 70 mL diphenyl ether and heated to reflux. Solution was refluxed for 20 minutes before cooling to room temperature and diluting with 100mL of diethyl ether (NOTE: if solution is not COMPLETELY cooled, addition of diethyl ether could result in explosion). Solution was stirred for 5 minutes and then filtered. Solid was dried under vacuum to yield 2.91g (82%) of a brown solid. 3.545 = 100

Crude product (2.853g) was crystallized directly from methanol to give a 2.53g (72%) yield of a glittery gold/brown solid.

1H NMR (500 MHz, DMSO) δ 12.55 (s, 1H), 8.82 (d, J = 2.7 Hz, 1H), 8.50 (dd, J = 2.7, 9.3 Hz, 1H), 8.13 (d, J = 9.3 Hz, 1H), 6.77 (s, 1H), 4.45 (q, J = 7.1 Hz, 1H), 1.39 (t, J = 7.1 Hz, 1H).

Ethyl 6-amino-2-carboxyquinol-4-one, 3

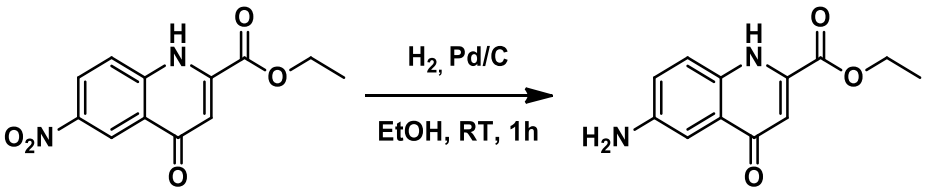

Ethyl 2-carboxy-6-nitroquinol-4-one (0.549g, 2.1 mmol) and 5% Pd/C (0.121g) were combined in ethanol (100 mL). Flask was sealed and flushed with H_2. After 3 hours, TLC (10% acetonitrile in dichloromethane) indicated starting material was no longer present.

Reaction was filtered through celite, and the celite was washed with hot ethanol until filtrate ran colorless. This was dried with magnesium sulfate and filtered again. The filtrate was concentrated via rotary evaporation and dried under vacuum to yield 0.4132g (84%) of a yellow solid.

1H NMR (500 MHz, DMSO) δ 11.81 (s, 1H); 7.68 (d, 1H); 7.07 (d, 1H); 6.47 (s, 1H); 5.47 (s, 1H); 4.34 (q, 2H); 1.34 (t, 3H)

Chlorination / bromination

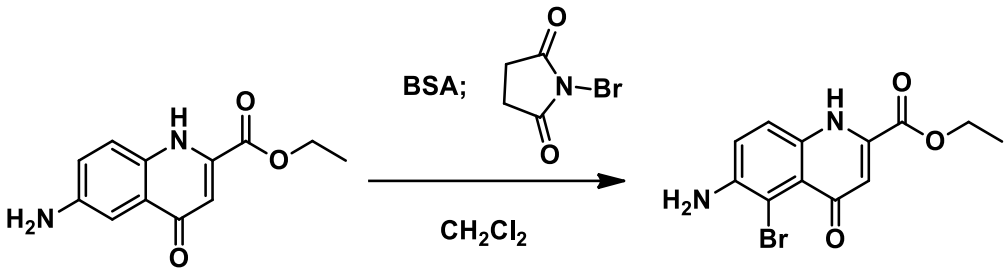

ethyl 6-amino-5-bromo-2-carboxyquinol-4-one, 4b, 4c
N,O-Bistrimethylsilylacetamide (1.2 mL) and 0.331g ethyl 6-amino-2-carboxyquinol-4-one (1.427mmol) were combined in CH_2Cl_2 and stirred until homogenous. 0.246g of N-bromosuccinimide (1.396 mmol) was then added resulting in an instantaneous darkening of the solution.

METHOD 1: Solution was stirred an additional 5 minutes and DI H_2O (15 mL) was then added and quickly swirled. Reaction mixture then placed at 4° overnight to crystallize the product with slow hydrolysis of the TMS ester. Solid collected via vacuum filtration and dried under reduced pressure to give a 43% yield.

METHOD 2: Solution was stirred an additional 30m, then quenched with 10mL of a 5% sodium thiosulfate solution. The reaction was then washed with water and the organic layer was put into a new flask. 10mL of water was added to the organic layer and swirled, then the reaction mixture was placed at 4° overnight to crystallize. Solid was collected via vacuum filtration and dried under reduced pressure to give a 45% yield.

Variations: NCS instead of NBS gives the chloride

1H NMR (500 MHz, DMSO) δ 7.88 (d, J = 9.1 Hz, 1H), 7.37 (d, J = 9.1 Hz, 1H), 6.91 (s, 1H), 4.42 (q, J = 7.1 Hz, 1H), 1.37 (t, J = 7.1 Hz, 1H).

Synthesis of 5-(methoxymethylene)-2,2-dimethyl-1,3-dioxane-4,6-dione, **5**

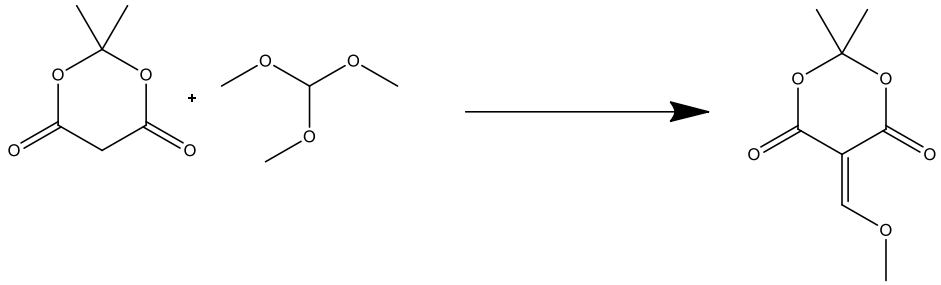

1.0061g Meldrum's Acid (6.93mmol) was combined with 1.25mL/1.21g of trimethyl orthoformate and heated to 60°C in an oil bath. The Meldrum's Acid solubilized within 10 minutes and turned the solution a yellow color. After a few hours, the reaction turned a dark red-brown and was done by TLC (10% MeOH in CH_3CN). The reaction was then removed from heat and concentrated via rotary evaporation to give a 1.14g (93%) yield of a red-brown solid. Solid is very hygroscopic and must be kept under vacuum.

1H NMR (500 MHz, DMSO) δ 8.18 (s, 1H); 4.30 (s, 1H); 1.75 (s, 6H).

Synthesis of 2,2-dimethyl-5-(((4-nitrophenyl)amino)methylene)-1,3-dioxane-4,6-dione, **5a**

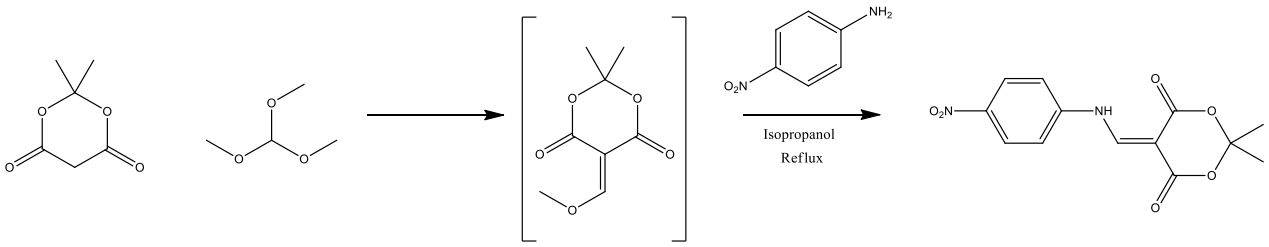

0.5309g of Meldrum's acid (3.68mmol) was combined with ~1.5mL of trimethyl orthoformate (13.70mmol) in a round bottom flask with a stir bar and a rubber septum. This was heated in an oil bath at approximately 60 degrees. The Meldrum's acid became soluble after 5-10 minutes, where the solution turned yellow, then red.

When finished by TLC 2h later (using a 1:1:1 Et_3N, CH_2Cl_2, EtOAc as eluent or 10% acetonitrile in dichloromethane), 0.5041g (3.65mmol) of *p*-nitroaniline was added to the reaction with toluene and set to reflux overnight.

The reaction was removed from heat and concentrated to give a 93% yield.

1H NMR (500 MHz, CDCl3) δ 11.40 (d, 2H); 8.71 (d, 1H); 8.35 (d, 2H); 7.39 (d, 2H); 1.77 (s, 6H)

*Notes: This reaction can be completed using almost any solvent after enol ether formation. Toluene is the fastest as it is the highest boiling, and when refluxing in toluene reaction is completed in 12h. Reaction also proceeds fully using MeOH, EtOH, and acetonitrile. Changing solvent does not appear to affect yield of enamine product, but does change reaction length due to varied reflux temperatures.

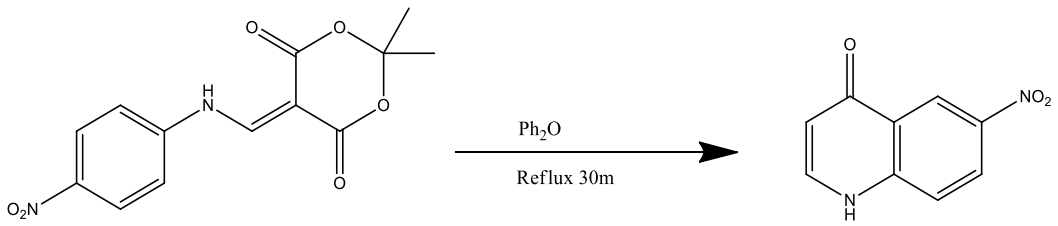

Synthesis of: 6-nitroquinolin-4(1H)-one, **6**

2,2-dimethyl-5-(((4-nitrophenyl)amino)methylene)-1,3-dioxane-4,6-dione (1.065g, 3.6mmol), was combined with 50mL of diphenyl ether and refluxed for 35m. This was cooled to room temperature (**NOTE: MUST BE AT ROOM TEMPERATURE BEFORE ADDING ETHER. Let cool approximately 45m)**, and 50mL ether was added and stirred for 5-10m. A precipitate formed, and the reaction was filtered and dried under vacuum to give a 90% yield.

HNMR (DMSO): 12.281 (s, 1H); 8.850 (d, 1H); 8.412 (q, 1H); 8.047 (d, 1H); 7.730 (d, 1H); 6.185 (d, 1H)

Preparation of: 6-aminoquinolin-4(1H)-one, **6a**

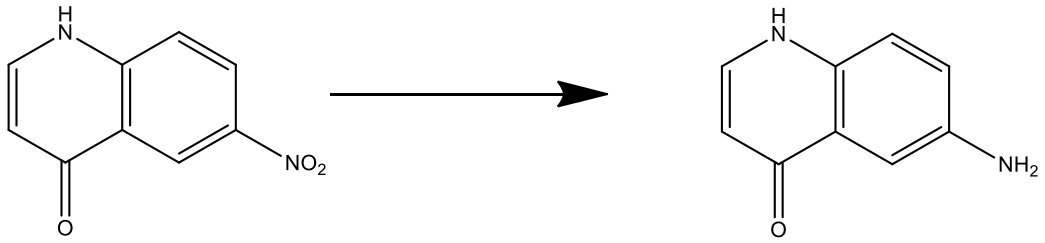

0.495g of 6-nitroquinolin-4(1H)-one (2.6mmol) was dissolved in ~30mL of THF in a flame dried round bottom flask. 0.041g of 5% Pd/C was added to the flask, a septum was put on top, and the flask was flushed with H_2.

Once completed, the reaction was filtered through celite, and hot THF was filtered through until the filtrate ran clear. The reaction was then concentrated via rotary evaporation for a yield of 0.39g = 92%

HNMR (DMSO): 11.15 (d, 1H); 8.38 (s, 1H); 8.35 (s, 1H); 7.21 (d, 1H 8.7Hz); 6.59 (d, 1H 8.7Hz); 5.31 (s, 1H)

ethyl 2-((4-nitrophenyl)amino)-2-oxoacetate **1c**

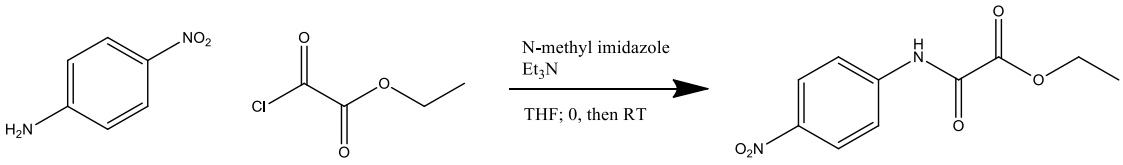

3.26g p-nitroaniline (23.6mmol) was combined with 7.1mL Et_3N (50.7mmol), 1mL N-Methyl imidazole (12.5mmol), and 6mL THF in a flame dried flask equipped with a stir bar. This flask was cooled to 0°C by ice bath, and 3.4mL ethyl chlorooxalate (30.4mmol) was added dropwise while keeping the temperature at 0°C. Once the ethyl chlorooxalate was fully added, the reaction was removed from ice and allowed to warm to room temperature and stir overnight.

The reaction is a thick, muddy texture and color. 10mL THF added, then reaction was concentrated via rotovap. Reaction was resuspended in ~100mL EtOAc, then washed with 1x75mL 2N HCl, 1x125mL $NaHCO_3$, and 1x75mL brine. The reaction was then dried over magnesium sulfate, filtered, and concentrated via rotovap.

Crude mass = 5.19g (93%)

Crystallized by dissolving in 150mL dichloromethane, heated to boiling. Once boiling, 45mL hexanes was added and heated. After about a minute of stirring, precipitation began, so was removed from heat, cooled to room temp, and put in the freezer. Crystalline yield = 3.97g (71% yield).

HNMR (CDCl3): 9.16 (s, 1H); 8.30 (m, 2H); 7.84 (m, 2H); 4.46 (q, 2H); 1.46 (t, 3H)

Preparation of: dimethyl 2,5-bis((3-hydroxy-1-methoxy-1-oxopropan-2-yl)amino)terephthalate

Common name: Bis-Serine Methyl Ester, **7**

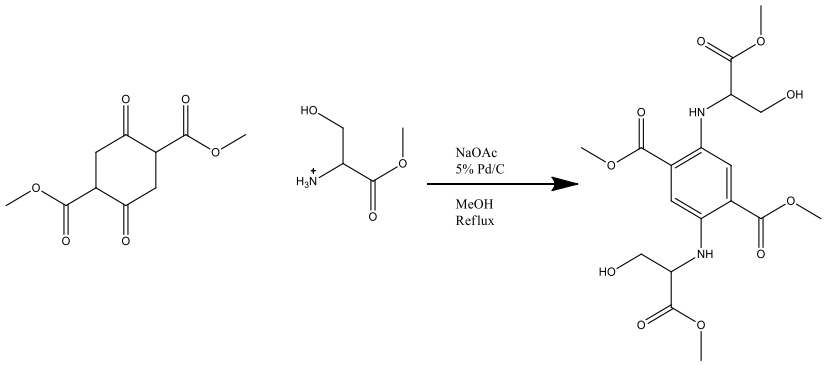

Combined serine methyl ester (1.308g, 8.4mmol) with DMSS (0.736g, 3.2mmol), 5% Pd/C (0.053g, 0.5mmol), and NaOAc (0.818g, 9.9mmol) in a flame dried RBF. 20mL of MeOH was carefully added to the reaction to ensure no sparking of the Pd/C. This was set to reflux and turned orange approximately 3.5h after beginning the reaction. Reaction went overnight until done by TLC (10% acetonitrile in dichloromethane). Once done, reaction was removed from reflux and filtered through celite. This was then concentrated down and resuspended in dichloromethane. It was washed twice with water and twice with brine, and was then dried over magnesium sulfate, filtered, and concentrated down to approximately 50mL. This was heated to boiling, and an equal amount of hexanes was added slowly. After a few moments of boiling, the solution turned cloudy and was removed from heat to cool to room temperature before putting in the freezer. Crystallized yield = 83.3% 1H NMR 500 MHz ($CDCl_3$): δ 7.33 (s, 2H), 4.30 (t, *J* = 3 Hz, 2H), 4.00 (m, *J* = 3 Hz, 4H), 3.91 (s, 6H), 3.78 (s, 6H)

13C-NMR 500 MHz ($CDCl_3$): δ 172.3, 167.8, 140.3, 117.9, 115.2, 63.0, 58.5, 52.5, 52.2

dimethyl 2,5-bis((Z)-(1-methoxy-1-oxopropan-2-ylidene)amino)terephthalate, **8**

From MsCl:

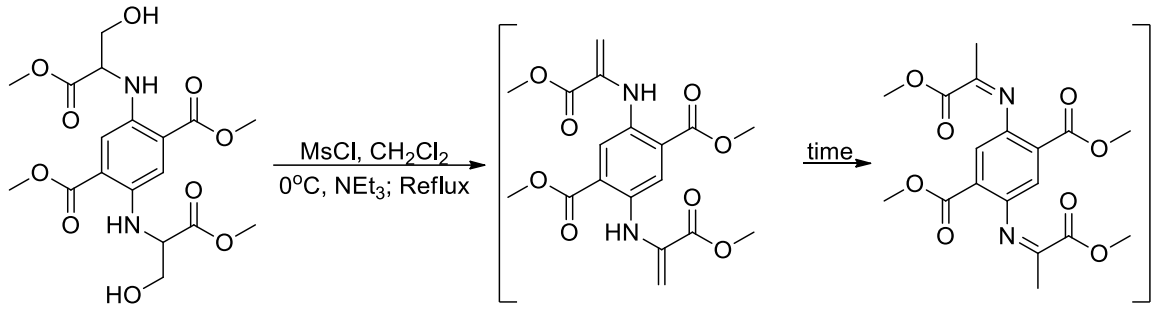

.4863g (1 mmol) of was dissolved into 20 ml of CH_2Cl_2 and chilled to 0 °C. .17 ml (2.0 mmol) of MsCl was added and while maintaining 0 °C, .51031g (5.1 mmol) of NEt_3 was added dropwise and slowly. After 15 minutes TLC indicated mesylation of starting material and the reaction mixture was heated to reflux. After 2 hours the reaction mixture was chilled and diluted to 50 ml of CH_2Cl_2. This was then washed with 500mL of sat. $NaHCO_3$ then 75 ml of sat. NaCl and the organics were dried over $MgSO_4$ before concentrating. The crude residue was crystallized from 55 ml of CH_2Cl_2 and 35 ml of hexanes. Yield: .30884g (79%), m.p. 172 – 173 °C

1H NMR 500 MHz ($CDCl_3$): δ 3.88 (6H, s), 3.93 (6H, s), 5.28 (2H, d, J = 1.5 Hz), 5.50 (2H, t, J = 1.3 Hz), 8.09 (2H, s), 9.33 (2H, s)

13C-NMR 500 MHz ($CDCl_3$): δ 167.1, 165.4, 136.3, 135.0, 120.4, 120.1, 95.9, 52.8, 52.5

dimethyl 4,9-dioxo-1,4,6,9-tetrahydropyrido[2,3-g]quinoline-2,7-dicarboxylate, **9**

From BAME-Ene:

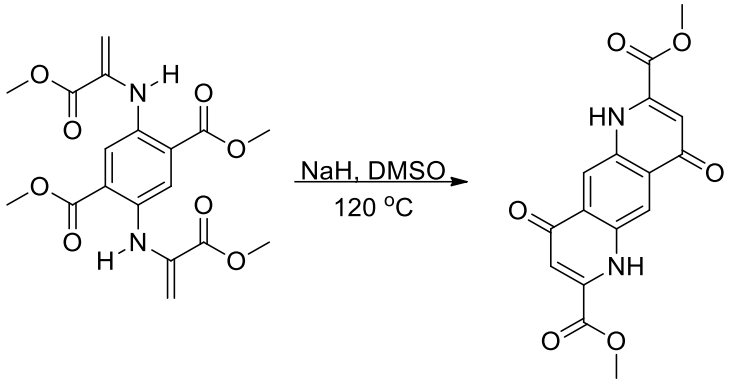

0.08346g (.23 mmol) was suspended into 20 ml of warm DMSO (60 °C) and stirred to dissolve. To this was added 0.034g (.9mmol) of NaH (60% disp in oil), which was washed with 4 ml of THF to remove oil then suspended in 2 ml of THF to transfer to the warm DMSO solution. Once bubbling had stopped the reaction mixture was warmed to 120 °C for 24 hours. The reaction mixture was cooled to room temperature before dilution into 200 ml MeOH: 10 ml AcOH. This solution was then stirred for 30 minutes before filtering and drying under reduced pressure. Yield: 0.05031g (89%), m.p. 348°C

Preparation of: ethyl 6-nitro-3-nitroso-4-oxo-1,4-dihydroquinoline-2-carboxylate, **10a, 11a**

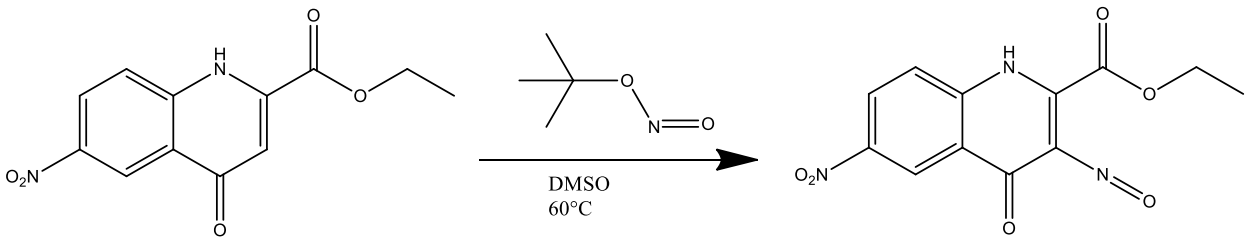

Combined 0.0997g (0.4mmol) of ethyl 2-carboxy-6-nitroquinol-4-one was dissolved in ~5mL of DMSO in a flame dried flask equipped with a stir bar. 0.1mL (0.8mmol) of t-butyl nitrite was added, and the flask was connected to a condenser. 1mL (>2eq) of 1M potassium t-butoxide in THF was added dropwise through the condenser. The reaction initially turned orange upon addition of t-butoxide and then became dark red. The reaction mixture became a goopy solid at room temperature, so it was connected to a variac and heated to ~60°C for 6 days. Reaction was done by TLC (10% acetonitrile in dichloromethane) after 5 days, but was left stirring/heating for a total of 9 days before workup.

Workup: Dump reaction mixture into vigorously stirring mix of 50mL water, 50mL dichloromethane, with 10mL of glacial acetic acid. This was stirred for 20 minutes, extracted with water 3x, then dried over magnesium sulfate and filtered. The dichloromethane layer was then evaporated to dryness and stored under vacuum.

HNMR (CDCl3): 9.31 (s, 1H); 8.51 (d, 1H); 7.59 (d, 1H); 4.57 (q, 2H); 1.57 (t, 3H)

Mass ion: 291.04 g/mol

Preparation of: Ethyl 4-chloro-6-nitroquinoline-2-carboxylate **2c**

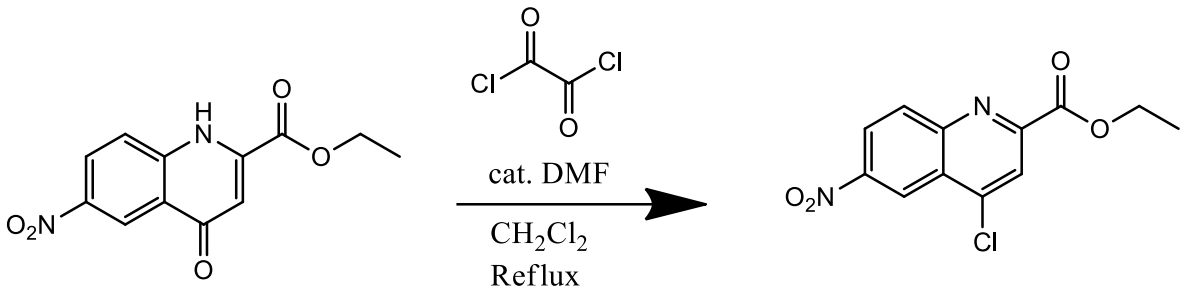

0.0518g of KDW-1-89 (0.2mmol) was placed into a flame dried flask with a stir bar. 5mL of dichloromethane and 0.08mL (0.8mmol, >2eq) of oxalyl chloride were added. The reaction mixture was yellow in color, and began to bubble slightly upon addition of oxalyl chloride.

2 drops of DMF were dissolved into 1.5mL of dichloromethane. This was added dropwise through the reflux condenser to the reaction until bubbling was seen. Once added, the reaction was heated to reflux and checked by TLC. Once heat was added, all starting material dissolved. After two hours, starting material was consumed by TLC (eluent 10%MeOH in CH_2Cl_2), but due to an intermediate being formed, the reaction was left to go longer to ensure completion. After 5h30m, the reaction was removed from heat and evaporated down via dry ice rotovap, and left on the rotary evaporator for 5m even after it appeared dry.

Crystallized from dichloromethane/hexanes. Dissolved in ~8mL dichloromethane, got to boiling, added ~3mL hexanes and saw solid precipitate out. Cooled to room temp and put into freezer overnight.

HNMR (CDCl3): 9.25 (d, 1H); 8.63 (q, 1H); 8.52 (d, 1H); 8.42 (s, 1H); 4.63 (q, 2H); 1.52(t, 3H)

Preparation of 3,6-dinitroquinolin-4(1H)-one, **10b, 11b**

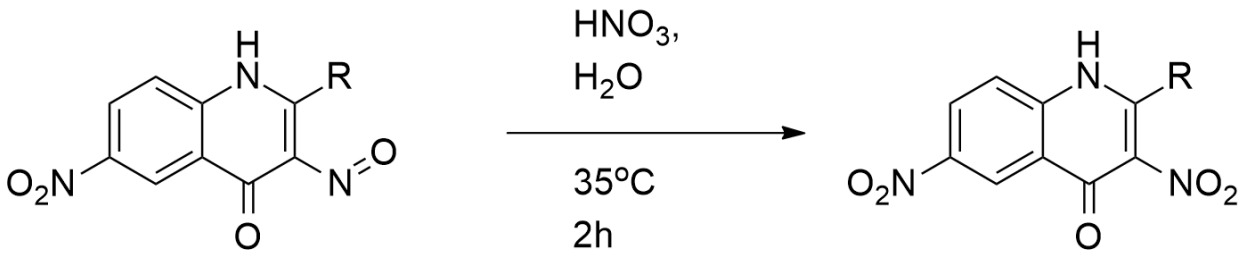

All of **10a or 11a (**0.21g) is dissolved in 10mL water and 1mL nitric acid and heated to 35 degrees with gentle stirring for 2h. Product precipitates out and is filtered and crystallized from 25mL dichloromethane/14mL hexanes to give a yield of 0.14g or 55%.

HNMR (DMSO): 11.11 (d, 1H); 8.38 (s, 1H); 8.14 (s, 1H); 7.25 (d, 1H 8.7Hz); 6.52 (d, 1H 8.7Hz);

Chapter III. Sensor Project

Introduction

Trace metals are commonly present in drinking water and are a rising source of concern to public health. The contaminating metals in water vary with location, but consist of Mn, Zn, As, Cu, Cd, Ni, Fe, and Pb [29,30,33,73]. Metals generally enter water through either waste or acidic water corroding metal-based pipes, with older pipes are often composed of Pb or Cu and releasing ions into solution. Some of these metals are largely harmless in small amounts but accumulation can cause harmful effects, such as Cu or Zn[30]. Other metals are harmful to consume in any amount, and their presence in drinking water presents a source of concern for public safety, such as Hg or Pb[33].

The Safe Water Drinking Act (SWDA) enacted by congress in 1974 allows the EPA to set guidelines for the amount of various metals and other contaminants allowed in public drinking water systems. This act does not regulate privately owned water systems, meaning approximately 10% of the US population is not covered by these guidelines [33]. Beyond issues of coverage, there are problems with violations in compliance. A study found nearly 9% of US water systems violated the health guidelines for metal content in drinking water. This effected at least 19% of the US population and up to 45 million people in 2015 alone[31]. The need for accessible water testing is great and can be achieved through development of an at-home system that could be sold to consumers worldwide [30,31,33].

The availability of water testing is limited and current testing kits out on the market have many flaws. Many commercially available testing kits require long waiting periods or lab testing and these kits are often not multi-use [52,68]. There is a need for a multi-use, real-time detection device that can test water in a consumer's home for unsafe levels of metals.

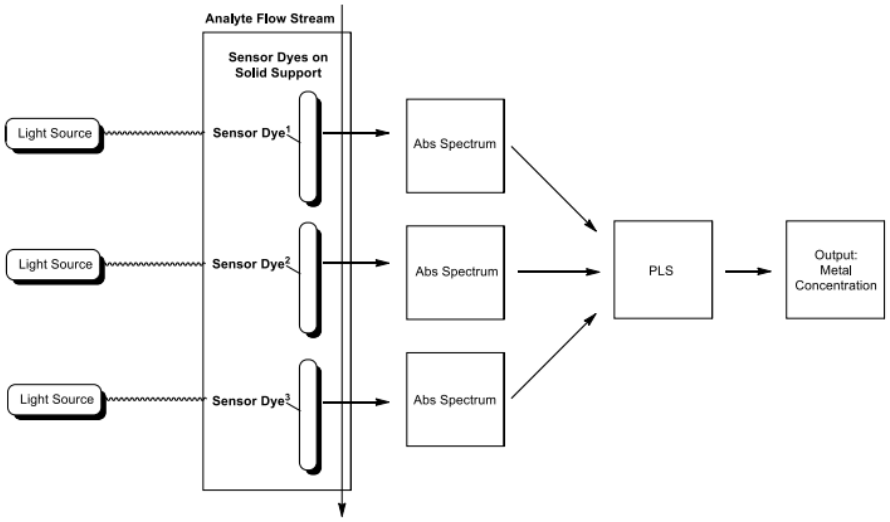

Figure 14: General System (Hagemann)

The design of a sensor array for metal detection and reporting was undertaken by the Schwabacher group in collaboration with a local business, Aquametals. The goal of this sensor array would make it so that anyone with access to the technology could test their own water at any time and the sensor would visibly change color if exposed to metals over a predetermined threshold. This works by securing a sensor to a solid support and passing drinking water over it. A light can then be shined onto the sensor and fed through a detector to receive an absorbance readout. This absorbance readout would change over time in response to metals and could be used to determine approximate amount of metal as well as metal identity, as it was demonstrated that there is linear relationship between absorbance change and exposure to metals at increasing concentrations in the sensors designed by Trevor Hagemann of the Schwabacher group.

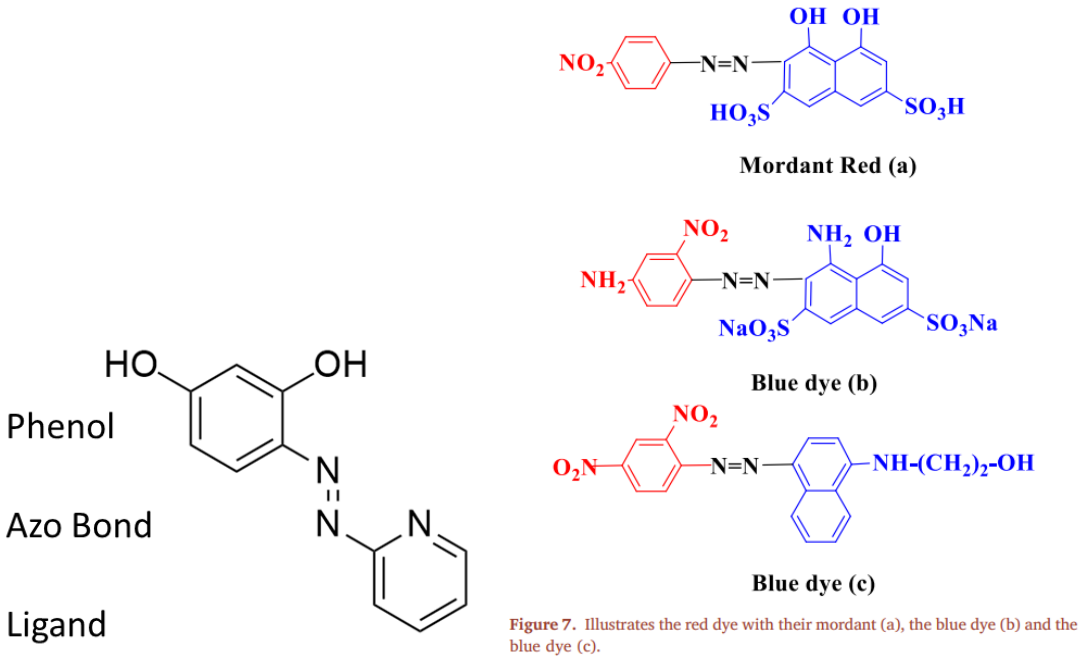

Figure 7. Illustrates the red dye with their mordant (a), the blue dye (b) and the blue dye (c).

Figure 15: a) General Structure of an Azo Dye b) variations of azo dyes and how small changes can cause large differences

Azo dyes are widely used compounds that make up 70% of dyes used in industry setting. Azo dyes are compounds that are made up of at least one azo bond (-N=N), a phenyl, and a functional group or ligand such as a hydroxyl or amine[38]. They are commonly synthesized through diazotization of an aromatic primary amine and then coupling to an electron rich nucleophile. Synthetic simplicity is a contributing factor to their utility[26,27].

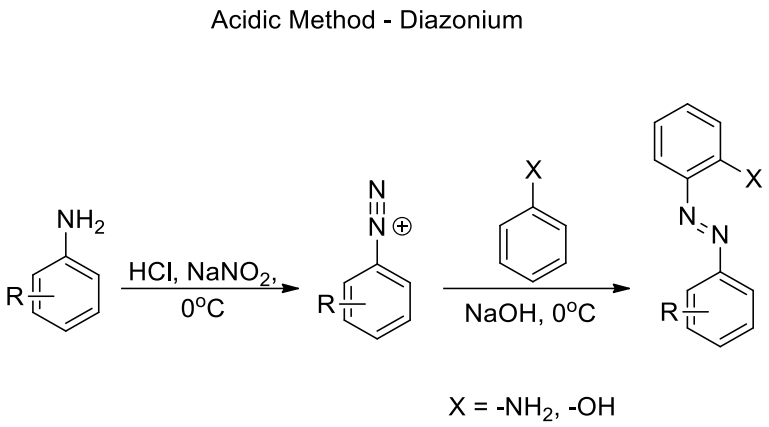

Scheme 8: Azo dye synthesis method

Azo dyes are highly variable in properties and color. Small changes to ligands or substituents can result in different characteristics or behavior[28,36].

As shown in *figure 15b*[28], small changes in structure of an azo dye can wildly vary color and functionality, meaning that a core molecule can be used to develop many different azo dyes with different properties and behaviors. In *figure 15b*, it is shown that a change of one hydroxyl to an amine, addition of an amine and change in position of the nitro, and the change to a salt caused the dye to shift from red to blue. However, change from an amine into a nitro, removal of sulfurs, and movement of ligands entirely did not cause a change in color in the sensor – it was still blue[26,28]! This demonstrates that many variations can be performed on an azo dye with different effects. In some cases, addition of new groups can cause a dramatic change in azo dye color. In other circumstances, the color can remain the same but properties can change to make the dye more soluble, more easily synthesized, or more reactive[24].

The Schwabacher group has been synthesizing molecular chemosensors that change color and absorbance in the presence of various metals. Each sensor has a different sensitivity and responds to different metals in solution. These sensors indicate the presence of metal at or above

a certain concentration by undergoing a visible color change and a shift in maximum absorbance. Initially, these sensors were used in the detection of metals such as Zn by covalent attachment to a gel polymer matrix.

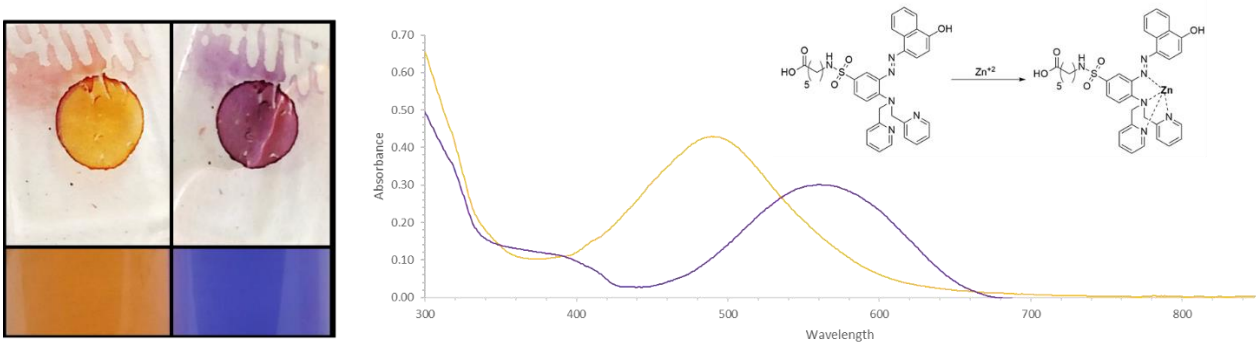

Figure 16: Demonstration of azo dye color change in response to metal

As shown above in *figure 16*, these sensors experience a visible color change when exposed to metals. *Figure 16* shows one of Hagemann's many dyes made for detection of small metal ions in an aqueous environment. On the left is an image of the sensor attached to polymer gel. This sensor, PAR, is orange before exposure to metal and purple after exposure to Zn. The structure for PAR can be found in the upper righthand side of *figure 16*, both before and after interacting with Zn, with the metal interactions shown. In this case, the Zn is binding to one of the nitrogens in the azo bond, as well as to three other nitrogens in the ligand portion of the molecule.

The last part of *figure 16* is an absorbance spectrum, showing the change in absorbance maximum and measurement before and after Zn exposure. Zn exposure caused the sensor to shift

from orange to purple, changed absorbance max from 490nm to 550nm, and decreased the absorbance measurement.

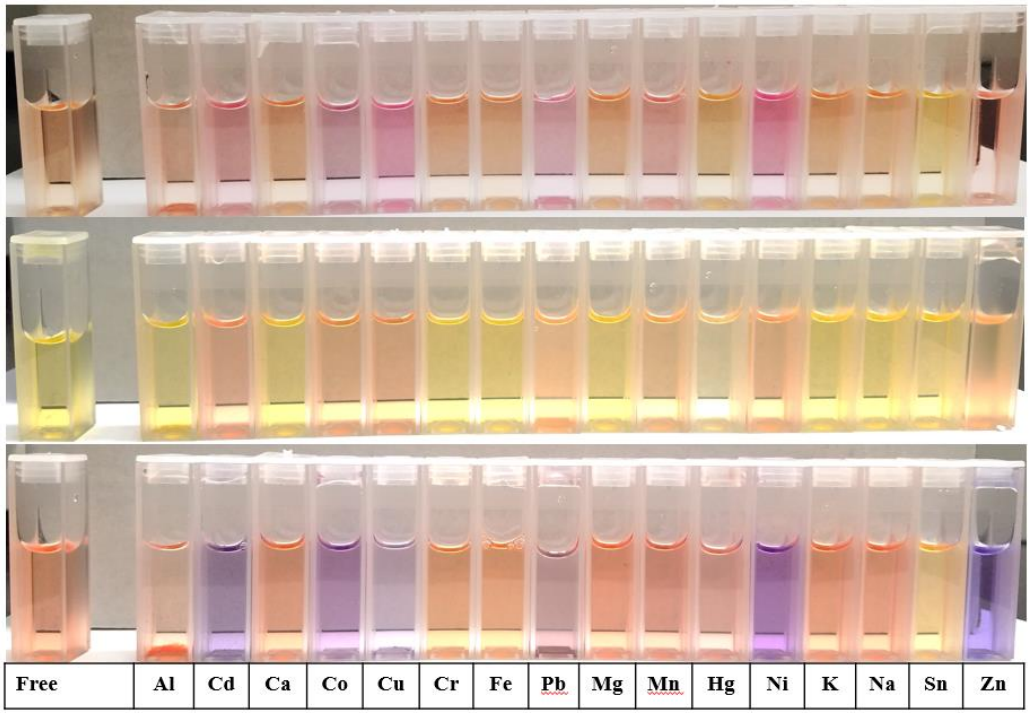

Figure 17: Sensor Color Changes

Figure 17 is a practical demonstration of how azo dye ligand variation or naphthol variation can change the color and response of the azo dye. This figure shows three different sensors, with the unbound sensor in the leftmost cuvette, and the sensor exposed to various metals on the right. Each sensor is shown to respond in a unique manner, with different colors, intensities, and different metals responded to.

This initial sensor project was in collaboration with Aquametals, a company seeking to identify and quantitate amounts of metal ions in drinking water. This collaboration was looking primarily at smaller metal ions such as Zn with Trevor Hagemann and Tyler Fenske of the Schwabacher group taking point on synthesis of azo dyes and polymers respectively.

Fenske created a method of synthesis for polymer dots. These polymer dots are bound to a glass slide with the end goal of acylation with a sensor, wherein these dots would be fully functional sensors in a machine. The procedure for polymer dots has been modified many times by Rebecca Dominguez after Fenske's graduation, and as of 2022 this method is no longer the optimal method for polymer synthesis. As of 2021, the polymers themselves have been changed to a different structure entirely.

This older scheme begins with activation of glass slides through soaking in concentrated sulfuric acid. These slides are then silanized in the gas phase, dehydrated, and then put in a methacroylyl chloride bath. Once removed, the polymerization occurs in an oven over three hours, as seen in *scheme 9.*

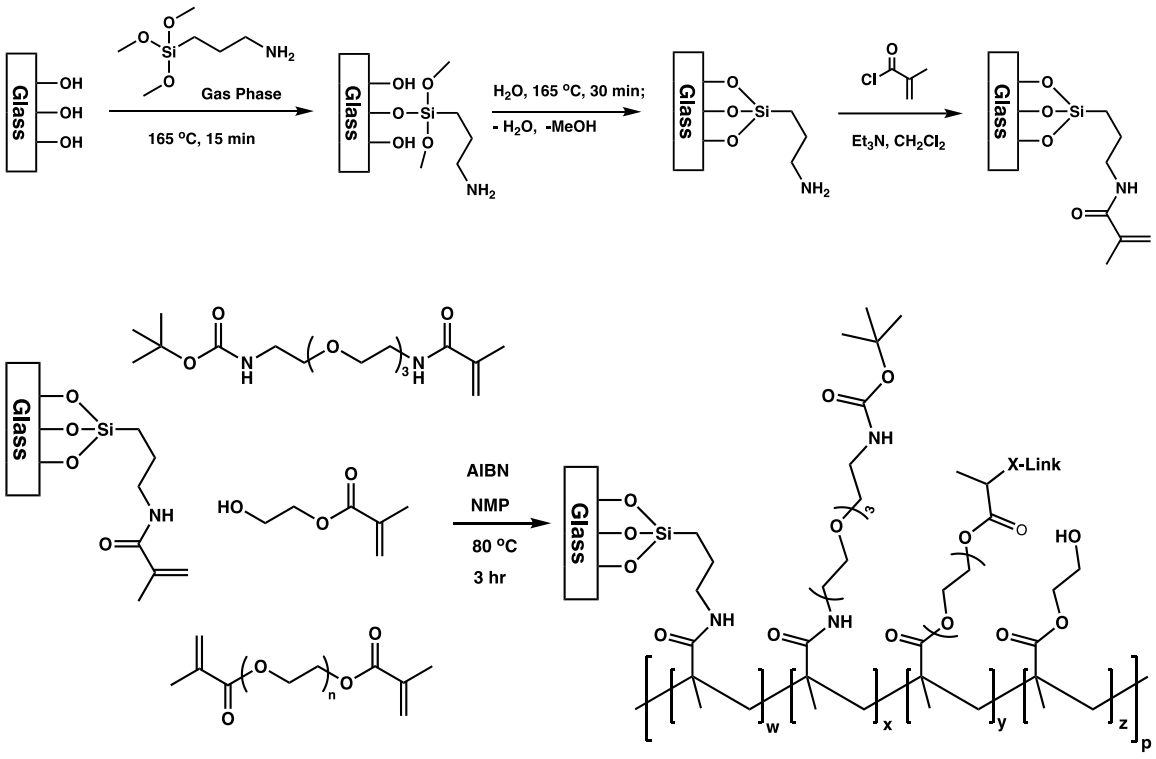

Scheme 9: Building of polymer dots

Unfortunately, these dots were difficult to synthesize and work with. The synthesis itself was a time-consuming process and required a workday of 10h or more and there were few checks mid-process that could determine whether the synthesis was working well or not. After the long day of synthesis, the polymer gels would sit in solution overnight and only then could success of the experiment be determined, meaning in some cases entire days of work were spent on an experiment that had failed in an early stage.

There should be twelve polymer dots per slide, but often Dominguez's slides contained between 7-10 polymer dots instead of the expected 12. This would be discovered the morning after synthesis when the slides had their templates removed. In addition to having a lesser number of viable dots per slide, often these dots were more fragile and would fragment off while acylating with sensor, causing further loss of dots through the process of acylation with sensor dye.

Dyes Loaded		
TMH-3-091c	TMH-4-024b	**TMH-4-062c**
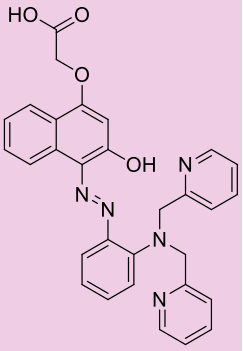	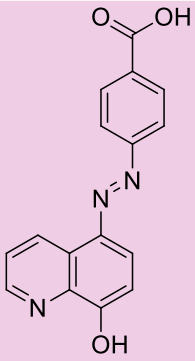	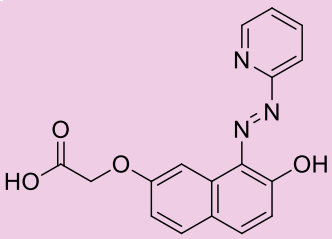

Table 3: Dyes loaded onto polymers

Some of Hagemann's sensors were loaded onto polymer dots synthesized by Dominguez, their structures are shown in *table 3*, above. In total, three dyes were used but over ten slides were loaded. Some dyes were loaded multiple times due to lower yield of dots or due to a higher need of the dye in question.

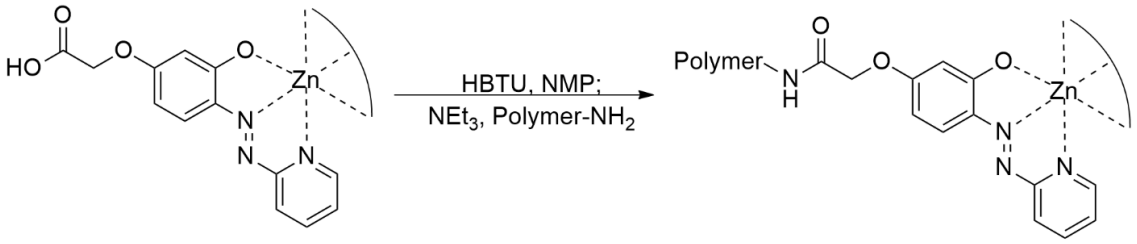

Scheme 10: Acylation of polymer dots by azo dyes

The acylation process begins with the slow movement of the slide of polymer dots from solution to solution. This must be done carefully and slowly to avoid dots swelling and shearing off the slide. As such, moving the slide from solution to solution until it was able to be placed in NMP usually took 10-12h in total, causing this to be a nerve-wracking and time-consuming experiment.

Once in NMP, the dots could be acylated by adding HBTU, triethylamine, and sensor into a crystallization dish with NMP and polymer dots. This was heated to approximately 55 degrees over three hours with gentle shaking to ensure uniform loading. After 3h the apparatus was cooled to RT and slowly moved from solution to solution to pull out excess dye and avoid stress of the loaded dots.

Since loading the dye was such a time-consuming process, often only one slide could be done per week due to limiting equipment numbers and the inability to acylate more than one slide at a time. If multiple slides were placed in the acylation solution at once, they would bump

into each other and shear off dots. At the end of the week these dots would be cut by hand, causing loss of more dots. Upon handoff, the collaborators would usually get 4-6 of a desired 10-12 dots. This was not ideal for a long-term strategy, and was not sustainable for development of a marketable device.

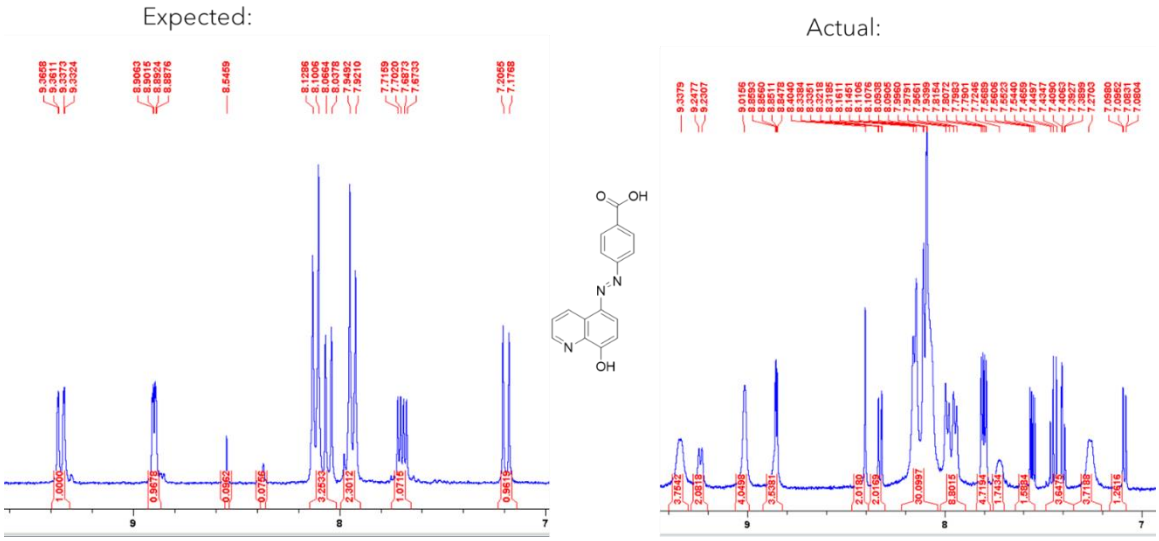

Figure 18: Degradation of previously synthesized sensors over time

Beyond the issues with loading times and polymer dot yield, there were issues with dye response once loaded. Unfortunately, the sensors on polymer dots were not responding as expected, with a decreased metal response and a less linear relationship between metal ion concentration and absorbance change. This was in part due to the degradation of the sensor dyes over time as seen in *figure 18.* This shows the expected spectrum versus the spectrum of the sensor that had been loaded. This data demonstrates that the sensors, when exposed to light or air, tend to isomerize or degrade. Azo dyes are known to photoisomerize from trans to cis with light[28,36]. This lead to sensors that did not perform optimally on polymer, which caused suboptimal results on the part of Aquametals during testing.

In addition to the sensor degradation, the collaborators had not tested things they had claimed to have tested, causing late-stage issues in development with issues that were thought to have been solved previously. This eventually ended with the dissolution of the collaboration and small metal sensing project.

Lead Sensors

When the first portion of the sensor project was scrapped, another avenue arose. The core of the project itself had been shown to work based on preliminary data, so using the framework from the original sensor project for a new sensor project was not a large leap. The Schwabacher group was approached by a new collaborator, Advanced Chemical Systems, with an interesting problem to help mitigate: the crisis of lead in drinking water.

There is an increasing need to detect Pb in drinking water, as Pb is one of the most toxic metals that can be present in tap water. [30,31,73] Flint, Michigan is one of the most well-known examples of a recent lead crisis: in early 2014 residents of Flint noticed their water was discolored and were advised to boil it to get rid of contaminants. It took over half a year for residents to be informed that there was lead in their water. Scientists tested water from Flint and found 13,000ppb Pb in the water. The acceptable level as declared by the EPA is 0ppb. The critical action level of Pb in the water is just 15ppb[31,71]. These residents had been exposed to 867 times the critical action level of Pb for over half a year. It is estimated up to 12,000 children were exposed to detrimental levels of Pb in the water[73]. This modern-day crisis in a highly developed country exemplifies the need for reliable and accessible Pb sensors for drinking water [31,72,74].

Milwaukee is also known for having elevated levels of metals such as lead in water, as between 1996-2016 almost a quarter million children were diagnosed as having lead poisoning [31,71]. Lead exposure in children is a serious concern, as it can cause slowed growth, anemia, learning difficulties, and in more severe cases can cause seizure, organ failure, and death[33]. In adults, exposure to lead can cause kidney, heart, and reproductive problems. Historically, Pb exposure is linked to many tragedies as can be seen with the fall of Rome, or more recently, with

the lack of empathy in the "boomer" generation, postulated to be due to lead poisoning which decreases empathy as well as other brain functions [22, 31, 71,72,74]. These are not insignificant effects, and lead exposure needs to be minimized. Lead exposure comes primarily from dust lead, but the secondary source of exposure is through drinking water[73]. This exposure through drinking water is largely due to Pb based pipes corroding and releasing Pb ions into water, generally without consumers being aware. Recent years have seen an increase in initiatives to replace lead based pipes, but many of these initiatives are behind and leave consumers vulnerable while they wait[76,77].

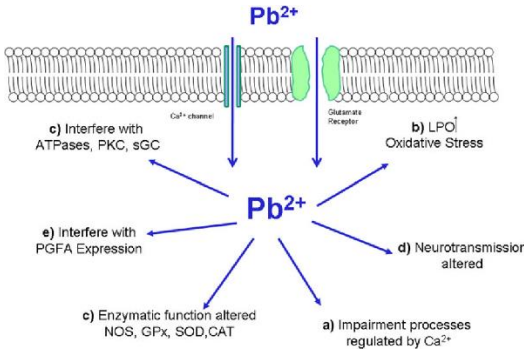

Heavy metal ions	Permissible limits (ppm) WHO[18]	US EPA[19]
As(III)/As(V)	0.05	0.01
Pb(II)	0.05	0.015
Cd(II)	0.005	0.005
Cr(VI)/Cr(III)	0.05	0.05
Hg(II)	0.001	0.002
Zn(II)	5.0	5.0
Cu(II)	1.5	1.3
Co(II)	0.01	—

Figure 19a: Consequences of Pb
Figure 19b: Acceptable amounts of metals in drinking water per WHO and EPA standards in ppm

Pb can get into cells through various channels and receptors, such as calcium channels and glutamate receptor. One of the biggest concerns of lead exposure are the effects on the brain, *figure 19*. Pb can get into the neurons and interfere with normal firing, which greatly inhibits brain function[24,30]. This disrupts the movement and storage of Ca inside of cells, which increases cell stress and can lead to neuron or cell death long term. Lead not only interrupts the storage of Ca, but is able to hijack the roles of Ca, such as communication between neurons [22, 23, 24].

More exposure means more inhibition and eventual brain death. Long term exposure can cause memory difficulties, an increase in sociopathic tendencies, a general increase in irritability

and depression rates, potential hallucinations, and increased prevalence of disorders such as attention deficit hyperactivity disorder or borderline personality disorder [23, 73,74].

A large source of exposure to lead is drinking water [23, 71,74]. As pipes erode, more lead and other metals can be introduced into the water running through them. Neglected systems are likely to have unhealthy levels of metal in them, and without consistent monitoring these systems can cause health problems undetected. Corrosivity of groundwater is an indicator of whether large amounts of metal will be present in drinking water [57, 58, 59], as more corrosive water will cause more metal to come through the pipes. As such, the USA measures water corrosivity to determine highest risk areas for metal poisoning in water [71,72,73,74]. In fact, the acceptable levels of lead in drinking water are not health-based, but rather a measure of groundwater corrosivity. The presence of more than 15ppb Pb in the water indicates highly corrosive groundwater and thus more metals in the water.

In *figure 19b* the permitted levels of metal ions per EPA and WHO standards are listed. The permissible level of Pb in water in the USA is 15ppb. The permissible level per WHO standard is 50ppb. The recommended level of Pb intake is 0ppb[31,33]. The required level of Pb in bottled water is only 5ppb which is 33% the amount allowed in tap water. Multiple studies have been done that show no Pb is safe to consume, especially for children. Amounts as low as 5ppb have been demonstrated to cause lead poisoning in children. The 15ppb standard for drinking water is too high and leaves many children, especially in poor areas, to suffer the lifelong consequences of lead exposure[31,71].

Government estimates state that 20% of the lead a person is exposed to comes from drinking water – this percent skyrockets up to 60% for bottle fed infants. In 1976, the passing of the SWDA set acceptable levels of lead at 0.2% for solder and flux and 8% for pipes. In

December of 2020, these guidelines were changed, and the new acceptable level of lead in pipes is 0.25% [27, 71,73]

Since lead is not absorbed through the skin, contaminated water is acceptable to use for activities such as bathing but is not acceptable for drinking. As such, contaminated water could be used for many purposes without causing a safety risk. The only true risk is ingestion, and awareness is key for limiting potential lead ingestion[72,73].

Once the first sensor collaboration with Aquametals was disbanded, Advanced Chemical Systems approached the Schwabacher group with the hopes of using this sensor technology to develop a functional lead sensor that could detect lead down to the low ppb in drinking water.

With this goal in mind, initial research was done on known Pb binders. The geometry, known structures, and behaviors were analyzed to direct synthesis efforts. Many effective Pb binders use large, soft atoms like S instead of atoms like O or N to increase the specificity of the molecule for Pb [47,49,50,52]. Smaller atoms increase the likelihood of binding to smaller metals such as Zn or Cu, meaning it will be less selective for Pb[53,55]. Additionally, many known Pb binders have asymmetric structures with the exception of crown-ether based sensors.

There are a fair amount of lead sensors with crown ethers: specifically, 18-C-6 crown ethers. Many known Pb binders have crown-ether like structures and approximately 6 ligating atoms in their ligand structure [54, 59, 60, 61, 62].

This concept was adapted into a proposed scheme, *scheme 11*. This scheme began with the dimesylation of tetraethylene glycol [56] followed by immediately moving onto reaction with a phenyldiethanolamine derivative. In the model case, this was done with phenyldiethanolamine but in the planned case this would have been performed with *o*-nitrophenyldiethanolamine to allow for hydrogenation and then azo coupling to produce a functional azo dye.

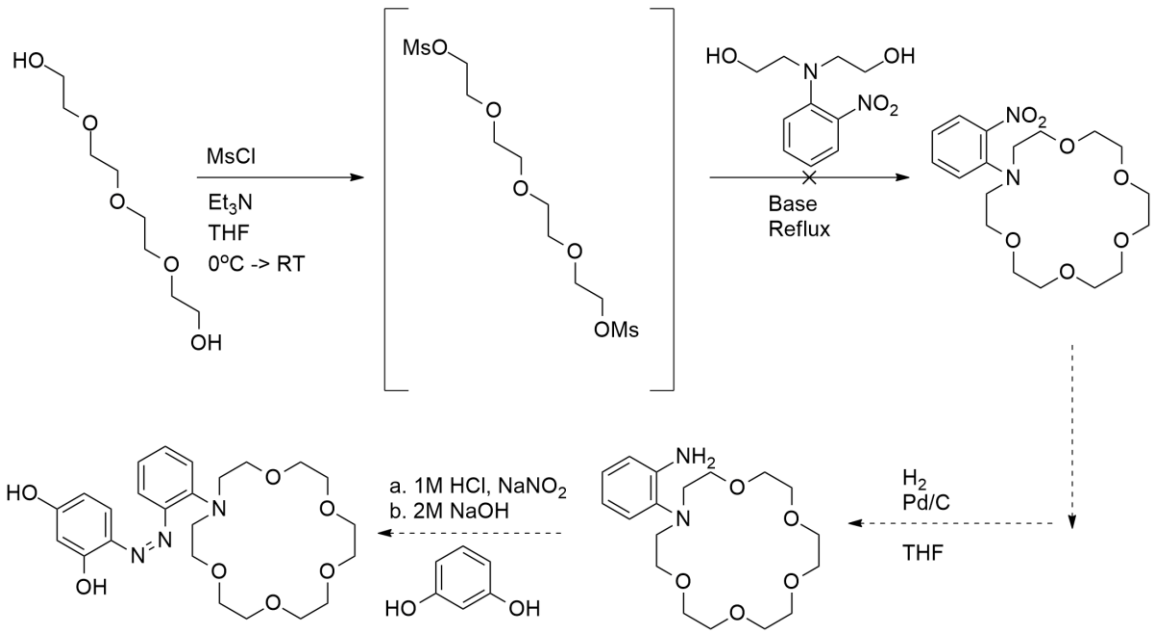

Scheme 11: Planned crown ether synthesis for a functional lead sensor

Scheme 11 shows the planned scheme to use tetraethylene glycol and nitro phenyl diethanolamine to form an 18-C-6 crown ether [5, 38, 54 59]. Before this reaction was tried, a model reaction was attempted as shown in *scheme 12*.

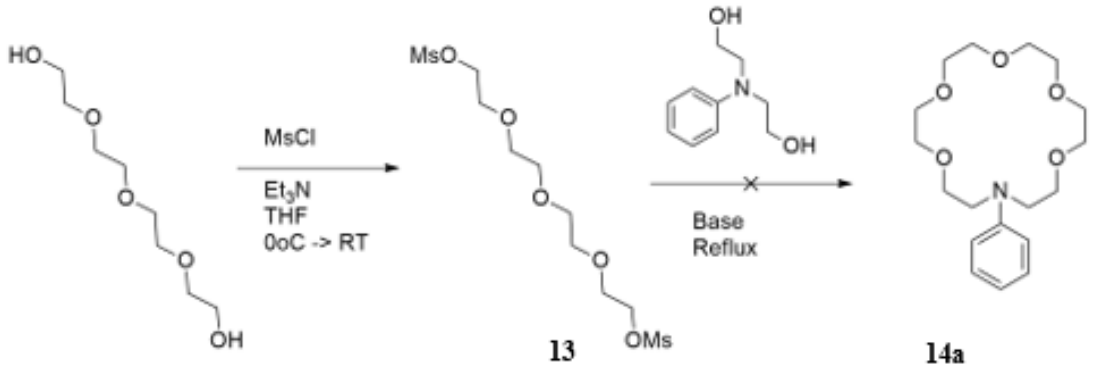

Scheme 12: Reactions to form crown in model synthesis

Scheme 12 began well, with the reaction to form the TEG dimesylate [70] working by TLC and NMR, however the reaction to form the crown was unsuccessful. *Table 4* shows the various

conditions tried to form the crown using TEG dimesylate and phenyl diethanolamine. Base was varied and strong base such as NaH was attempted, as well as weaker bases such as carbonate and hydroxide. Solvent was varied with minimal effect and switching to TEG ditosylate did not change the lack of reaction. By TLC reaction had completed but by NMR no product was formed in any of the attempts.

Starting Material	Base	Solvent	Temp	Time
TEG dimesylate	Potassium t-butoxide	THF	Reflux	14h
TEG dimesylate	NaH	THF	Reflux	12h
TEG dimesylate	KOH	Water	Reflux	24h
TEG ditosylate	Potassium t-butoxide	THF	Reflux	24h
TEG ditosylate	NaH	THF	Reflux	8h
TEG dimesylate	KOH	MeOH	Reflux	20h

Table 4: Conditions tried for crown ether synthesis

This attempt at synthesizing a crown ether was rather ambitious as reactions to form crown ethers generally involve intensive and sensitive reactions with low yields[4,5] and there were a variety of problems that cropped up during reaction. Initially, the TEG dimesylate was added via addition funnel over time to a heated solution of base and solvent with phenyl diethanolamine present. The dimesylate precipitated out of all solvents attempted, so the reverse was tried where phenyldiethanolamine was added to a solution of TEG dimesylate and base. The phenyldiethanolamine *also* precipitated out in the addition funnel. At this point a TEG ditosylate

was attempted, and while this was more soluble it was still precipitating out over the course of addition. Regardless of base, solvent, or starting materials used no product was ever found to be formed by NMR.

These reactions made a lot of side products and required separation by column. Even after column chromatography there was no recognizable product found by NMR, likely indicating the product was not forming during reaction. This could be due to the speed of addition, lack of proper base, or a reluctance to react in these conditions.

Since the reactions to form the crown were unsuccessful and an 18-C-6 has the potential to bind to smaller metals such as potassium [4,5,37], this avenue was scrapped in favor of a synthesis that more closely resembled the successful dyes used in the small metal sensing project, *scheme 13*.

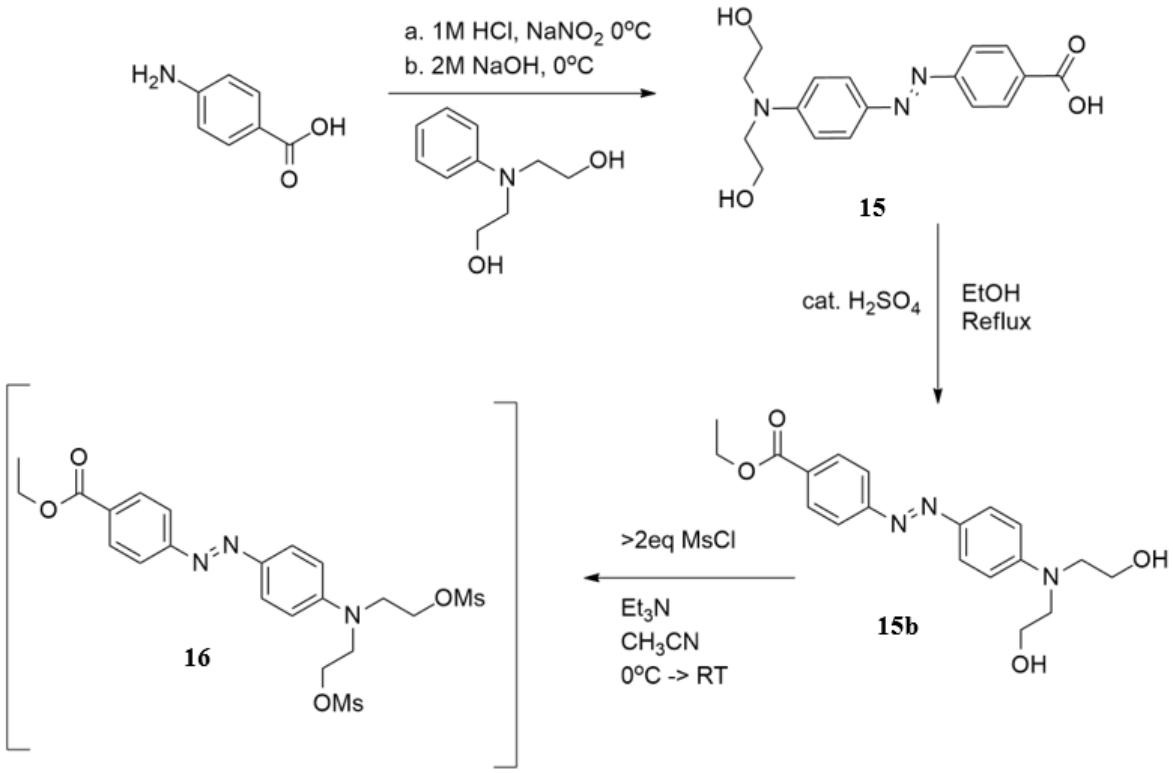

Scheme 13: New sensor direction with an ortho-azo bond

The new scheme, *scheme 13*, began with an azo coupling of *p*-aminobenzoic acid with phenyl diethanolamine using an acidic method of coupling. This provided compound 15 in 89% yield. While it was not always esterified, later down the line it was discovered esterification makes the dye much easier to work with creating 15a in 68% yield. Once esterified, this sensor was much more soluble and was able to be dimesylated much more easily. In general, esters make these azo dyes much more soluble and manageable to work with in solution, as the carboxylic acid form sticks to everything, is not as soluble, and is not very mobile by TLC. In comparison, the ester form is significantly more soluble and can be looked at via TLC with a much wider range of eluents.

The dimesylate (15b) was never isolated due to the properties of the intermediate. This intermediate is a mustard, meaning it is very dangerous. Historically, various mustard agents have been used as war gases as they are generally vesicants which cause blistering of the skin, and they are also known to cause respiratory irritation. These mustard agents are cytotoxic and capable of alkylation[75]. This mustard intermediate was handled very carefully by adding in a large excess of ligand through the reflux condenser, well over two equivalents to ensure all mustard was fully reacted. Adding excess ligand did ensure that this reaction was much safer to perform, however it added a significant amount of time to the end of this reaction. Purifying these sensors away from the excess ligand and any potential side products proved to be difficult and time consuming as it required a column and a silica plug to get these sensors clean.

Exp #	Form	Ligand (Eq)	Time	Yield?
1-167	Acid	KDW-1-152	24h	0%
1-170	Acid	8-hydroxyquinoline	16h	62% crude
1-173	Acid	8-hydroxyquinoline	16h	110% crude
1-179	Acid	KDW-1-152	24h	0%
1-181	Acid	KDW-1-152	72h	81% crude
1-182	Ester	8-hydroxyquinoline	24h	24%
1-183	Ester	KDW-1-152	3h	7%
1-187	Ester	KDW-1-152	3h	9%
1-191	Ester	8-hydroxyquinoline ; KDW-1-152	16h	0%
2-2	Ester	8-hydroxyquinoline ; KDW-1-152	48h	0%

Table 5: Substitution conditions for new sensor scheme

As seen in *table 5*, the substitution worked inconsistently and was never isolated from the acid form of the sensor. This was because of the lack of solubility of compound 15 as an acid which created many problems in isolation, since this reaction could not be put onto a column or silica plug without it getting stuck to the silica gel. When using 15b, the ester form of this sensor, these reactions were much more successful as were the isolations. The substitutions were done with 8-hydroxyquinoline and a sulfur ligand synthesized from bromoacetic acid and thiourea. Both substitutions did occur successfully and were isolated, but neither product was a successful lead sensor.

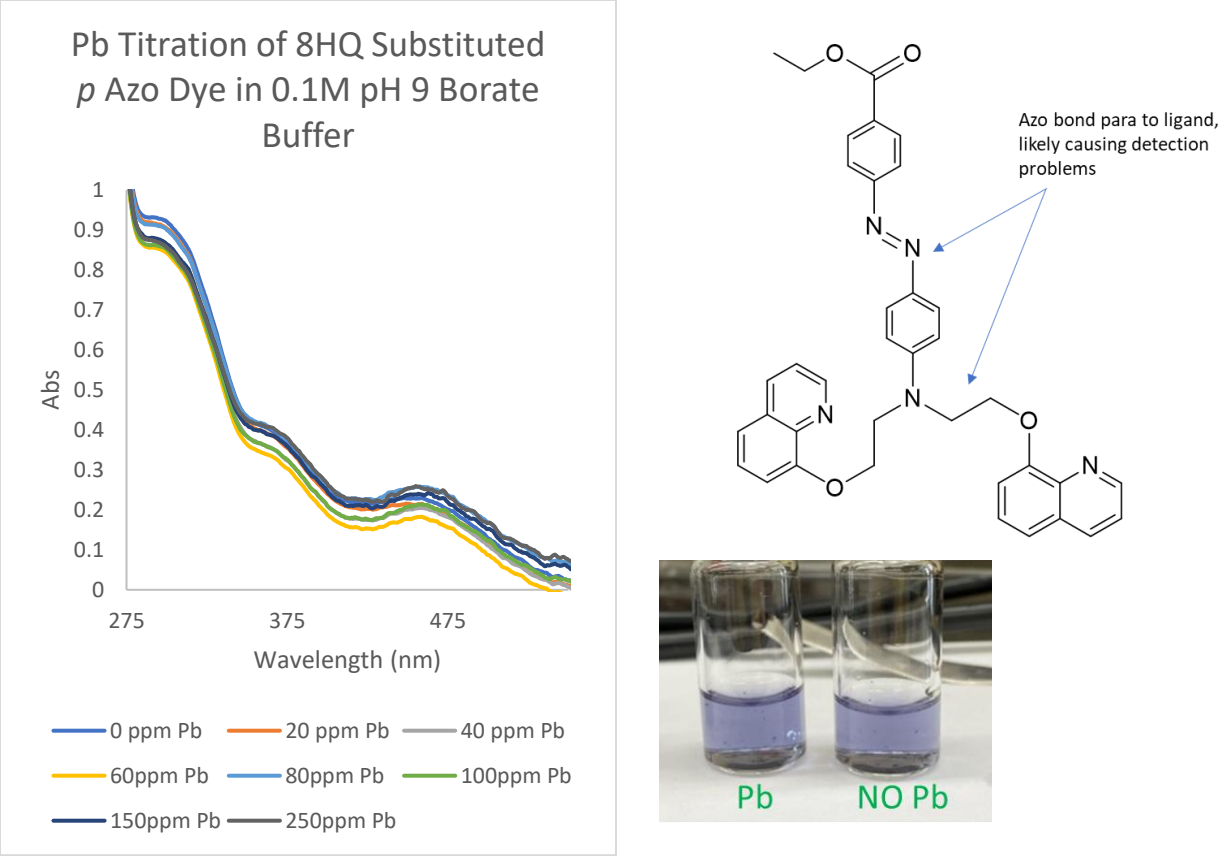

Figure 20: Results of compound 16a as a Pb sensor

Upon analysis of the end-stage product, compound 16a, it was discovered that this structure shows no response when exposed to lead. *Figure 20* shows a titration with compound 16a with a lack of response from 0ppm Pb to 250ppm Pb. There was no visual response at any concentration of Pb and no response when analyzing absorbance spectra.

The desired structure did not appear respond to lead which created a question: why? The reason is thought to have to do with the position of the azo bond. In the Schwabacher group's most successful sensors the azo bond is ortho to the ligand and metal is able to interact with the azo bond. In the structure synthesized from *scheme 13* the *para*-azo bond is unable to interact with metal if the metal is interacting with ligand. As such, there is no visual response to lead.

This does not mean that lead isn't binding, however the results regarding lead binding to this structure were inconclusive. It is thought that this structure does bind to lead but is unable to signal due to azo bond positioning, as the isomerization from cis to trans is what causes a shift in absorbance.

A new scheme was designed that would put the azo bond ortho to the ligand. This target scheme is shown below in *scheme 14.*

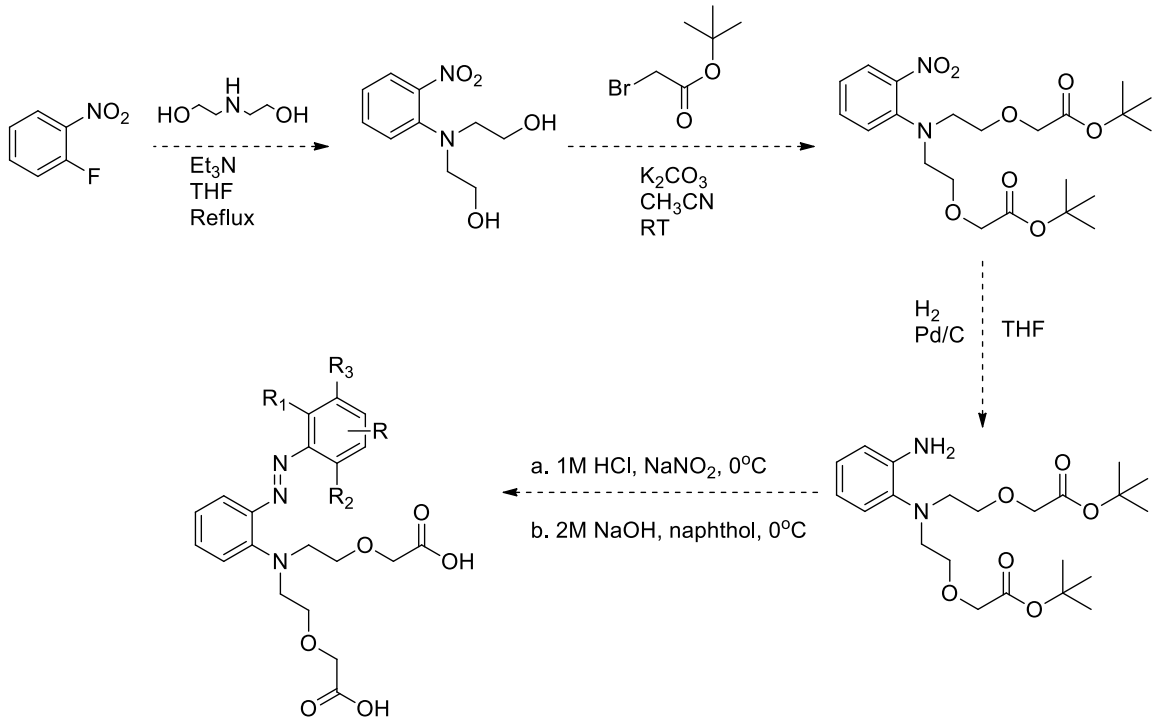

Scheme 14: Planned synthesis route for lead sensors

This planned scheme began with a substitution which was followed by alkylation, hydrogenation, and then an azo coupling to form a symmetric sensor. It was thought that the dialkylation would provide good ligands for lead but not for other, smaller metals.

The substitution gave the desired product, 17, in a 97% yield, but the alkylation did not provide the desired product. The dialkylation reaction had been previously performed by Trevor Hagemann, and the procedure had been anticipated to give the dialkylated product. This is not

what occurred, and instead there was a very fortunate but unexpected result which made synthesis of successful lead sensors possible.

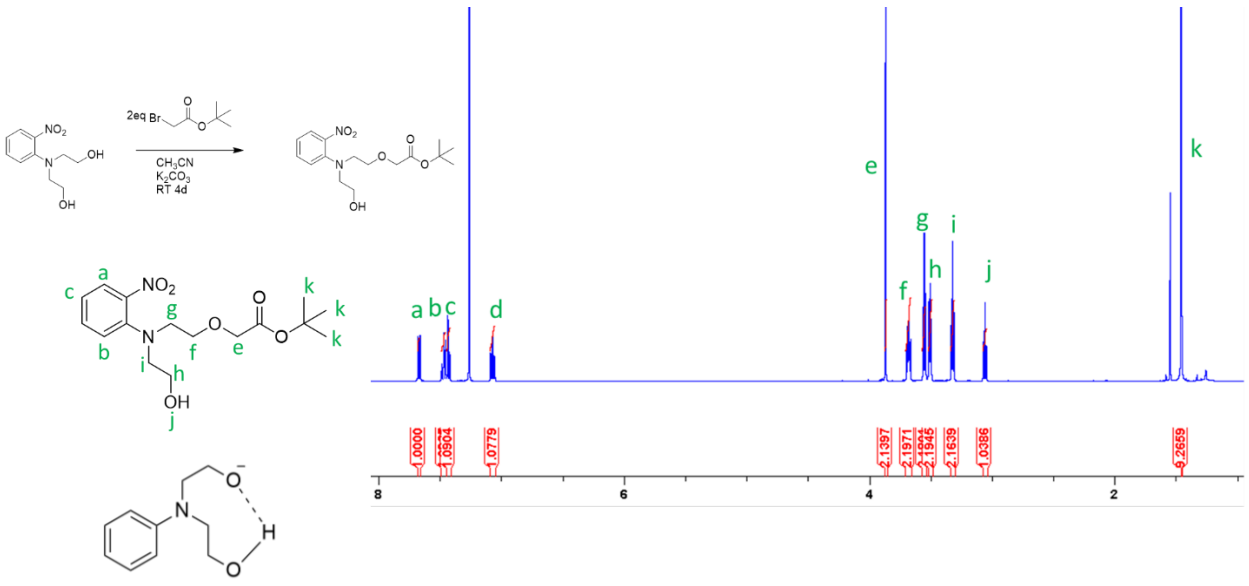

Figure 21: Monoalkylation NMR and proposed intramolecular H-bond

Instead of forming the desired dialkylated product, a monoalkylated product, 18 was selectively formed instead as seen in *figure 21*. It is thought that an intermolecular H-bond allows for deprotonation, *figure 21*, and stabilizes the molecule to allow one alkylation to occur but the molecule is not able to undergo a second alkylation without a stronger base present. Potassium carbonate is too weak a base to allow for dialkylation and so the reaction stops at the monoalkylated product.

This reaction formed 18 in a 71% yield after column chromatography using ethyl acetate as eluent. This compound was able to be hydrogenated and azo coupled to form a successful lead sensor. This compound was also able to be modified to make multiple varied “families” of lead sensors, and is the basis for all three major families, all stemming from one grandparent molecule, compound 17.

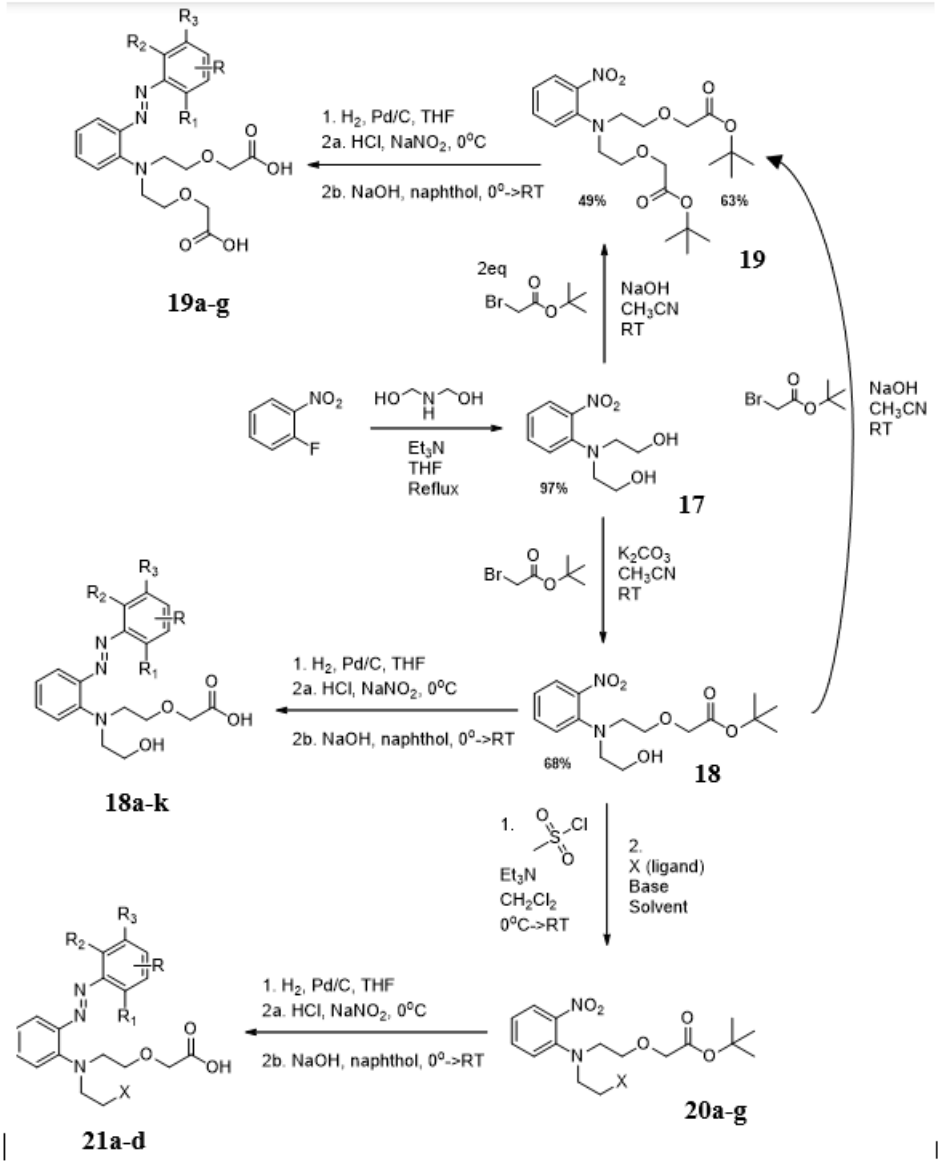

Scheme 15: Scheme for synthesis of all three major lead sensor "families."

Scheme 15 shows the three different major paths to form the three different sensor families. All syntheses were shown to provide successful Pb sensors and all three schemes begin from the same reaction: the substitution of ortho-nitrofluorobenzene with diethanolamine, which proceeds to form compound 17 in a 97% yield over 5 days. This reaction, while slow, produces a clean and high yielding product.

The route to PbSF1 (Lead sensor family 1) starts with that substitution to form 17, followed by the monoalkylation to form 18, and then hydrogenation and azo coupling to form an end stage sensor.

Once the monoalkylation was shown to lead to a functional Pb sensor, conditions for dialkylation were sought out as it was thought that the dialkylated sensor would be more specific than the monoalkylated. This was why the dialkylated form was the initial target: the monoalkylated product was a happy accident but had not been anticipated to work very well. Many methods of dialkylation were tried using a total of four different starting materials as well as many different bases, temperatures, and solvents. *Table 6* is a summary of the various conditions used for alkylations, both mono and di.

Number	Starting Material	Alkylating agent	Base	Solvent	Temp	Conversion	Yield
1	Boc-diethanolamine	t-butylbromoacetate	K_2CO_3	CH_3CN	RT	0	0
2	Boc-diethanolamine	t-butylbromoacetate	t-butoxide	THF	0	100	0
3	Boc-diethanolamine	Ethyl bromoacetate	t-butoxide	THF	-15	100	0
4	Boc-diethanolamine	t-butylbromoacetate	NaOH	CH_3CN	RT	0	0
5	Boc-diethanolamine	t-butylbromoacetate	KOH	CH_3CN	Reflux	100	0
6	Boc-diethanolamine	Ethyl bromoacetate	K_2CO_3	CH_3CN	RT	0	0
7	Boc-diethanolamine	t-butylbromoacetate	t-butoxide	THF	Reflux	100	0
8	Boc-diethanolamine	t-butylbromoacetate	t-butoxide	THF	RT	75	0
9	o-nitrophenyldiethanolamine	t-butylbromoacetate	K_2CO_3	CH_3CN	RT	99	0
10	o-nitrophenyldiethanolamine	t-butylbromoacetate	t-butoxide	THF	0	100	0
11	o-nitrophenyldiethanolamine	Ethyl bromoacetate	t-butoxide	THF	-15	100	0
12	o-nitrophenyldiethanolamine	t-butylbromoacetate	KOH	CH_3CN	Reflux	100	0
13	o-nitrophenyldiethanolamine	Ethyl bromoacetate	K_2CO_3	CH_3CN	RT	50	0
14	o-nitrophenyldiethanolamine	t-butylbromoacetate	t-butoxide	THF	Reflux	100	0
15	o-nitrophenyldiethanolamine	t-butylbromoacetate	t-butoxide	THF	RT	100	0
16	tert-butyl 2-(2-((2-hydroxyethyl)(2-nitrophenyl)amino)ethoxy)acetate (MONOALK)	t-butylbromoacetate	K_2CO_3	CH_3CN	RT	0	0
17	Monoalk	t-butylbromoacetate	t-butoxide	THF	RT	99	0
18	Monoalk	t-butylbromoacetate	NaOH	CH_3CN	RT	99	56
19	Monoalk	t-butylbromoacetate	KOH	CH_3CN	Reflux	80	0
A	o-nitrophenyldiethanolamine	t-butylbromoacetate	K_2CO_3	CH_3CN	RT	100%	64%
B	o-nitrophenyldiethanolamine	t-butylbromoacetate	t-butoxide	CH_3CN	RT	-	0%
C	o-nitrophenyldiethanolamine	t-butylbromoacetate	NaOH	CH_3CN	RT	99%	0%
D	o-nitrophenyldiethanolamine	t-butylbromoacetate	Cs_2CO_3	CH_3CN	RT	100%	60%
E	o-nitrophenyldiethanolamine	t-butylbromoacetate	Na_2CO_3	CH_3CN	RT	100%	58%
F	Boc-diethanolamine	t-butylbromoacetate	K_2CO_3	CH_3CN	RT	0%	0%
G	phenyldiethanolamine	t-butylbromoacetate	K_2CO_3	CH_3CN	RT	100%	17%
H	p-nitrophenyldiethanolamine	t-butylbromoacetate	K_2CO_3	CH_3CN	RT	50%	33%
I	o-nitrophenyldiethanolamine	t-butylbromoacetate	K_2CO_3	CH_3CN	Reflux	100%	41%
J	o-nitrophenyldiethanolamine	t-butylbromoacetate	K_2CO_3	CH_3CN	RT	99%	53%
K	Boc-diethanolamine	t-butylbromoacetate	K_2CO_3	CH_3CN	Reflux	0%	0%

Table 6: Alkylation conditions: dialkylations are noted by numbers 1-19, monoalkylation conditions are noted by letters A-K

As shown in *table 6*, most conditions for dialkylation were unsuccessful. Boc-diethanolamine was unable to be either mono or dialkylated, while all other molecules were able

to be either mono or dialkylated, if not both. The highest yielding reactions were performed with ortho-nitrophenyldiethanolamine, potentially due to the o-EWG allowing for more activation in the diethanolamine. p-nitrophenyldiethanolamine did work in a lower yield, so it appears that a p-EWG does work but is not as activating as the o-nitro. Phenyldiethanolamine was able to be alkylated in a low yielding monoalkylation, which lends to the theory that an EWG is activating, but also provides a theory that an aromatic ring is necessary for reaction to occur as alkylations were not able to occur without one. This could be due to the stability added by having the aromatic ring present.

For dialkylations, many bases were tried. Potassium tert-butoxide was too strong of a base and lead to many undesired products in the reaction flask. By TLC, attempted alkylations with t-butoxide as a base typically provided 7-9 spots.

Carbonate was too weak of a base to allow for dialkylation. Hydroxide at an elevated temperature produced a lot of side products in the initial attempts and did not give the desired product. However, compound 18 was dialkylated successfully with hydroxide per entry 18 in *table 6*. The dialkylated product was achieved in a 56% yield.

The successful conditions consisted of powdered sodium hydroxide with t-butylbromoacetate in acetonitrile at RT. This was able to be adapted to successfully dialkylate o-nitrophenyldiethanolamine (17), which formed the desired product in a lower yield of 48%. Interestingly, performing this reaction on compound 17 vs compound 18 showed more than just a difference of yield. There were different side products formed as shown by both TLC and NMR, providing more difficulties in working up the reaction starting with compound 17. Beginning from the monoalkylated (compound 18) provides cleaner and more easily isolable

product. The drawback of this is that it adds approximately a week to the scheme when going through the monoalkylated compound, as the monoalkylation reaction takes 5d and must be run through a column.

The dialkylated compound (19) was able to be subsequently hydrogenated and turned into a family of sensors through an azo coupling per *scheme 15*. This set of sensors was awarded the name PbSF2.

Table 6 also demonstrates conditions used to replicate the monoalkylation on different molecules. It was interesting that the monoalkylated product was selectively formed from potassium carbonate, t-butyl bromoacetate, and acetonitrile at RT. This was done with phenyl diethanolamine as well as *p*-nitrophenyldiethanolamine with moderate success. *Figure 20* showed the downsides of having an azo bond para to the ligand, but to check that the azo bond's position was essential, a para version of the successful monoalkylated sensor was made, *scheme 16.*

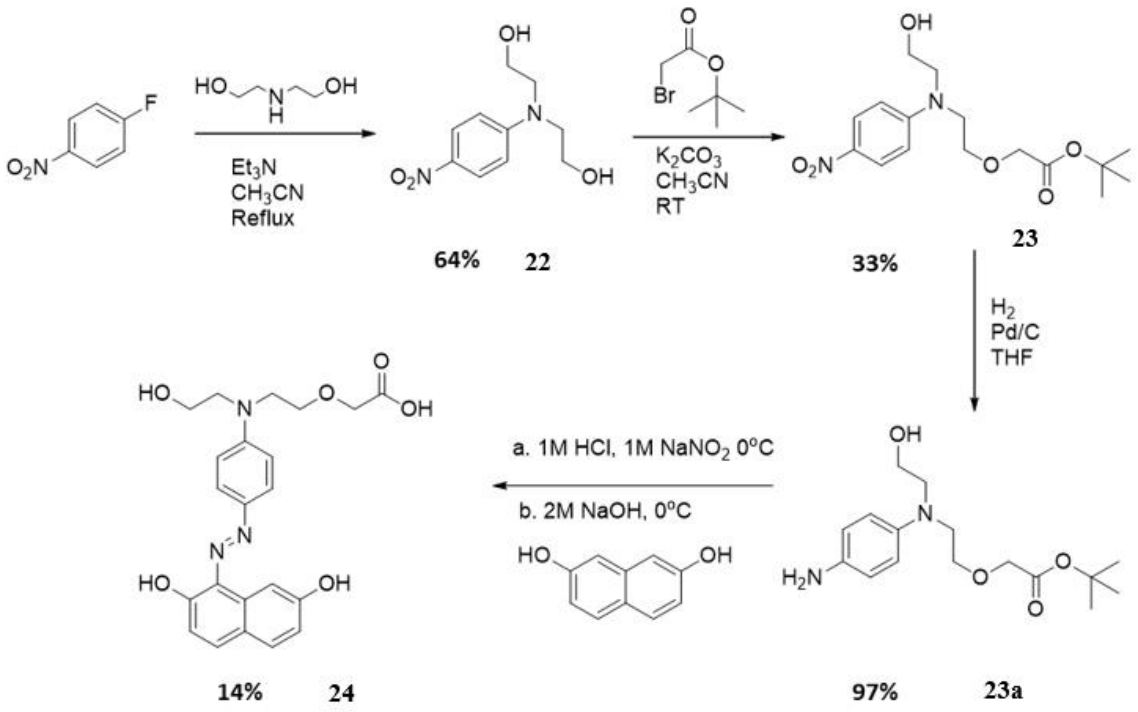

Scheme 16: Synthesis of *p* version of monoalkylated sensor

Scheme 16 shows the substitution of p-nitrofluorobenzene with diethanolamine to form 22. This scheme had a lower yield than *scheme 15*, 64% vs 97%. The monoalkylation occurred in a lower yield as well, 33% of 23 vs 71% of 18, but 23 was able to be moved on and coupled successfully to form a sensor with 2,7-dinaphthol, compound 24, in a 14% yield. This seems to lend evidence to the idea that the o-nitro group helps activate the nitrofluorobenzene toward substitution with diethanolamine. This also suggests that the nitro group participates in the monoalkylation, perhaps through stabilizing the intermediate for monoalkylation when it is ortho.

The results from this scheme demonstrated that the *para*-analogue of this sensor is in fact less able to detect and signal in response to metals. Compound 24 demonstrated limited ability to

respond to small metals such as Cu and showed no ability to respond to Pb. This is similar to what Hagemann found as his sensors seemed to be more responsive to smaller metals and less responsive to larger metals when the azo bond is para to the ligand. This supports the hypothesis that the *ortho* azo bond is important for metal sensing capabilities, as shown in the sensors from *scheme 15.*

Another hypothesis about the unsuccessful sensor from the *para* sensor *scheme 13*, compound 16a, was that the 8-hydroxyquinoline is not a good ligand for sensing Pb. As such, a scheme was designed to allow for 8-hydroxyquinoline to be added onto the molecule to allow it to be present in an endstage sensor. *Scheme 15* above shows the synthesis pathway while *scheme 17* below shows the substitution reaction itself.

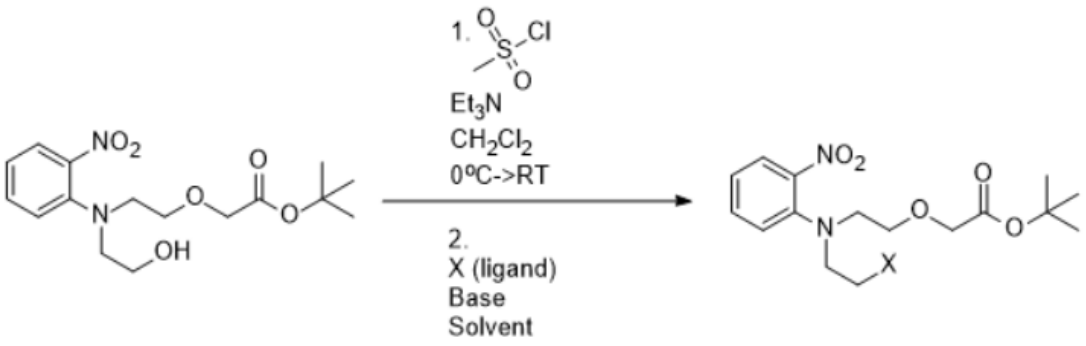

Scheme 17: Substitution conditions starting with compound 18

The substitution reaction begins with the monoalkylated compound, 18, and leads to "Pb sensor family 3." Compound 18 is mesylated and immediately substituted using ligand of choice. Many ligands were tried in an attempt to find one that provided optimal Pb sensing capabilities. These ligands are listed in *table 7* and shown in *figure 22*.

Exp #	Ligand	Base	Solvent	Yield	Conversion
KDW-2-001	Thiourea	Et_3N	CH_2Cl_2	0%	100%
KDW-2-002	8-hydroxyquinoline	K_2CO_3	CH_3CN	8%	95%
KDW-2-040	8-hydroxyquinoline	K_2CO_3	CH_3CN	12%	90%
KDW-2-093a	8-hydroxyquinoline	K_2CO_3	CH_2Cl_2	19%	100%
KDW-2-093b	KDW-1-152	K_2CO_3	CH_2Cl_2	0%	73%
KDW-2-093c	Methyl salicylate	K_2CO_3	CH_2Cl_2	0%	99%
KDW-2-109	8-hydroxyquinoline	K_2CO_3	CH_2Cl_2	33%	90%
KDW-2-120	Glycine	K_2CO_3	CH_3CN	28%	50%
KDW-2-129	Sarcosine methyl ester HCl	K_2CO_3	CH_3CN	35%	86%
KDW-2-143	Tryptophan	K_2CO_3	CH_3CN	19%	78%
KDW-2-144	Methyl salicylate	K_2CO_3	CH_3CN	17%	89%
KDW-2-145	2-(methylamino) pyridine	Et_3N	CH_3CN	21%	93%
KDW-2-149	Methyl salicylate	K_2CO_3	CH_3CN	8%	90%
KDW-2-150	Ammonium hydroxide	-	-	0%	0%
KDW-2-151	Thiourea	-	CH_3CN	0%	100%
KDW-2-152	4-aminobenzoic acid	Et_3N	CH_3CN	22%	56%

Table 7: Substitutions tried under various conditions on compound 20 to form 20a-g. Entries grayed out indicate failed reactions

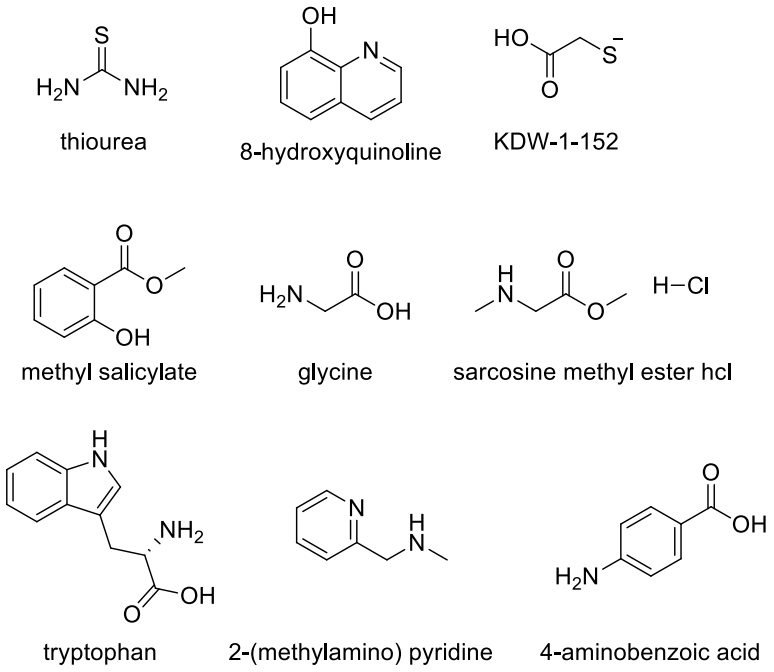

Figure 22: Substitution structures used in *table 7*

As shown in *table 7* and *figure 22*, many different ligands were used with varying rates of success. The ligands from *scheme 13* were utilized in *scheme 17* to determine if azo bond position was the primary problem with sensors 16a and 16b or if ligand contributed to lack of binding. These ligands were chosen because literature showed similar structures as known Pb binders. For example, some sensors have a tryptophan ligand, sulfur atoms, or structures with three to five ligating atoms such as oxygen or nitrogen[38,40,56]

PbSF3 was the most complex family of sensors synthetically, as this family took the most time to get to an end stage sensor and had the most variability. Scouting one substituted compound for Pb detecting activity would not yield information about other substitutions and their potential responses. Ligands shown to work in the literature were not guaranteed to work on this structure or type of sensor, so research on known Pb binders was only semi-helpful in this circumstance.

This set of reactions began with compound 18 being mesylated and substituted. The mesylate was never isolated, which introduced potential reaction variability. Once mesylation was complete by TLC, substitution was attempted by adding in excess ligand and base. Yields for this substitution were consistently low, between 0-35%. Many ligands never substituted, such as thiourea. Those that did substitute were difficult to isolate, and could require as many as three columns and two silica plugs which could be very time consuming. Evidence of this can be seen in *figure 23* below. Determining isolation methods and then performing them often took up weeks of time per substituted product only to produce a yield <35%.

Once the substituted product was isolated, it would be hydrogenated and azo coupled. This is where the second major problem with PbSF3 arose: not all substituted products would

survive or undergo azo coupling. After weeks of work, sometimes the compounds would spontaneously precipitate out of solution and refuse to undergo coupling even under varied conditions or over multiple attempts.

Those compounds that did couple to form sensors in PbSF3 were unpredictable. Not all of these sensors would respond to Pb, and those that did often had responses to other metals more strongly. This family of sensors provided the most interesting responses visually, as they often changed different colors entirely in response to different metals, as seen in *figure 23.*

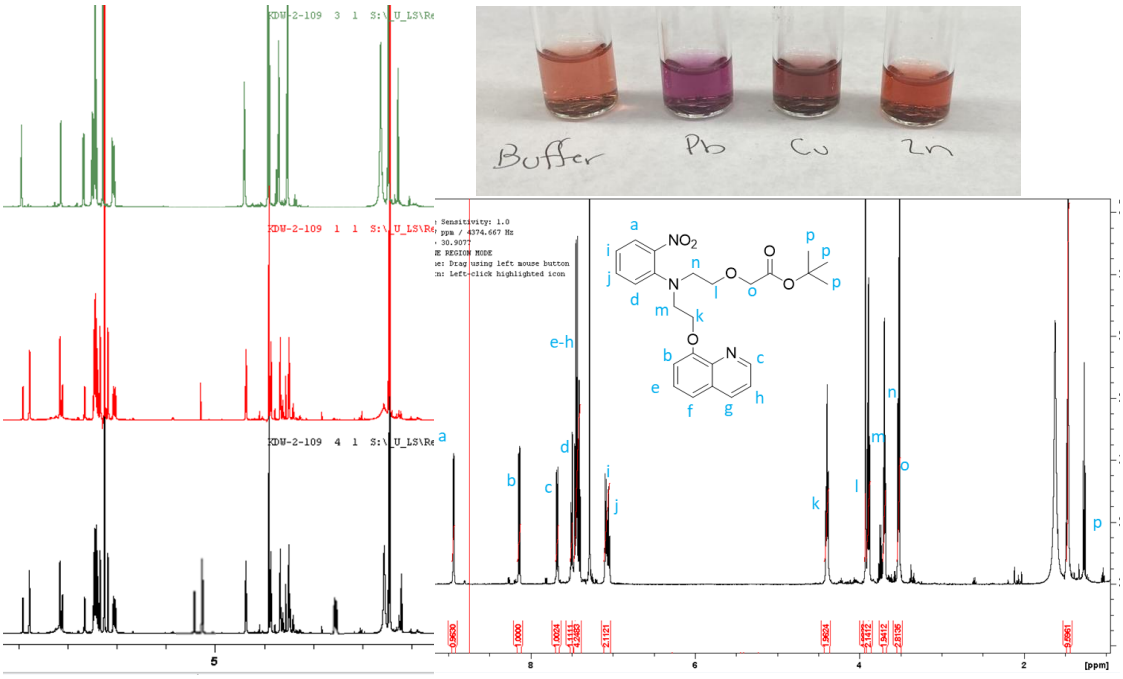

Figure 23a) Trouble with purifying PbSF3 sensors
Figure 23b) Image of 21b's color with no metal, Pb, Cu, Zn
Figure 23c) HNMR of purified substitution using 8-hydroxyquinoline

Figure 23a demonstrates some of the problems with the substitution reaction. The bottom spectrum shows compound 20a after its first column, the red after its second column and first

silica plug, the top after the second column and second silica plug. *Figure 23c* shows the mostly purified spectrum of compound 20a which was hydrogenated and moved on to make sensor 21b. Unfortunately, this sensor did not show any color change in response to any metal after synthesis. This was not encouraging for this family of sensors, however there was another sensor in this family synthesized in tandem with 21b – sensor 21a.

Figure 23b shows the response of sensor 21a. This sensor, made from 20b, demonstrates a different color change in response to different metals. This was not was the collaborators wanted, and as such was not studied as much as the sensors from PbSF1. However, the drastic color change from metal to metal is promising because it shows the sensor is responding to multiple metals but is likely to have a distinct spectral shift for each metal.

Many ligands that did work to sense Pb often also had responses to small metals, as was known per the literature. Tryptophan, for example, worked in the substitution and azo coupling and did respond visually to the presence of Pb. It also responded to small metals Zn and Cu. This was somewhat expected to happen, and these sensors are not best for detection of Pb for this reason.

While PbSF3 sensors were difficult to synthesize and purify, they were some of the most rewarding sensors in terms of their variety in response. Distinct color changes were often found for Pb vs Zn or Cu. This family of sensors had more varied metal responses than PbSF1 or PbSF2, but was the least studied family.

All three families of sensors have different strengths and weaknesses and each family has different uses for the end-stage product of a functional sensor array.

Coupled To:	Pb response?	Yield	Name	Ligand	Compound #
Resorcinol	Y	34%	PbSF1-R	Monoalkylated (MA)	18a
1-naphthol	Y	41%	PbSF1-1n	MA	18b
2-naphthol	Y	43%	PbSF1-2n	MA	18c
1,3-dihydroxynaphthalene	Y	35%	PbSF1-1,3	MA	18d
2,7-dihydroxynaphthalene	Y	46%	PbSF1-2,7	MA	18e
1,5-dihydroxynaphthalene	N	28%	PbSF1-1,5	MA	18f
4-methyl resorcinol	Y	8%	PbSF1-4mR	MA	18g
4-chlororesorcinol	Y	11%	PbSF1-4cR	MA	18h
Resorcinol	Y	22%	PbSF2-R	Dialkylated (DA)	19a
1-naphthol	N	32%	PbSF2-1n	DA	19b
2-naphthol	N	36%	PbSF2-2n	DA	19c
2,7-dihydroxynaphthalene	N	14%	PbSF2-27	DA	19d
1,3-dihydroxynaphthalene	N	11%	PbSF2-13	DA	19e
2,7-dihydroxynaphthalene	Y	23%	PbSF3-27,MAP	2(methylamino)pyridine	21b
Resorcinol	N	11%	PbSF3-R,8HQ	8-hydroxyquinoline	21a
2,7-dihydroxynaphthalene	Y	17%	PbSF3-27,Trp	Tryptophan	21c
Resorcinol	N	0%	PbSF3-R,MS	Methyl salicylate	21d

Table 8: Table of all sensors synthesized from *scheme 15*

Above, *table 8* shows all sensors synthesized using *scheme 15*. The majority of these sensors were all able to detect lead in different concentration ranges and with different spectral and visual changes. The general yield for sensors in any of these families was low, with 46% (PbSF1-27) being the highest overall yield for any one sensor. This is somewhat expected and is what Hagemann found when synthesizing the sensors for the original project. Often, these yields are low due to multiple factors such as incomplete reaction, degradation, and often leaving some

sensor behind during workup. These sensors are difficult to work with and are reluctant to be extracted out of water, so yield does tend to suffer for those reasons.

Fortunately, very small amounts of sensor are needed for a large response. When acylating sensor onto polymer in the initial project, only 6mg of dye was measured out for acylation of 12 polymer dots. With this in mind, a low yielding reaction that provides 100mg of product would be enough to acylate approximately 200 polymer dots.

These syntheses, while time consuming and not without their struggles, have been shown to be effective enough to move forward in development of the sensor array. Each sensor is able to be synthesized and isolated, even if in low yield. With isolated sensors in hand the focus of the lead sensor project was shifted to analysis of the sensor's responses to metal ions in aqueous solution.

Sensor Analysis

Once synthesized, these sensors were tested for their response to metal ions, in particular their response to Pb. Every sensor was initially tested for Pb response in solution, and a positive response led to further study. A lack of response to Pb often caused a sensor to drop to the bottom of the list of viable sensors for this project.

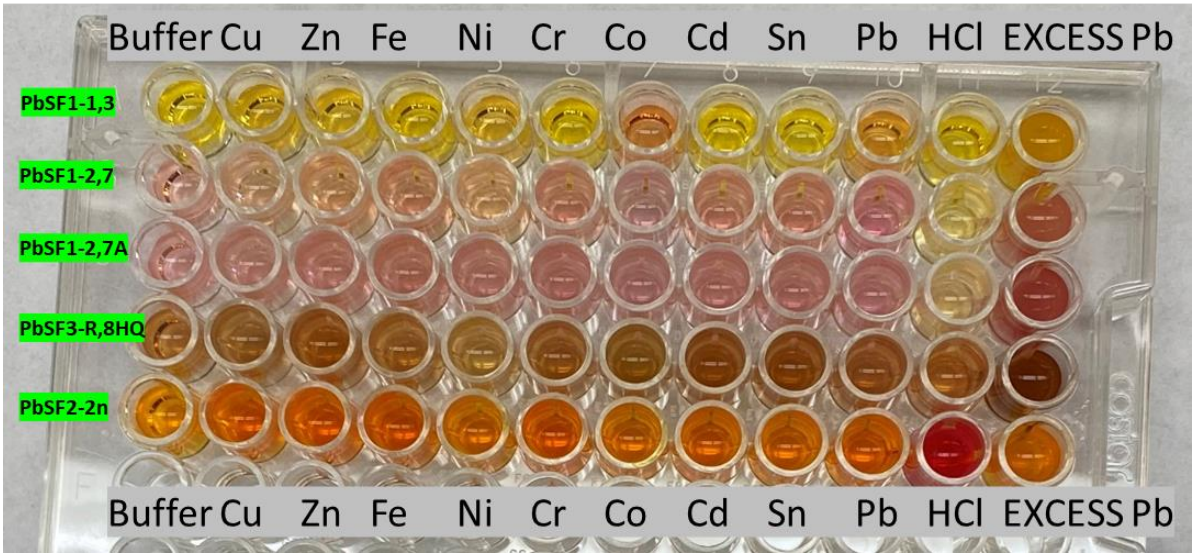

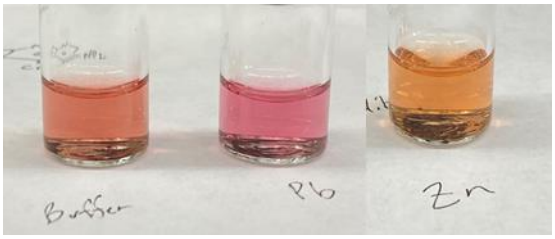

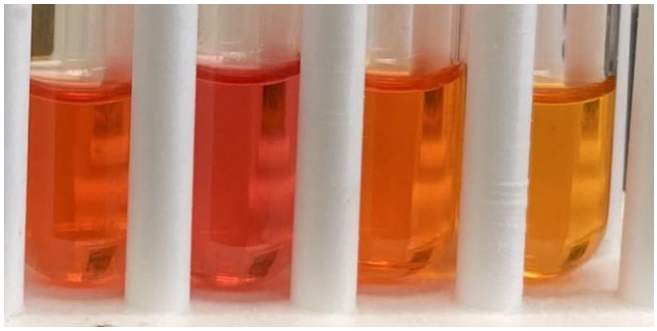

Figure 24a: Well plate of sensors reacting with different metals
Figure 24b: PbSF1-27 in pH 9 buffer, with Pb, with Zn
Figure 24c: PbSF1-2n in pH 9 buffer, with Pb, with Cu, with Zn

As shown in *figure 24a*, even though many of these sensors are structurally similar, small changes such as the naphthol coupled to can cause a large change in response. Sensors within

the same family respond vastly differently to one another. The difference between PbSF1-2n and PbSF1-2,7 is minor: PbSF1-2,7 has an extra hydroxyl group, but this isn't near the ligand that binds to Pb. Still, these sensors respond very differently and to different metal ions, as demonstrated in *figure 24b* and *figure 24c*. Small changes in structure can make large spectral differences. In the case of the 2,7-dinaphthol vs the 2-naphthol, there is a much better response with the 2,7-dinaphthol coupled sensor in terms of detection limit, visual, and spectral response. This goes to show that seemingly insignificant structural changes can provide big results. In *figure 24*, it is shown that PbSF1-27 is a red-pink in borate buffer, pink with Pb, and orange with Zn. In contrast, PbSF1-2n is red-orange in borate buffer, red with Pb, orange-red with Cu, and orange with Zn. Both sensors turn orange with Zn, but the sensors themselves start as different colors and respond to Pb differently when looked at with the naked eye. These differences are significant when looked at by the eye, and these differences are much more apparent when looked at spectroscopically through absorbance measurements and titrations.

It is of particular interest to have a sensor with a spectrally unique signature in response to Pb, meaning a spectrum with a distinct absorbance shift and, ideally, an isosbestic point. Isosbestic points allow for more certainty in detection, as responses to different metals should provide different isosbestic points, or alternatively, a lack of isosbestic point in response to some ions. This makes the spectrum more distinct and allows for more definitive determination of which metal ion is present in solution.

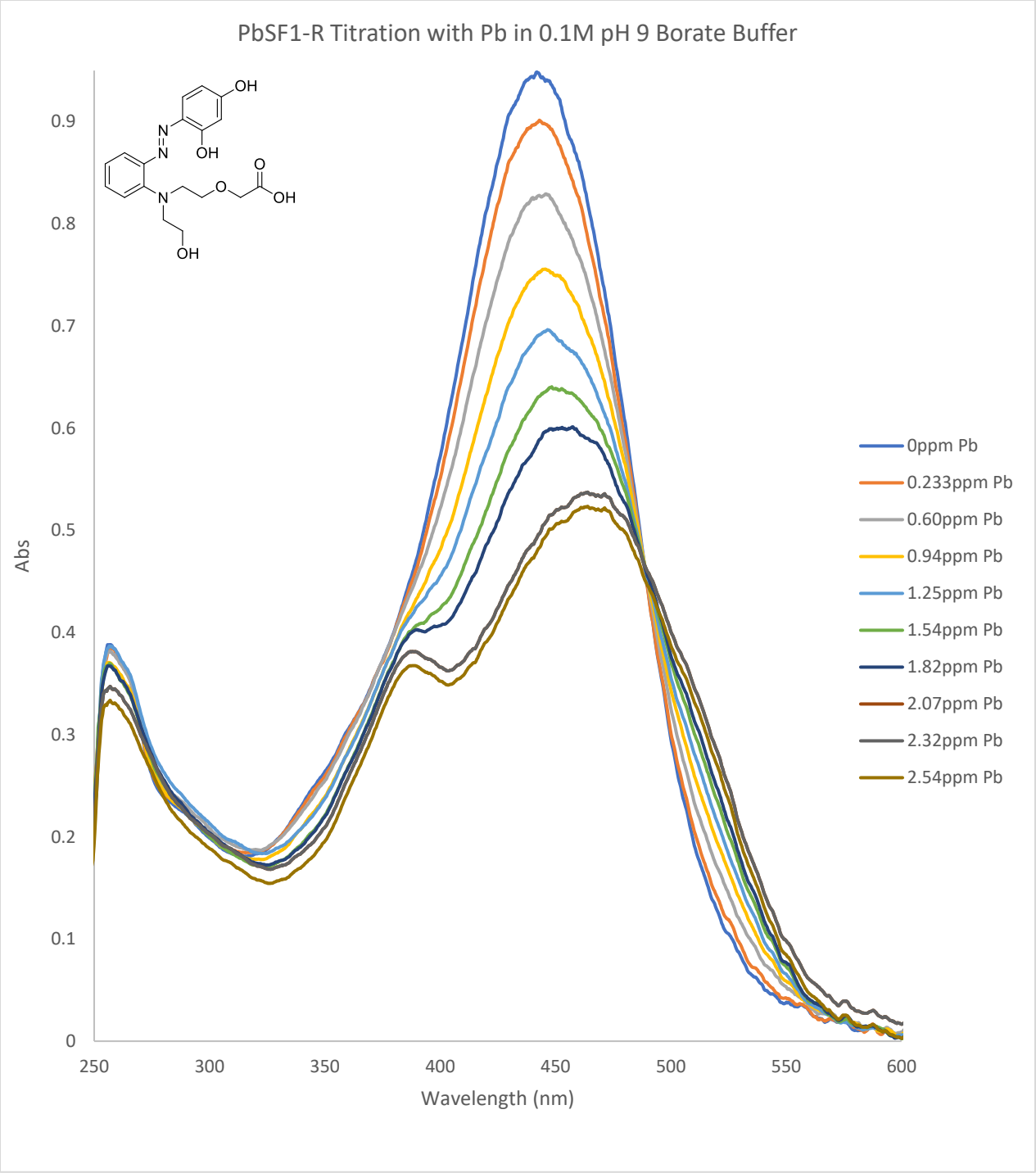

Figure 25: First titration of successful Pb sensor, PbSF1-R in 0.1M borate at pH 9 in DI water.

Figure 25 shows the first titration of a successful Pb sensor, PbSF1-R. This sensor showed promising spectral changes, such as a decrease and shift in absorbance around 450nm, an isosbestic point at 488nm, and a range of absorbance increase between 490-530nm. Unfortunately, this sensor's response range was not optimal, as it was able to detect in the 100ppb range but not much lower. The optimal sensor for this project had a goal of detecting under 10ppb Pb in solution – the lower, the better, considering the ideal safe consumption of Pb is 0ppb. Detection at or under 15ppb is needed for this device to serve its ultimate purpose of detecting lead above the legal limit in drinking water.

While sensors in PbSF1 largely responded to Pb, some of the sensors in this family also responded to other metals or did not have the required detection range. *Figure 26* shows some of the problems with the sensors in PbSF1.

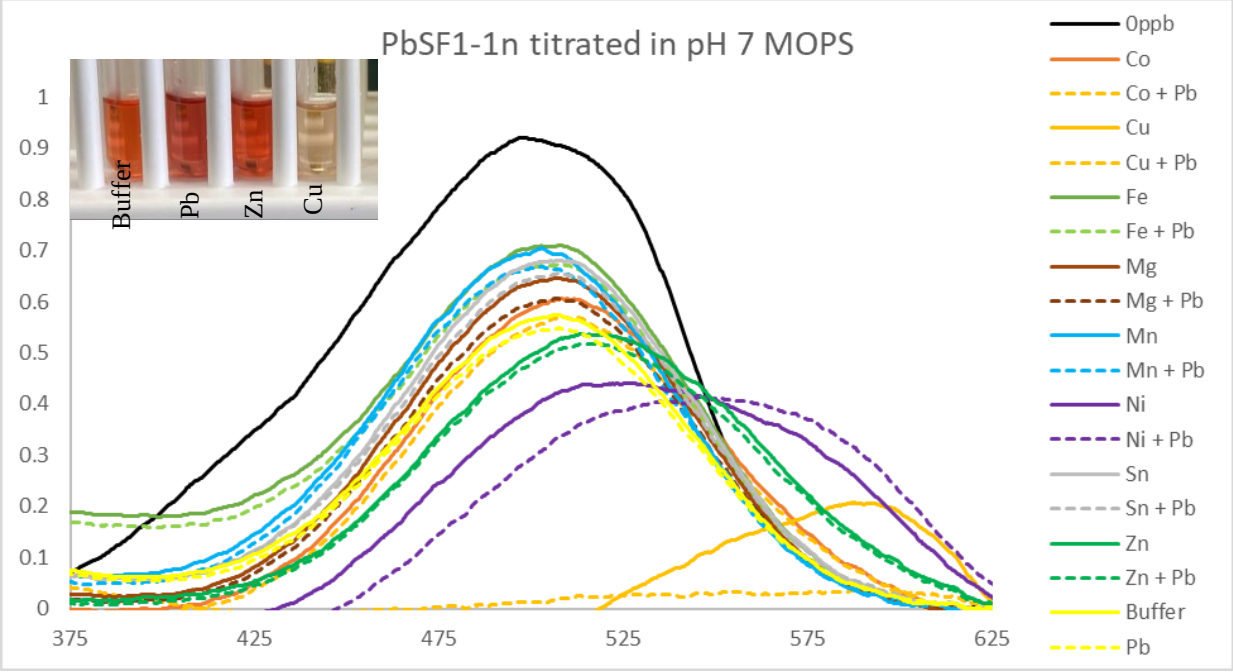

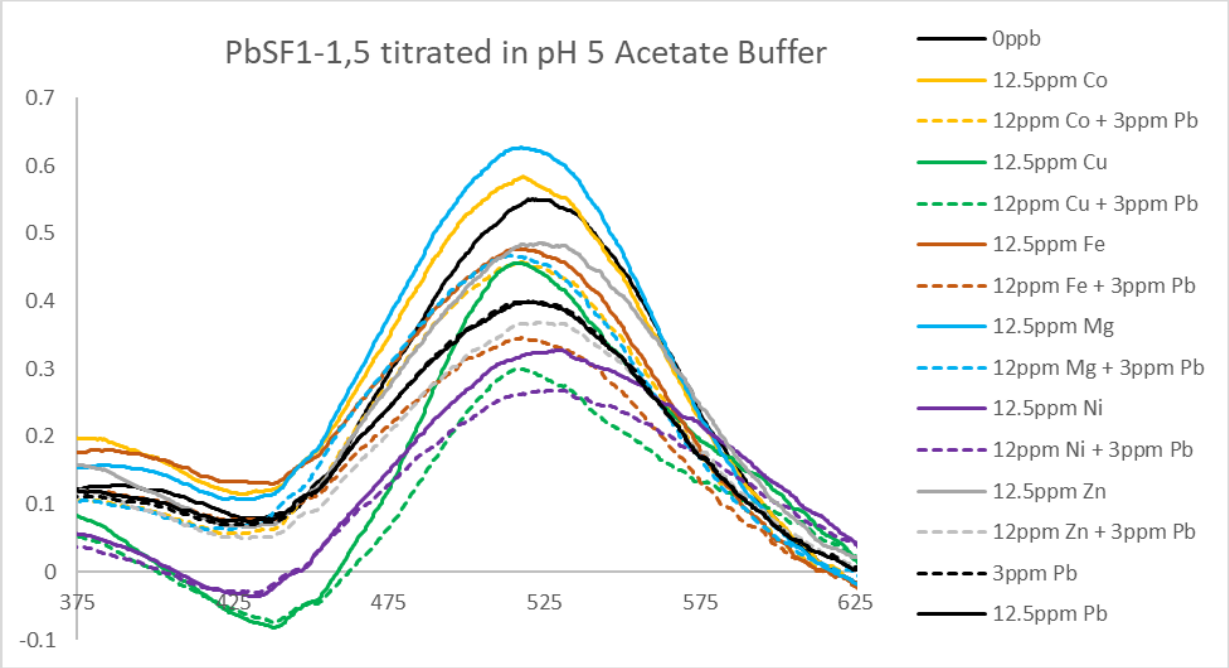

Figure 26a: PbSF1-1n visual response with pH 9 buffer, Pb, Zn, and Cu; PbSF1-1n titrated with various metals in pH 7 MOPS buffer
Figure 26b: PbSF1-1,5 titrated with various metals in pH 5 acetate buffer

Figure 26a shows PbSF1-n. The goal of this sensor was to remove the para hydroxyl on the naphthol, as having a para hydroxyl is thought to increase small metal binding. Without this para hydroxyl, the molecule may be more selective for Pb. This is because the hydroxyl allows for small metals to coordinate to the sensor without binding all atoms of the ligand. Without this hydroxyl, there are not enough electronegative atoms in proximity for small metals such as Zn to reach very well. This would not be a problem for Pb, a large atom. This sensor served as a check of sorts to see if that para-hydroxyl was needed for Pb binding and signaling or if the sensor would bind to Pb better without that hydroxyl present.

However, this sensor, when exposed to Cu, goes completely colorless. The sensor's color is unable to be regenerated, and Cu is permissible in water above the levels at which this

change occurs. This disappearance of color likely indicates oxidative cleavage of the azo bond by Cu.

As such, PbSF1-1n is unable to be used for the project's desired goal, and PbSF1-1n was not studied further. This sensor also had very similar spectral results for different metals and only had a decrease in intensity in response to many metals. This was not very distinct and would likely have metal interference issues when trying to detect Pb.

Figure 26b shows PbSF1-1,5 and its response to various metals. PbSF1-1,5 unfortunately shows no visible color change upon Pb exposure. Beyond that, the spectral change in response to Pb is minimal, and the spectral change in response to other metals such as Zn, Cu, or Ni are significantly larger than the change to Pb. This also knocked PbSF1-1,5 out of the choices for this project, as sensing Pb is the goal.

Some other sensors in this family, such as PbSF1-cR and PbSF1-2n also fell into similar issues. Generally, the three issues with sensors in this family are 1) no response to Pb, 2) higher response to other metals, and 3) low sensitivity to Pb. Some sensors, PbSF1-27 and PbSF1-13, did not have these issues and were thus determined the "most promising" Pb sensors and were set aside for further analysis at a later time.

Other sensor families, PbSF2 and PbSF3 were analyzed at this time as well, as it was thought that the different ligands would allow for more selectivity or sensitivity compared to PbSF1. *Figure 27* shows some of the studies of PbSF2, which was the initial target sensor family.

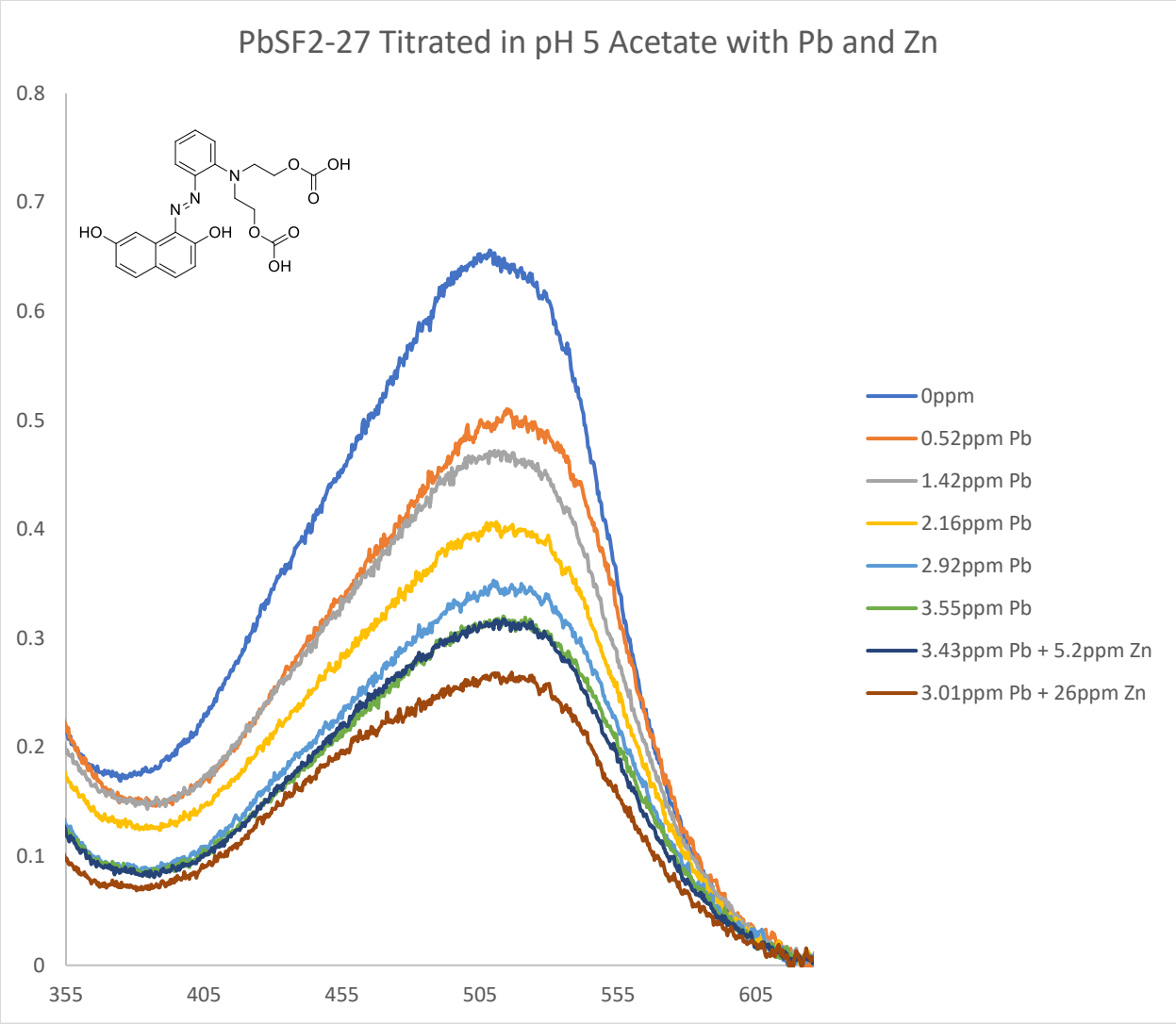

Figure 27: Titrations of PbSF2, dialkylated symmetric sensor coupled to 2,7-dinaphthol

As shown above in *figure 27*, the sensors in PbSF2 are not as sensitive as the sensors in PbSF1, as they respond in the high ppb. This automatically made them less desirable, as this was true for both visible color change to the naked eye and in spectral data. These sensors did not

typically show lead response until the ppm range was reached as opposed to the desired ppb range.

Another issue with these dialkylated sensors is that they are spectrally not very distinct. The change in response to lead is largely just a decrease in absorbance, which could be in part due to dilution. However, in *figure 27* there was an addition of Zn at the end of the Pb titration. This Zn addition used 1.5x the amount of Pb in solution and there was almost no change in absorbance. Upon an additional Zn addition of over 8.6x the amount of Pb, the graph change was much smaller than would be expected for an equivalent amount of Pb. This lends evidence to the sensors in this family being more selective for Pb than for small metals such as Zn, which is

expected as there is a greater number of ligands in the PbSF2 sensor family, which would favor Pb binding as Pb is a larger ion.

This dialkylated family of sensors was the original target when switching to this general, ortho-azo structure for this reason. It was anticipated that more ligands would allow for more Pb selectivity, but it was not anticipated that this would also mean a lower sensitivity.

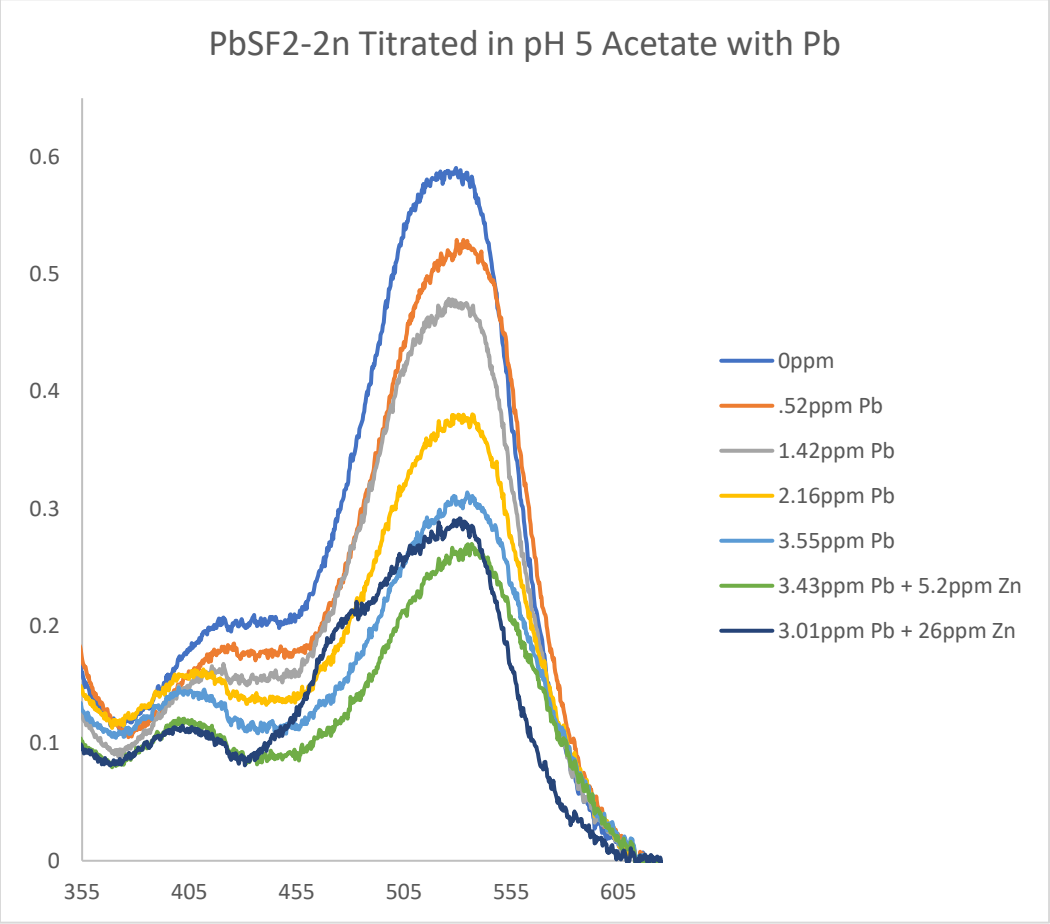

Figure 28: PbSF2-2n titrated in pH 5 acetate buffer with Pb

Figure 28 shows another sensor from PbSF2, the sensor that utilized 2-naphthol. In this sensor, the addition of 8.6x Zn:Pb causes a shift in the spectrum and absorbance maximum, meaning that Zn will directly interfere with Pb binding and detection. Some of the sensors in

PbSF2 did not have this problem, while others did. Many small metals tended to interfere with sensors that only had one hydroxyl on the naphthol, particularly when that hydroxyl was ortho to the azo bond. There was less interference in sensors that had a dinaphthol present and more unique spectra were found when using dinaphthols.

These sensors are, unfortunately, not sensitive enough to serve the collaborator's desired purposes. However, these sensors do allow for a "check" of sorts. In a sensor array, these PbSF2 sensors could be used to alert to high amounts of Pb in the water and are less likely to be interfered with by Zn. This allows for a redundancy and a self-check of the desired apparatus.

Once PbSF2 was found to be suboptimal, PbSF3 was studied. These sensors were, by far, the most interesting visually as they tended to visually change to different colors with the

addition of each metal. However, this also meant these sensors were more sensitive to metals that were not intended to be detected, as illustrated in *figure 29*, below.

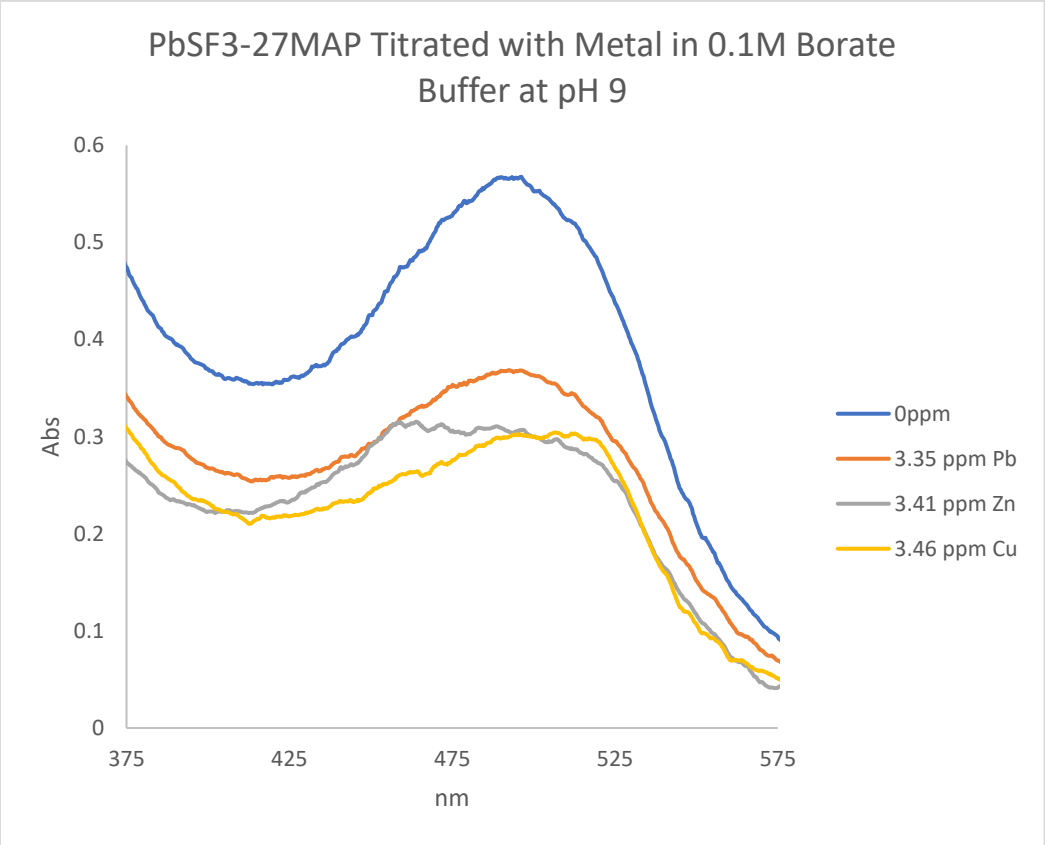

Figure 29: PbSF3-27MAP sensor titrated with different metals

As shown in *figure 29*, this sensor, while it did respond to Pb, was not as sensitive as desired and detected in the ppm range. Beyond that, this sensor responded more strongly to Cu and Zn than to Pb. There were distinct spectra in regard to each metal tested and so these sensors are able to determine which metal is in solution, but does not bind Pb as strongly as needed. Unfortunately, when these sensors were able to be synthesized they often ended up like this: not

functional for the purposes of the collaboration. This group of sensors could be used in a sensor array for determination of what other metals are in solution.

For example, if Zn interferes with Pb detection in the sensors with high sensitivity, the sensors in PbSF3 could be used to show whether there is Zn present in solution. Since these sensors are more sensitive to Zn than to Pb, it would be easy to visually or spectroscopically determine if there is Zn in solution. If this sensor in the array reported no Zn, it could be assumed that the Pb response in the PbSF1 sensor is not due to Zn response.

While this family of sensors did not serve the desired purpose, they do allow for more self-checks and for redundancy. Between all three families of sensors there is a family for detection of low levels of Pb, PbSF1; a family for detection of high levels of Pb, PbSF2; and a family for detection of other, potentially interfering metals, PbSF3. On top of these three families working together, Trevor Hagemann's small metal sensor dyes can also be utilized in conjunction with this array to allow for even more system checks and redundancies to avoid false positive results due to other contaminating metals.

After the discovery that PbSF2 and PbSF3 would not lead to highly sensitive sensors for Pb, PbSF1 was explored further. More sensors were synthesized using different dinaphthols, as dinaphthols seemed to give the best spectral data and the best results in general. Not only were the dinaphthol coupled sensors more sensitive and more spectrally interesting, but they were generally much easier to synthesize and isolate.

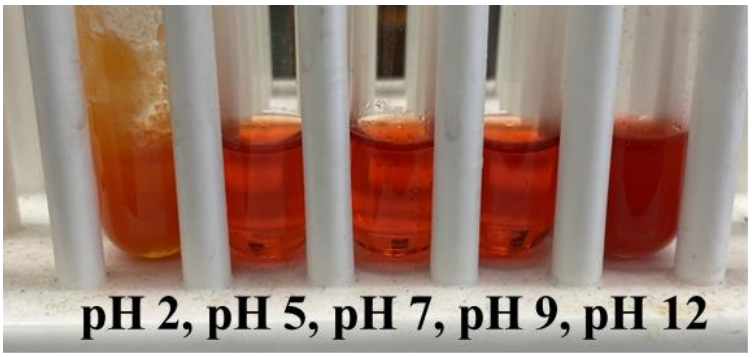

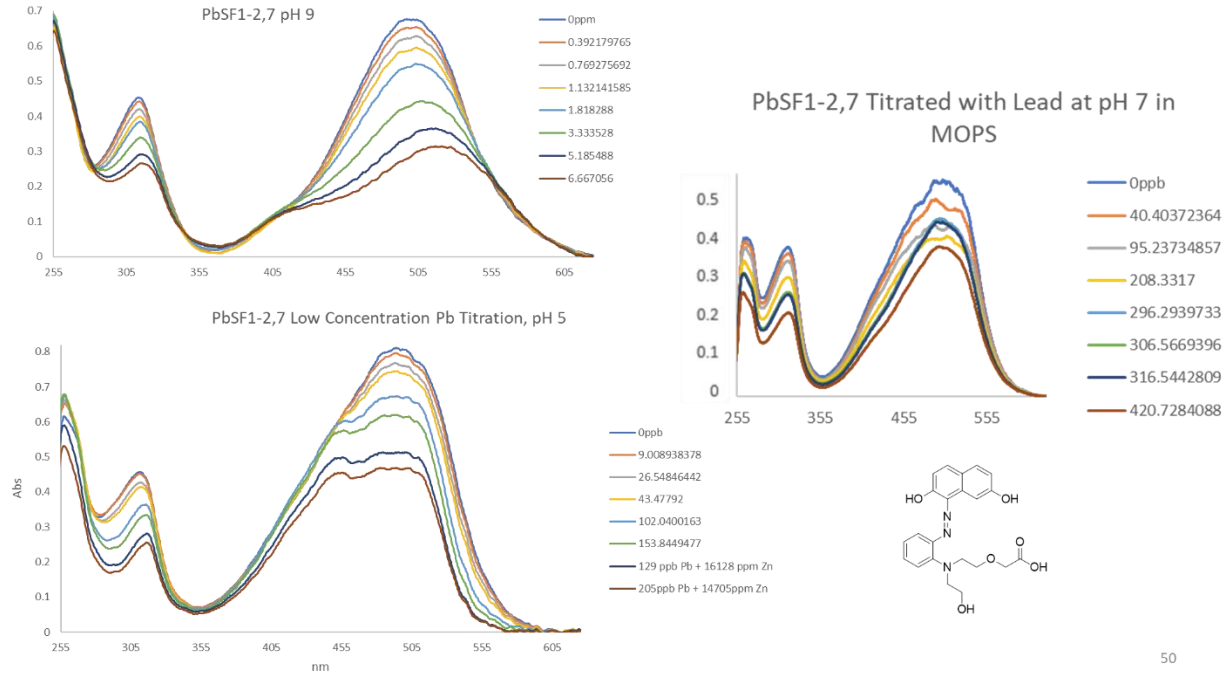

Figure 30a: pH scouting of sensors
Figure 30b: PbSF1-27 titrations at different pHs

Figure 30a demonstrates the pH scouting used for these sensors. pH 2 and 12 were too extreme and caused precipitation of sensor, as expected. A pH range from 5-9 was adopted moving forward, as sensors all remained in solution and demonstrated ability to respond to metals within that range.

Figure 30b shows PbSF1-2,7 titrated with Pb at different pHs. pH 9 was used initially as that is what Trevor Hagemann had used in a lot of his titrations during the initial sensor project

and it was shown to provide good results. pH 7 was used as well, as water should be pH 7. The last pH that was used was pH 5, as acetate buffer is cheap and nontoxic. All three pHs showed different sensitivities, absorbance maximums, and results. pH 7 was the least consistent set of results, as some titrations showed a decrease in absorbance while others showed an increase. This was not always the case when using MOPS buffer to titrate, but approximately 20% of the titrations performed at pH 7 showed inconsistent and randomized results. pH 9 showed a lower sensitivity than pH 5 but pH 9 seemed to show more consistent and replicable results over longer periods of time. As such, these pHs were used moving forward.

pH 9 has the advantage of isosbestic points. pH 9 is the *only* pH at which these isosbestic points seem to appear. This pH has the most consistently unique spectral data directly after sensor synthesis. Unfortunately, this does not appear to be the most selective pH and actually appears to have a slightly lower binding than at pH 5.

pH 5 *also* showed one very interesting characteristic: less metal interference. In the pH 5 titration a very large excess of Zn (125x) was added to solution and minimal change was shown in absorbance and the sensor was shown to respond to another addition of Pb in a manner that was similar to what was expected of the sensor at this pH. This data is very promising and

shows that other metals in water may not cause as many problems as anticipated if pH and a few other factors are accounted for.

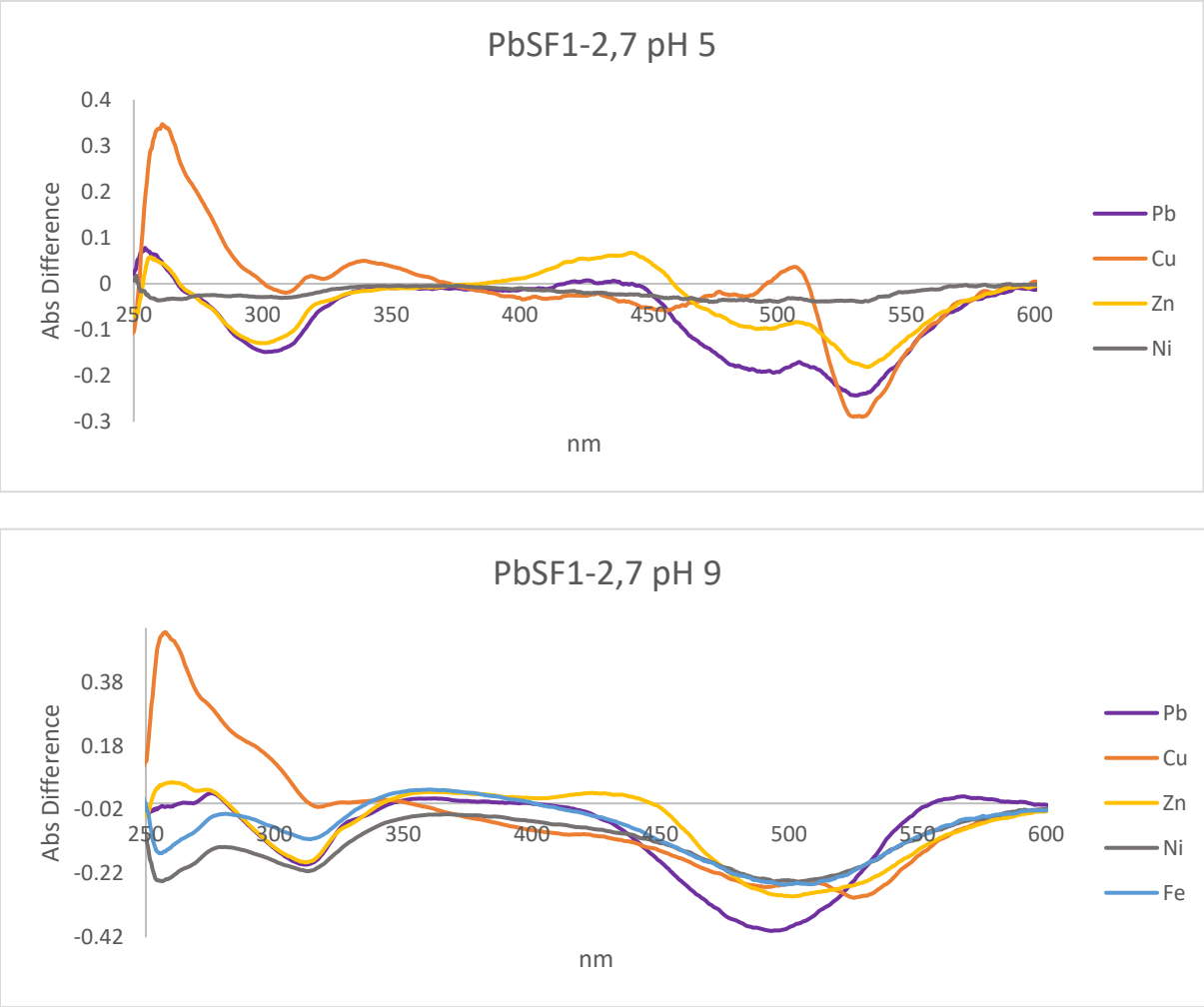

Figure 31: Metal difference graphs

Figure 31 shows some metal difference graphs. Sensor PbSF1-27 was titrated with the same amount of each metal, enough that there was a large excess of metal over sensor, and the metal-bound graph was subtracted from the free dye graph. The metals that are bound by the dye change based on pH. At pH 5, there is less spectral response to metals such as Ni and Fe which could point to less interference or, at the least, more distinct interference. This reinforces the idea that pH 5 is the optimal pH for Pb detection with these sensors.

At both pHs there are overlapping spectra. At pH 9, Pb looks similar to Ni, Fe, and Zn. While this is not optimal, there are some small ranges where there are spectral differences distinct to Pb. A program could be developed to look at the entire spectrum. This program could read the absorbance change at the maximum and look at the wavelengths that just response to Pb to determine whether response is due to Pb or another metal.

At pH 5, Zn looks very similar to Pb. But, as shown and discussed regarding *figure 30b,* it appears that this sensor can still detect Pb in the presence of excess Zn. How much this Zn interferes is yet to be determined, but from preliminary data it appears that it can be worked out through a combination of a sensor array and a program that can take ratios of absorbance at different points to determine whether the signal in question is in response to Zn, Pb, or another metal entirely. A ratio of absorbance is much more distinct than plotting simple absorbance vs concentration because it eliminates the need to account for sensor concentration.

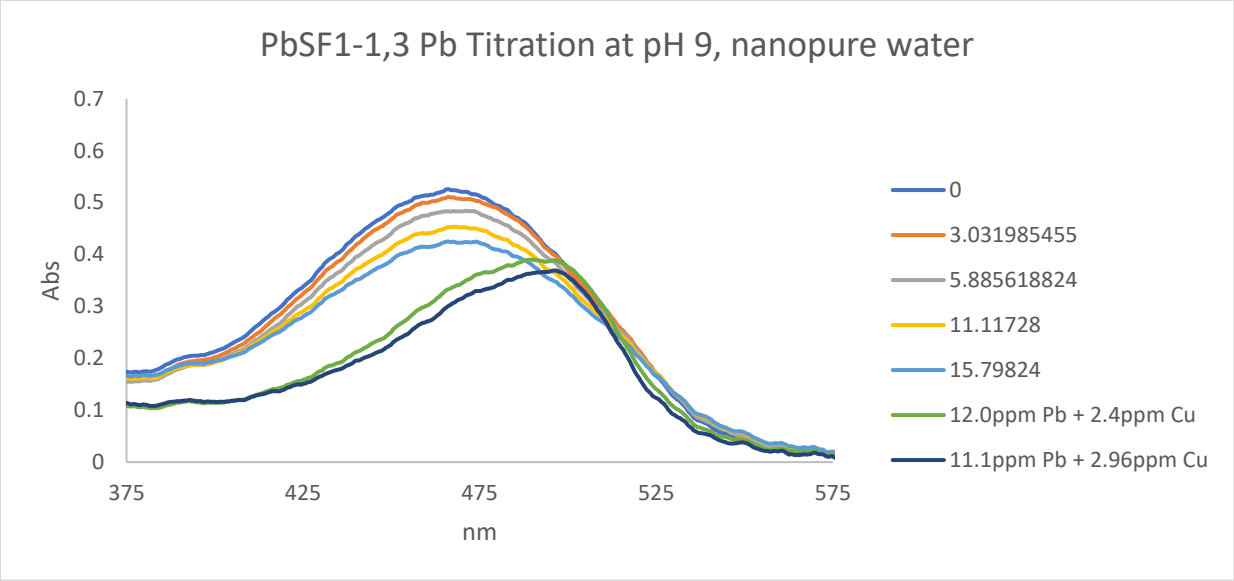

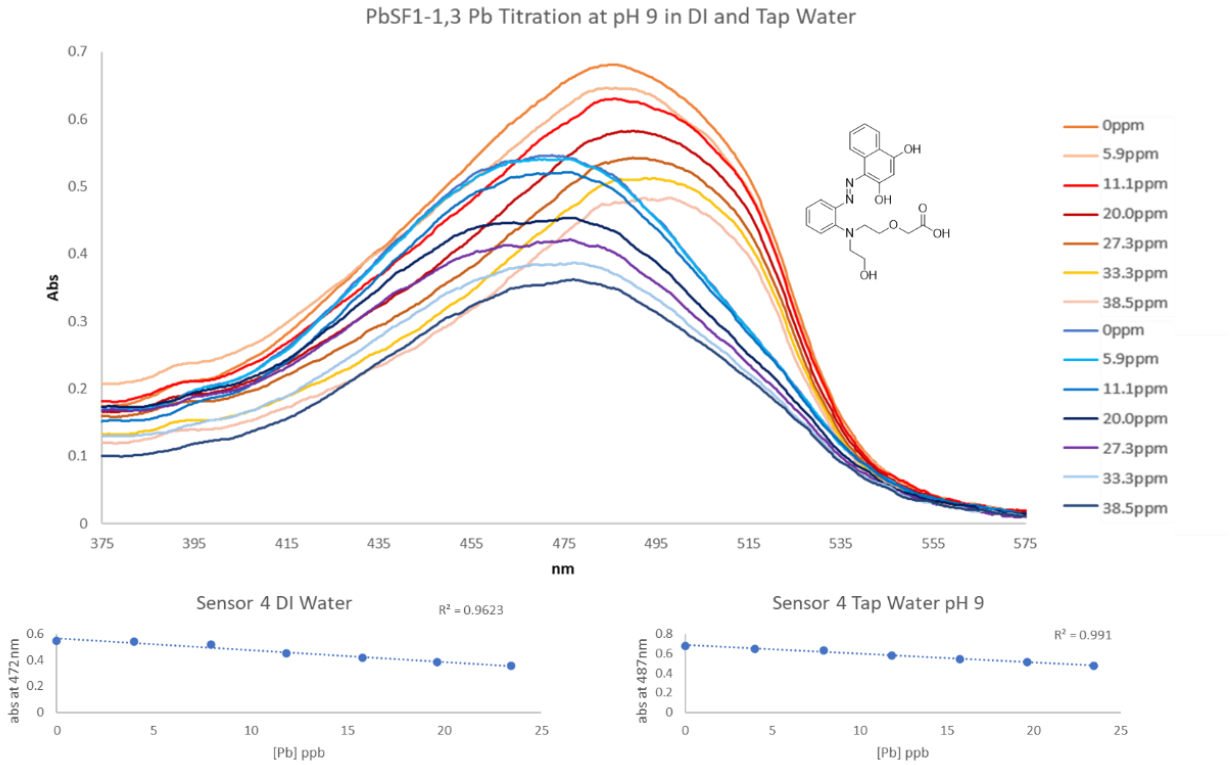

Figure 32a: PbSF1-1,3 titrated at pH 9 in nanopure water
Figure 32b: DI and Tap water with R^2 values for Pb binding

Figure 32a is a titration of PbSF1-1,3 titrated in different water sources. The top is PbSF1-1,3 titrated at pH 9 in nanopure water, starting with small amounts of Pb with the

eventual addition of Cu. This graph shows that Cu presence directly interferes with Pb detection, as it changes the spectral appearance and absorbance maximum entirely from 468nm to 497nm. Cu seems to consistently be the most problematic metal for Pb detection and for all three families of sensors, and immediately changes the maximum absorbance even in small amounts. Pb is still able to be detected to some degree with Cu in solution, but Cu is the most difficult metal to work around because of the high sensitivity of the sensors to Cu ions.

Figure 32b shows a spectrum with the same sensor titrated at pH 9 again, yet this time in DI water (warm colors) and tap water (cool colors). Both water sources have metal contaminants. The DI water starts higher and has a shifted maximum absorbance closer to 480nm than the expected 470nm. The Pb detection is relatively accurate and when plotted absorbance vs concentration, the R^2 value is a 0.96.

The cool colored tap water titration starts even lower than the DI water spectrum and is shifted left instead of right. The absorbance maximum here is closer to 460nm than to 470nm, but over time there is a shift in this absorbance maximum until it gets to approximately 470nm. The R^2 value for this is 0.99, which is even closer to linear than before. This shows that these titrations can be completed in tap water with competing ions, however the mystery of how to account for that in calculations to get an accurate reading is still being solved and is a mystery for an analytical chemist or programmer. This is promising as it appears to show that other metal ions in solution will not prevent the sensor from detecting Pb in the sample. It is known that there is Fe, Mg, Cu, and Zn in the tap water that was used for this experiment, and it is known that the DI water also has Fe present in it from prior testing done by Hagemann and Joe Labeots during the initial sensor project. This appears to be a sample representative of the average US citizen's water supply and while further testing in more varied samples of tap water need to be

done, this result is encouraging for the project as a whole. This was replicated with the PbSF1-2n sensor and similar results were found.

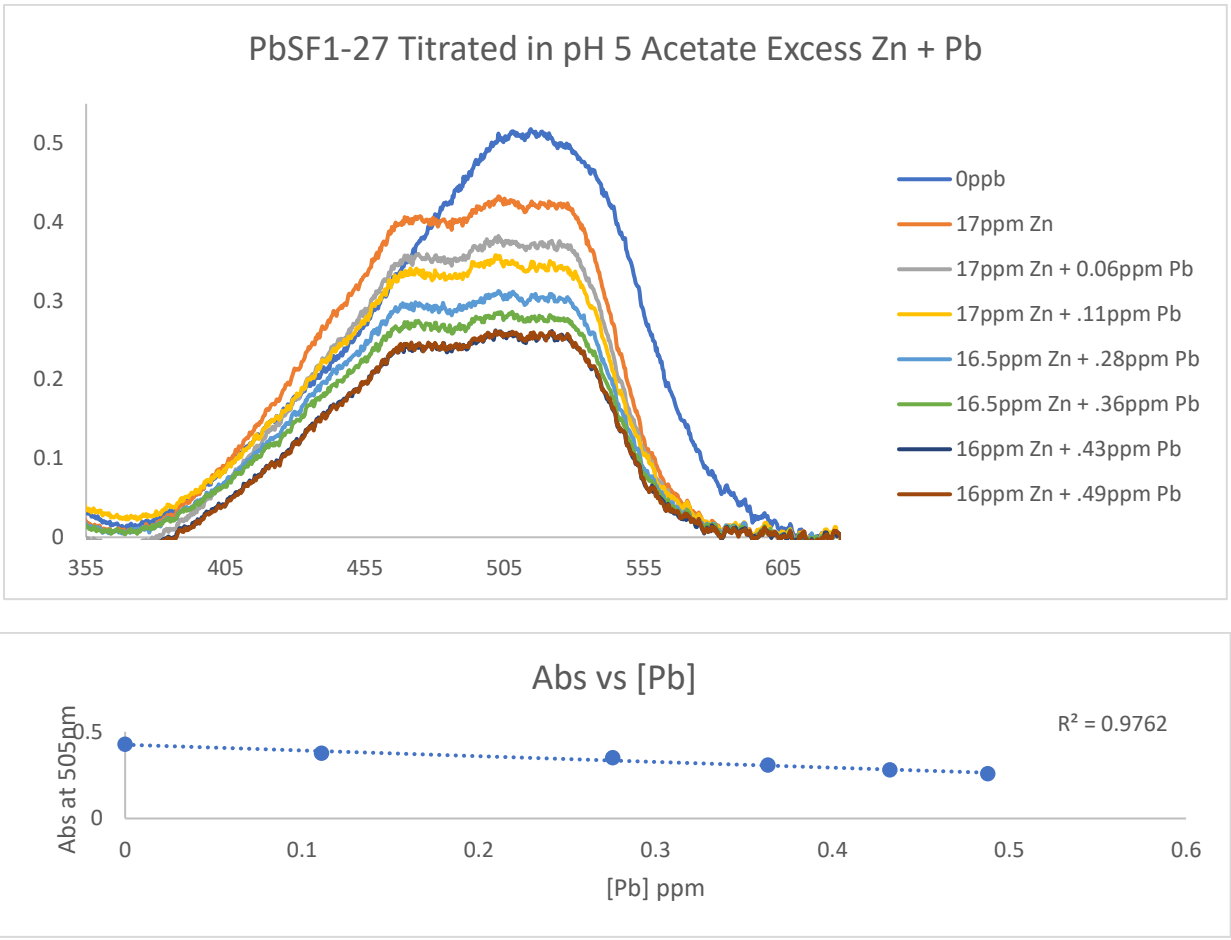

Figure 33: Titration of PbSF1-27 at pH 5 with Zn and Pb, Abs vs [Pb]

At this point, the biggest obstacles were reproducibility and potential interference by small metals. As such, sensor PbSF1-27 was titrated in a myriad of different ways to determine whether its sensing ability would be viable for the desired purpose. 17ppm Zn was added to the sensor and the sensor was then titrated with Pb. The amount of Pb started at .4% the amount of Zn and went up to 3% the amount of Zn. While the sensor responded to Zn and took on the spectrum of the Zn-bound dye, it was still able to detect Pb in solution.

When this was put into a graph comparing Abs with [Pb], the R^2 value of the line is .89 when taking the spectrum of the free dye into account. While this value is not ideal, the blank spectrum is vastly different from the metal-bound spectrum but the concentration of Pb is the same, which destroys linearity in this case. When the blank is not accounted for, the change is much closer to linear between the initial Zn-bound spectrum and the Zn-bound spectra with Pb present. This value was much closer to the desired value and was a 0.97. Taking the blank out of the equation fixes this value because the shift in absorbance is drastic when going from free dye to metal-bound sensor. This shows a mostly linear relationship between [Pb] and Abs, even with an excess of over 200x the amount of Zn to Pb. In this case, the dye was fully saturated with Zn before Pb addition but was still able to detect Pb which suggests that the affinity of sensor PbSF1-27 is higher for Pb than for Zn.

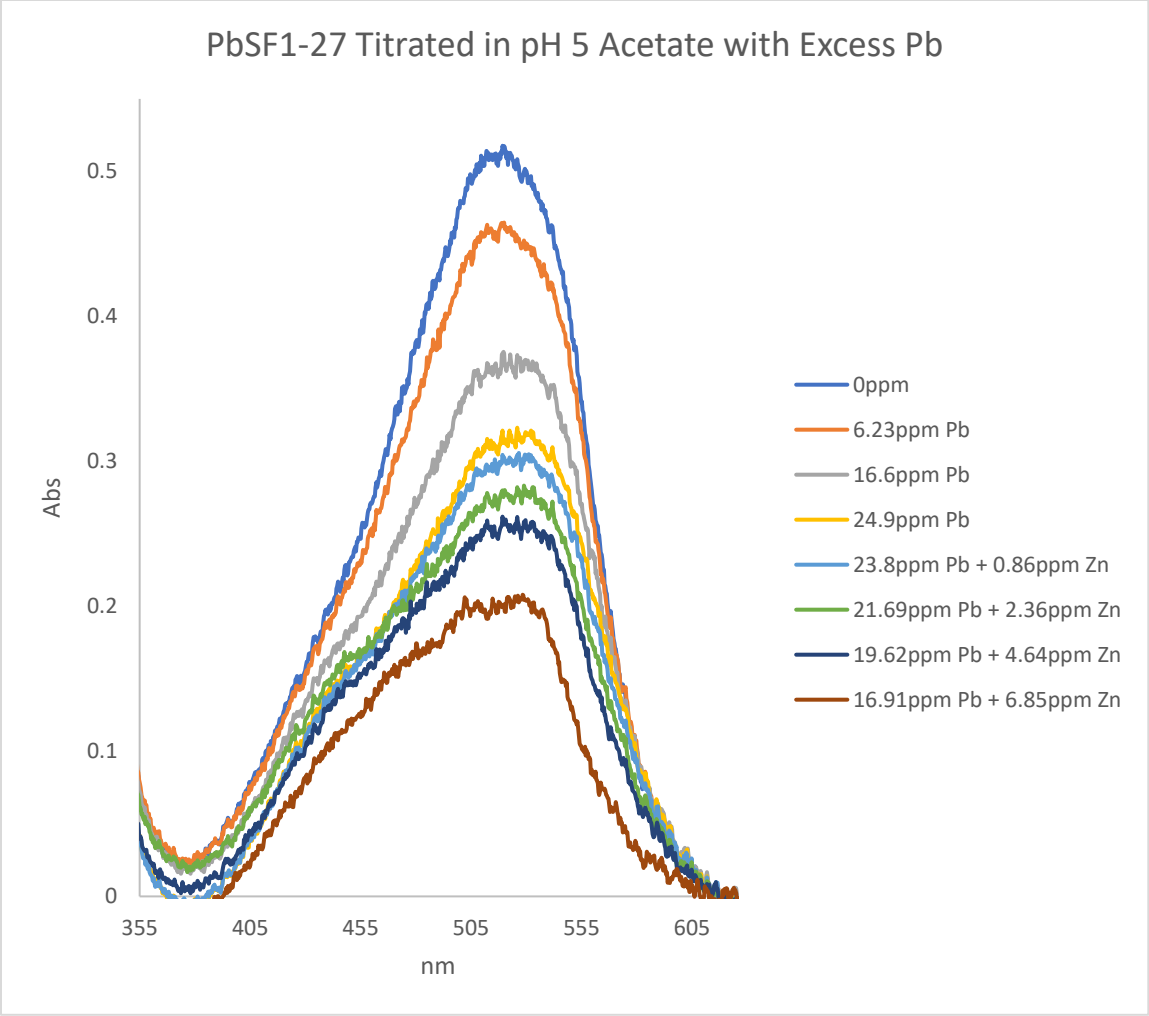

Figure 34: Titration of PbSF1-27 at pH 5 with excess Pb and Zn

In *figure 34*, PbSF1-27 was titrated with a higher concentration of Pb followed by Zn addition and titration. While this sensor does appear to respond to amounts of Zn in the low ppb, the response is drastically reduced when compared to the Pb response at a similar concentration. The spectrum changes shape and broadens slightly once almost 7ppm Zn was added, approximately a 1:2.5 ratio of Zn:Pb.

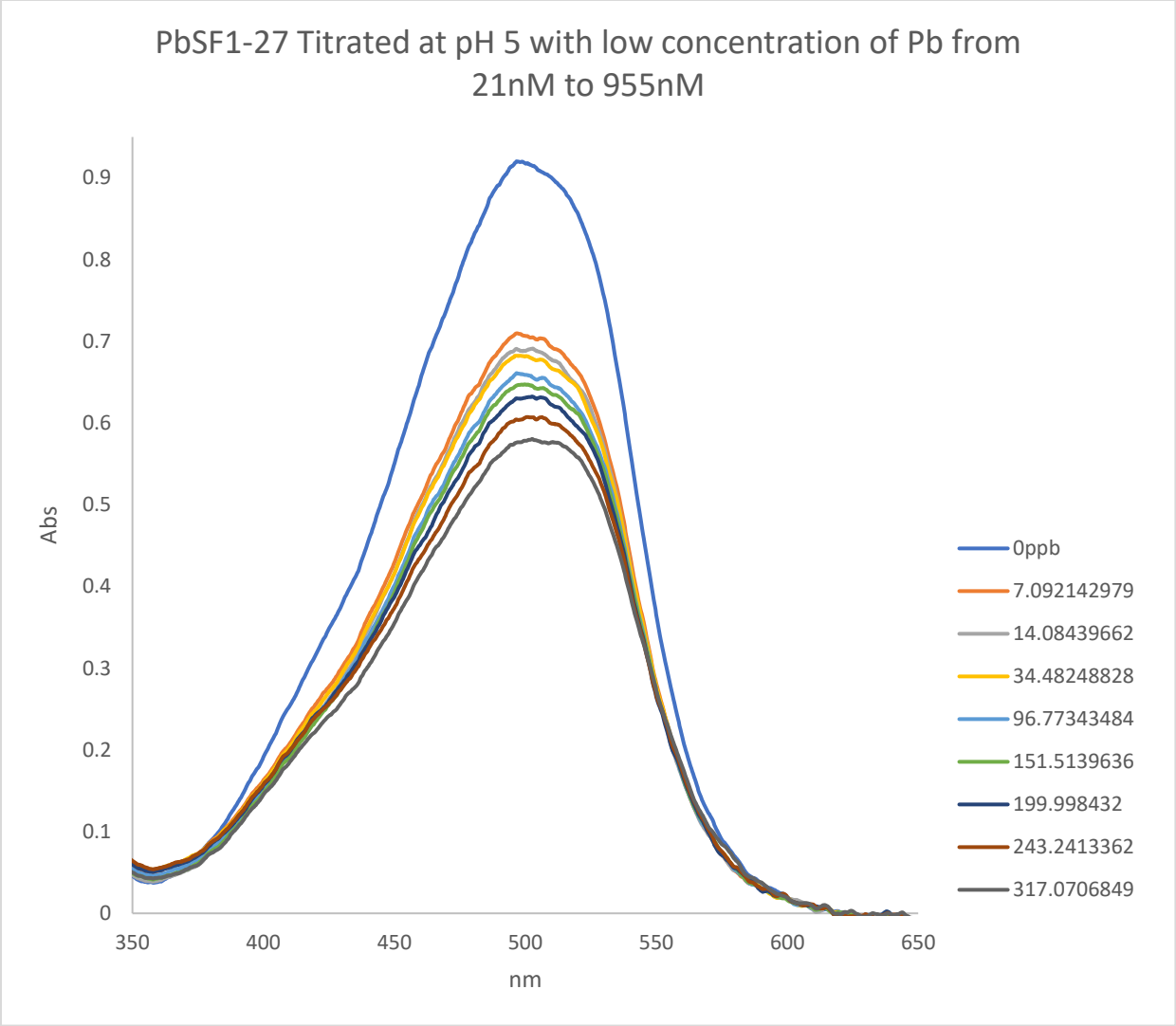

Figure 35: Titration of PbSF1-27 with low ppb Pb

Figure 35 shows a titration of PbSF1-27 at pH 5 with Pb starting in the low nM and going to high nM concentrations. This dye was titrated 4 weeks after synthesis and was stored in a vacuum desiccator under active vacuum, but the spectral shift when detecting Pb was still different than expected. This sensor showed a response to Pb through a decrease and minor shift in absorbance maximum. The absorbance of PbSF1-27 changes at 450 when exposed to Zn, so this ratio could be used to determine the presence of Zn in solution vs the presence of Pb, as the sensor does respond to both metals.

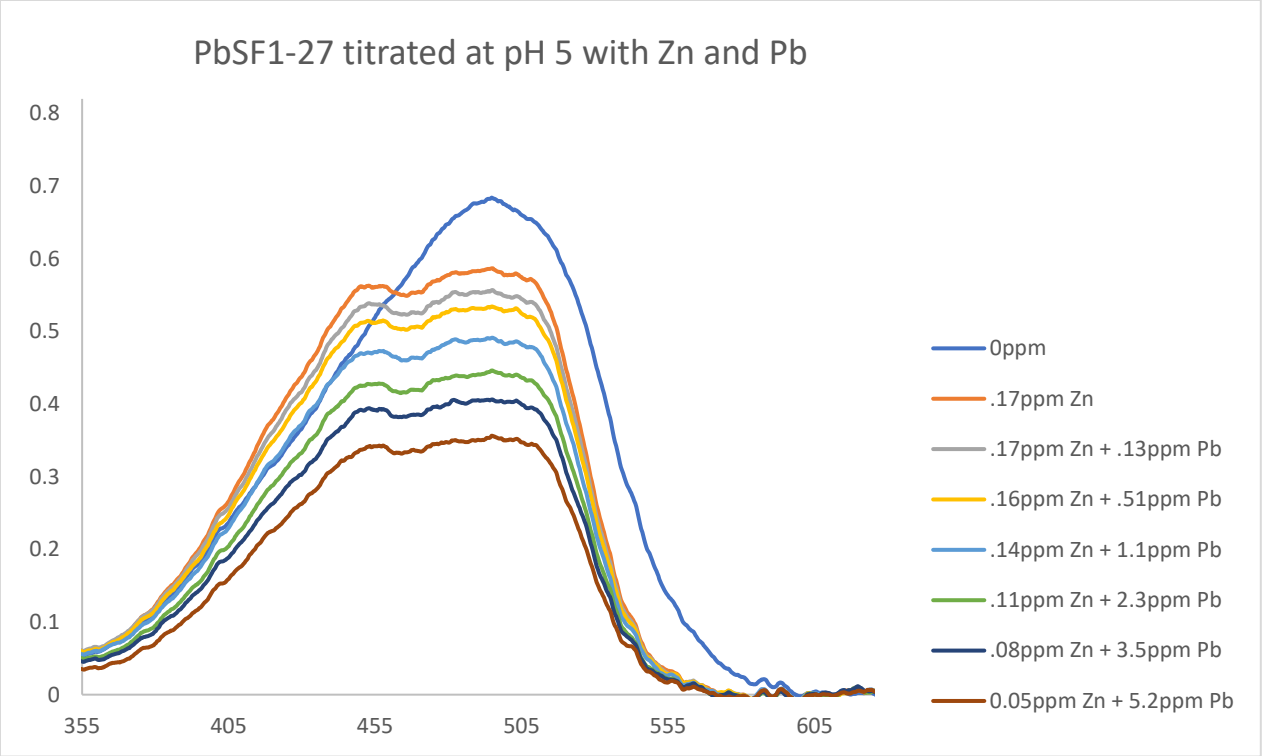

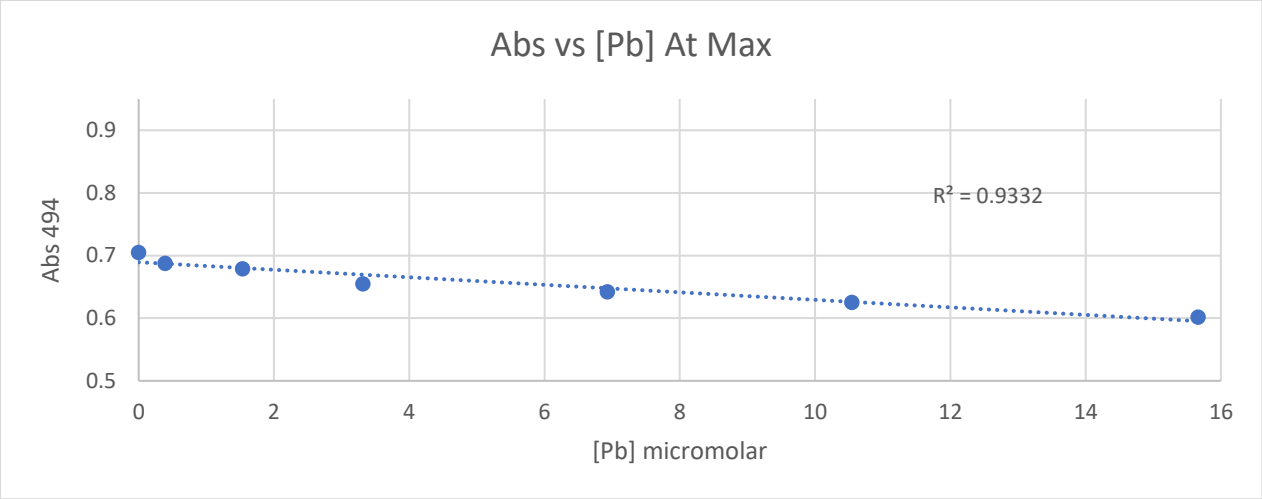

Figure 36: Titration of PbSF1-27 with Pb with a small amount of Zn in solution, [Pb] plotted vs Abs

Above, *figure 36* shows a titration of PbSF1-27 at pH 5 with a small amount of Zn in solution. 0.17ppm Zn is added to the sensor followed by a titration with Pb. As the concentration of Pb rises and Zn falls, the spectrum still looks like the Zn bound with even a small amount of

Zn and an excess of Pb present. This sensor does still detect Pb as and there is a gradual shift in absorbance maximum as the concentration of Pb rises. When [Pb] is plotted against absorbance, the R^2 value is only 0.93, indicating Zn is interfering with Pb detection. This result is highly replicable and occurs with any amount of Zn in solution.

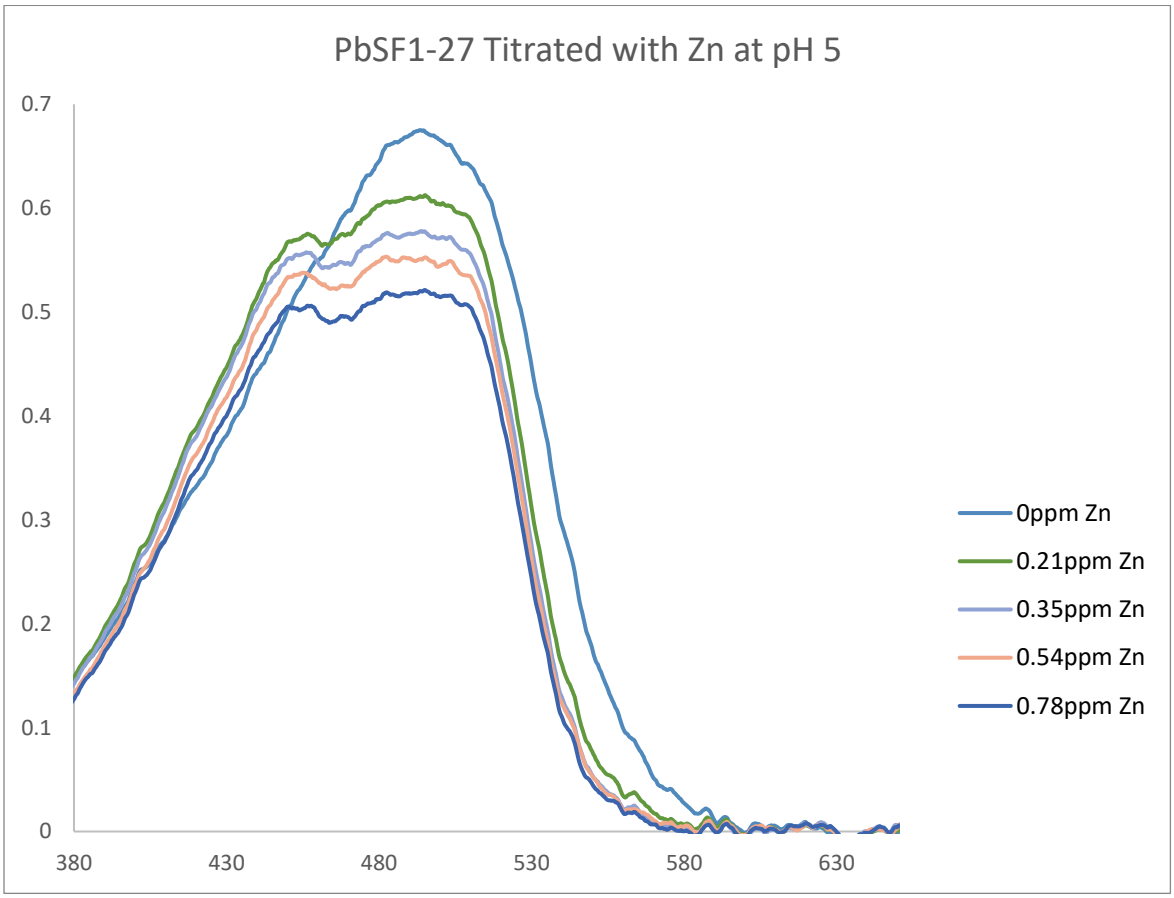

Figure 37: Titration of PbSF1-27 with Zn

For comparison, *figure 37* shows a titration of PbSF1-27 with Zn at pH 5 and the change in absorbance that comes with it. The ratio of absorbance at 494/450 vs [Zn] has an R^2 value of 0.608, different from the Zn/Pb bound of 0.23 and different from the Pb bound of 0.78. This shows that there is a difference in ratio between Zn bound, Zn and Pb bound, and Pb bound. This is promising as it indicates that the identity of metal can be determined through using a ratio of absorbances. While this is not as simple as having different isosbestic points for each metal, it

does indicate that this sensor is still viable for Pb sensing purposes. It has been demonstrated in *figure 36* that this sensor can still detect Pb even with small amounts of Zn present in solution, and it has been demonstrated in *figure 33* shows that Pb can be detected even with an excess of Zn over dye in solution. This result does appear to be consistent, as does the dramatic spectral change with even a small amount of Zn present.

The presence of small metals like Zn or Cu alter the spectrum of the Pb sensors drastically, but preliminary evidence suggests that the sensors are functioning to detect Pb even with these spectral changes. This can be accounted for through development of a computer program that looks at various parts of the spectrum and runs calculations, such as absorbance ratios at predetermined wavelengths, to determine the identity of the metals in solution and verify whether a signal detected is in response to Pb ions or another metal in solution.

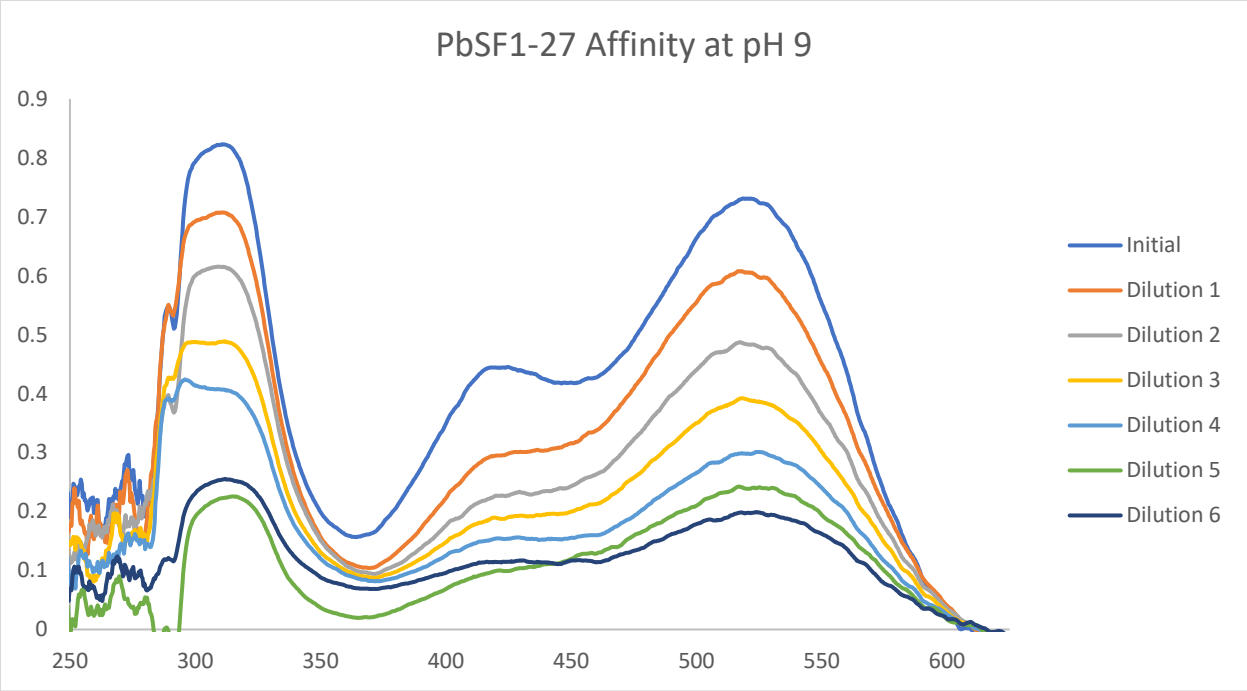

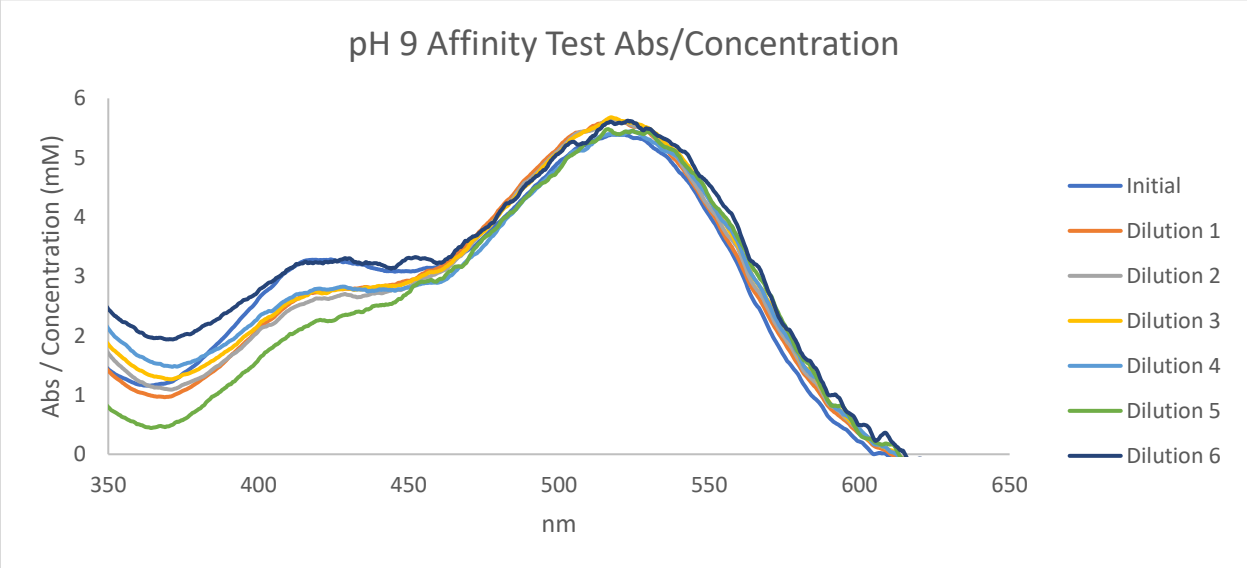

Figure 38a: PbSF1-27 affinity tests at pH 9
Figure 38b: Absorbance/Concentration for dilution tests to determine affinity

Affinity tests were conducted on PbSF1-27 by mixing an equal concentration of Pb and dye in borate buffer. The absorbance spectrum was measured and then this was diluted six times in a ratio of 0.5mL dye:metal solution to 1.5mL buffer, meaning a 1:3 dilution. With every

dilution a spectrum was taken, and then these spectra were compiled as shown in *figure 38a*. Each dilution has a very similar spectral profile with a decreased absorbance. These spectra were then compiled into *figure 38b*, which took absorbance/concentration and overlaid the spectra. Since the spectra were all the same when concentration was accounted for, this means the sensor is a high affinity sensor as there is no dissociation down to the nanomolar range.

A high affinity sensor is typically used to mean this sensor has a low dissociation rate under 10^{-5} s^{-1} and a low equilibrium dissociation constant, which means under 10^{-9}M, or nanomolar. This indicates that the sensor should be able to bind to Pb at the desired low ppb concentrations, as 1ppb Pb is approximately $3.021*10^{-9}$M.

After affinity determination, data was compiled and analyzed to find patterns. At this stage it was determined that much of the data was inconsistent. Sensors would behave differently upon being tested at different times, meaning data could not be replicated. Absorbance maximums and general responses would change and become less unique. Sensors that showed isosbestic points or very distinct spectra would later give spectra without unique features. Many of these sensor titrations were compiled into a table, *table 9*, below.

Dye	**pH**	**Max free**	**Max Pb**	**Max Zn**	**Max Cu**	**Date**
PbSF1-R	9	441	445-465 max, 470i 472-548+	467		9.15.20
PbSF1-R	9	441-447	450			1.11.21
PbSF1-1n	9	501	499			2.4.21
PbSF1-1n	9	501	499			2.10.21
PbSF1-1n	9	498	501		515	2.11.21
PbSF1-2n	9	510	519	506		12.21.20
PbSF1-2n	9	508	515			2.11.21
PbSF1-2n	9	508	515			2.11.21
PbSF1-2n	9	505	519			4.5.21
PbSF1-2n	9	512	521			4.5.21
PbSF1-15	9	541	541			2.22.21

PbSF1-13	5	485	485, 476i			7.12.21
PbSF1-13	7	465	477	501		4.9.21
PbSF1-13	9	458	463	490	494	4.11.21
PbSF1-13	9	474	478			4.6.21
PbSF1-13	9	486	499			4.6.21
PbSF1-13	9	474			497	5.18.21
PbSF1-13	9	468	472	486		4.9.21
PbSF1-13	9	470	472			2.22.21
PbSF1-13	9	474	476			2.22.21
PbSF1-27	5	510	515			3.23.22
PbSF1-27	5	512	525	507		3.17.22
PbSF1-27	5	508	516	510		3.23.22
PbSF1-27	5	508	518	511	524	3.23.22
PbSF1-27	5	512	531	532		3.17.22
PbSF1-27	5	503	505			4.23.21
PbSF1-27	5	501	503			4.23.21
PbSF1-27	5	499	503			5.6.21
PbSF1-27	5	498	503	497	508	5.6.21
PbSF1-27	7	504	504			11.14.21
PbSF1-27	9	504	517	498	509	4.23.21
PbSF1-27	9	503	520, 554i, 554-570+	499	508	4.29.21
PbSF1-27	9	508	516			6.28.21
PbSF1-27	9	502	518		508	4.8.21
PbSF1-27A	9	503	508			9.18.21
PbSF1-27A	9	502	506	506	505	11.23.21

Table 9: Table of sensor absorbance data with dates and absorbance wavelengths for metals tested

Upon compilation, the data shown in *table 9* demonstrates a few clear patterns regarding sensor data. It appears the best and most distinct data comes from newly synthesized sensors. Directly after synthesis, these sensors perform optimally, with less interference from other metals and more distinct spectra with isosbestic points. Over time, these sensors have altered responses, as demonstrated below in *figure 39*. This could be due to degradation or isomerization, likely caused by exposure to air and light [43, 66,69]. After initial analysis, it appears that light is the

primary factor in the degradation as these sensors were generally stored under active vacuum when not in use.

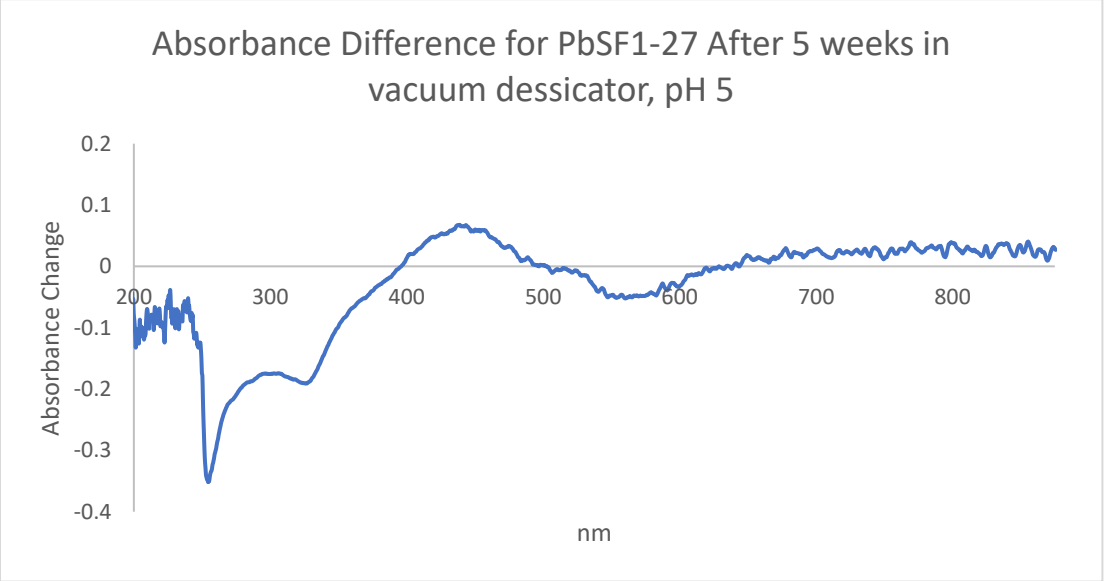

Figure 39: Change in PbSF1-27 absorbance after five weeks under vacuum

Figure 39 shows sensor PbSF1-27 in pH 5 acetate buffer and is a difference spectrum. This spectrum was made from two separate trials of PbSF1-27 at pH 5 done five weeks apart. The no-metal spectrum was normalized at the maximum absorbance by multiplication of a constant and then one spectrum was subtracted from the other. In *figure 36*, this shows the difference over time. After five weeks there are multiple ranges of decrease and increase in absorbance, showing that the spectrum does in fact change over time and with exposure to light and air.

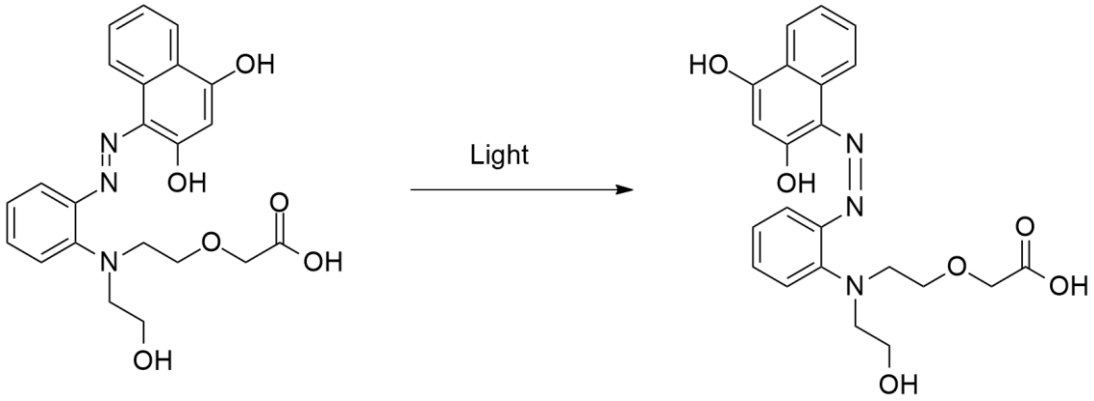

Figure 40: Proposed photoisomerization of azo dyes under vacuum

Figure 40 shows one theory for the degradation: photoisomerization. Azo dyes are known to photoisomerize with light[42,50] and while this concept is what makes the project work, it also creates a problem with consistency in detection if these sensors were not recently synthesize. When a freshly synthesized azo dye is used for titrations, spectra have a higher baseline absorbance and decrease over time upon exposure to metal. This metal exposure causes a shift from trans to cis in the azo bond. This decrease in absorbance is partially due to more of the cis isomer being present. It makes sense that over time and with photoisomerization these sensors would have a lower baseline absorbance but would look spectrally similar in some aspects.

In addition to photoisomerization, these dyes degrade oxidatively in solution at a very fast rate. This degradation also occurs when the dye is in its solid form, albeit slower, which would cleave the azo bond over time. This azo bond cleavage results in different compounds being present in the sample and thus alter the spectrum if used without purification.

One thing to note is that even with this degradation occurring, Pb sensing is still able to be performed, albeit with different absorbance data. These sensors do still respond visibly to Pb when exposed even after degradation. Upon testing directly after synthesis, these sensors appear to be more Pb specific and less able to be interfered with by other metals. These sensors also

tend to have more interesting spectral data such as an isosbestic point or more dramatic absorbance shift upon Pb exposure when they have been recently synthesized, as evidenced in *table 9*. In particular, it has been discovered that the presence of isosbestic points only occurs directly after synthesis and in titrations performed at pH 9. At pH 5 no isosbestic point is present in any titration in any sensor tested. Instead, pH 5 appears to minimize potential interference by other metals as well as causes development of a spectral "shoulder" upon exposure to certain metals.

This sensor degradation, while unfortunate, is not unexpected. Hagemann's sensors from the initial, small metal sensing project also degraded over time. However, in the initial sensor project it was shown that when these sensors are put onto polymer that they do not degrade in the same way and are stable for a much longer period of time. As such, it is reasonable to assume that these sensors would behave in much the same way and will be able to be used for more consistent results once on polymer. It was also assumed that conversion into an amide, which is required for putting onto polymer, would make these sensors more specific and sensitive to lead ions.

In the polymer-bound form the amide would be used, as the polymers synthesized by Rebecca Dominguez are benzylamine based. As such, some of these sensors were turned into amides by the following method, *scheme 18.*

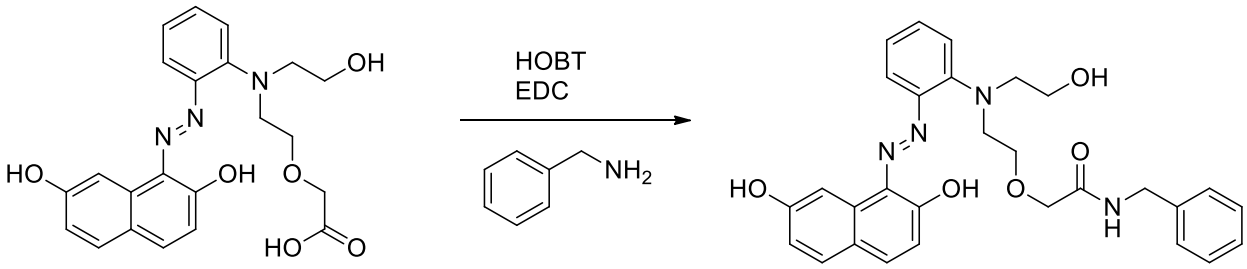

Scheme 18: Turning sensor PbSF1-2,7 into an amide using HOBT, EDC, and benzylamine

Scheme 18 shows the reaction used to synthesize amides using PbSF1 sensor dyes. This reaction was done on a variety of sensors, compounds 25a-d, with the most successful being the reaction shown which provided product in a 31% yield. This was an unfortunately low yielding reaction, likely due in large part to solubility of the starting compound and contaminants in the benzylamine. While the reaction was low yielding, this is fine as very small amounts of azo dye are needed for testing or reaction.

With the amide in hand, this was titrated and showed very promising results for limited metal interference.

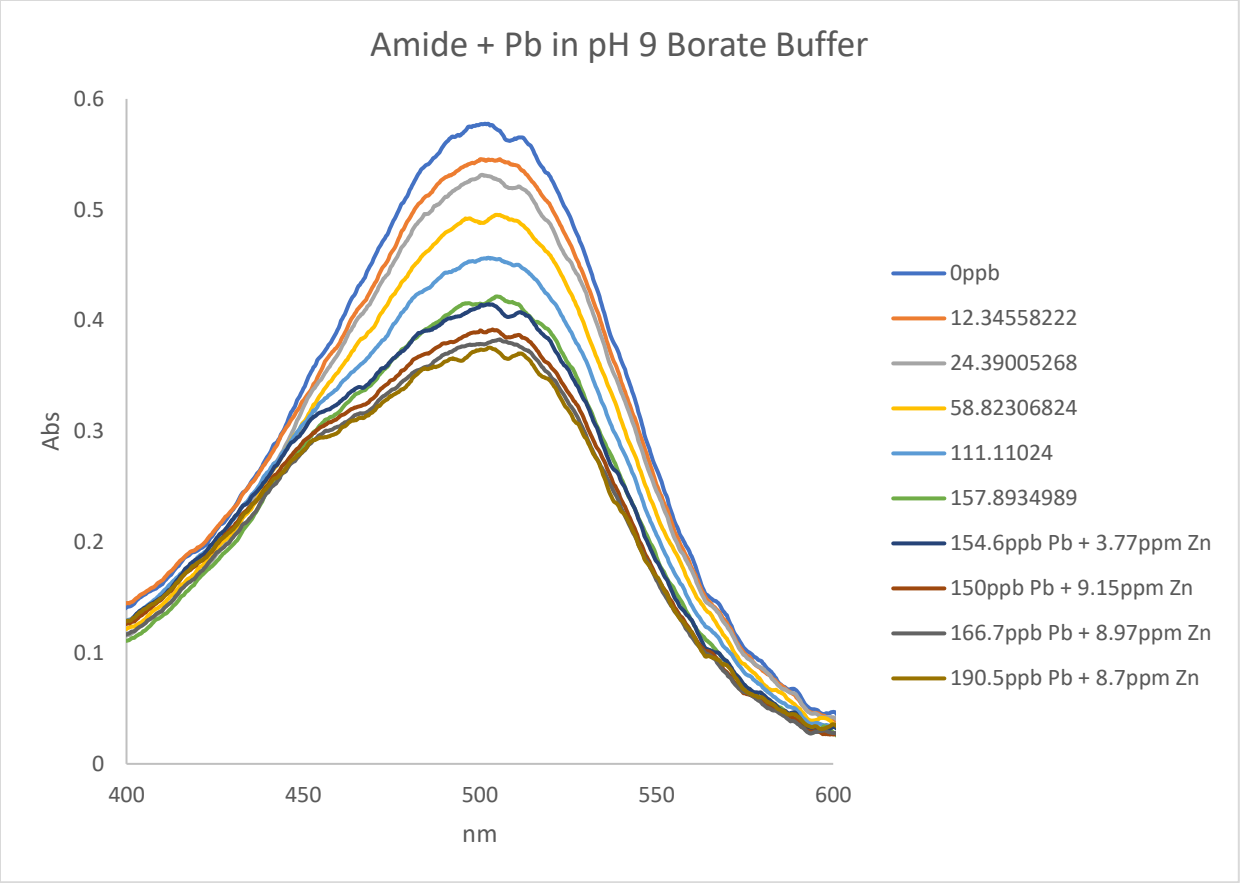

Figure 41: Titration of PbSF1-27A with Pb followed by Zn addition

Figure 40:

Figure 41 shows the first titration with the converted sensor, PbSF1-27A. This sensor demonstrated the ability to respond to Pb in the low ppb, starting with an absorbance decrease with 12ppb Pb in solution. This sensor was titrated with lead until it reached approximately

158ppb Pb, and then a large excess of Zn was added. Close to 4ppm Zn, or 25x the amount of Pb in solution, was added to the dye. There was almost no change in the spectrum at this point. This sort of Zn addition had showed a spectral change when the acid was used instead of the amide. This lends to the belief that the amide form of this sensor is more specific to lead. Upon tripling the amount of Zn, which is 75x the amount of Pb, there is still very little spectral change. Again, this shows a much higher sensitivity for Pb than for Zn. When more Pb was added, there was a small decrease in absorbance showing there is still Pb response.

When this was plotted as a function of Abs vs [Pb], it was found that the R^2 value is exactly 1. This means the line is perfectly straight, even with the Zn addition, and demonstrates that the sensor is able to respond to and detect Pb with a high degree of accuracy. This value was based on a simple decrease in absorbance which is not ideal because it can allow for error in detection. A "ratiable" spectrum is highly preferred, as it gives a second point of reference to ensure the decrease in absorbance is due to response and not something else. In this case, the ratio of 501/440nm has an R^2 of 0.96 and the absorbance of 550nm-440nm plotted vs [Pb] has an R^2 value of 0.98. Both of these are mostly linear, which demonstrates these ratios can be used to determine the concentration of Pb in solution. At the very least, these ratios can serve as a self-check to ensure the decrease in absorbance at 501nm is in fact due to metal ion response.

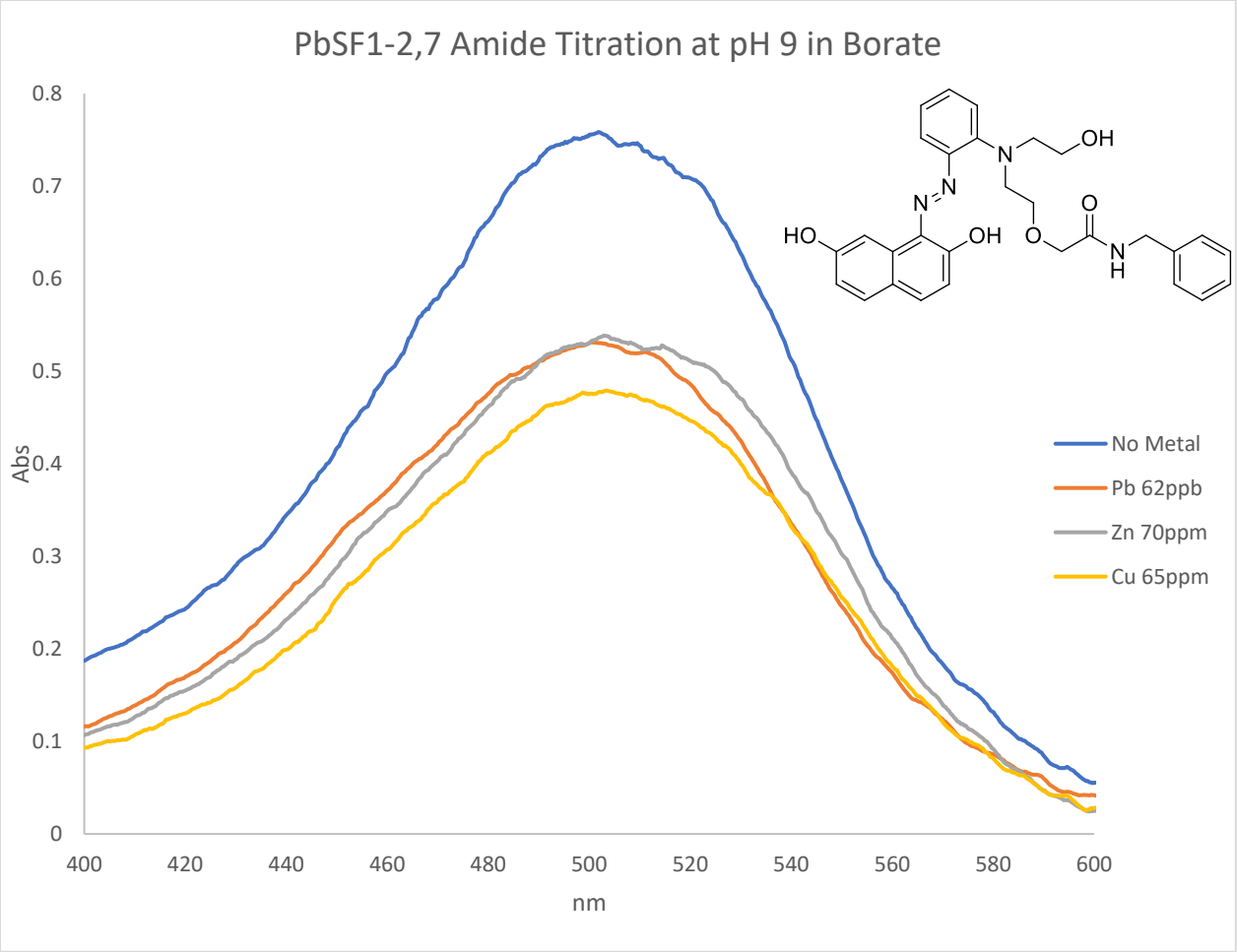

Figure 42: Titration of PbSF1-27A with Pb, Zn, and Cu

Figure 42 further illustrates the higher specificity for Pb that this sensor shows. This sensor is shown to respond in a similar fashion to Pb, Zn, and Cu but at vastly different concentrations. The response to 62ppb Pb is similar to the response to 70ppm Zn or 65ppm Cu. This is a difference of approximately 100x the concentration, meaning PbSF1-27A is around 100x more sensitive to Pb than to Cu or Zn. It was anticipated that the amide form of this sensor would have less of an affinity for small metals than the acid form, but this drastic difference is very promising, as the polymer-bound form of these sensors found in an end stage product would be in amide form.

Unfortunately, the Cu and Zn bound spectra do look very similar to the Pb bound spectrum, but since the sensitivity is so much lower to these smaller ions that it may not be a cause of concern, especially if an array is designed to mitigate any chance of misassigning signal of one metal to another.

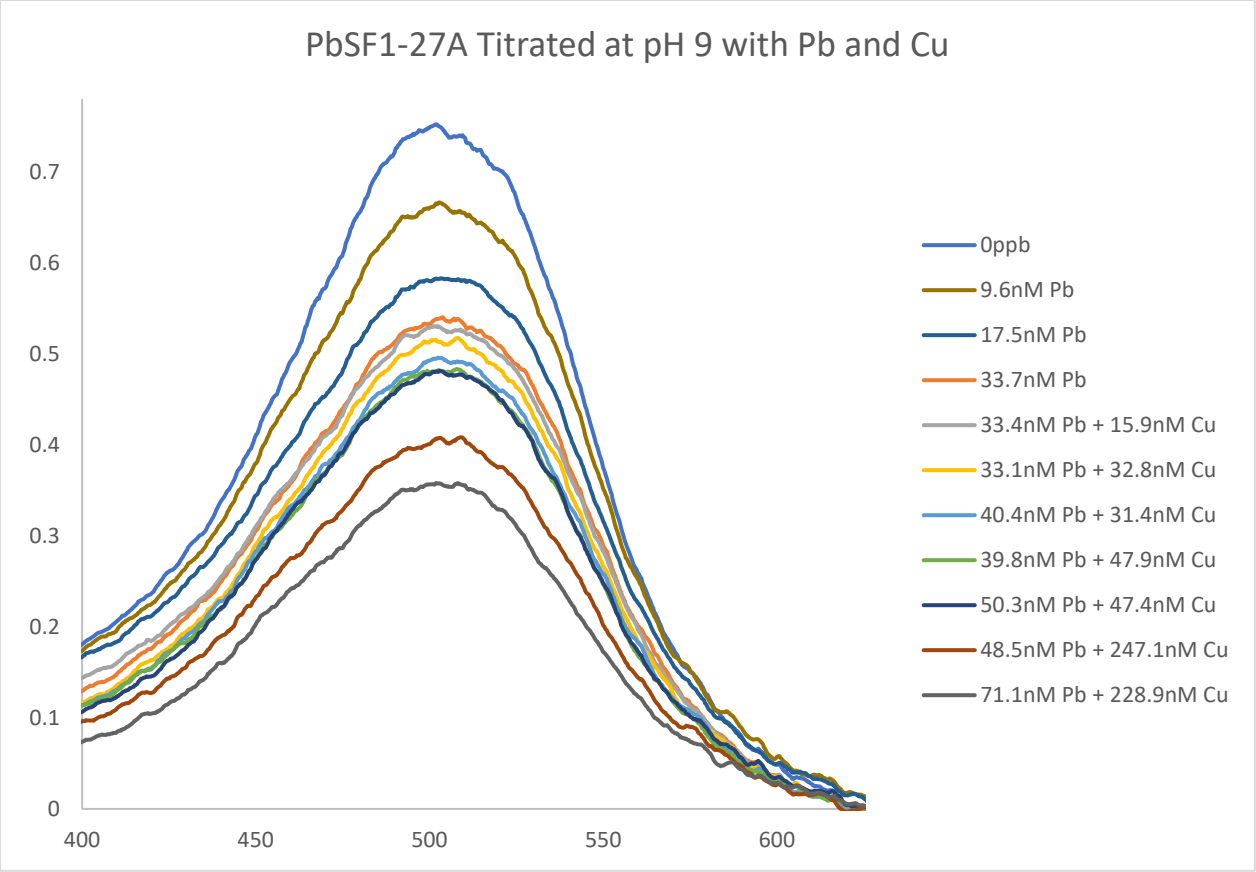

Figure 43a: Titration of PbSF1-27A with Pb and Cu
Figure 43b: Plot of absorbance at max vs [Pb]

Cu is particularly concerning when it comes to having other metals present in solution with these sensors. In every acid form of these sensors, Cu caused a drastic shift in absorbance immediately upon addition, even if the addition was small. *Figure 43a* shows the titration of

PbSF1-27A with Pb in the low ppb range, starting at 3ppb or 9.6nM Pb. The sensor was titrated with Pb up to 33.7nM and then approximately 16nM of Cu was added to solution. The absorbance change upon Cu addition was incredibly minor, and subsequent additions of Cu seem to make minimal changes to the spectrum. There is no shift in absorbance upon binding Cu.

When this is plotted as a function of absorbance vs [Pb] in *figure 43b*, the absorbance at the maximum decreases with an R^2 value of 0.96 despite the additions of Cu. This data is mostly linear despite there being more than 3x the amount of Cu than Pb in solution. In the acid form of this sensor, even a small amount of Cu was enough to entirely upset the spectrum in general appearance and maximum wavelength. Here, the spectrum remains mostly unchanged when Cu is added and the absorbance maximum remains constant. While this absorbance maximum only decreasing instead of shifting is not ideal, it does appear to sense metal ions despite a lack of distinct spectral fingerprint.

This data is promising, as it shows these sensors do work to sense Pb despite inconsistency in data and with other metals in solution. Putting these sensors onto polymer where they are more stable will likely eliminate many detection problems by increasing Pb sensitivity and selectivity as well as dye stability. Turning the sensor into the amide-bound form shows that it increases sensitivity of the sensor for Pb as well as increases selectivity for Pb and decreases response to metals such as Cu and Zn.

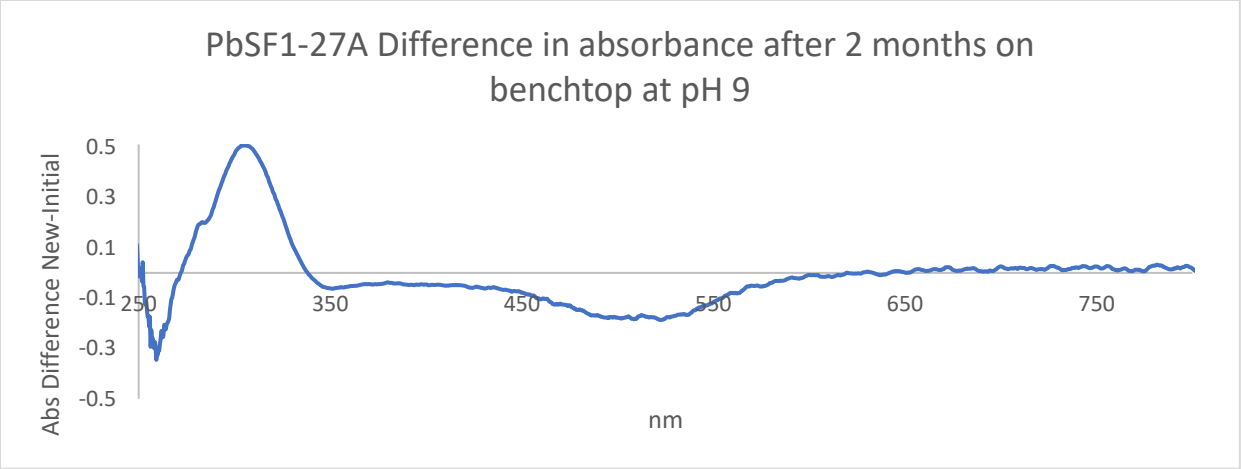

Figure 44: Difference graph showing the net change in absorbance of free dye of PbSF1-27A after 60 days on benchtop

Above, *figure 44* demonstrates the net change in absorbance in the amide form of the sensor after being left on the benchtop for two months with exposure to air and light. There is a net increase in the UV range but a net decrease in the range where the spectral response is shown. This could explain the somewhat lower affinity for Pb that is shown over time with these sensors.

Despite this net change in absorbance, the sensor *does* still respond to Pb after being left out for this extended period of time, and it responds in much the same way as before being left out.

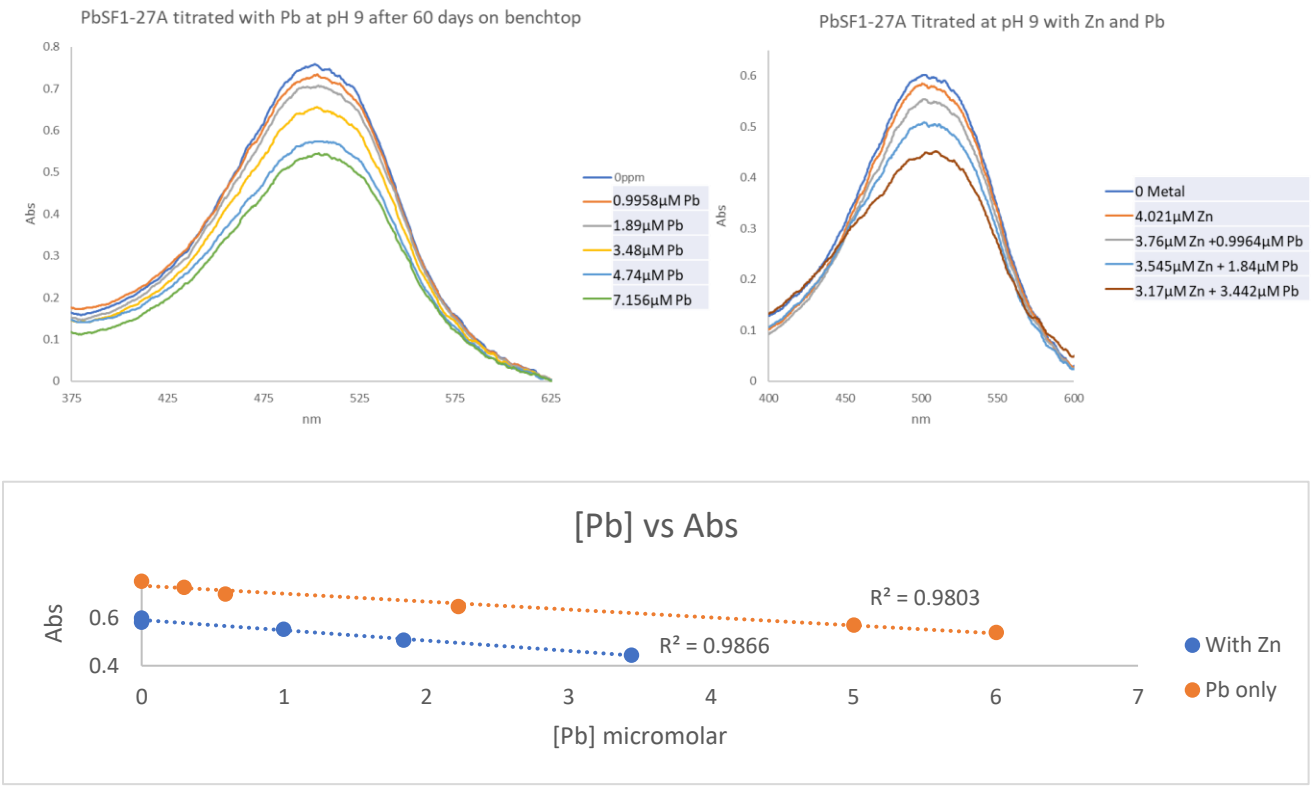

Figure 45a: Titration of PbSF1-27A after 60 days on benchtop with Pb
Figure 45b: Titration of PbSF1-27A after 60 days on benchtop with Zn and Pb
Figure 45c: [Pb] vs Abs graph of titrations

Figure 45 demonstrates the sensor's Pb sensing ability after being left on the benchtop. The sensor is still responding to Pb with a similar maximum absorbance and response. When the sensor is titrated with Pb and the absorbance is plotted against [Pb], the R^2 value is 0.98. This is not quite as good as when the sensor is freshly synthesized ($R^2 = 1$) but demonstrates that the sensor, even after being left out, does respond to Pb. It appears that regardless of contamination or decomposition, these sensors do still work after time has passed – they just appear to be a little bit less ideal. It is suspected that placement onto a polymer would significantly help with this stability.

Since it was determined that these sensors can still be used after time, *figure 45b* shows the sensor titrated by first adding Zn and then titrating with Pb in similar concentrations as

shown in *figure 45a*. When the absorbance vs [Pb] is plotted for this titration with Zn, the R^2 value actually goes *up* to 0.987. This appears to show this sensor can detect Pb even with the presence of Zn in solution, which is very promising. More studies need to be done, particularly with these sensors on polymer.

Placement of these sensors onto polymer is expected to increase their stability and therefore their shelf life. This could prolong ideal response to last for more tests or over the course of weeks if not months.

Even with issues in detection, this proposed device can fulfill a great need as even the best of sensors available commercially have long detection times up to two weeks, are not regenerable, and are not consumer friendly. [66,67,68]

The University of Michigan developed a Pb sensor in 2017 that, while very cost effective, requires a nine-day waiting period before the presence of lead can be determined in the water [50,52]. The proposed sensing device would be nearly instantaneous. This proposed device, while more expensive than some other commercially available Pb tests, is much faster and is able to last longer. With time and enough uses, this machine could become as cost efficient as the University of Michigan's $20 electronic lead sensor. [68] This device will not be less than $20 when it reaches development, as it needs a spectrometer to be functional. However, instead of having to send results off to a lab for development, the device proposed by Advanced Chemical Systems/Novie and the Schwabacher group *would* provide an instant result and could be reused for potentially dozens of tests, if not more. If the array degraded, a new slide with the array could be repurchased at a lower cost than the entire device, making this more affordable after a one-time expense. The results from this device could be interpreted by someone with minimal

chemistry background or understanding, making this a more accessible device to people without formal education.

Proposed Future Directions

This project will continue in the Schwabacher group in collaboration with Advanced Chemical Systems and their new company, Novie. A provisional patent is being issued with intention to pursue a patent and an SBIR grant for further research and development.

Considering the major issue with these sensors is stability, future syntheses will need to be stored in a manner that allows for long term stability. This could be done by limiting exposure to oxygen by storing under active vacuum or under nitrogen. This could also be helped by removing light as well, as sometimes light can cause isomerization of the sensors. One method of storage to try is placing the sensor into a vial in a desiccator under nitrogen and then placing it into the freezer. This way, the sensors will be away from both light and air which would likely give them an extended shelf life. Alternatively, these sensors could be synthesized and directly moved onto the polymer stage to avoid degradation over time.

The primary focus of this project in upcoming years will be placement of lead-specific sensor dyes onto a soluble polymer. Following this, the polymer can be tested in solution and behavior can be analyzed. If these sensors respond well on the soluble polymer, they will then be made into hydrogel polymers on glass.

These sensors could also be modified chemically to provide a stronger response to Pb, by adding functional groups such as a sulfonyl (*scheme 19*), converting already synthesized sensors into amides (*scheme 20*), or converting the OH to an SH (*scheme 21*).

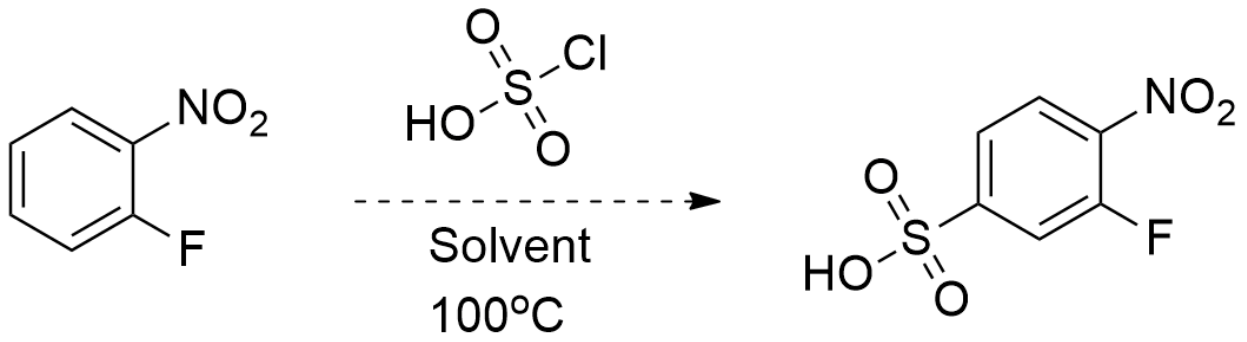

Scheme 19: proposed addition of a sulfonyl group onto sensor

The addition of a sulfonyl group, as shown in *scheme 19* could allow for different changes in absorbance as shown in Trevor Hagemann's dyes in the initial sensor project. The presence of a sulfonyl could cause a more distinct absorbance shift when exposed to metals. This sulfonation has been done before in yields of approximately 54%, and once product is in hand it could be reacted as the non-sulfonated molecule would be to form an end stage sensor in any of the three families. PbSF1 derivatives of this would be of particular interest, as they are the most responsive.

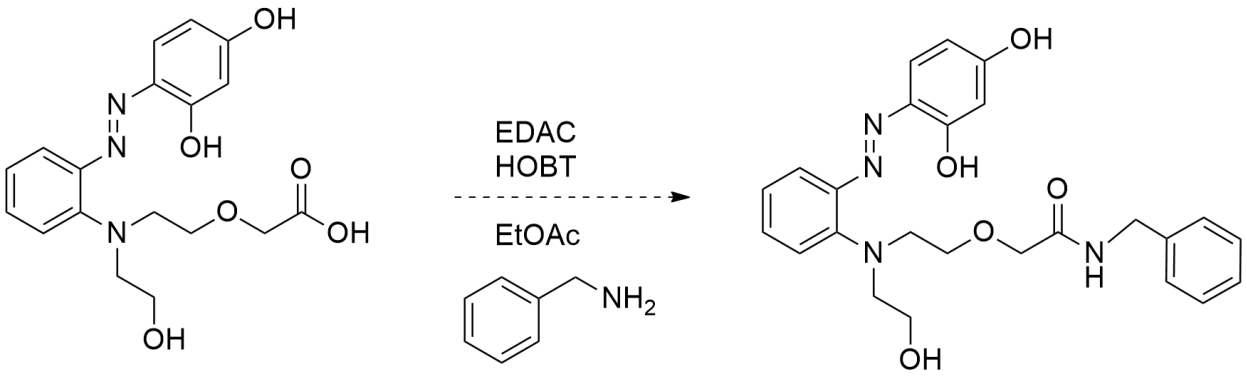

Scheme 20: proposed conversion of sensors such as PbSF1-R into an amide

Another way to increase specificity and sensor response is to convert more of these sensors into amides as shown in *scheme 20.* Conversion into an amide is necessary for putting these sensors onto polymer and has been demonstrated to increase Pb response and decrease

response to other metals in solution. The method used would be the same method that had been used previously to synthesize PbSF1-27A and PbSF1-13A.

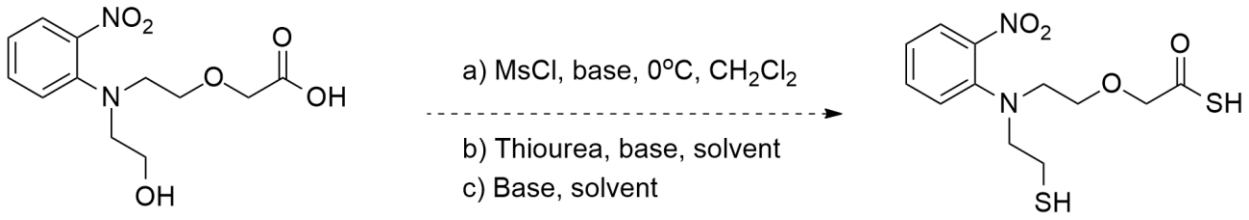

Scheme 21: proposed conversion of hydroxyl to SH on compound 18

If conversion into amide and addition of a sulfonyl are not enough to get a Pb-specific response, changing the carboxylic acid to a thioacid as well as conversion of the OH to an SH may increase specificity, as there is evidence that suggests larger atoms bind better to larger metals such as Pb and Hg and less to small metals such as Zn or Mg. A proposed scheme is shown above in *scheme 21*, with conversion from OH to a mesylate and then to SH using thiourea. There are many ways conversion from an O to a S can be performed and this can be done at nearly any stage in the sensor synthesis scheme.

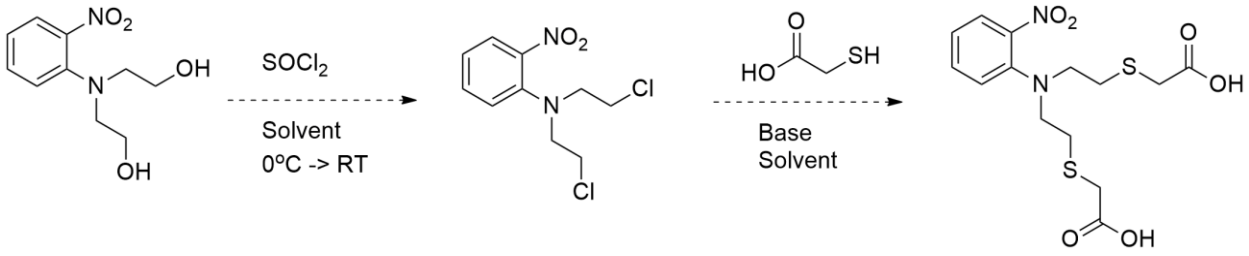

Scheme 22: proposed reaction with thionyl chloride and then reaction with thioglycolic acid

Above, *scheme 22* shows another proposed reaction that could result in a sulfur-based ligand. In this case, a reaction with thionyl chloride would allow for the hydroxyls to become chlorides, and then an alkylation reaction with thioglycolic acid would allow for dialkylation and a product with two sulfur atoms. With careful stoichiometry, it is possible that this reaction could be used to create a monoalkylated product that could be separated by column

chromatography, but it is likely that the dialkylated product would be more stable and could give stronger Pb binding and less small metal binding.

CONCLUSION

Overall, the proposed sensor device fulfills a need that is seen worldwide. This device would be able to detect lead, a harmful and toxic metal, in drinking water in a manner that is widely accessible. The device will be reusable and provide real-time results that can be interpreted with minimal chemistry knowledge, something that is missing from currently commercially available water testing kits.

The synthesized sensors have been demonstrated to work for the desired purpose in the desired detection range of low ppb Pb ions in solution. Future directions for this project will need to focus on putting these sensors onto polymer and performing further testing to determine whether alterations in structure need to be made to get optimal results. An array of these sensors still needs to be determined, but this array can be built of all three Pb sensor families described in *scheme 15,* as well as some of Hagemann's small metal sensors that have been characterized as well in the previous metal sensing collaboration.

This project shows a lot of promise but must undergo further testing before it is finished. Should these sensors pass through the next testing phase, a device could then be developed for their use in testing drinking water. A provisional patent is being sought after in regard to the new sensor dyes made for this project with the end-goal of producing a marketable device for widespread use of this technology.

Experimental

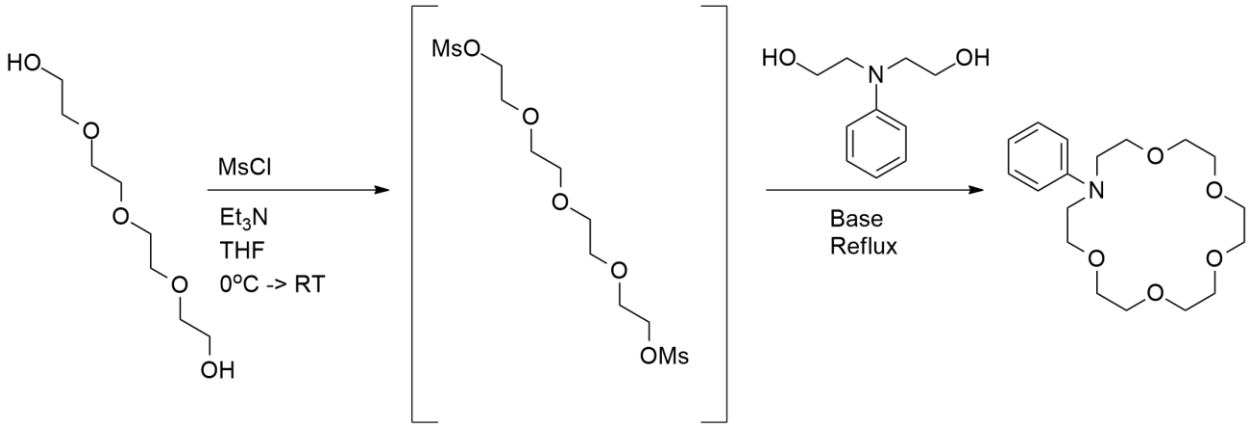

Preparation of 13a, 14

5mL of tetraethylene glycol was suspended in toluene by heating and then concentrated to dryness to avoid the presence of water. This was then suspended in THF with triethylamine and mesyl chloride at 0 degrees and let warm to RT overnight.

Method 1: Once reaction was complete by TLC, base was added and the reaction mixture was heated and stirred. Phenyl diethanolamine in THF was added in an addition funnel over the course of multiple hours. This was allowed to react until all starting material gone by TLC and was then diluted into EtOAc and washed with water and brine and concentrated to dryness.

Method 2: Once reaction was complete by TLC the mixture was concentrated to dryness and resuspended in solvent. Base was warmed in THF with phenyl diethanolamine and TEG dimesylate was added dropwise over the course of hours. This was then worked up by concentrating to dryness and running a silica plug in 40% EtOAc in hexanes.

Method 3: Once reaction was complete by TLC it was put into an addition funnel with phenyl diethanolamine and this was added dropwise to warm base. Once complete by TLC, this was concentrated to dryness.

Preparation of **15**

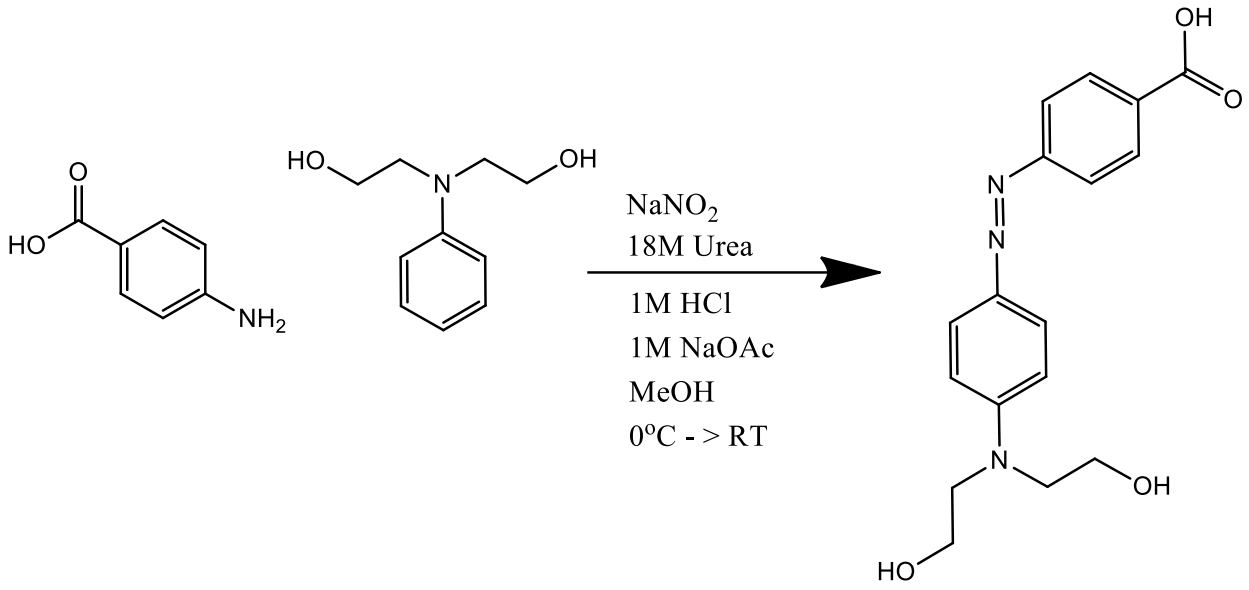

Dissolve 4-aminobenzoic acid (0.26g / 0.064mmol) in 10mL 1M HCl and chill to 0. Added 1.8mL of 1M $NaNO_2$ while keeping temperature below 5. Added nitrite until positive to KI paper. Then, added 18M urea dropwise and tested on KI paper until negative.

Then, in a separate flask, N-phenyl diethanolamine (0.32g / 1.8 mmol) was combined with 20mL of 1M NaOAc (2x the volume of HCl) with 8mL of MeOH for solubility. This solution was chilled to 0, and then the aminobenzoic acid solution was added dropwise, keeping temperature below 5. This was then allowed to warm to RT overnight, and was pH tested to ensure it was pH >3 but <7. Then the reaction was filtered and put under vacuum.

Yield = 0.54g = 93%

Note: During the nitrite addition, if temperature rises to quickly NO will be produced. Brown/orange gas. If aminobenzoic acid/nitrite solution has any color to it, nitrite was added a little too quickly.

Preparation of: 4-((4-(bis(2-(quinolin-8-yloxy)ethyl)amino)phenyl)diazenyl)benzoic acid

16a

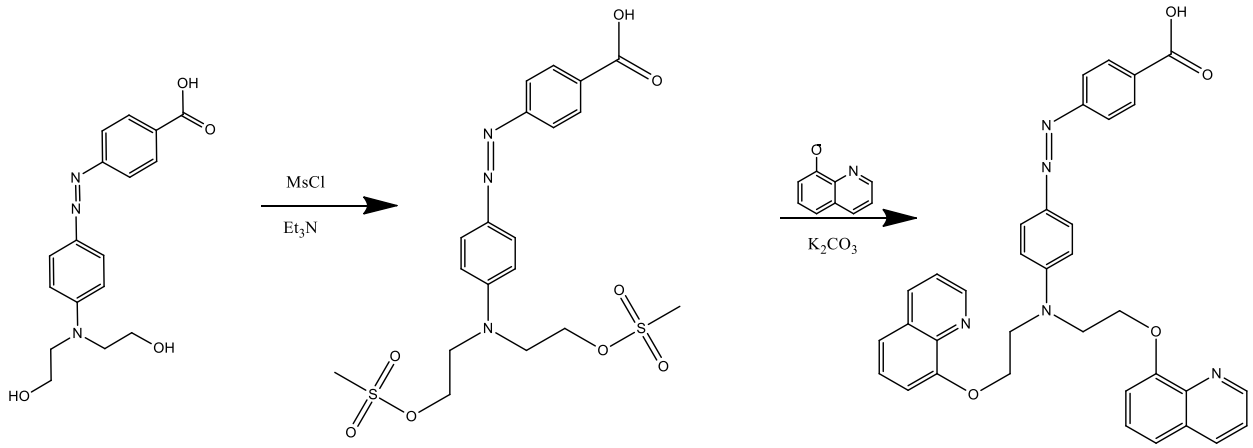

15 was dissolved in CH_2Cl_2 and chilled to 0. 2+ equivalents of Mesyl Chloride was added, and then 2+ equivalents of Et_rN was added. The condenser was attached, the reaction mix was warmed to RT, and this was allowed to react until TLC showed the starting material was gone.

NOTE: this reaction makes a “mustard” and thus this intermediate is not isolated.

Once the starting material is reacted, 3+ equivalents of 8-hydroxyquinoline and a couple scoopfuls of potassium carbonate were added to the reaction mixture. This was allowed to react at RT overnight.

The reaction was washed 3x75mL of water, and 1x75mL brine. Then the dichloromethane was dried over sodium sulfate, filtered, and concentrated and put under vacuum.

Preparation of: ethyl 4-((4-(bis(2-hydroxyethyl)amino)phenyl)diazenyl)benzoate **15a**

Notebook page reference: KDW-1-184

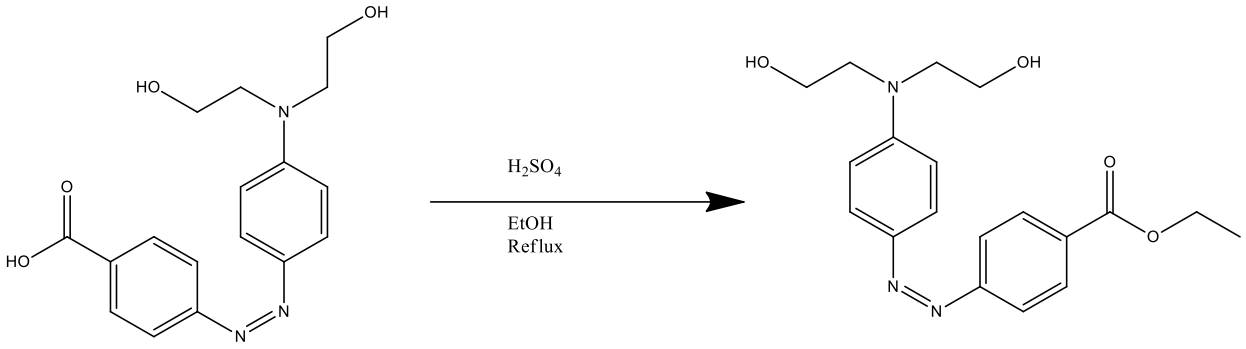

Put 4-((4-(bis(2-hydroxyethyl)amino)phenyl)diazenyl)benzoic acid (acid form of dye, **15**) into ethanol with 2 drops of sulfuric acid. Set to reflux. When done by TLC, concentrated to dryness, resuspended in dichloromethane, washed 2x75mL saturated bicarb, 2x75mL water, 1x75mL brine, dried over sodium sulfate, filtered, concentrated and put under vacuum. Crystallized from dichloromethane/hexanes.

HNMR (500): 8.15ppm (D,2); 7.89 (Q,2); 6.79 (D,2); 4.42 (Q,2); 3.97 (T, 4); 3.75 (M, 4); 1.42 (T, 3); 1.25 (T,2)

Preparation of: 2,2'-((2-nitrophenyl)azanediyl)diethanol ; ortho nitrophenyldiethanolamine, **17**

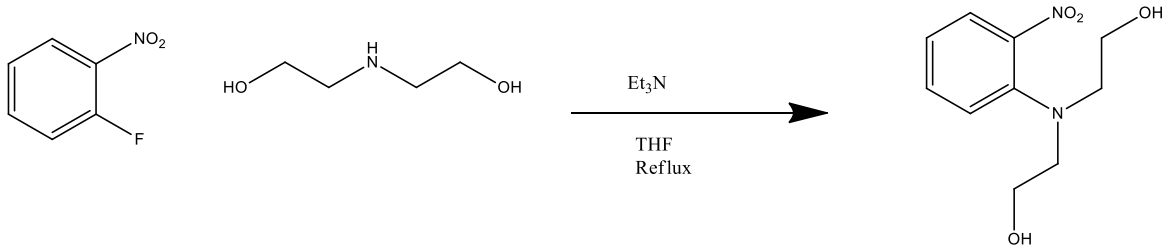

1-fluoro-2-nitrobenzene (0.12mL / 1.05mmol) was combined with diethanolamine (0.1mL / 1mmol) in a dried RBF in dry THF. Triethylamine was added, and the reaction was set to reflux.

When finished by TLC (10% MeOH in CH_2Cl_2), the reaction was poured into EtOAc and extracted with 3x50mL of 0.5M HCl (pH tested to make sure acidic enough). The acidic layer was combined with dichloromethane and saturated carbonate until basic to pH paper. Product was extracted from the acidic layer with dichloromethane (3x30mL) and concentrated.

HNMR (CDCl3): 7.70 (d, 1H); 7.57 (d, 1H); 7.40 (d, 1H); 7.15 (d, 1H); 3.69 (t, 4H); 3.36 (t, 4H)

Preparation of: tert-butyl 2-(2-((2-hydroxyethyl)(2-nitrophenyl)amino)ethoxy)acetate, **18**

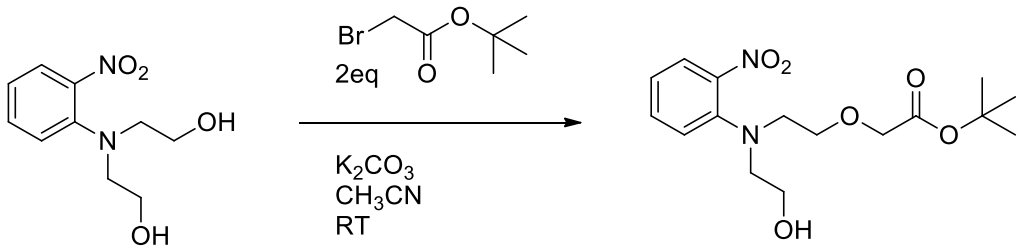

1.28g nitrophenyl diethanolamine **17** (5.66mmol) was combined with 1.8mL t-butyl bromoacetate (12.2 – excess) in acetonitrile with an excess of potassium carbonate and left to stir at room temp for 5 days. When done by TLC (10% acetonitrile in dichloromethane), the reaction was filtered, concentrated, and resuspended in dichloromethane. This was washed with water and brine, dried over sodium sulfate, and then concentrated. This was purified by column using EtOAc to get a yield of 68%.

HNMR (CDCl3): 7.70 (d, 1H); 7.51 (t, 1H); 7.42 (d, 1H); 7.03 (t, 1H); 4.53 (t, 4H); 3.55 (t, 2H); 3.52 (t, 2H); 3.47 (t, 2H); 3.19 (t, 2H); 1.39 (s, 9H)

Preparation of: di-tert-butyl 2,2'-((((2-nitrophenyl)azanediyl)bis(ethane-2,1-diyl))bis(oxy))diacetate **19**

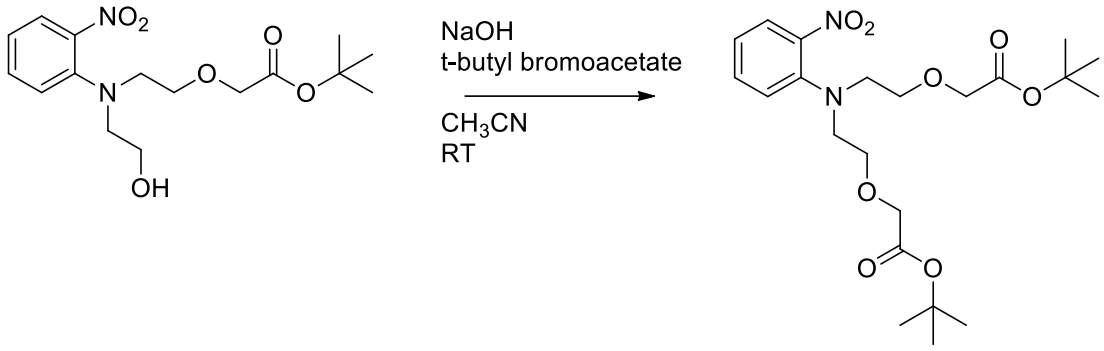

Dissolved **18** in acetonitrile and added powderized NaOH. Added t-butyl bromoacetate and allowed to stir overnight. Worked up by washing with hexanes 2x75mL, concentrating to dryness, resuspending in dichloromethane, washing with water with acetic acid 1x75mL, water 2x100mL, brine 1x50mL. Dried over magnesium sulfate, filtered, concentrated to dryness.

Preparation of: di-tert-butyl 2,2'-((((2-aminophenyl)azanediyl)bis(ethane-2,1-diyl))bis(oxy))diacetate

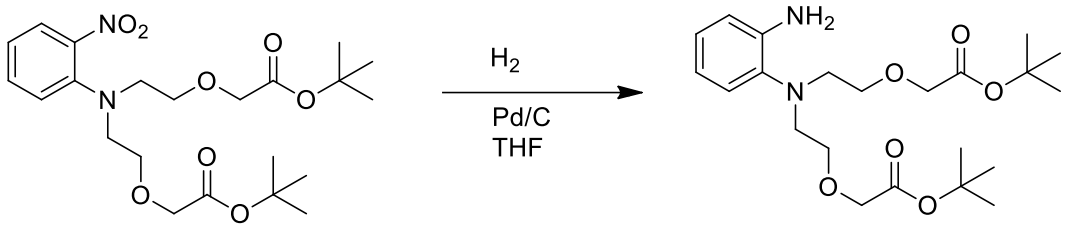

1.32g of **19** was suspended in 50mLTHF with 0.021g Pd/C, and the flask was flushed with H_2. Reaction was left stirring at RT for 18h. Once finished, the reaction was filtered through celite and concentrated to dryness. Product is a clear oil, 99% yield. Not stable in air.

Preparation of: *tert*-butyl 2-(2-((2-nitrophenyl)2-(quinoline-2-yloxy)ethyl)amino)ethoxy)acetate **20a**

Structure:

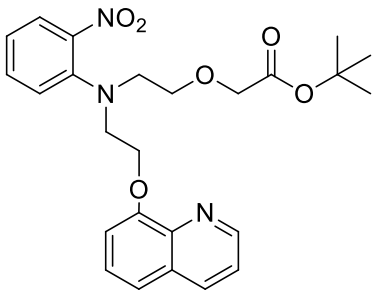

0.304g (0.73mmol) of compound **20** was dissolved in acetonitrile. 0.155g (1.1mmol) of 8-hydroxyquinoline and multiple scoops of potassium carbonate were added to solution. The reaction mixture was refluxed overnight, and was done by TLC ~18h later (10% acetonitrile in dichloromethane).

The reaction was filtered and concentrated to dryness, and then resuspended in dichloromethane. This was then washed with water 2x75mL, dilute acetic acid (2mL acetic acid in 50mL water), and then brine 1x75mL. The organic layer was dried over magnesium sulfate and concentrated to dryness via rotary evaporation.

The resulting solid was contaminated with 8-hydroxyquinoline, so it was triturated in ether and then filtered, and the filtrate was concentrated to dryness. This trituration procedure was repeated. Following this, a silica plug was run on the solid left behind. The 8-hydroxyquinoline was pushed through first using 10% acetonitrile in dichloromethane. The product was collected using methanol. The methanol fraction was concentrated to dryness and resuspended in dichloromethane. This was then dried using magnesium sulfate and concentrated to dryness once more for a yield of 0.111g, or 33%*

Product is a yellow/brown oil.

*Some product was lost during triturations, filtration, etc.

HNMR (CDCl3): 8.94 (d of d, 1H); 8.15 (d of d, 1H); 7.69 (d of d, 1H); 7.49 (d, 1H); 7.46 (m, 4H); 7.10 (d of d, 2H); 4.41 (t, 2H); 3.93 (s, 2H); 3.91 (t, 2H); 3.71 (t, 2H); 3.54 (t, 2H); 1.46 (s, 9H)

Preparation of: (E)-2-(2-((2-hydroxyethyl)(2-((2-hydroxynaphthalen-1-yl)diazenyl)phenyl)amino)ethoxy)acetic acid **18b**

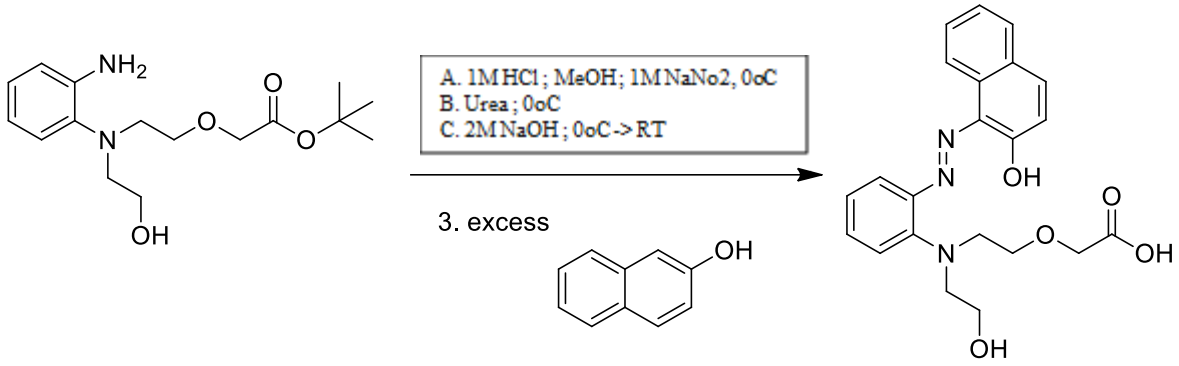

Dissolved amine (~0.2mmol) in 1M HCl and chilled to 0. Added 0.3mL of 1M $NaNO_2$ dropwise, and then added saturated urea to get rid of excess nitrite.

Dissolved 2-naphthol in 2M NaOH (same volume as HCl) and chilled to 0. Added acid solution dropwise, keeping temperature under 5 degrees. Once addition finished, allowed to warm to RT.

After 12h, acidified with acetic acid, extracted into EtOAc, washed with carbonate and then brine, dried, and filtered.

Triturated in ether, concentrated. Purified via silica plug using 10% acetonitrile in dichloromethane.

HNMR (CDCl3): 8.50 (d, 1H); 8.13 (q, 1H); 7.74 (d, 1H); 7.58 (t, 2H); 7.43 (t, 3H); 7.33 (q, 1H); 6.85 (d, 1H); 4.09 (s, 2H); 3.68 (q, 4H); 3.28 (t, 2H); 2.10 (s, 1H)

Preparation of: (*E)*-2-(2-((2-((2,7-dihydroxynaphthalen-1-yl)diazenyl)phenyl)(2-hydroxyethyl)amino)ethoxy)acetic acid, PbSF1-27, **18e**

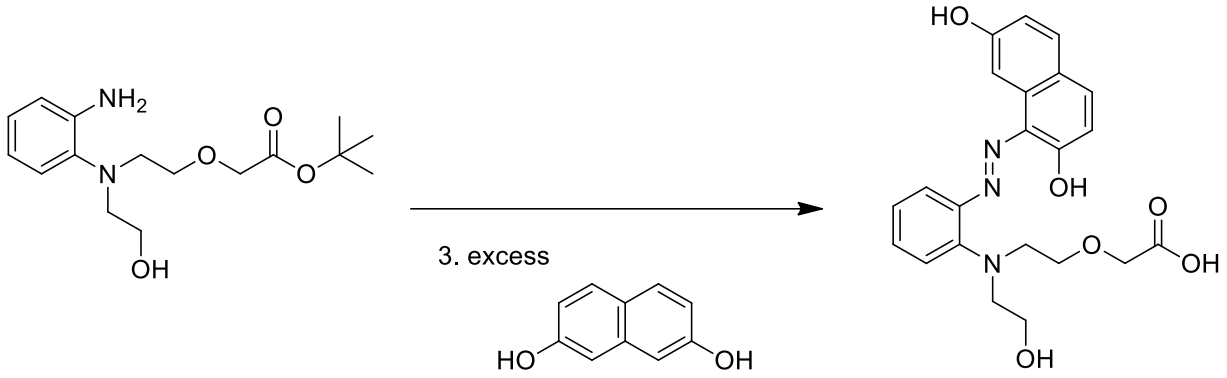

0.26mmol of amine compound was dissolved in 1M HCl and chilled to 0 degrees. 0.2mL (0.2mmol) of 1M NaNO2 was added to solution, careful to keep temperature under 5 degrees. 18M urea was added to solution and solution was stirred 5m to neutralize excess nitrite.

In a separate flask, 0.048g (0.31mmol) of 2,7-dihydroxynaphthalene was dissolved in 2M NaOH (2x the volume of 1M HCl) and chilled to 0 degrees.

The acidic solution was added to the basic solution, allowed to warm to RT and stirred overnight.

The solution was made acidic with acetic acid, and extracted into ethyl acetate. The ethyl acetate was washed with brine and dried over magnesium sulfate (some product is lost to Mg sulfate) and then filtered and dried via rotary evaporation.

The resulting solid was purified by dissolving in acetate, excess naphthol was extracted into ether. The acetate was then acidified using HCl, and the product was extracted into ethyl

acetate, dried over magnesium sulfate, filtered, and dried via rotary evaporation. Following this, the product was purified via silica plug using 10% acetonitrile in dichloromethane followed by rotary evaporation.

Preparation of: (E)-2-(2-((2-((2,4-dihydroxyphenyl)diazenyl)phenyl)(2-hydroxyethyl)amino)ethoxy)acetic acid (any PbSF1 sensor)

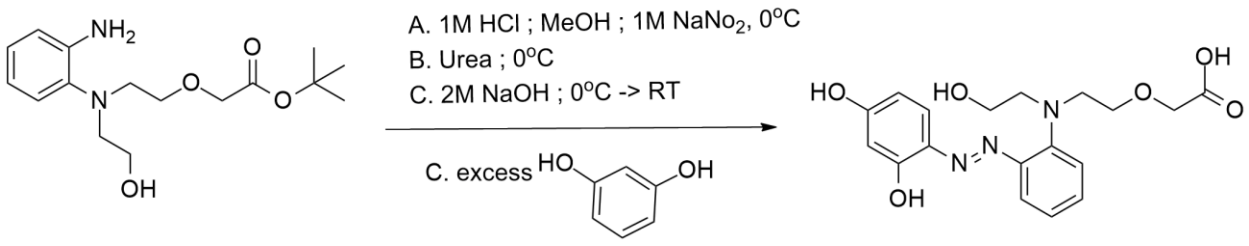

Amine of **18** suspended in 7mL of 1M HCl. This was chilled to 0, and 2.4mL of 1M $NaNO_2$ was added dropwise, keeping temp <5. Urea was added to consume excess nitrite (until negative to KI paper – if not negative after ~1mL, move on anyway).

0.23g of naphthol (in this case, resorcinol) (0.201mmol) was suspended in 14mL of 1M NaOH (2x acid) with ~5mL of methanol for solubility. This was chilled to 0. The acid solution was added dropwise, keeping temp <5. Once addition was complete, reaction was allowed to warm to RT overnight.

Reaction was acidified using acetic acid, and extracted into ethyl acetate. This was washed 3x with carbonate, 2x brine, and concentrated to dryness. This was then tritrated in ether at room temp over the weekend to get rid of excess naphthol. Sensors are purified through silica plug using 10% acetonitrile in dichloromethane, followed by 10% ethyl acetate in hexanes, followed by 10% ethanol in dichloromethane, followed by methanol to remove sensor from silica.

Synthesis of sensors **19a-g; PbSF2**

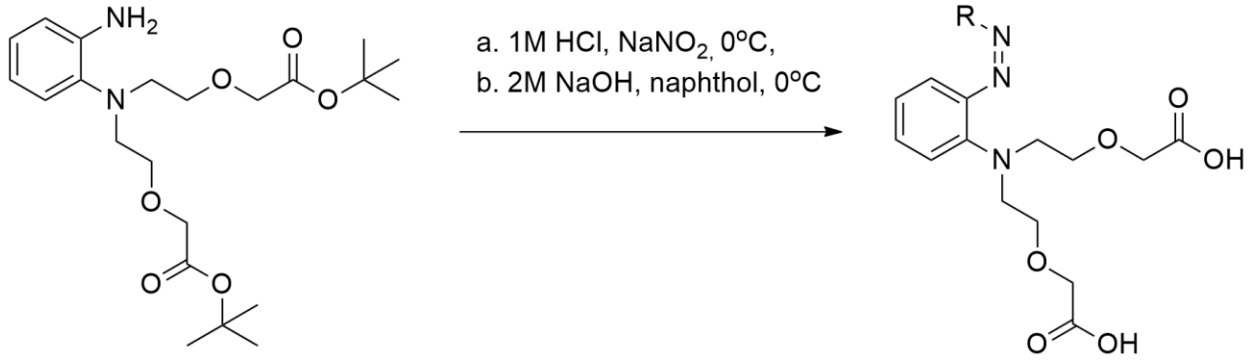

Amine of **19** is suspended in 1M HCl and chilled to 0 degrees. 1M sodium nitrite was added slowly dropwise keeping temperature at 0 degrees. Urea was added to consume excess nitrite and reaction was stirred 15m.

A separate flask with 2M NaOH and naphthol was prepared and chilled to 0 degrees. The acidic solution was added dropwise to the basic solution and reaction was left to stir overnight,

Workup was performed by acidifying with acetic acid and extracting into EtOAc followed by a wash with brine. This was concentrated to dryness and triturated with diethyl ether overnight, followed by a silica plug with 10% acetonitrile in dichloromethane.

Yields range from 11-29%

Synthesis of **20**

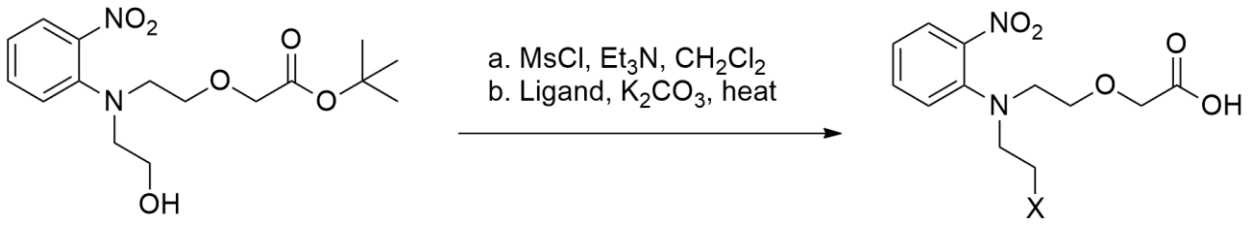

Compound **18** was suspended in dichloromethane with mesyl chloride and triethylamine at 0 degrees and allowed to warm to RT overnight until done by TLC. The reaction could then either have ligand added directly in excess with carbonate and heat until reaction is marked complete by TLC, OR the reaction can be washed with brine and concentrated to dryness before resuspending in solvent and reacting with excess ligand.

Workup proceeds by washing with water and brine, followed by drying over sodium sulfate and then rotary evaporation until dry.

Isolation is highly varied but generally involves a silica plug of 10% acetonitrile in dichloromethane followed by a column and/or crystallization.

Yields for these reactions ranged from 0-35%

(E)-N-benzyl-2-(2-((2-((3,6-dihydroxynaphthalen-2-yl)diazenyl)phenyl)(2-hydroxyethyl)amino)ethoxy)acetamide

Preparation of any version of compound **25**

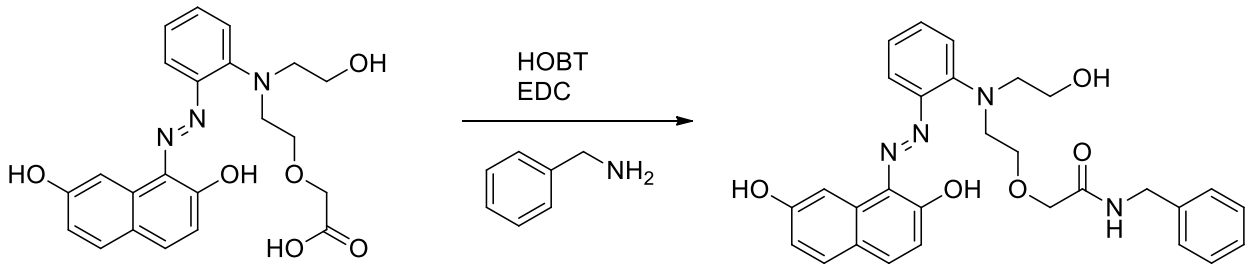

Dissolved 0.0078g (0.02mmol) KDW-2-158b (monoalkylated 2,7 sensor) in EtOAc and added 0.0117g (0.09mmol) HOBT and stirred 10m. Added 0.025mL (0.23mmol) of benzylamine and stirred 5m. Added 0.0126g (0.08mmol) EDAC and stirred overnight until complete by TLC (10% CH3CN in CH2Cl2 ; EtOAc).

Once complete by TLC, washed with 50mL water + 5mL acetic acid, then 2x75mL water, then brine. Dried over sodium sulfate, filtered, and concentrated to dryness. Yield of 31%. Product is a red solid, less water soluble than starting material, runs differently by TLC in amino acid eluent.

References

(1) Kyba, E. P.; Helgeson, R. C.; Madan, K.; Gokel, G. W.; Tarnowski, T. L.; Stephen Moore, lb S.; Cram, D. J. *Host-Guest Complexation. 1. Concept and Illustration13*; UTC, 2021; Vol. 20.

(2) Braegelman, A.S.; Webber, M. J. Integrating Stimuli-Responsive Properties in Host-Guest Supramolecular Drug Delivery Systems; *Europe PMC* **2019**, 9(11):3017-3040

(3) Zhang, X.; Whitten, D. G. Preface to the Supramolecular Chemistry at Interfaces Special Issue. *Langmuir*. February 15, 2011, p 1245. https://doi.org/10.1021/la104879j.

(4) Pedersen, C. J. Cyclic Polyethers and Their Complexes with Metal Salts. *J. of the Am. Chem. Soc.* **1967**, *89* (10). https://doi.org/10.1021/ja00986a052.

(5) Izatt, R. M. Charles J. Pedersen's Legacy to Chemistry. *Chem. Soc. Rev.* **2017**, *46* (9). https://doi.org/10.1039/C7CS00128B.

(6) Sears, M. E. Chelation: Harnessing and Enhancing Heavy Metal Detoxification—A Review. *The Scientific World Journal* **2013**, *2013*. https://doi.org/10.1155/2013/219840.

(7) Smulders, M. M. J.; Zarra, S.; Nitschke, J. R. Quantitative Understanding of Guest Binding Enables the Design of Complex Host-Guest Behavior. *J. of the Am. Chem. Soc.* **2013**, *135* (18), 7039–7046. https://doi.org/10.1021/ja402084x.

(8) Host-Guest Chemistry. http://www1.biologie.uni-hamburg.de/b-online/library/newton/Chy251_253/Lectures/HostGuest/Host-Guest.html

(9) Breijyeh, Z., Jubeh, B., & Karaman, R. (2020). Resistance of Gram-Negative Bacteria to Current Antibacterial Agents and Approaches to Resolve It. *Molecules (Basel, Switzerland)*, *25*(6), 1340. https://doi.org/10.3390/molecules25061340

(10) Spedding, F. H.; Porter, P. E.; Wright, J. M. *The Acid Dissociation Constants of Diethylenetriaminepentaacetic Acid and the Stability Constants of Some of Its Metal Chelates1*; 1952; Vol. 74.

(11) Olson, D. C.; Margerum Vol, D. W.; C Olson, B. D.; Margerum, D. W.; Theor, E.; HeYClg Exptl, assuming. *Downloaded via UNIV OF WISCONSIN-MILWAUKEE On*; UTC, 1952; Vol. 74.

(12) Rodell, C. B.; Mealy, J. E.; Burdick, J. A. Supramolecular Guest-Host Interactions for the Preparation of Biomedical Materials. *Bioconjugate Chemistry*. American Chemical Society December 16, 2015, pp 2279–2289. https://doi.org/10.1021/acs.bioconjchem.5b00483.

(13) Noinaj, N.; Gumbart, J.C.; Buchanan, S.K. The Beta-barrel assembly machinery in motion, *Nature Reviews Microbiology* April 2017, Vol 15, 197-204

(14) Hagan, C.L.; Silhavy, T.J.; Kahne D. Beta-Barrel Membrane Protein Assembly by the Bam Complex. *Annual Reviews Biochemistry* 2011 vol 80 189-210

(15) Hagan, C. L.; Westwood, D. B.; Kahne, D. Bam Lipoproteins Assemble BamA in Vitro. *Biochemistry* **2013**, *52* (35), 6108–6113. https://doi.org/10.1021/bi400865z.

(16) Freinkman, E.; Okuda, S.; Ruiz, N.; Kahne, D. Regulated Assembly of the Transenvelope Protein Complex Required for Lipopolysaccharide Export. *Biochemistry* **2012**, *51* (24), 4800–4806. https://doi.org/10.1021/bi300592.

(17) May, K. L.; Grabowicz, M. The Bacterial Outer Membrane Is an Evolving Antibiotic Barrier. *Proceedings of the National Academy of Sciences* **2018**, *115* (36). https://doi.org/10.1073/pnas.1812779115.

(18) Doerner, P. A.; Sousa, M. C. Extreme Dynamics in the BamA β-Barrel Seam. *Biochemistry* **2017**, *56* (24). https://doi.org/10.1021/acs.biochem.7b00281.

(19) Tomasek, D.; Rawson, S.; Lee, J.; Wzorek, J. S.; Harrison, S. C.; Li, Z.; Kahne, D. Structure of a Nascent Membrane Protein as It Folds on the BAM Complex. *Nature* **2020**, *583* (7816). https://doi.org/10.1038/s41586-020-2370-1.

(20) Plummer, A. M.; Fleming, K. G. BamA Alone Accelerates Outer Membrane Protein Folding In Vitro through a Catalytic Mechanism. *Biochemistry* **2015**, *54* (39). https://doi.org/10.1021/acs.biochem.5b00950.

(21) Heuck, A.; Schleiffer, A.; Clausen, T. Augmenting β-Augmentation: Structural Basis of How BamB Binds BamA and May Support Folding of Outer Membrane Proteins. *Journal of Molecular Biology* **2011**, *406* (5). https://doi.org/10.1016/j.jmb.2011.01.002.

(22) Kemp, D. S.; Bowen, B. R.; Muendel, C. C. Synthesis and Conformational Analysis of Epindolidione-Derived Peptide Models for .Beta.-Sheet Formation. *The Journal of Organic Chemistry* **1990**, *55* (15). https://doi.org/10.1021/jo00302a033.

(23) Nowick, J. S. Exploring β-Sheet Structure and Interactions with Chemical Model Systems. *Accounts of Chemical Research* **2008**, *41* (10), 1319–1330. https://doi.org/10.1021/ar800064f.

(24) Graf, G.I., et al The Synthesis of Aromatic Diazatricycles from Phenylenediamine-bis(methylene Meldrum's acid) derivatives *Tetrahedron*, 58 (44), 9095-9100

(25) Doyle, M.P.; Terpstra, J.W.; Pickering, R.A.; LePoire, D.M.; Hydrolysis, nitrosyl exchange, and synthesis of alkyl nitrites *J. Org. Chem.* 1983, 48, 20, 3379–3382

(26) Nowick, J.S.; Kreutzer, A.G.; Elucidating the structures of amyloid oligomers with macrocyclic beta-hairpin peptides: insights into Alzheimer's Disease and other amyloid diseases *Acc. Chem. Res.* 2018, 51, 706-718

(27) Weiner, W.S.; Hamilton, A.D.; Synthesis and binding studies of a 1-alkyl-3,6-diamino-4-quinolone based receptor for N-acylated dipeptides *Bioorg. & Med. Chem. Lett.* 8 (1998) 681-686

(28) Michne, W.F.; Shroeder, J.D.; Design and synthesis of a beta-strand inducer *Peptide Process Rev.* 47 (1996) 2-8

(29) Jaishankar, M.; Tseten, T.; Anbalagan, N.; Mathew, B. B.; Beeregowda, K. N. Toxicity, Mechanism and Health Effects of Some Heavy Metals. *Interdisciplinary Toxicology* **2014**, *7* (2). https://doi.org/10.2478/intox-2014-0009.

(30) Rabin, R. The Lead Industry and Lead Water Pipes "A MODEST CAMPAIGN." *American Journal of Public Health* **2008**, *98* (9). https://doi.org/10.2105/AJPH.2007.113555.

(31) Dingle, A. The Flint Water Crisis: What's really going on? https://www.acs.org/content/acs/en/education/resources/highschool/chemmatters/past-issues/2016-2017/december-2016/flint-water-crisis.html.

(32) Reddy, A.; Braun, C. L. Lead and the Romans. *Journal of Chemical Education* **2010**, *87* (10). https://doi.org/10.1021/ed100631y.

(33) Payne, M. Lead in Drinking Water. *Canadian Medical Association Journal* **2008**, *179* (3). https://doi.org/10.1503/cmaj.071483.

(34) Wani, A. L.; Ara, A.; Usmani, J. A. Lead Toxicity: A Review. *Interdisciplinary Toxicology* **2015**, *8* (2). https://doi.org/10.1515/intox-2015-0009.

(35) Azeh Engwa, G.; Udoka Ferdinand, P.; Nweke Nwalo, F.; N. Unachukwu, M. Mechanism and Health Effects of Heavy Metal Toxicity in Humans. In *Poisoning in the Modern World - New Tricks for an Old Dog?*; IntechOpen, 2019. https://doi.org/10.5772/intechopen.82511.

(36) Hauptman, M.; Bruccoleri, R.; Woolf, A. D. An Update on Childhood Lead Poisoning. *Clinical Pediatric Emergency Medicine* **2017**, *18* (3). https://doi.org/10.1016/j.cpem.2017.07.010.

(37) Renner, R. Exposure on Tap: Drinking Water as an Overlooked Source of Lead. *Environmental Health Perspectives* **2010**, *118* (2). https://doi.org/10.1289/ehp.118-a68.

(38) Tchounwou, P. B.; Yedjou, C. G.; Patlolla, A. K.; Sutton, D. J. Heavy Metal Toxicity and the Environment; 2012. https://doi.org/10.1007/978-3-7643-8340-4_6.

(39) Renu; Agarwal, M.; Singh, K. Heavy Metal Removal from Wastewater Using Various Adsorbents: A Review. *Journal of Water Reuse and Desalination* **2017**, *7* (4). https://doi.org/10.2166/wrd.2016.104.

(40) Fu, F.; Wang, Q. Removal of Heavy Metal Ions from Wastewaters: A Review. *Journal of Environmental Management* **2011**, *92* (3). https://doi.org/10.1016/j.jenvman.2010.11.011.

(41) Baysal, A.; Ozbek, N.; Akm, S. Determination of Trace Metals in Waste Water and Their Removal Processes. In *Waste Water - Treatment Technologies and Recent Analytical Developments*; InTech, 2013. https://doi.org/10.5772/52025.

(42) BEEK, H. C. A. van; HEERTJES, P. M. Fading by Light of Organic Dyes on Textiles and Other Materials. *Studies in Conservation* **1966**, *11* (3). https://doi.org/10.1179/sic.1966.016.

(43) The Staffs of the Textile Research Institute and The Textile. Review of Research and Development in the Field of Textiles During 1949. *Textile Research Journal* **1950**, *20* (5). https://doi.org/10.1177/004051755002000507.

(44) Liss, T. A.; Baer, D. R. Metal Complexes of Azo Dyes. I. Quadridentate Complexes from Bidentate Azo Compounds and Alkanediamines or Ethanolamine. *Inorganic Chemistry* **1969**, *8* (6). https://doi.org/10.1021/ic50076a026.

(45) Jezorek, J. R.; Freiser, Henry. 4-(Pyridylazo)Resorcinol-Based Continuous Detection System for Trace Levels of Metal Ions. *Analytical Chemistry* **1979**, *51* (3). https://doi.org/10.1021/ac50039a012.

(46) Dingle, A. The Flint Water Crisis: What's really going on? https://www.acs.org/content/acs/en/education/resources/highschool/chemmatters/past-issues/2016-2017/december-2016/flint-water-crisis.html.

(47) Ma, L., Liu, Y., Wu, Y.; A tryptophan-containing fluoroionophore sensor with high sensitivity to and selectivity for lead ion in water. *Chem. Commun.*, 2006, 2702–2704

(48) Fluorescent and colorimetric sensors for detection of lead, cadmium, and mercury ions *Chem. Soc. Rev* .,2012,41,3210–3244

(49) A Selective Fluorescent Sensor for Detecting Lead in Living Cells *J. Am. Chem. Soc.* **2006** *128,* 9316-9319

(50) Grudpan, K.; Taylor, C. G. Some Azo-Dye Reagents for the Spectrophotometric Determination of Cadmium. *Talanta* **1989**, *36* (10). https://doi.org/10.1016/0039-9140(89)80183-3.

(51) Wang, M.; Funabiki, K.; Matsui, M. Synthesis and Properties of Bis(Hetaryl)Azo Dyes. *Dyes and Pigments* **2003**, *57* (1). https://doi.org/10.1016/S0143-7208(03)00011-1.

(52) Benkhaya, S.; M'rabet, S.; el Harfi, A. Classifications, Properties, Recent Synthesis and Applications of Azo Dyes. *Heliyon* **2020**, *6* (1). https://doi.org/10.1016/j.heliyon.2020.e03271.

(53) Douaihy, R.E., *et al.* Diaminoanthraquinone-Linked Polyazamacrocycles: Efficient and Simple Colorimetric Sensor for Lead Ion in Aqueous Solution *Org. Lett.* 11(*4*), 2009

(54) Rapid and selective lead (II) colorimetric sensor based on azacrown ether-functionalized gold nanoparticles *Nanotechnology* vol 21 **2010**, 315503-315511

(55) Lee, K.M., Chen, X., Fang, W., Kim, J.-M. and Yoon, J. (2011), A Dual Colorimetric and Fluorometric Sensor for Lead Ion Based on Conjugated Polydiacetylenes. Macromol. Rapid Commun., 32: 497-500.

(56) Ensafi, A.A., Far, A.K., Meghdadi S. (2009) Highly selective optical sensing film for lead II determination in water samples *J. Haz. Mat.* Vol 172 (2-3) 1069-1075

(57) Thakur, A., Mandal, D., Ghosh, S. Sensitive and selective redox, chromogenic, and turn on fluorescent probe for Pb(II) in aqueous environment *Anal. Chem.* 2013, 85, 3, 1665–1674

(58) Synthesis of triazole linked fluorescent amino acid and carbohydrate bio-conjugates: a highly sensitive and skeleton selective multi-response chemosensor for Cu(II) and Pb(II)/Hg(II) ions. *Rsc. Adv.*, **2014,** 4, 1918-1921

(59) Izatt, R. M. Charles J. Pedersen's Legacy to Chemistry. *Chem. Soc. Rev.* **2017**, *46* (9). https://doi.org/10.1039/C7CS00128B.

(60) Sears, M. E. Chelation: Harnessing and Enhancing Heavy Metal Detoxification—A Review. *The Scientific World Journal* **2013**, *2013*. https://doi.org/10.1155/2013/219840.

(61) Jezorek, J. R.; Freiser, Henry. 4-(Pyridylazo)Resorcinol-Based Continuous Detection System for Trace Levels of Metal Ions. *Analytical Chemistry* **1979**, *51* (3). https://doi.org/10.1021/ac50039a012.

(62) Sharma, V.; McKone, H. T.; Markow, P. G. A Global Perspective on the History, Use, and Identification of Synthetic Food Dyes. *Journal of Chemical Education* **2011**, *88* (1). https://doi.org/10.1021/ed100545v.

(63) Potera, C. DIET AND NUTRITION: The Artificial Food Dye Blues. *Environmental Health Perspectives* **2010**, *118* (10). https://doi.org/10.1289/ehp.118-a428.

(64) Wang, M.; Funabiki, K.; Matsui, M. Synthesis and Properties of Bis(Hetaryl)Azo Dyes. *Dyes and Pigments* **2003**, *57* (1). https://doi.org/10.1016/S0143-7208(03)00011-1.

(65) Benkhaya, S.; M'rabet, S.; el Harfi, A. Classifications, Properties, Recent Synthesis and Applications of Azo Dyes. *Heliyon* **2020**, *6* (1). https://doi.org/10.1016/j.heliyon.2020.e03271.

(66) Affordable lead sensor for home, City Water Lines. https://news.umich.edu/affordable-lead-sensor-for-home-city-water-lines/.

(67) Lin, W., Li, Z., Burns, M.A., A Drinking Water Sensor for Lead and Other Heavy Metals *Anal. Chem.* **2017**, 89(17), 8748-8756

(68) Affordable lead sensor for home, City Water Lines. https://news.umich.edu/affordable-lead-sensor-for-home-city-water-lines/ (accessed Apr 10, 2022).

(69) Khalik, W.F., Ho, L., Ong, S., Wong, Y., Yusoff, N, Lee, S., Revealing the influences of functional groups in azo dyes on the degradation efficiency and power output in solar photocatalytic fuel cell J Environ Health Sci Eng. 2020 Dec; 18(2): 769–777.

(70) Schwabacher, A.W., Lane, J.W, Schiesher, M.W., Leigh, K.M., Johnson, C.W. Desymmetrization reactions: efficient preparation of unsymmetrically substituted linker molecules *J. Org. Chem* **1998** 63(5), 1727-1729

(71) Troubled Waters: Lead Lurking in US Water Supplies https://www.earthmagazine.org/article/troubled-waters-lead-lurking-us-water-supplies

(72) Ground Water and Drinking Water: Basic Information about Lead in Drinking Water https://www.epa.gov/ground-water-and-drinking-water/basic-information-about-lead-drinking-water

(73) Lead Toxicity: Who is at Risk? https://www.atsdr.cdc.gov/csem/leadtoxicity/who_at_risk.html

(74) Mason, L.H., Harp, J.P, Han, D.Y., Pb Neurotoxicity: Neurophysical Effects on Lead Toxicity *Biomed. Res. Int.* 2014 240547

(75) Krishna, G., Goel, S.; *Handbook of Toxicology of Chemical Warfare Agents (Second Edition)* **2015,** 657-673

(76) Milwaukee City Water Works "Lead and Water." https://city.milwaukee.gov/water/WaterQuality/LeadandWater

(77) Martinez, M., *Milwaukee Neighborhood New Service,* **2020** https://www.greatlakesnow.org/2020/08/milwaukee-significantly-behind-lead-pipes-by-end-of-year/

(78) Kemp., D.S, Bowen, B.R, Muendel, C.C, *J. Org. Chem.,* **1990**, *55*, 4650-4657

(79) Nowick, J.S., *Acc. Chem. Res.* **2008**, 41(*10*), 1319-1330

(80) Nowick, J.S., Tsai, J.H., Quoc-Chuong, D.B, Maitra, S., *J. Am. Chem. Soc.* **1999**, *121*, 8409-8410

(81) Pastor, A., Martinez-Viviente, E., *Coord. Chem. Rev.* **2008**, *252*(21-22), 2314-2345

(82) Qu, D., Wang, Q., Zhang, Q., Ma, X., Tian, H., *Chem. Rev.* **2015**, *115*(15), 7543-7588

(83) Cheng, P., Pham, J.D., Nowick, J.S., *J. Am. Chem. Soc*. **2013 Apr 17**; 135(15): 5477–5492.

Appendix: Compound Characterization Spectra

[1]HNMR of Compound 1

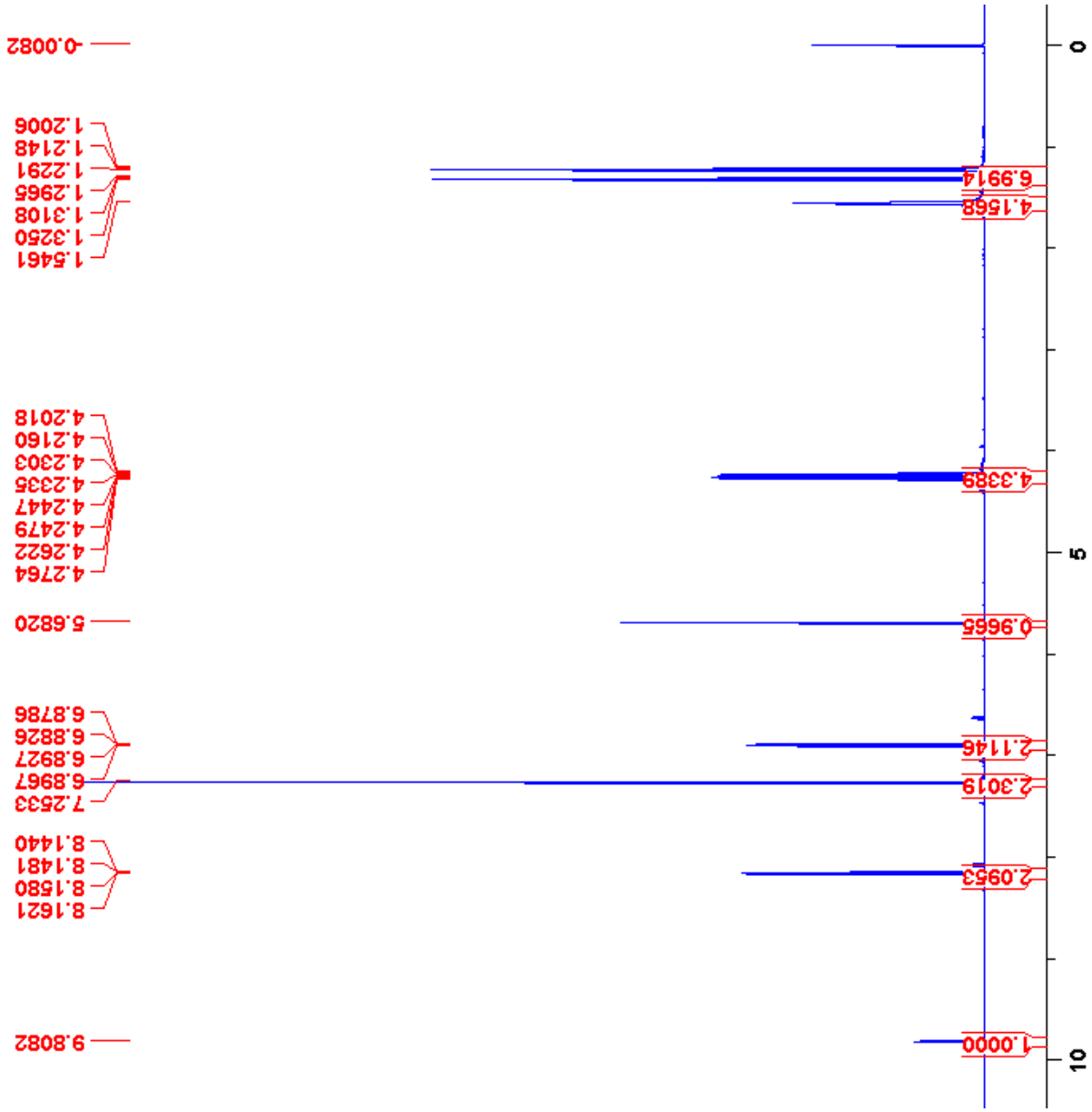

Spectrum 1 1H NMR (500 MHz, CDCl3)

^{1}HNMR of Compound 2

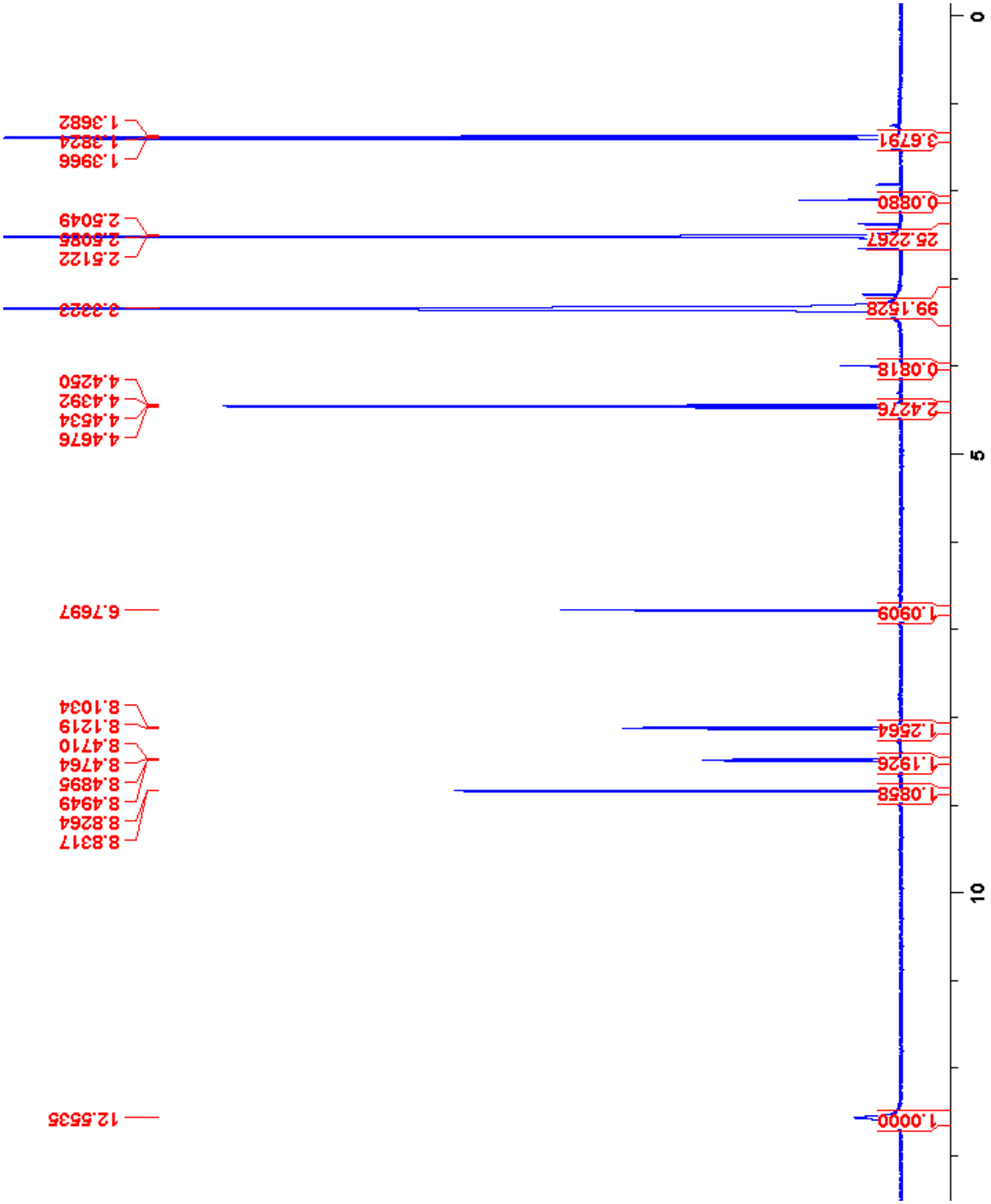

Spectrum 2: 2 **1H NMR (500 MHz, DMSO)**

LCMS of Compound 2

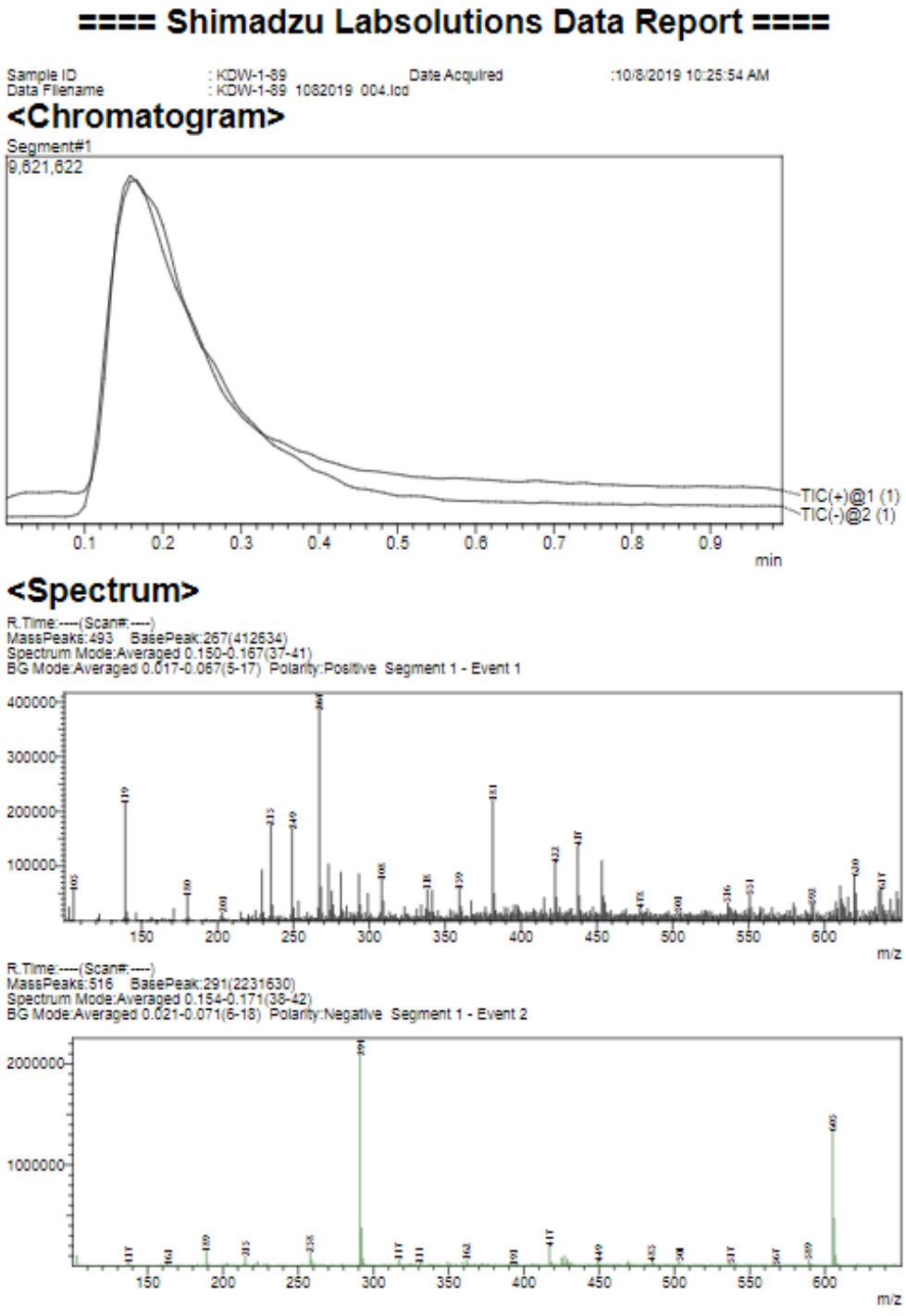

Spectrum 3: 2 ESI-LCMS Report

^{1}HNMR of Compound 3

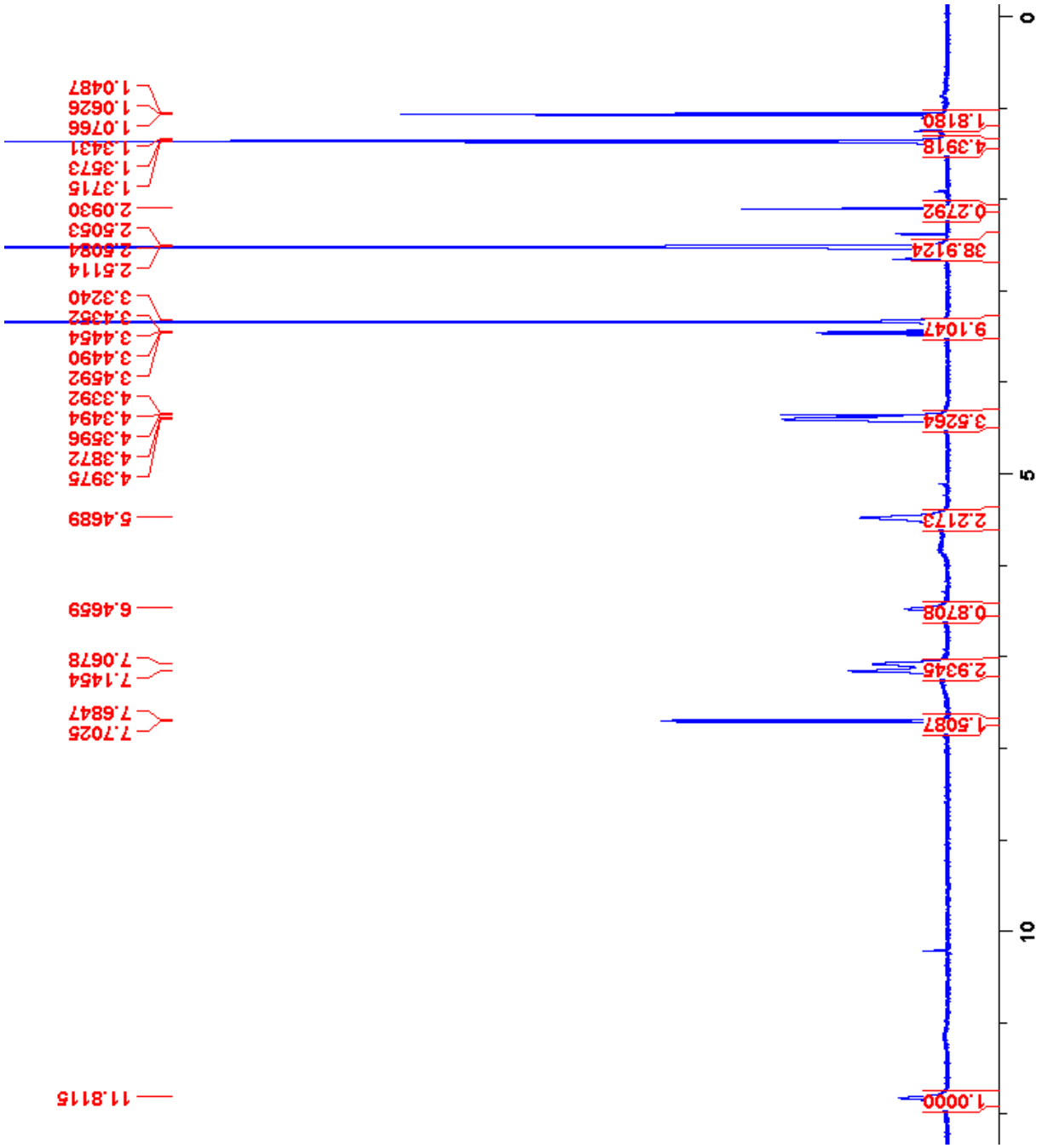

Spectrum 4: 3 1H NMR (300 MHz, CDCl3)

^{1}HNMR of Compound 4b

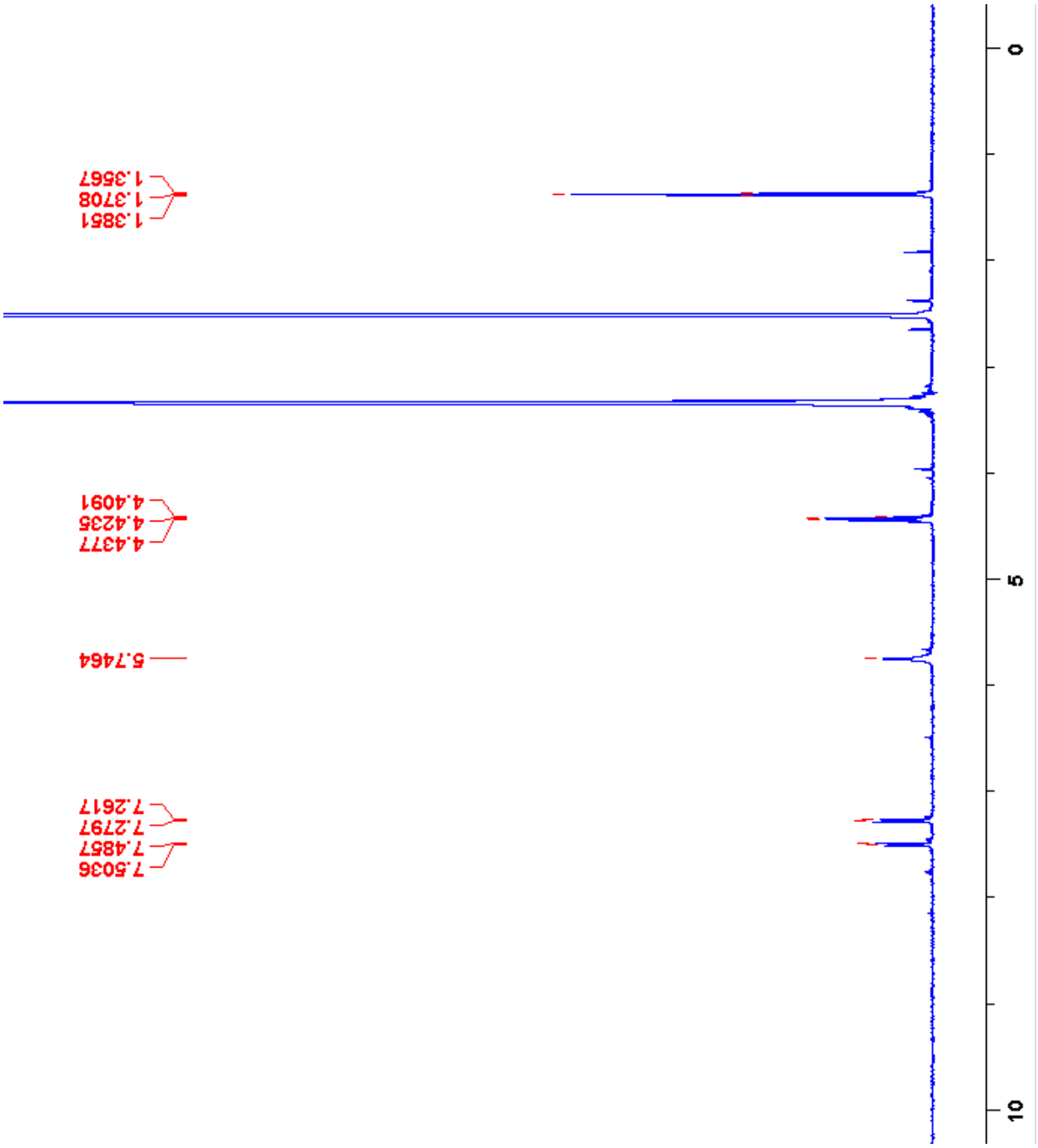

Spectrum 5: 4b 1H NMR (500 MHz, DMSO-d6)

LCMS of Compound 4c

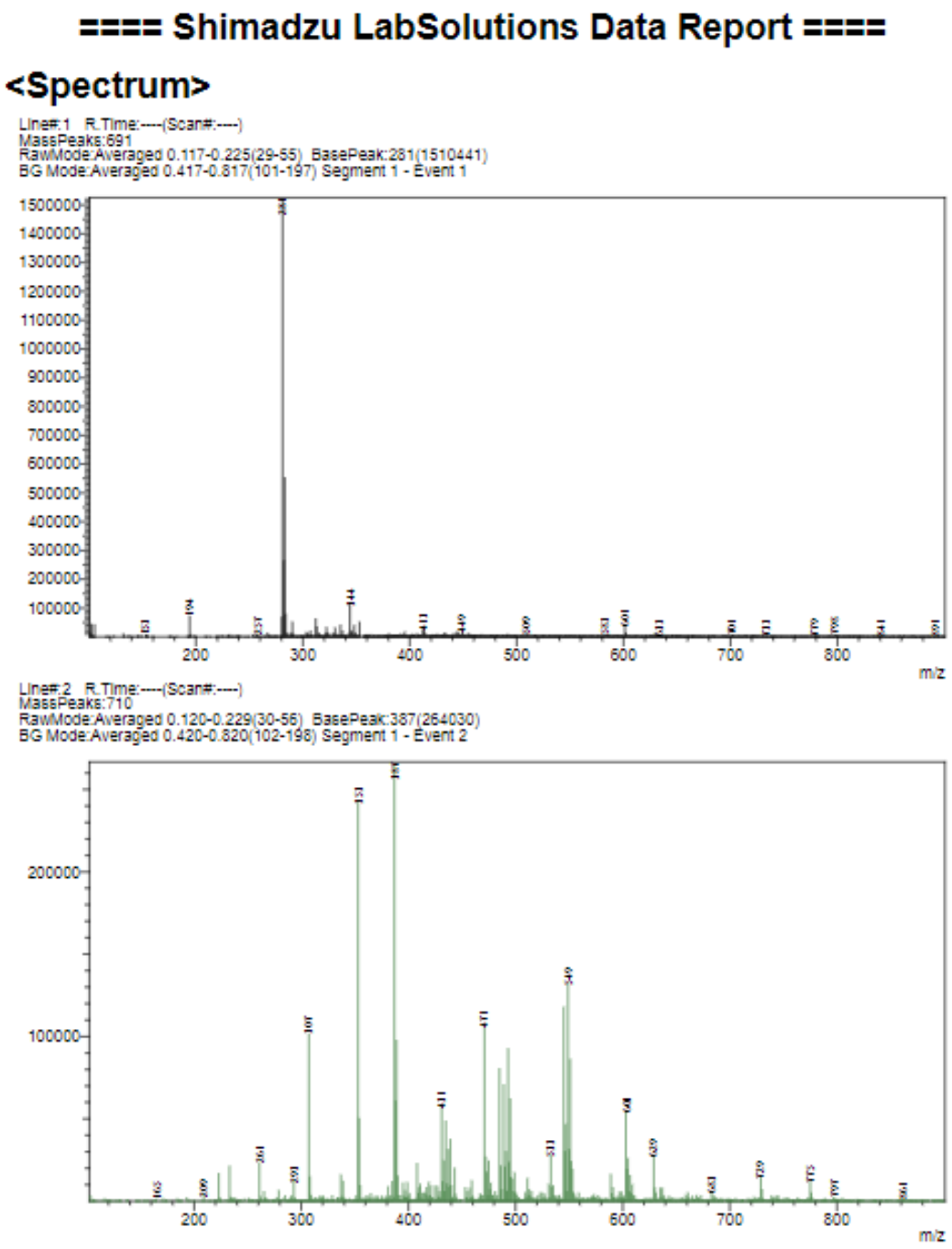

Spectrum 6: 4c ESI-LCMS Report

[1]HNMR of Compound 5

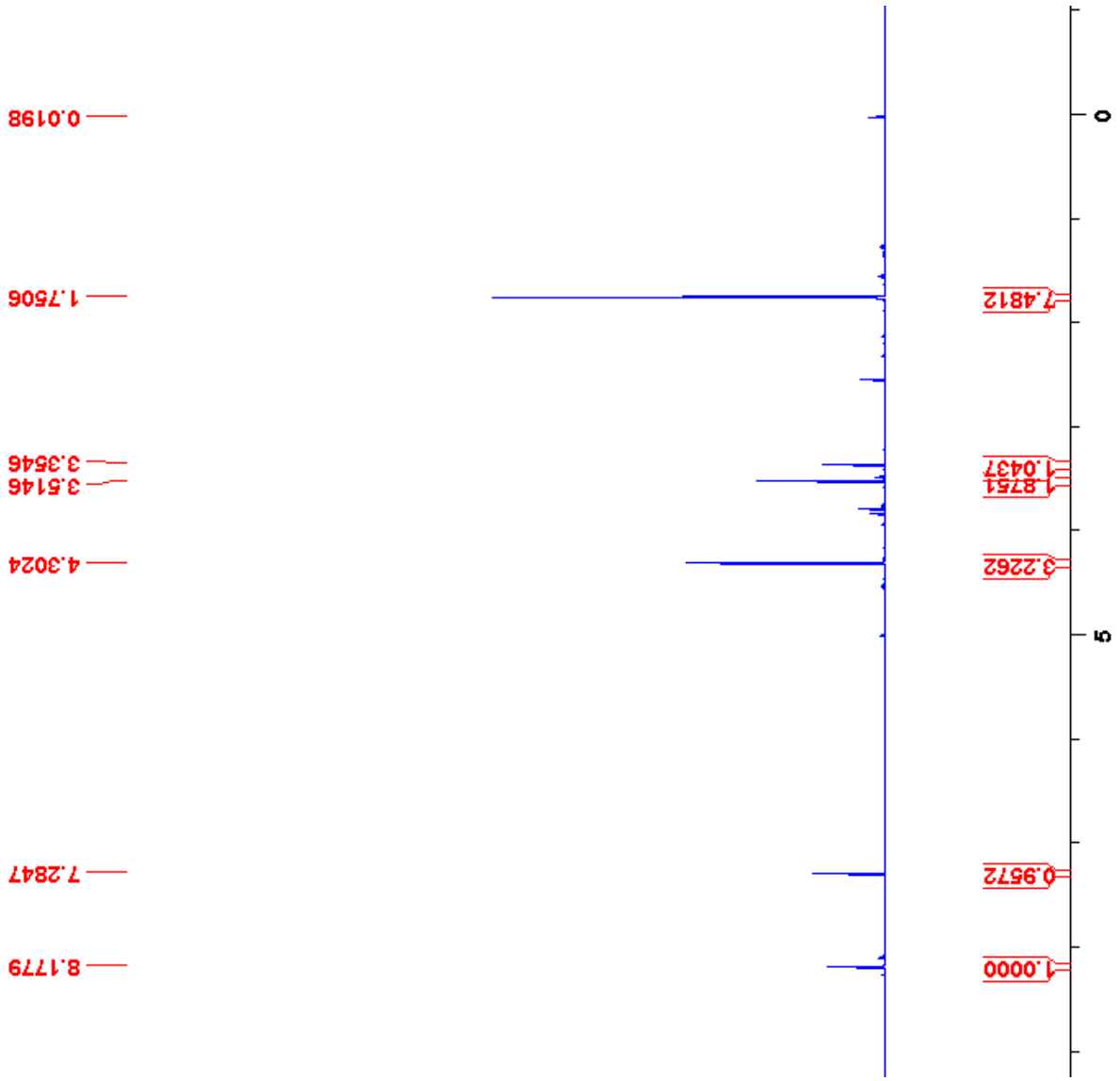

Spectrum 7: 5 **1H NMR (500 MHz, CDCl3)**

[1]HNMR of Compound 5

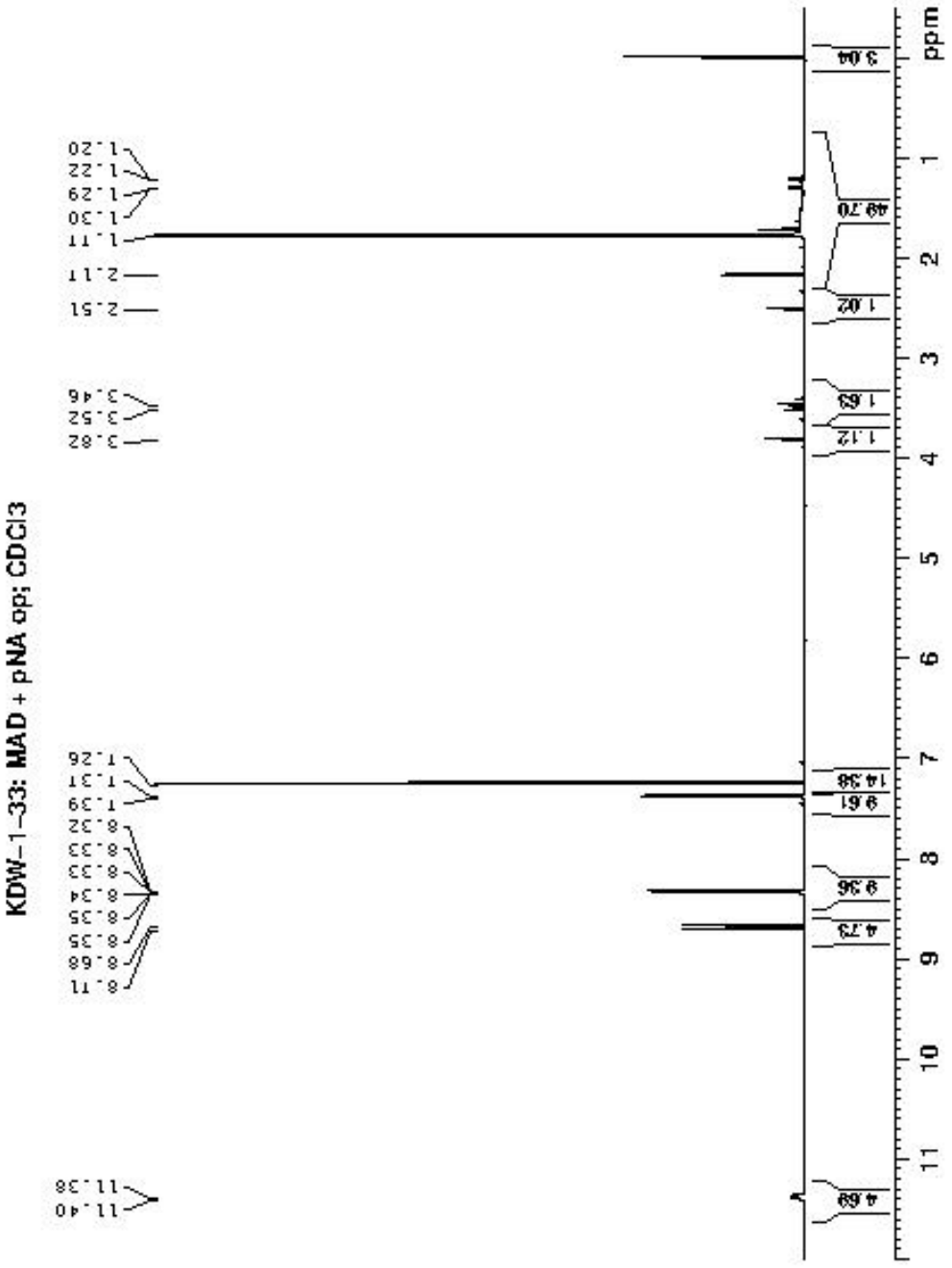

Spectrum 8: 5 1H NMR (500 MHz, CDCl3)

[1]HNMR of Compound 5a

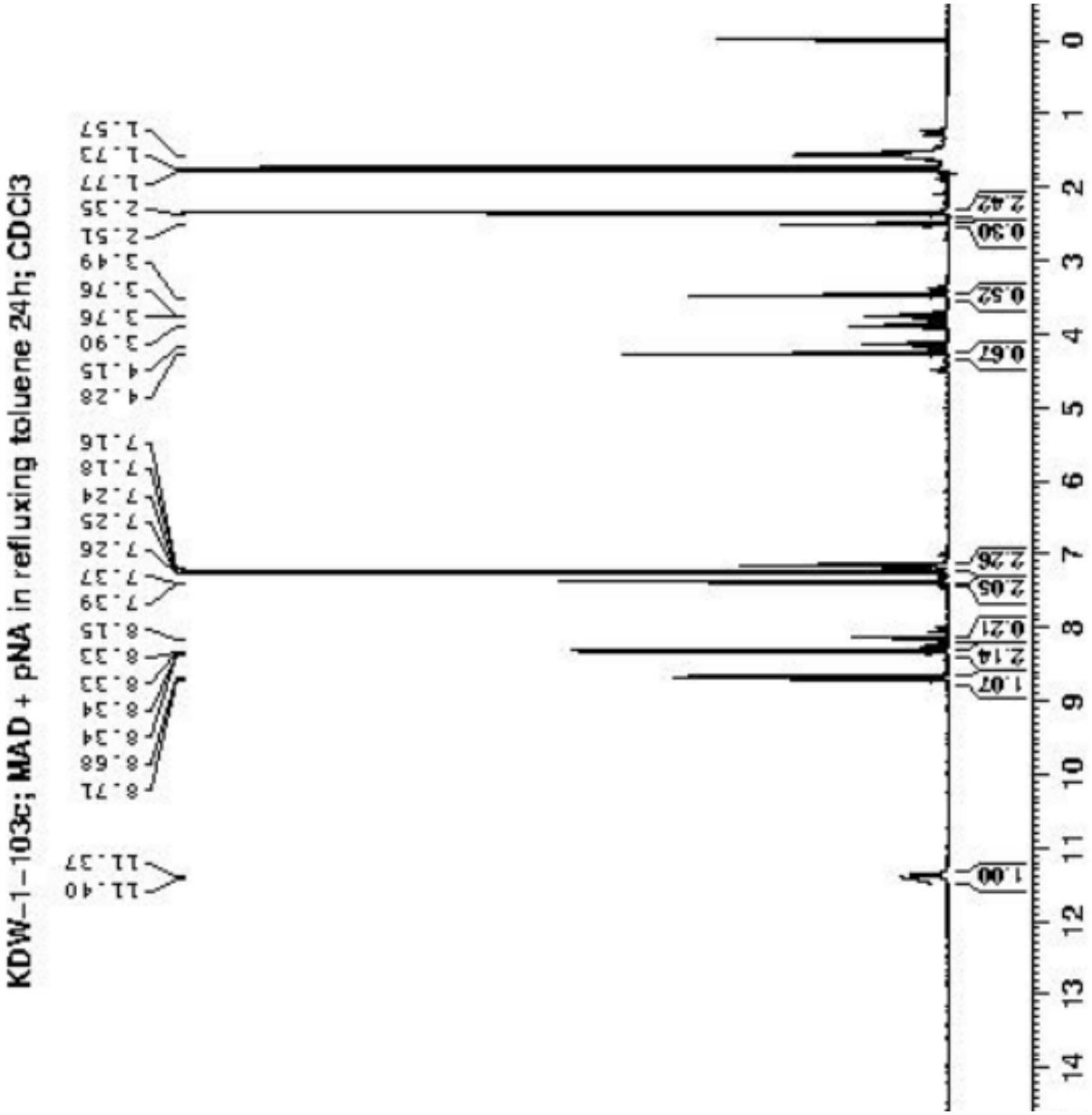

Spectrum 9: 5a 1H NMR (500 MHz, CDCl3)

[1]HNMR of Compound 6

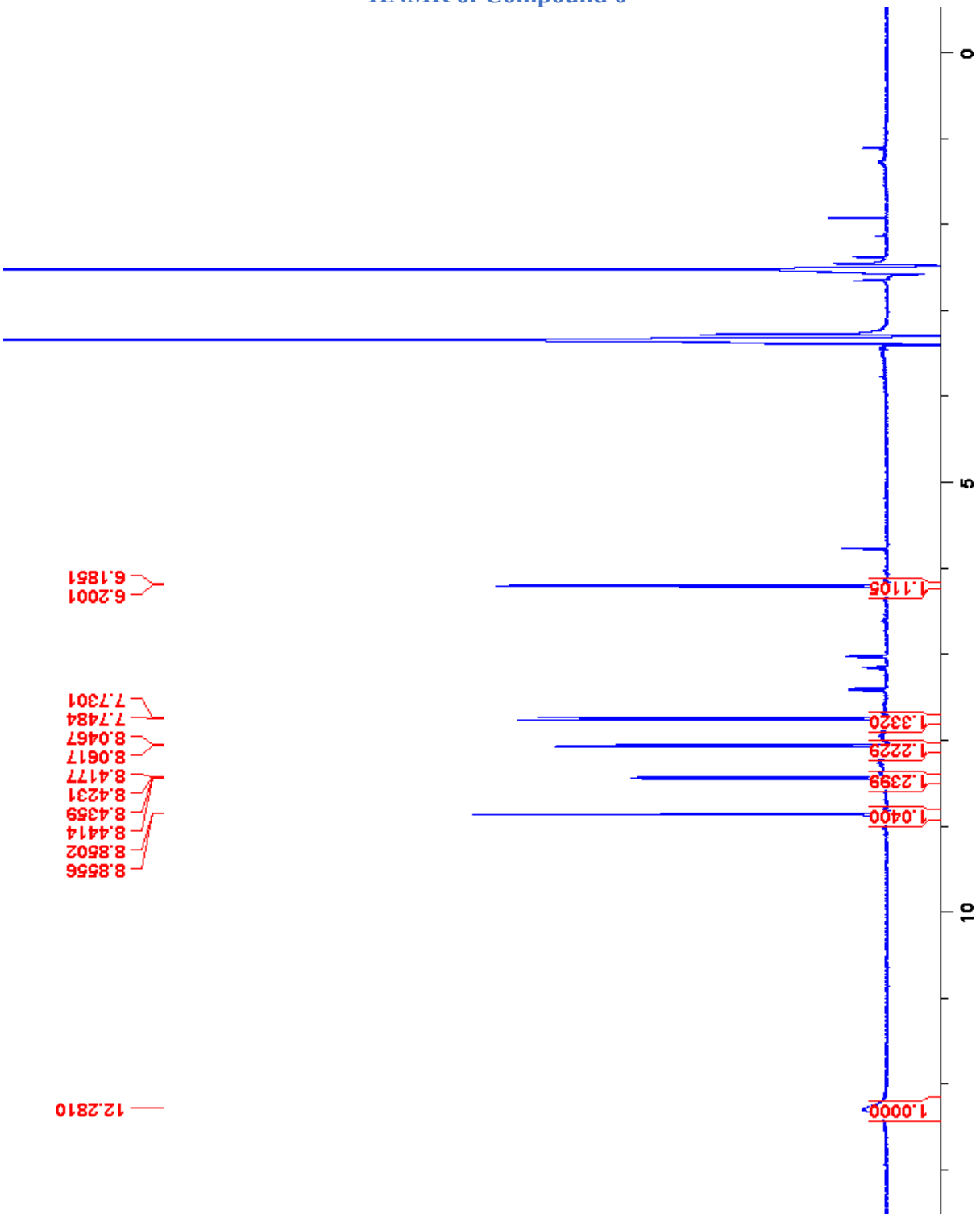

Spectrum 10: 6 1H NMR (500 MHz, DMSO-d6)

^{1}HNMR of Compound 7

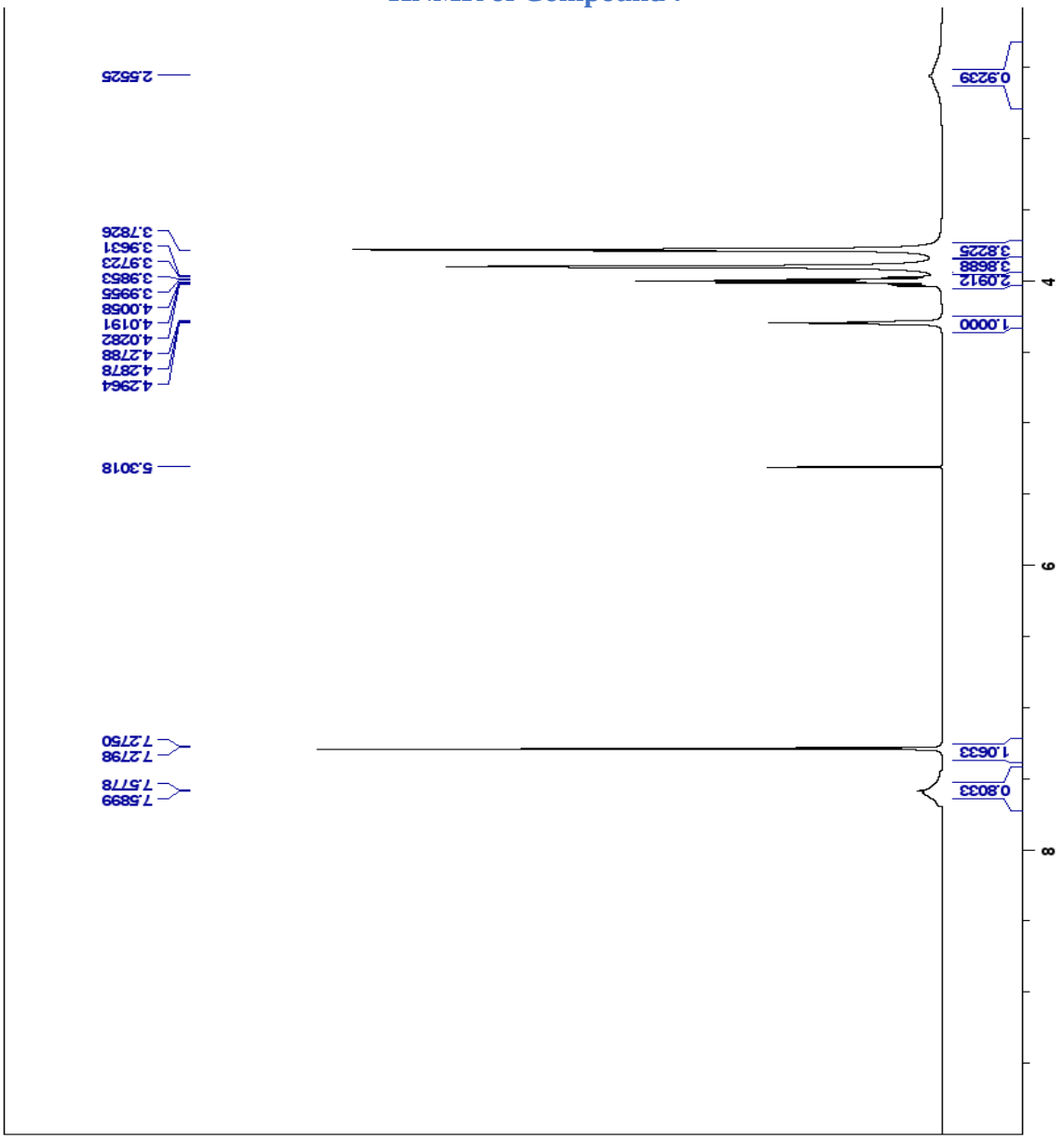

Spectrum 11: 7 1H NMR (500 MHz, CDCl3)

^{13}CNMR of Compound 7

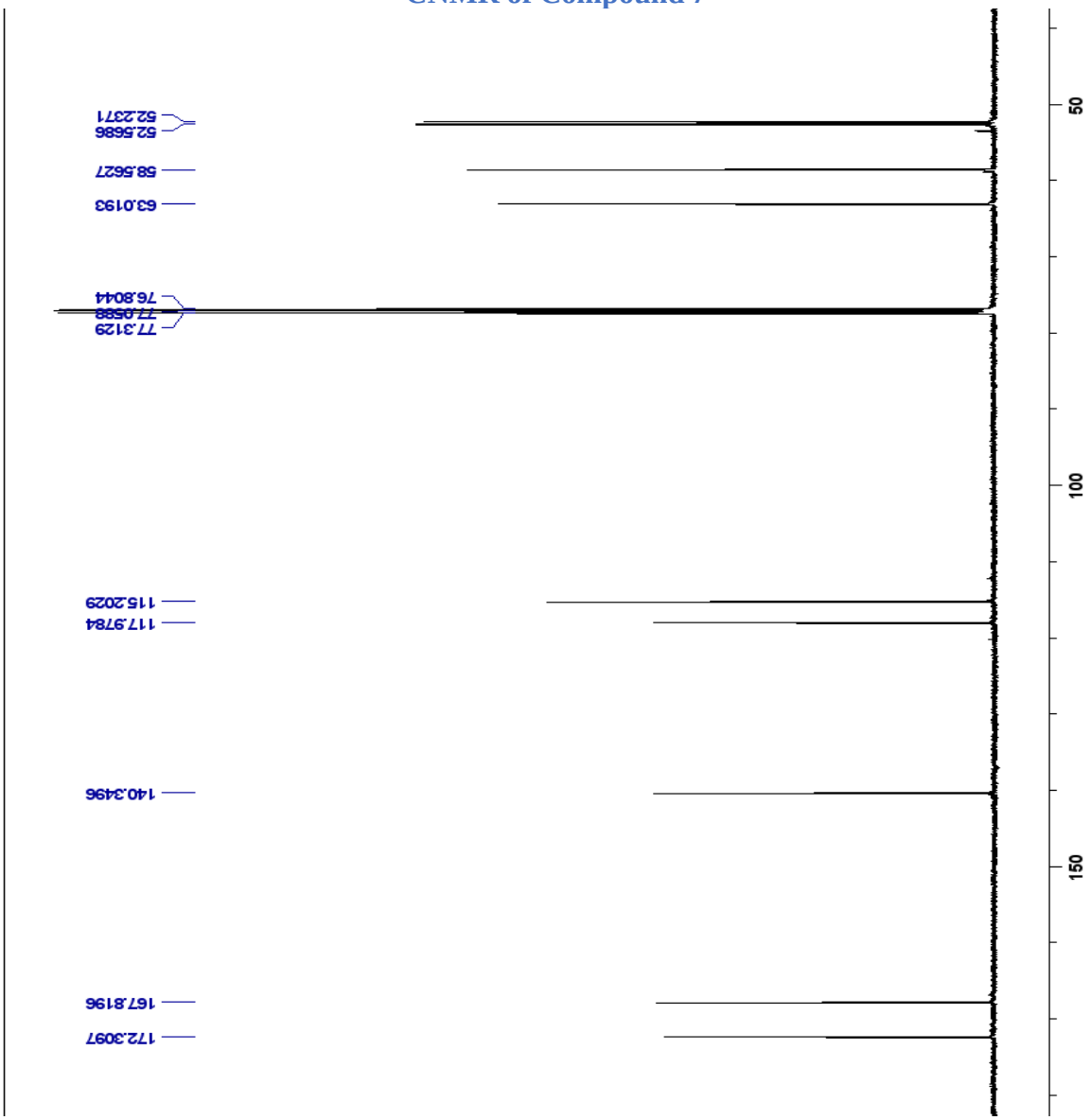

Spectrum 12: 7 13C NMR (500 MHz, CDCl3)

[1]HNMR of Compound 8

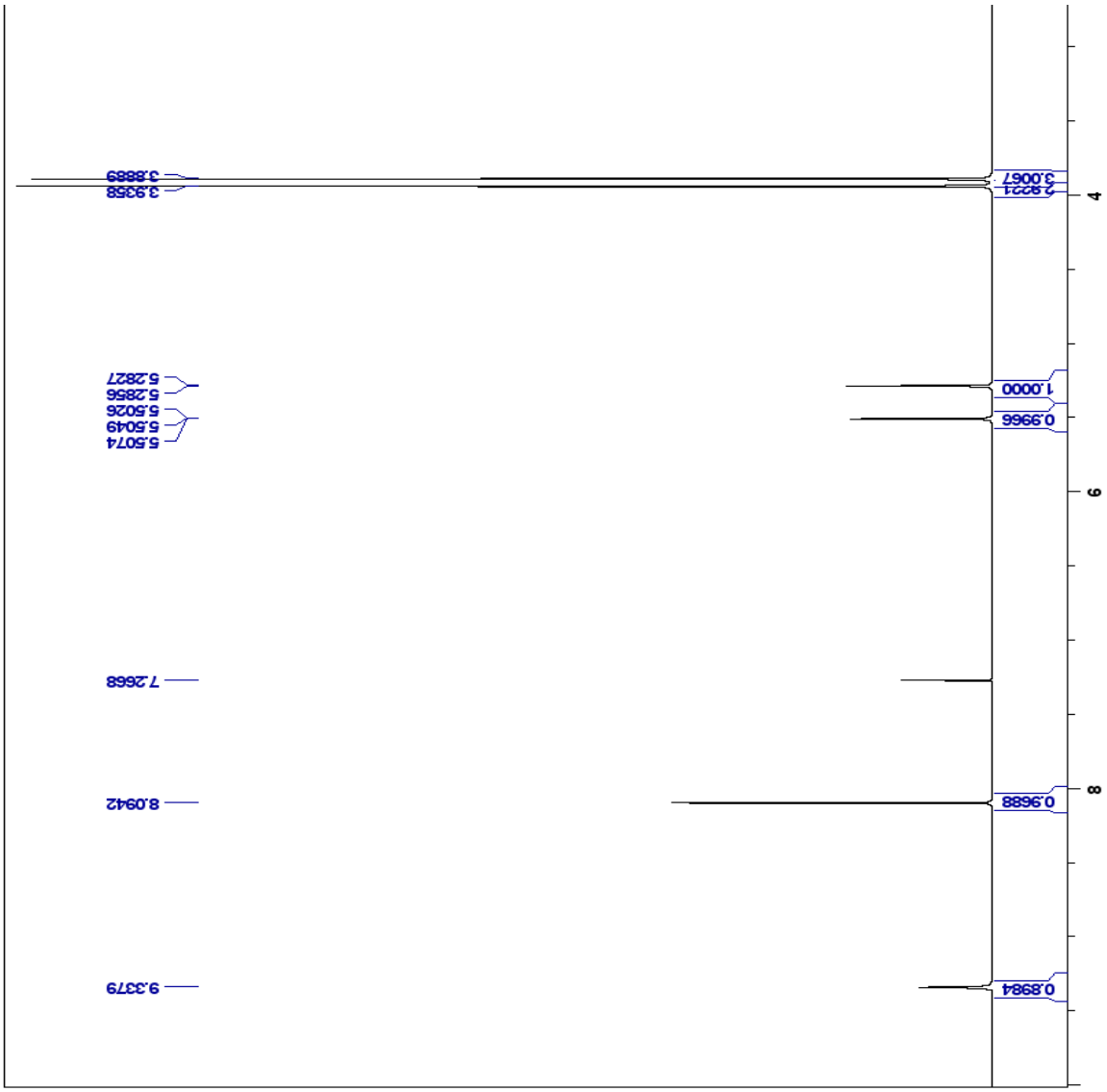

Spectrum 13: 8 1H NMR (500 MHz, DMSO-d6)

^{1}HNMR of Compound 9

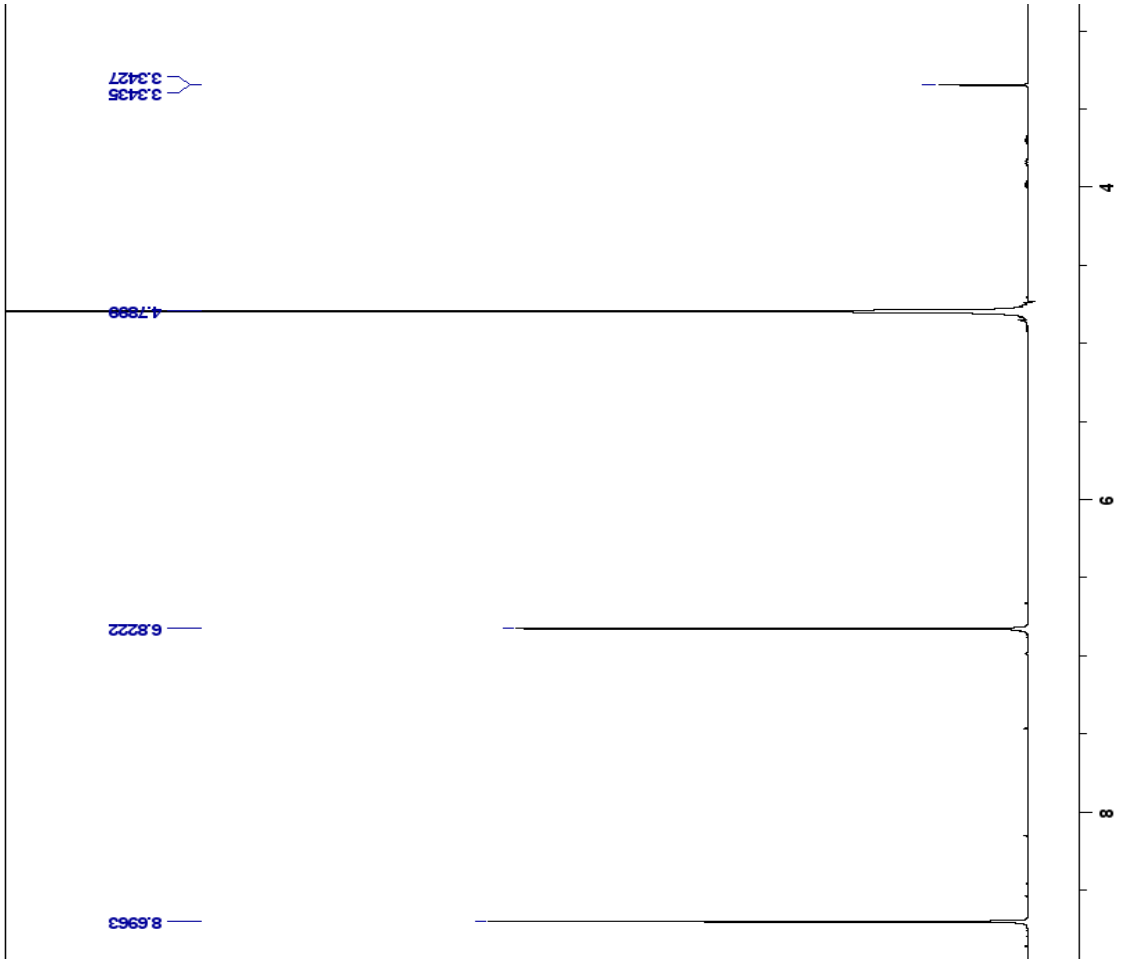

Spectrum 14: 9 1H NMR (500 MHz, D2O + KOH)

[1]HNMR of Compound 6, 10a, 11a

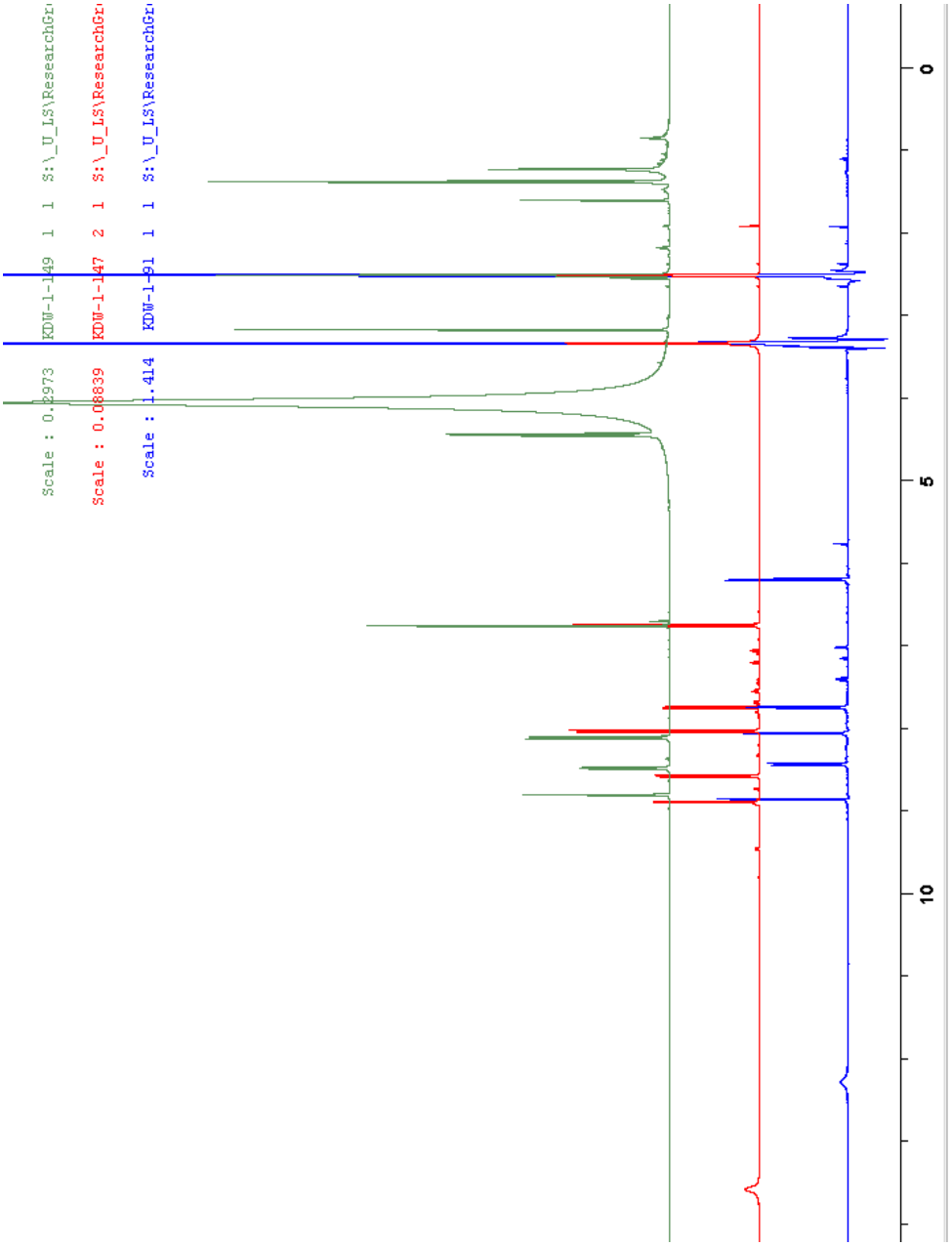

Spectrum 15: 6a, 10a, 11a, 1H NMR (500 MHz, DMSO-d6)

LCMS Report for Compound 11a

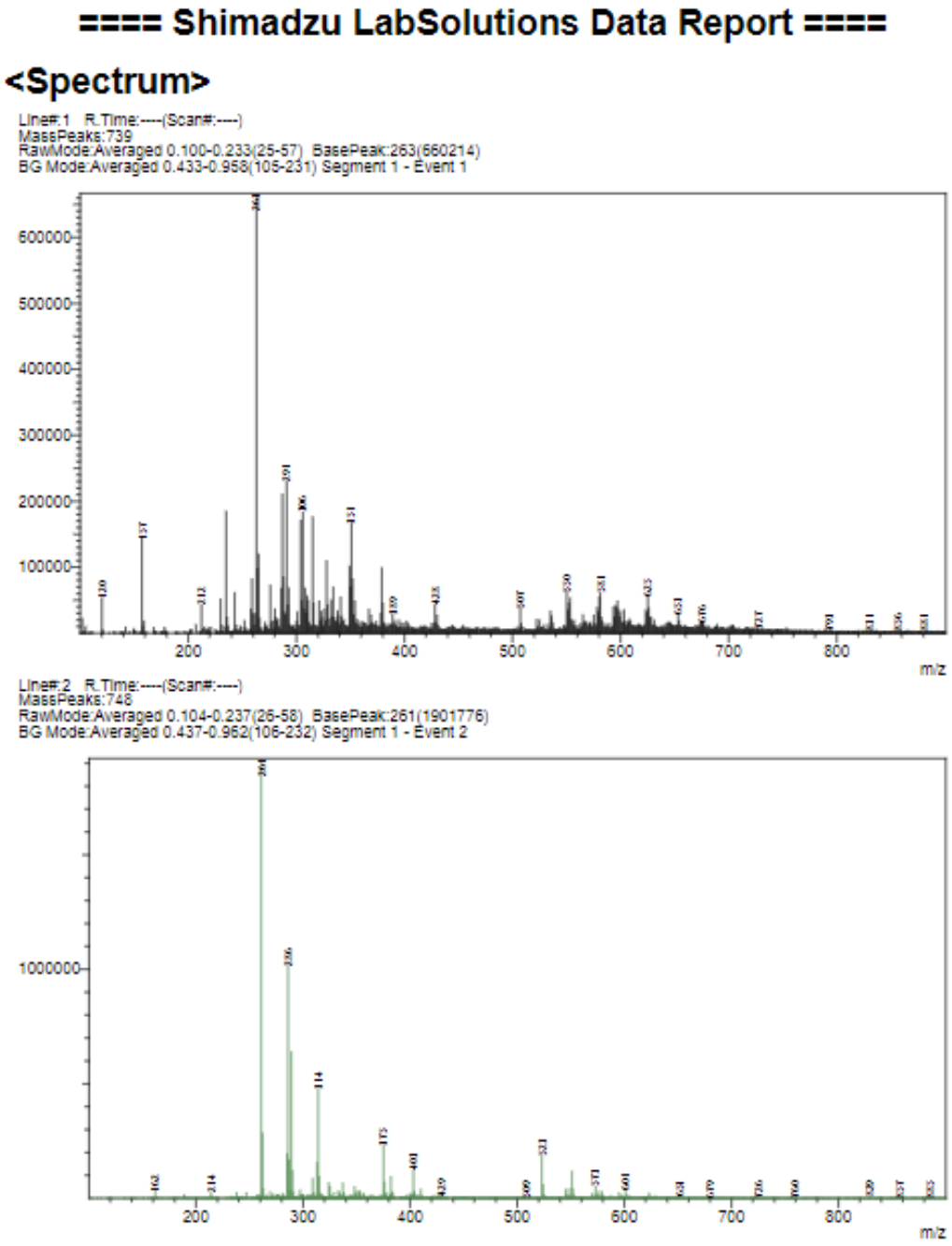

Spectrum 16: 11a ESI-LCMS Report

[1]HNMR of Compound 15 (acid form of dye)

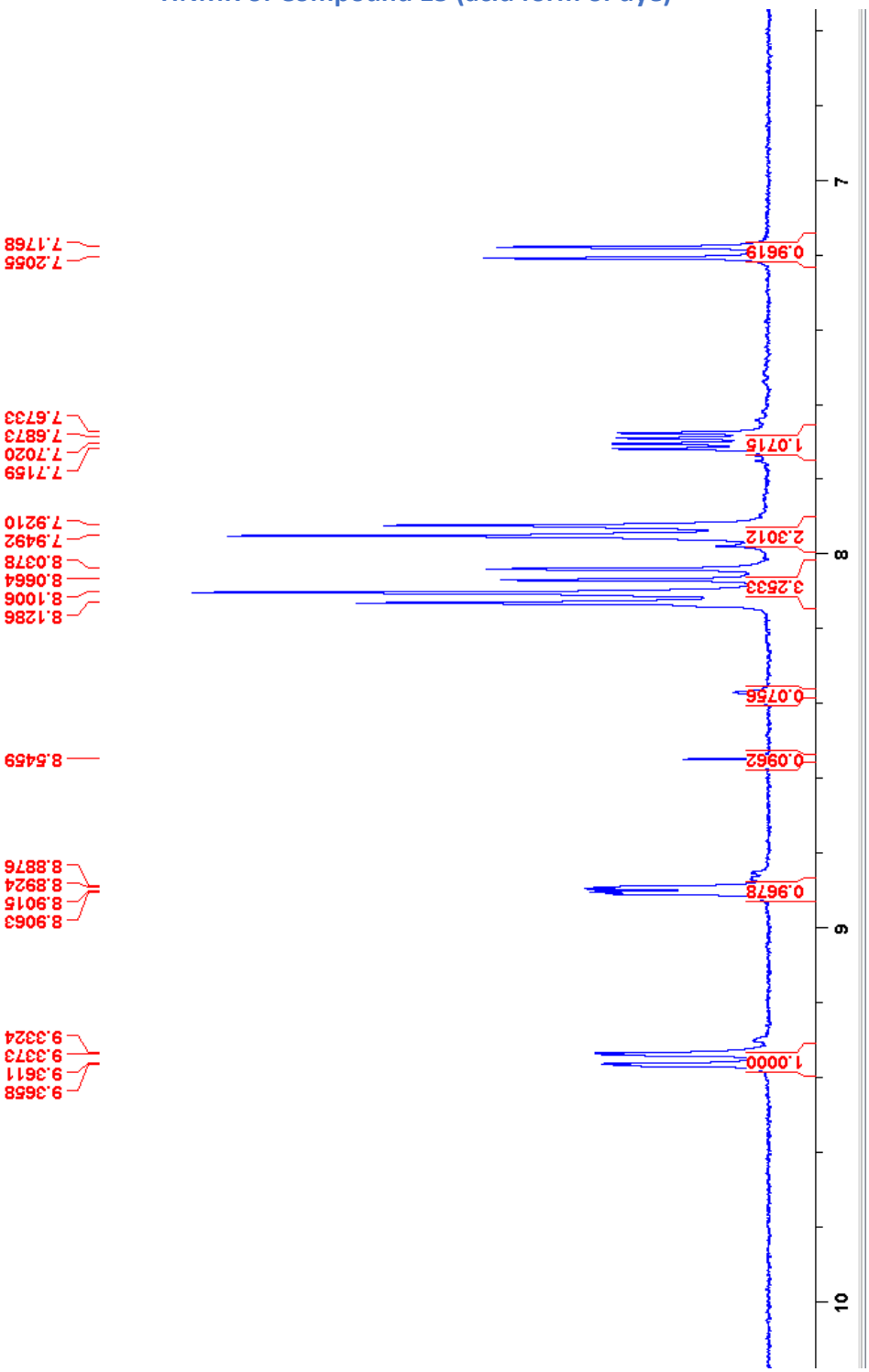

Spectrum 17: 15 1H NMR (500 MHz, DMSO-d6)

^{1}HNMR of Compound 15

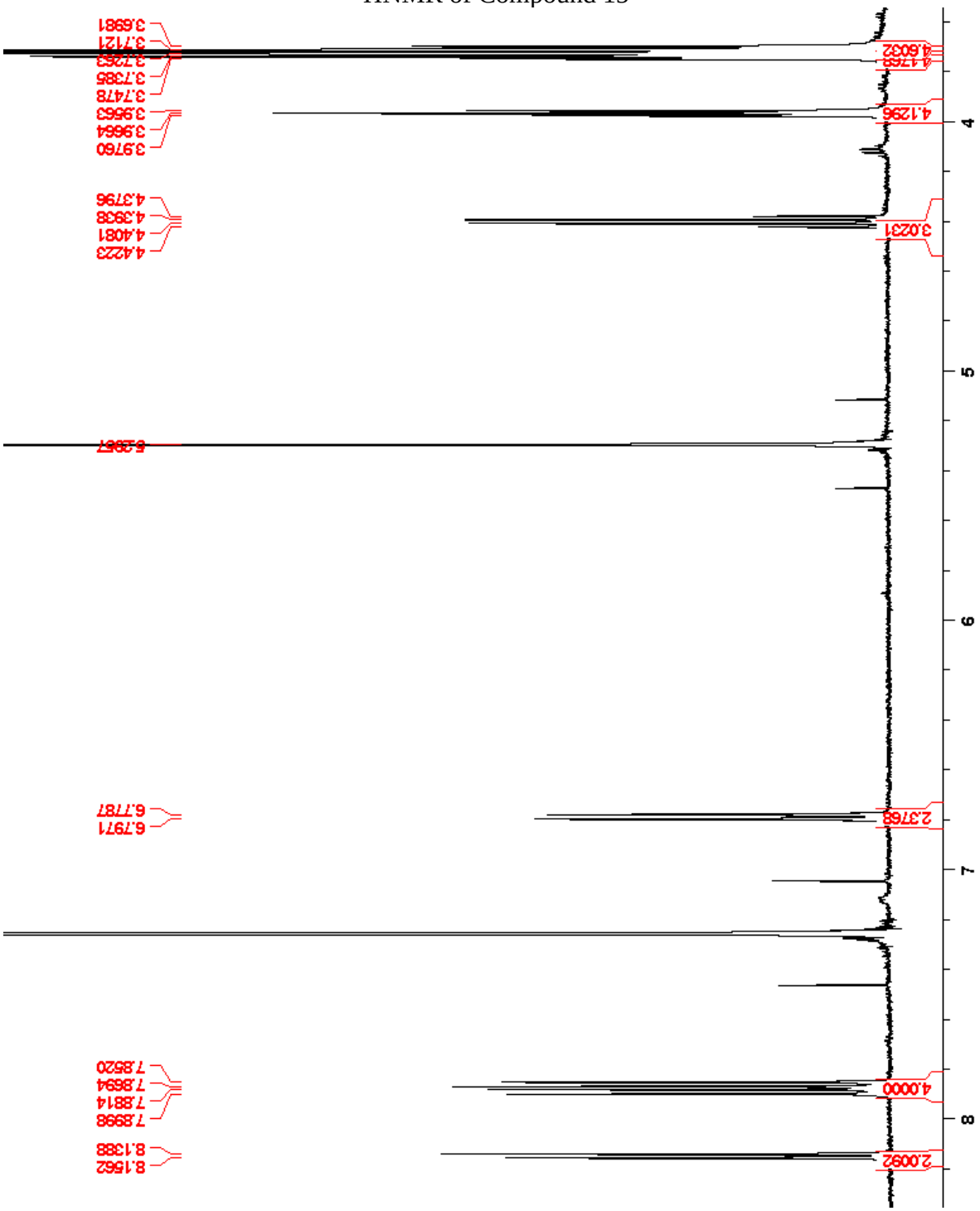

Spectrum 18: 15 1H NMR (500 MHz, DMSO-d6)

[1]HNMR of Compound 16a

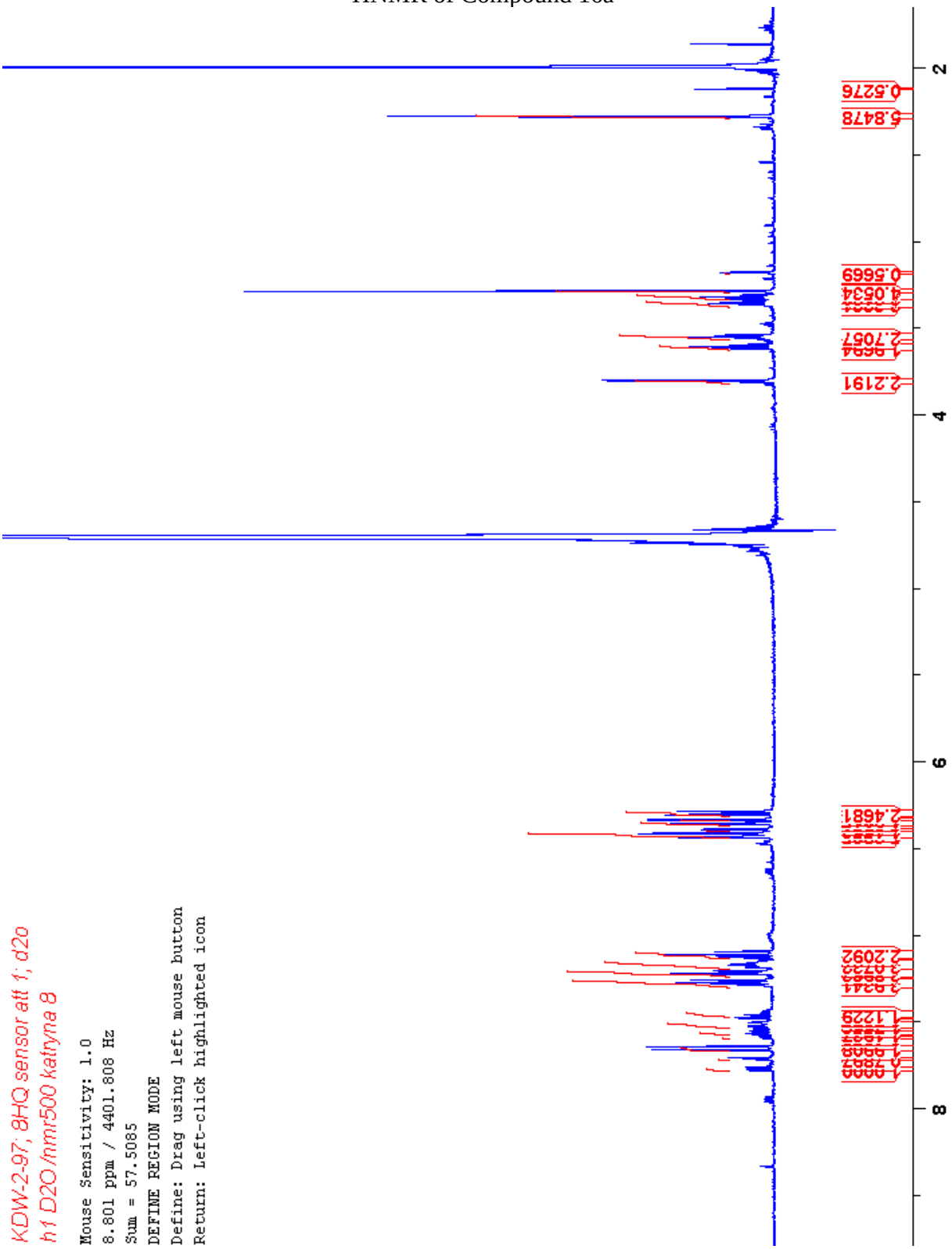

Spectrum 19: 16a 1H NMR (500 Mhz, D2O)

^{1}HNMR of Compound 17

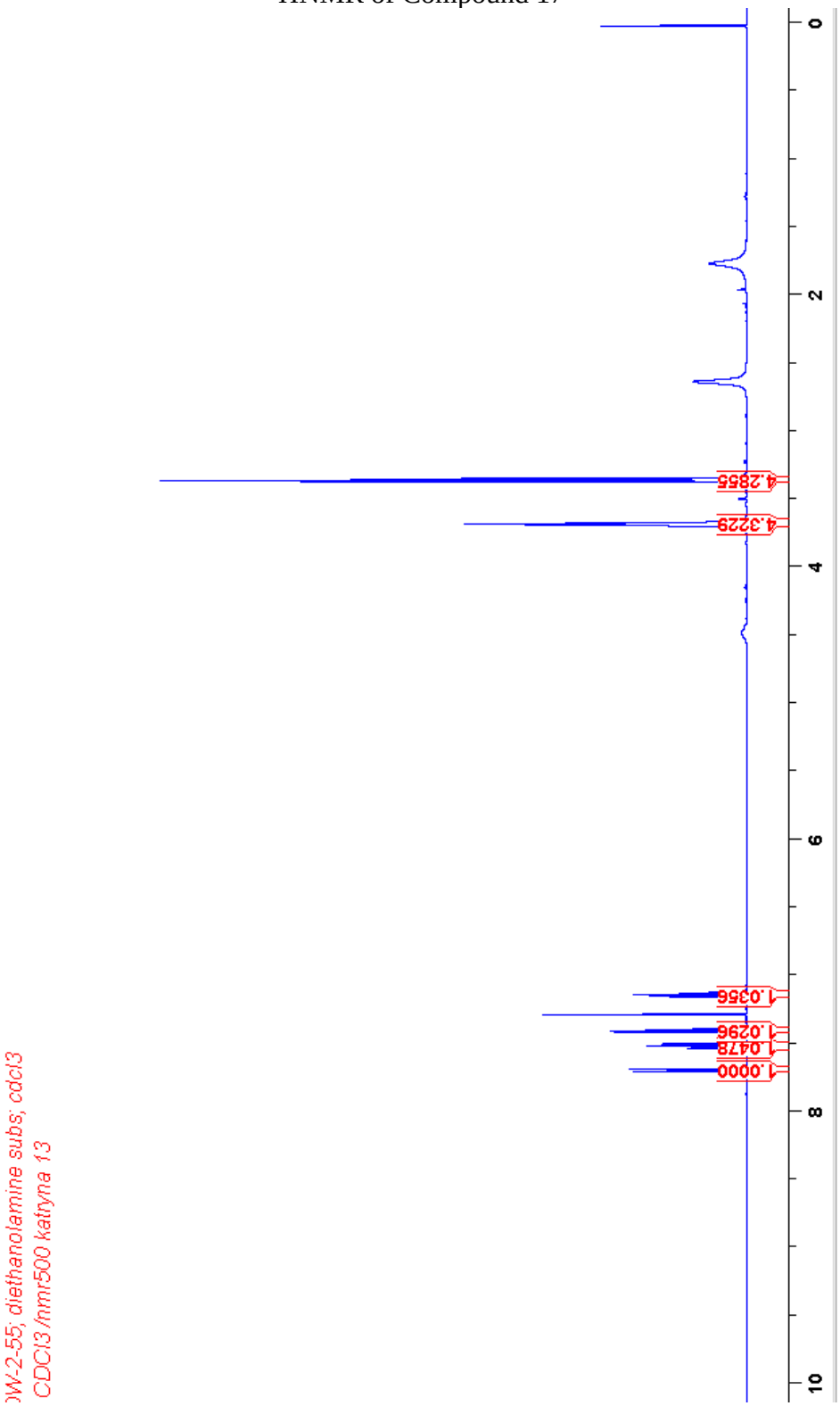

Spectrum 20: 17 1H NMR (500 MHz, CDCl3)

^{13}CNMR of Compound 18

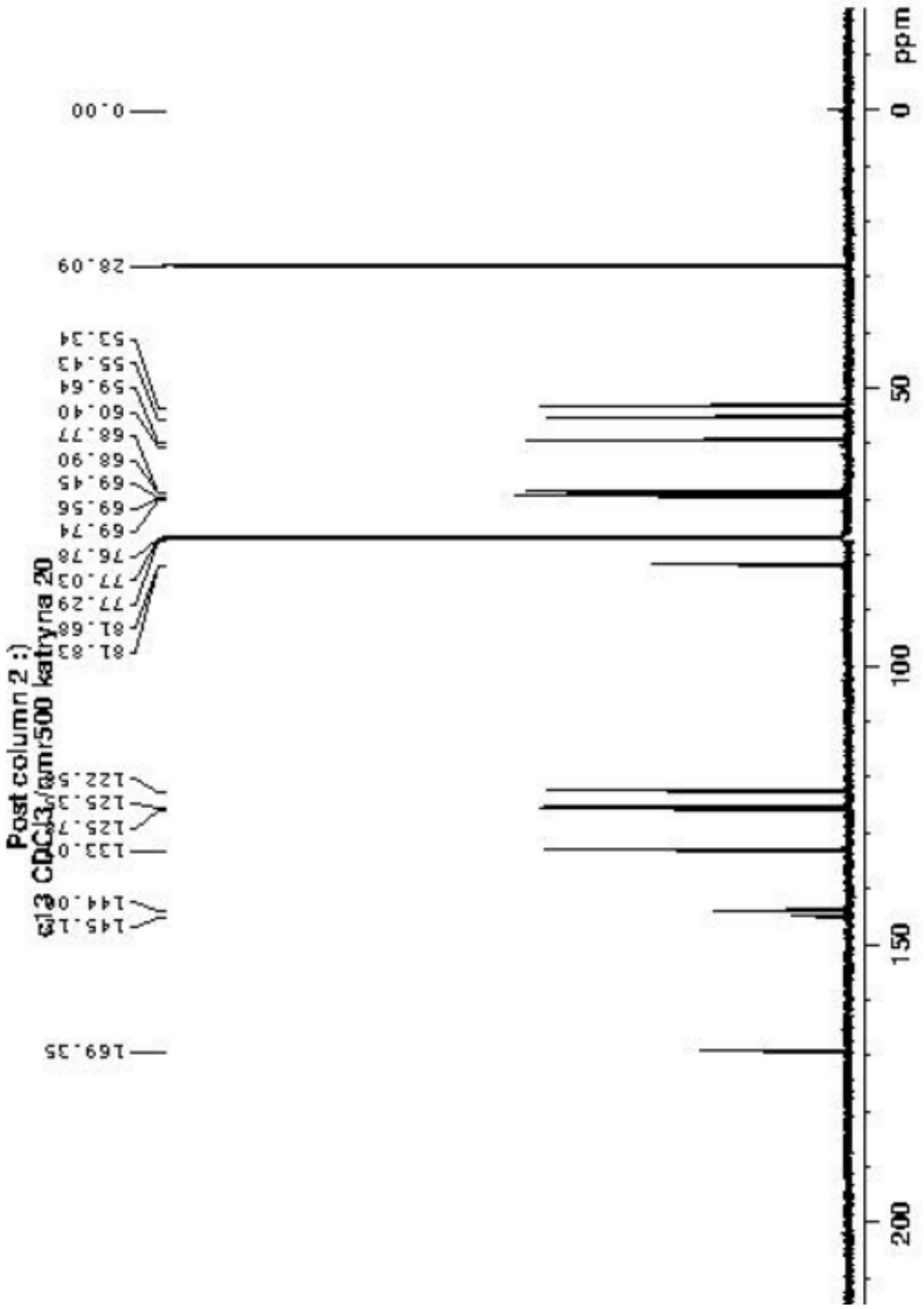

Spectrum 21: 18 13C NMR (500 MHz, CDCl3)

^{1}HNMR of Compound 18

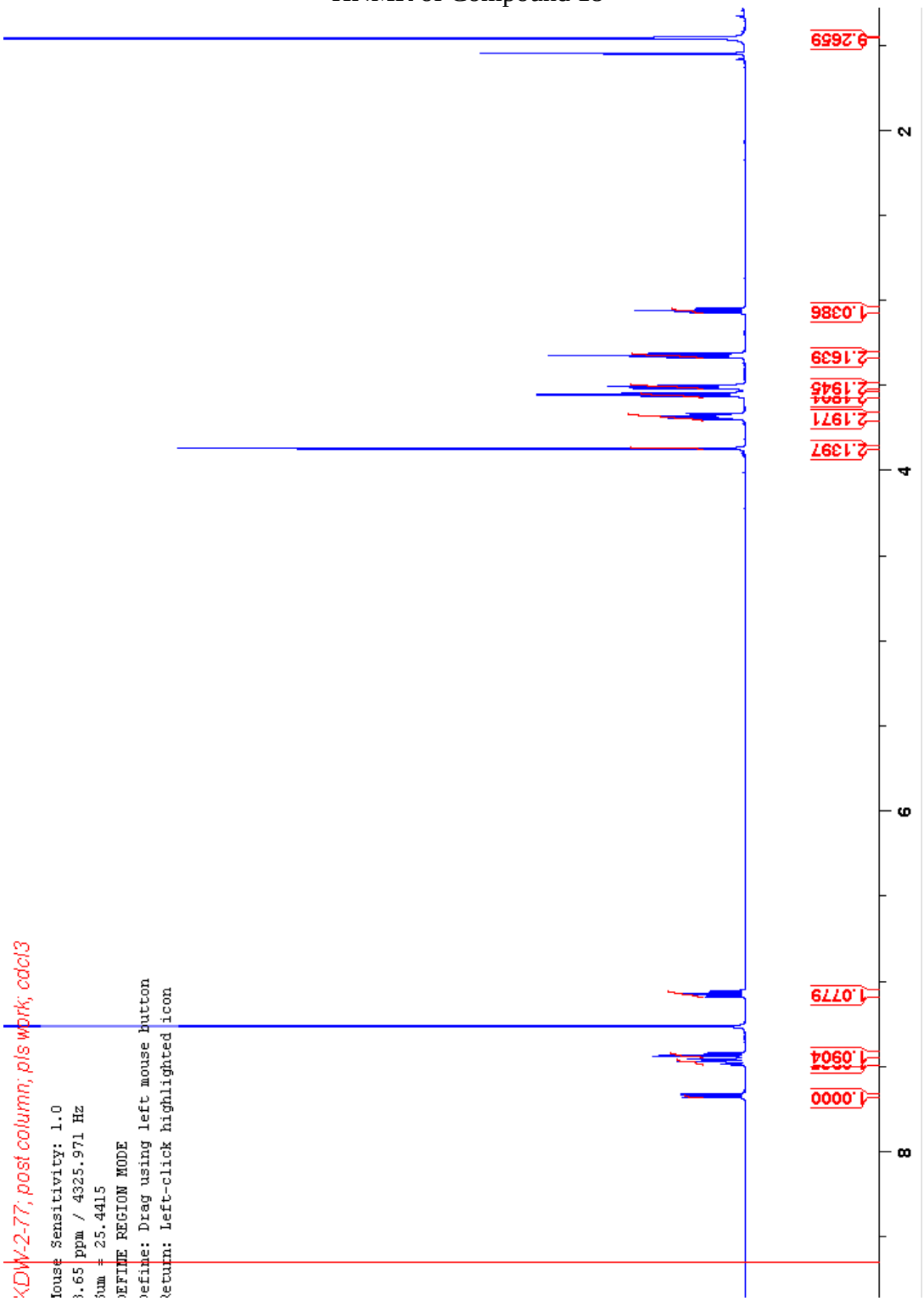

Spectrum 22: 18 1H NMR (500 MHz, CDCl3)

[1]HNMR of Compound 18a (PbSF1-R)

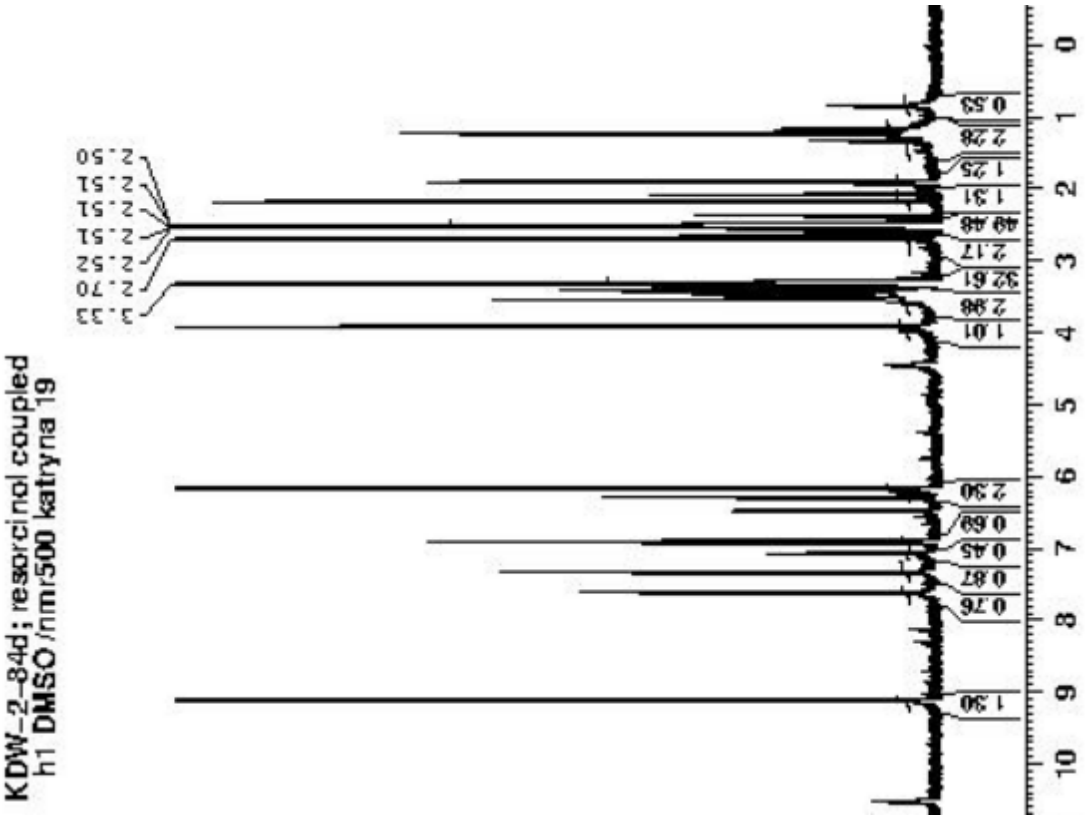

Spectrum 23: 18a 1H NMR (500 MHz, DMSO-d6)

[1]HNMR of Compound 18b (PbSF1-1n)

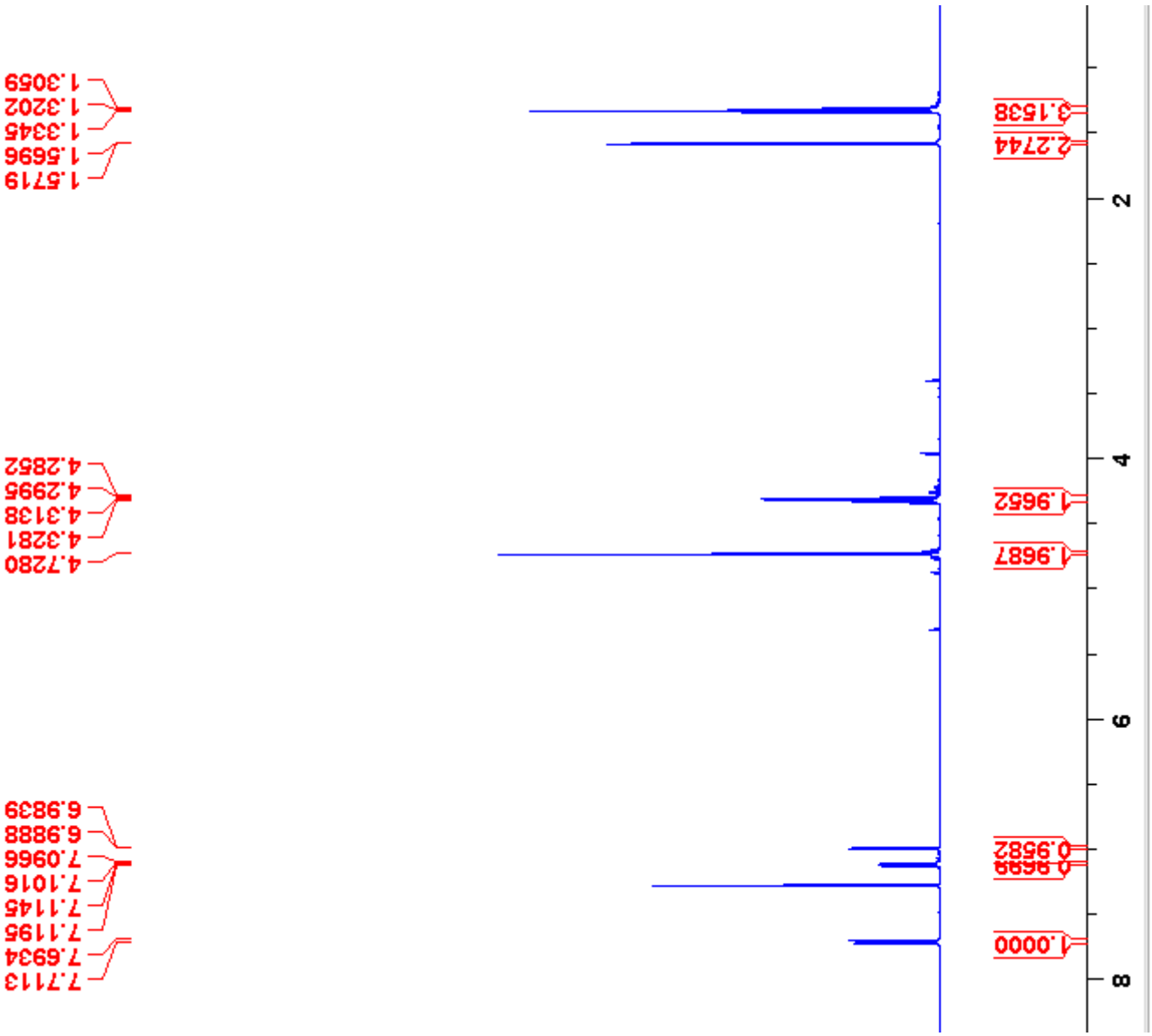

Spectrum 24: 18b 1H NMR (500 MHz, DMSO-d6)

^{13}CNMR of Compound 18b (PbSF1-1n)

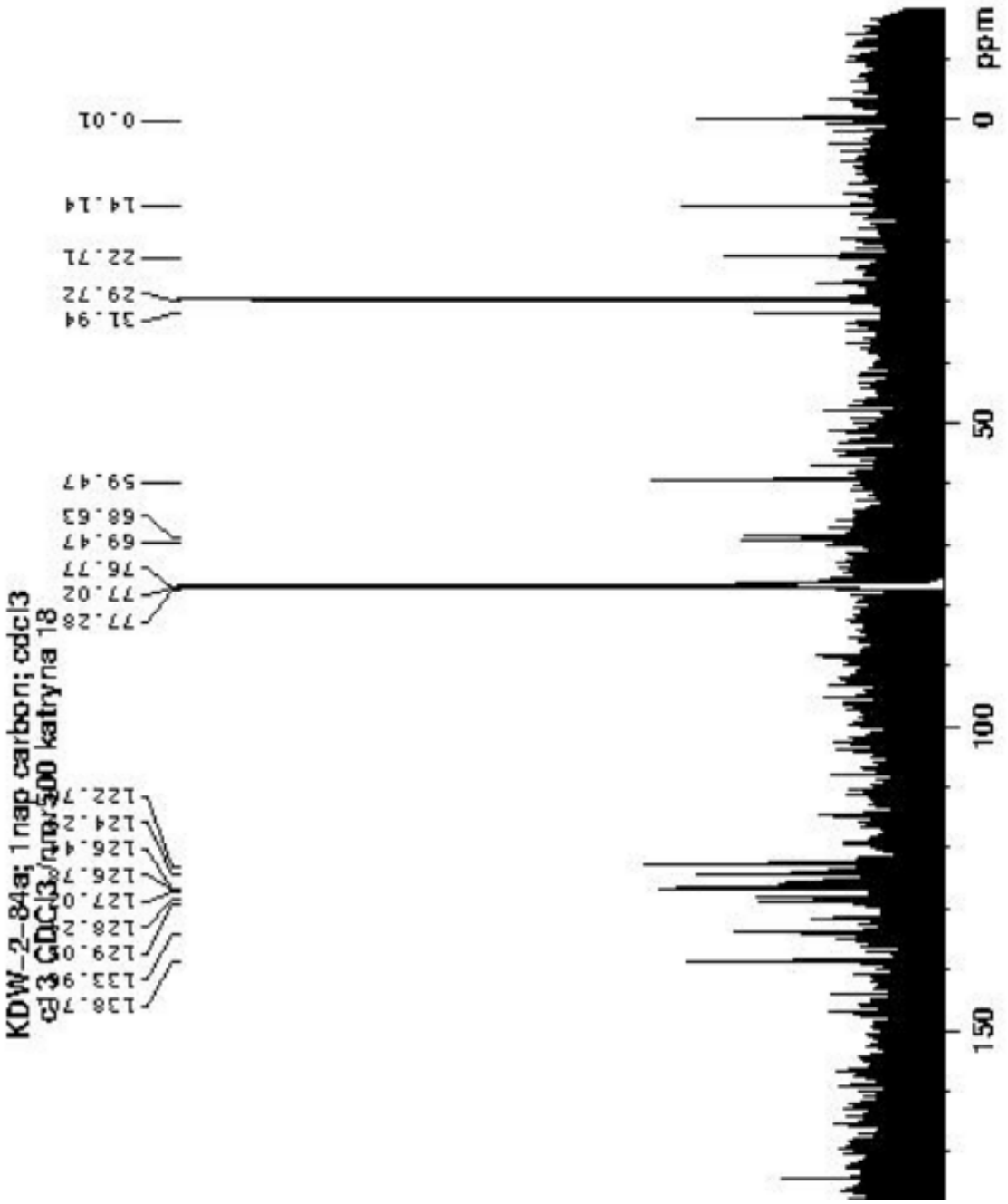

Spectrum 25: 18b 13C NMR (500 MHz, DMSO-d6)

^{1}HNMR of Compound 18c (PbSF1-2n)

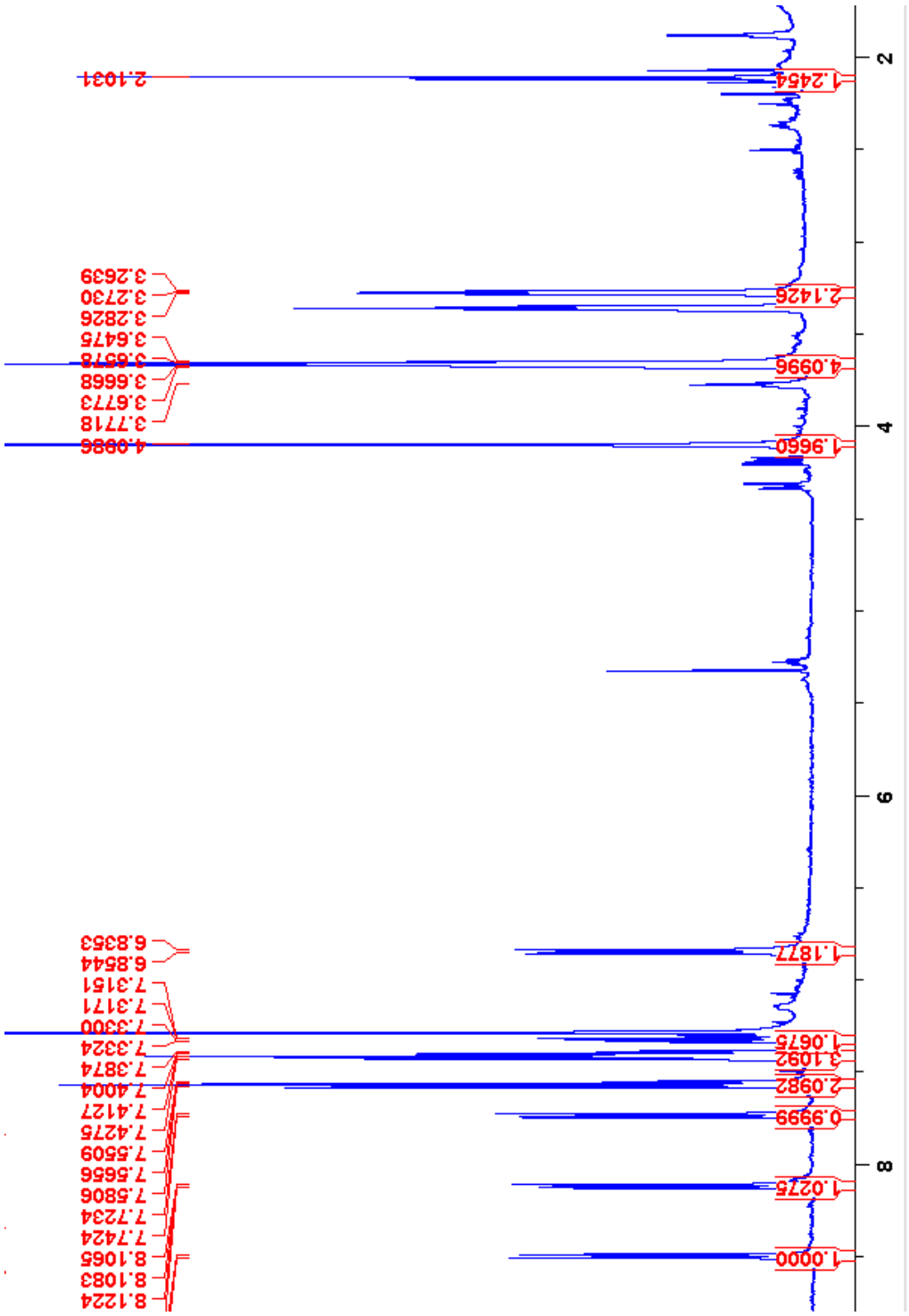

Spectrum 26: 18c 1H NMR (500 MHz, DMSO-d6)

^{13}CNMR of Compound 18c (PbSF1-2n)

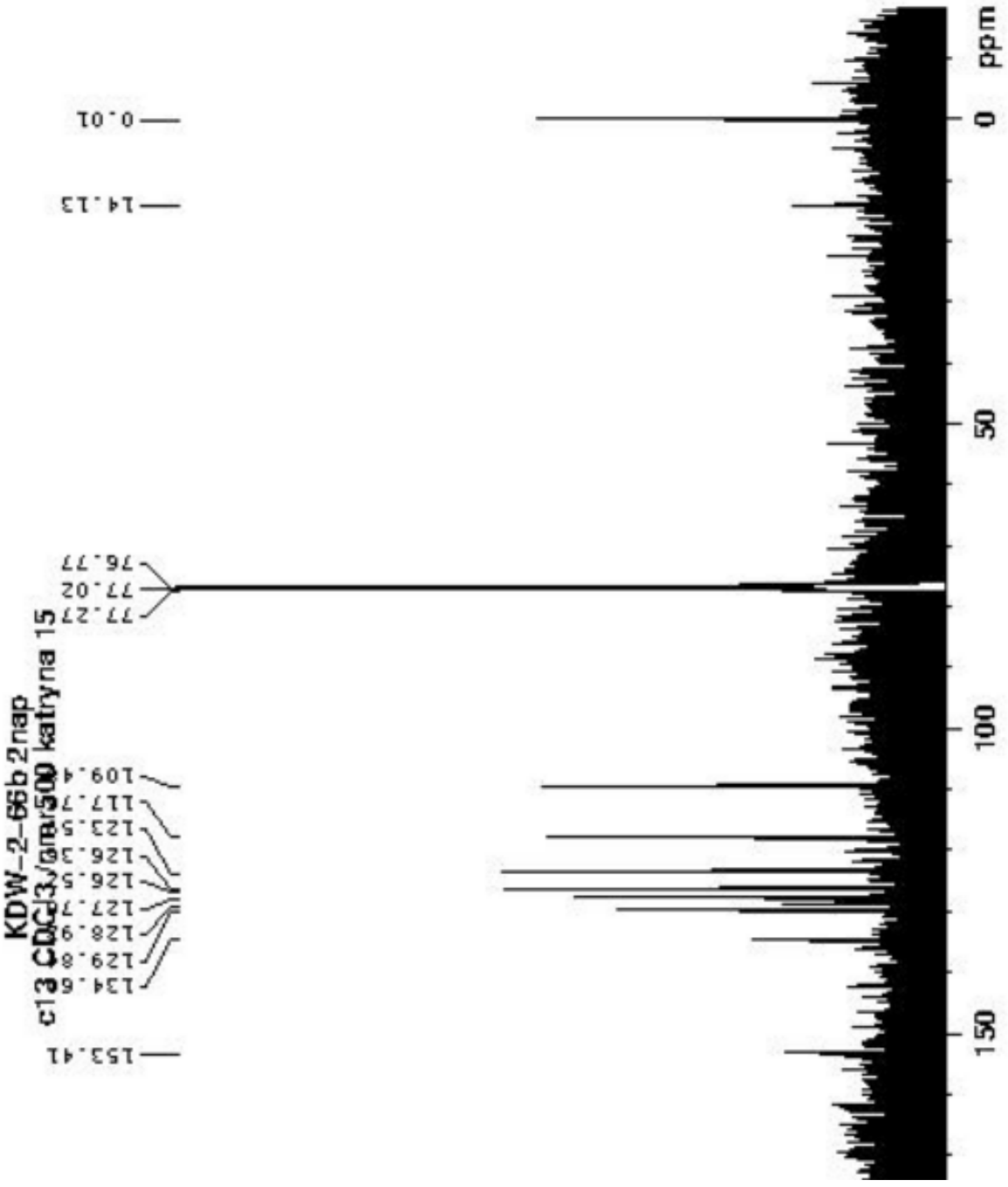

Spectrum 27: 18c 13C NMR (500 MHz, DMSO-d6)

[1]HNMR of Compound 18d (PbSF1-13)

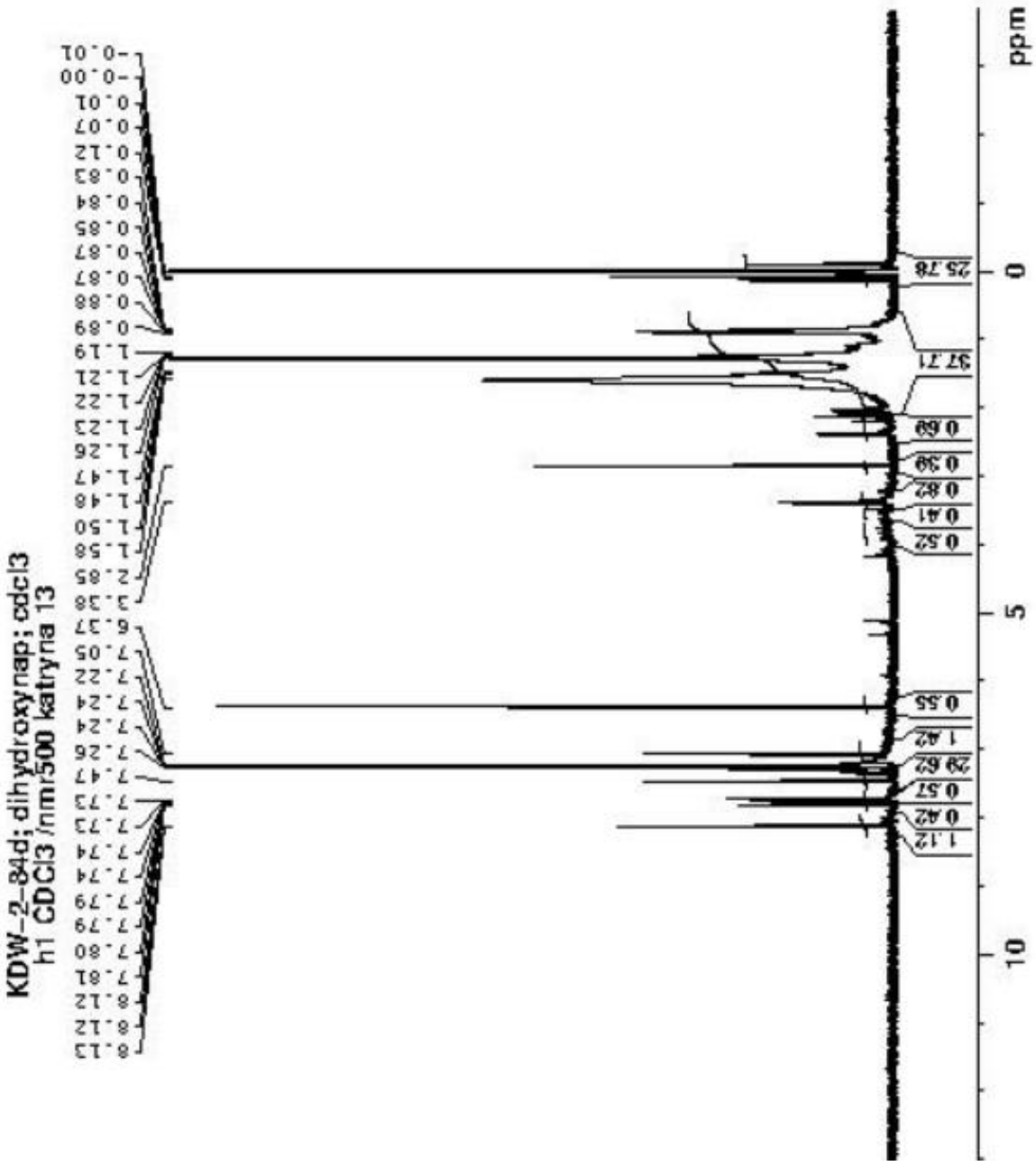

Spectrum 28: 18d 1H NMR (500 Mhz, DMSO-d6)

^{13}CNMR of Compound 18d (PbSF1-13)

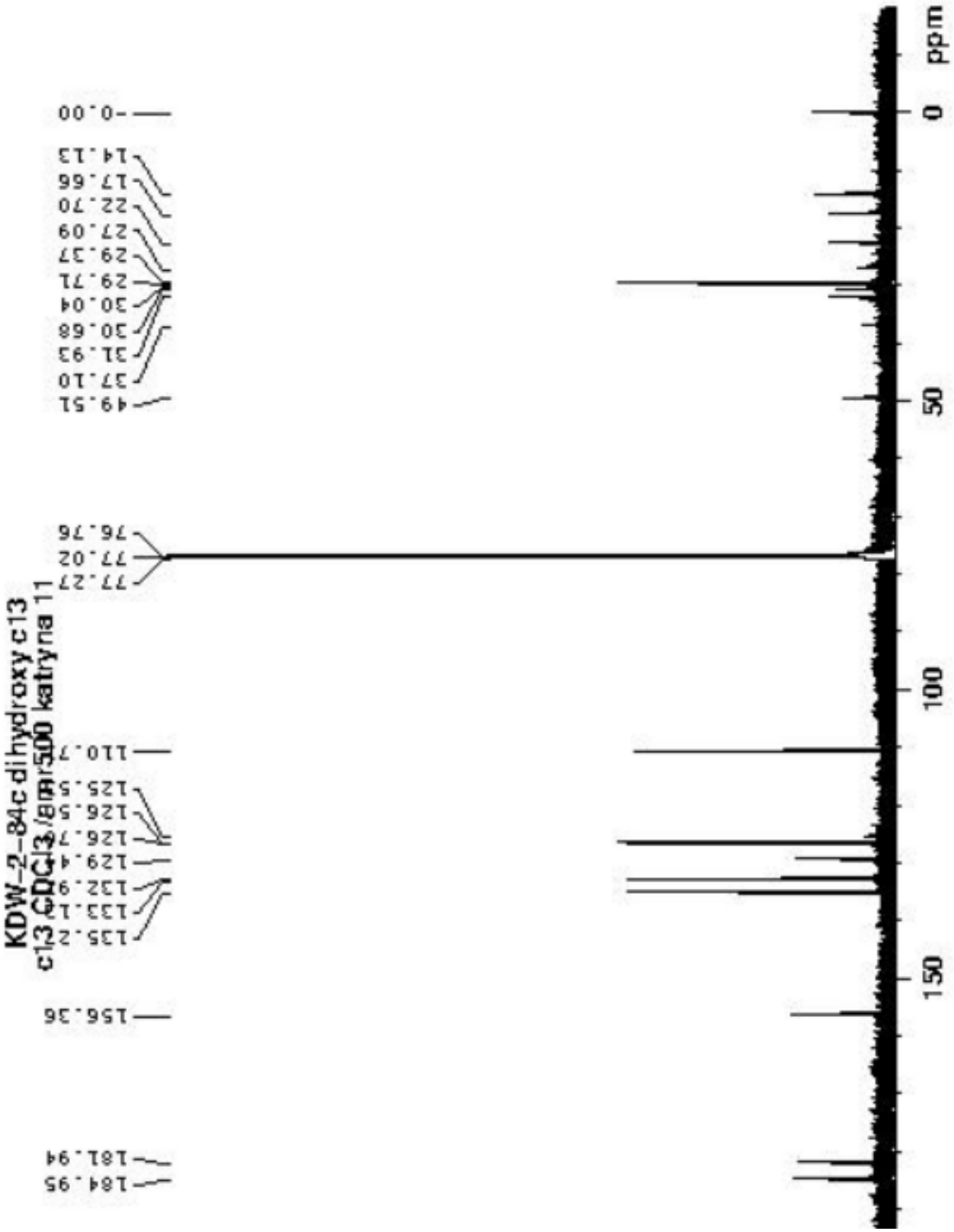

Spectrum 29: 18d 13C NMR (500 Mhz, DMSO-d6)

^{1}HNMR of Compound 18e (PbSF1-27)

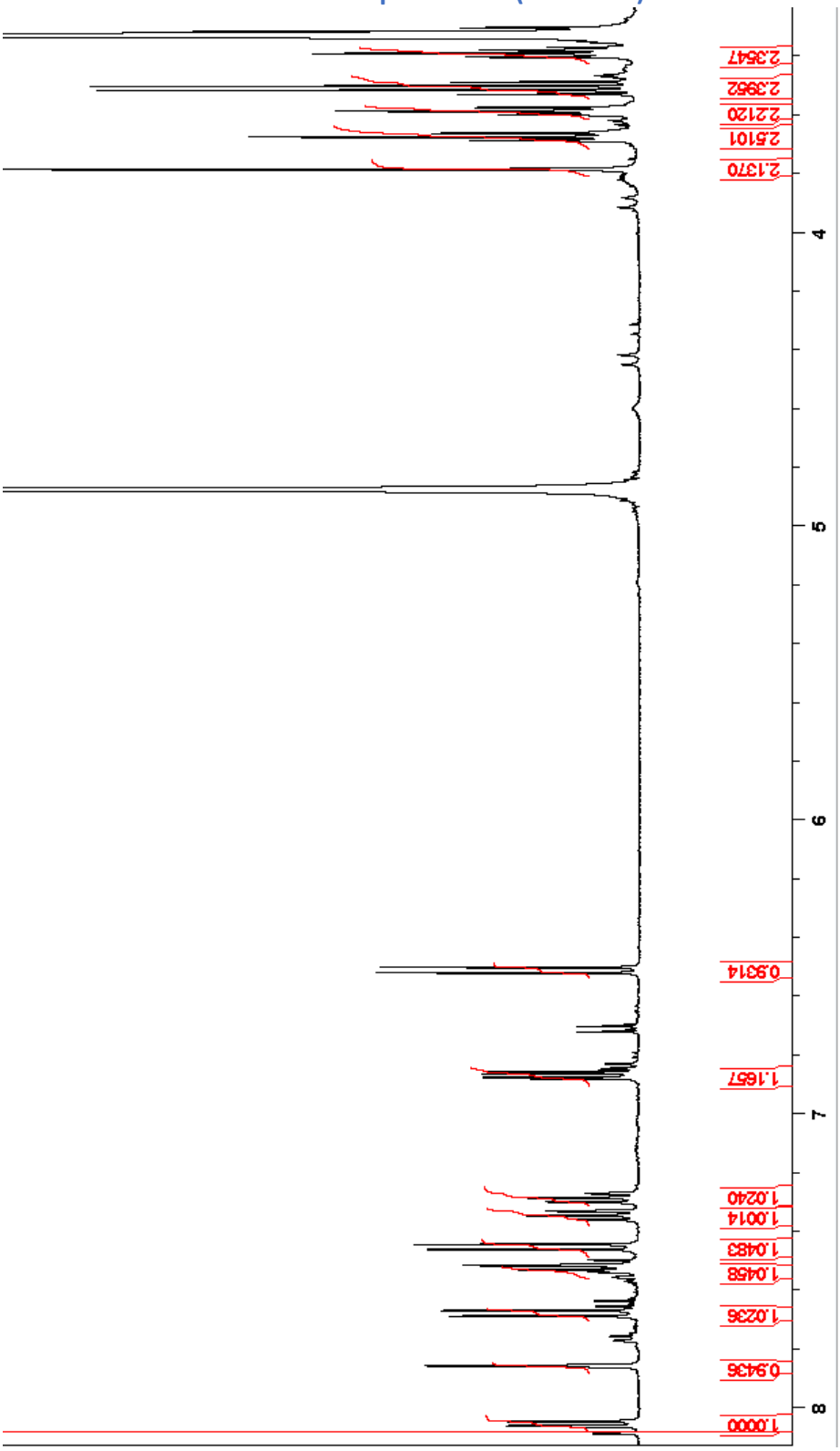

Spectrum 30: 18e 1H NMR (500 MHz, DMSO-d6)

^{13}CNMR of Compound 18e (PbSF1-27)

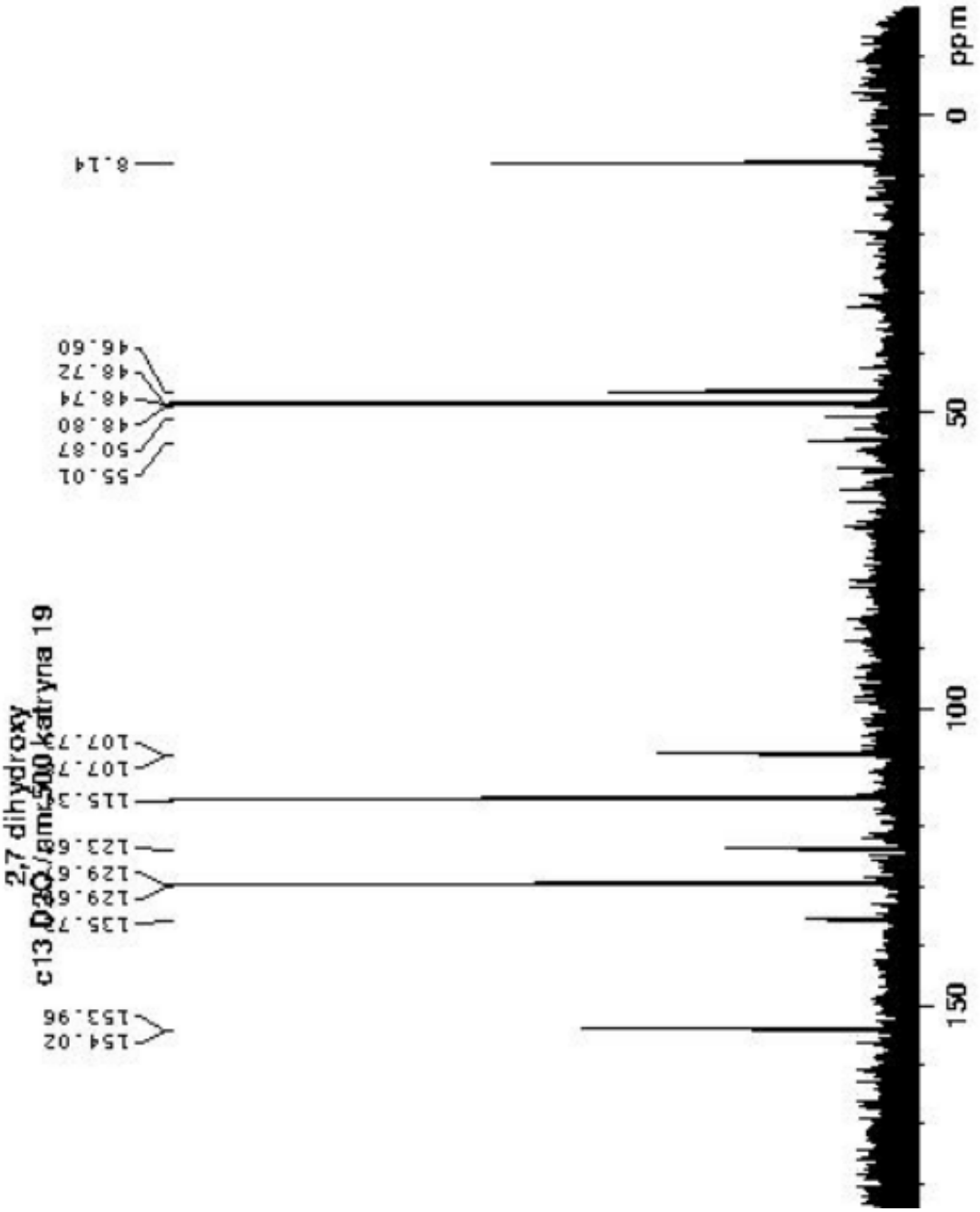

Spectrum 31: 18e 13C NMR (500 MHz, D2O)

[1]HNMR of Compound 18f (PbSF1-cR)

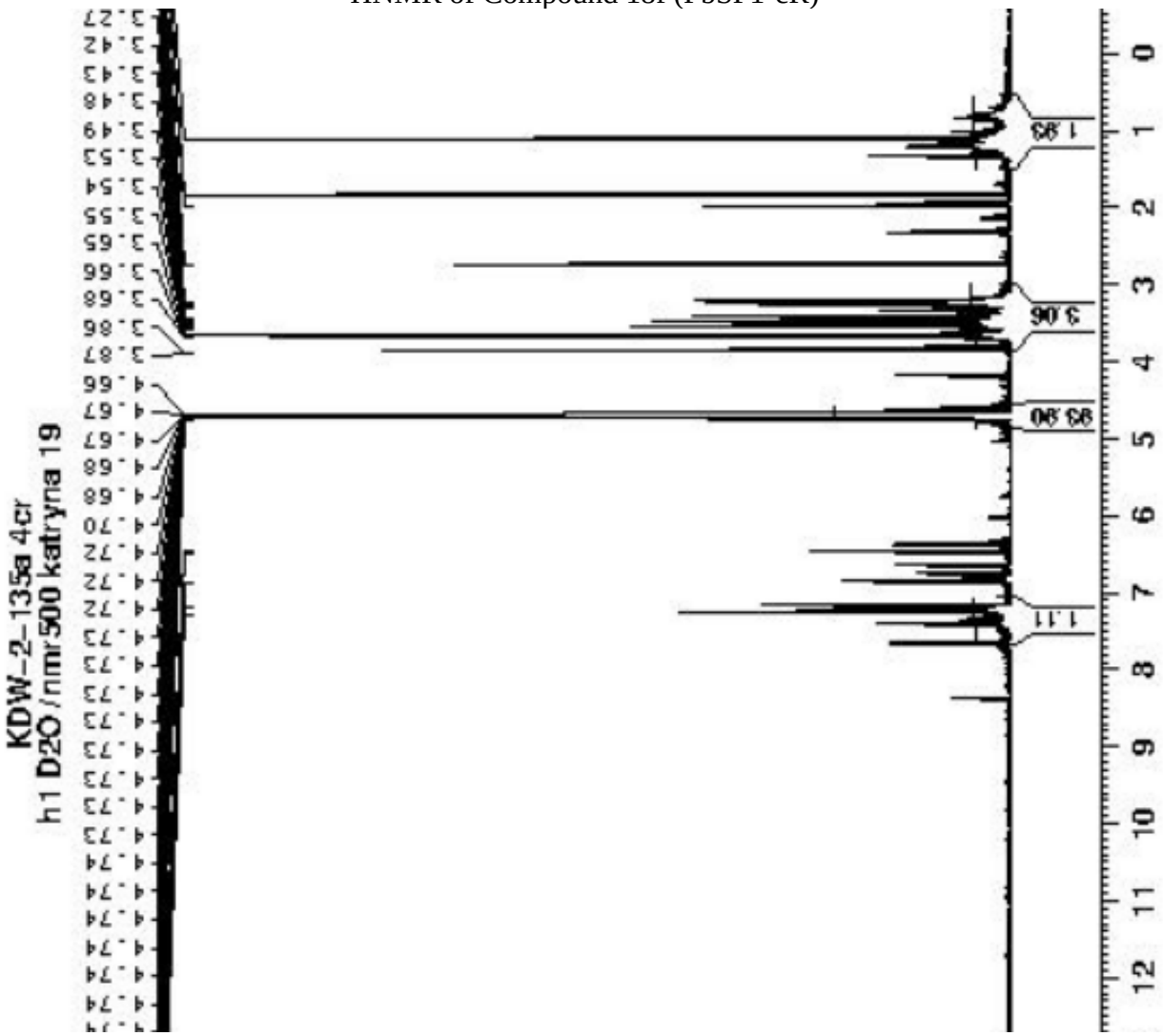

Spectrum 32: 18f 1H NMR (500 MHz, D2O)

^{1}HNMR of Compound 19

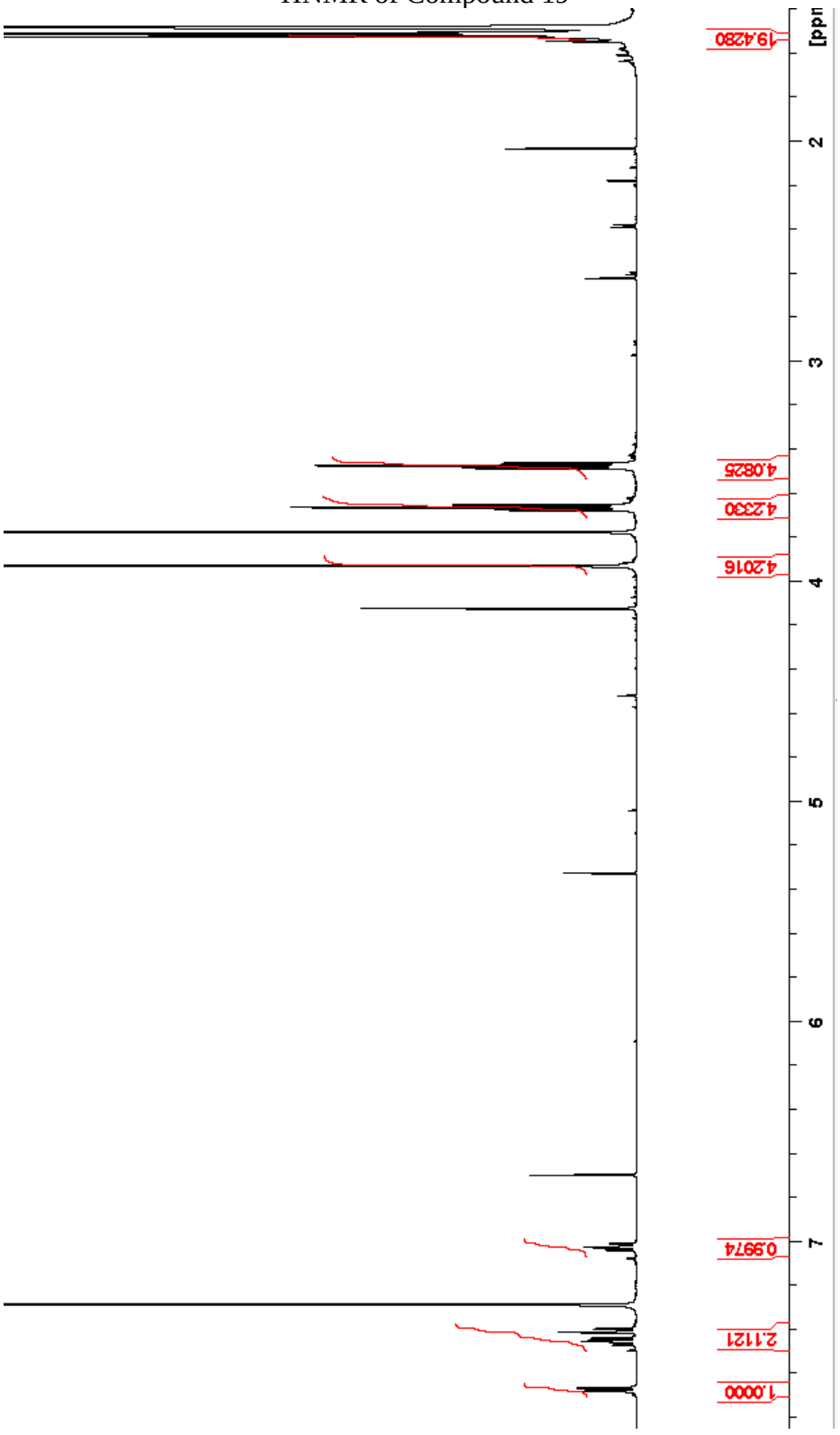

Spectrum 33: 19 1H NMR (500 MHz, CDCl3)

^{1}HNMR of Compound 19a

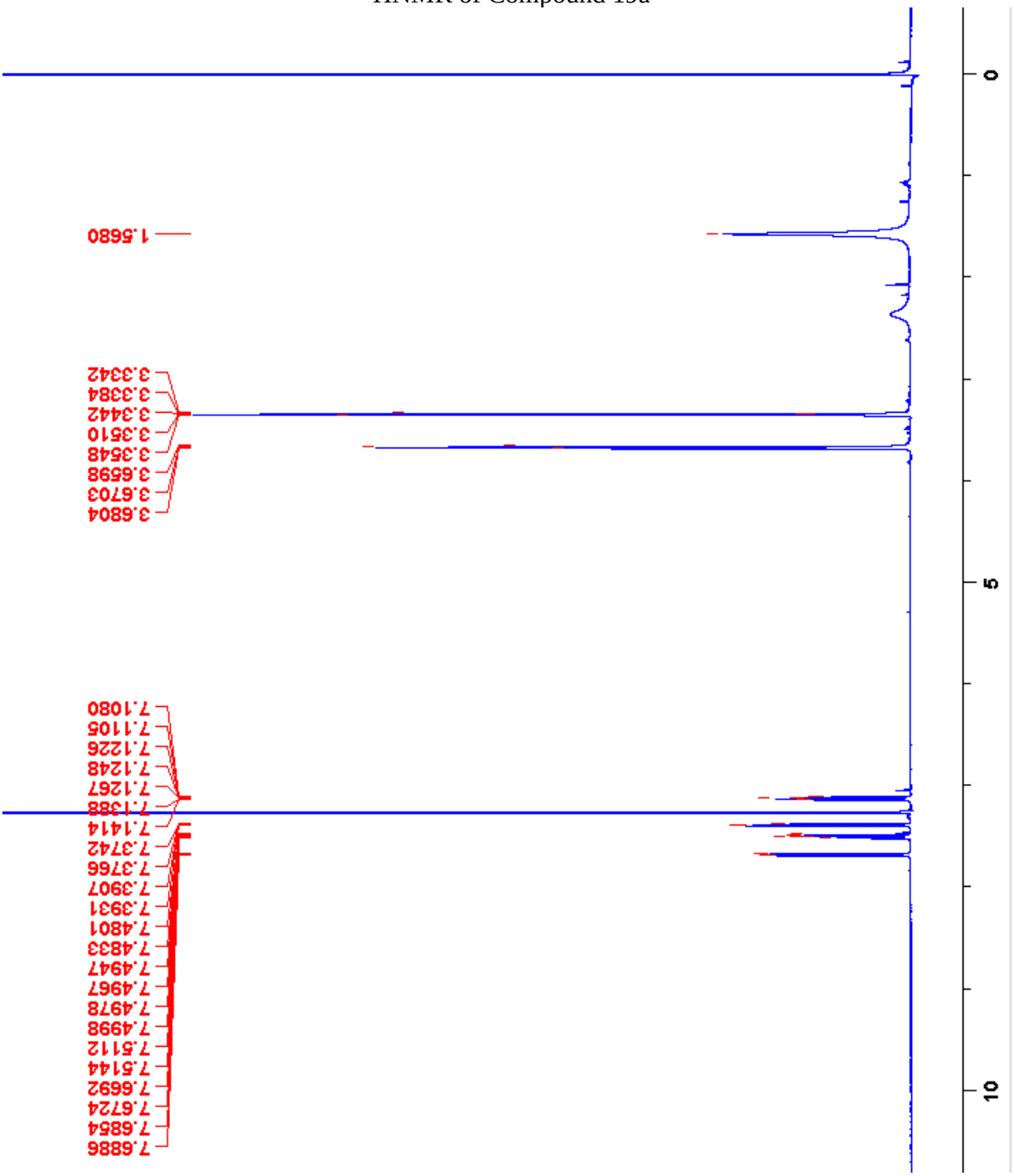

Spectrum 34: 19a 1H NMR (500 MHz, CDCl3)

[1]HNMR of Compound 19b

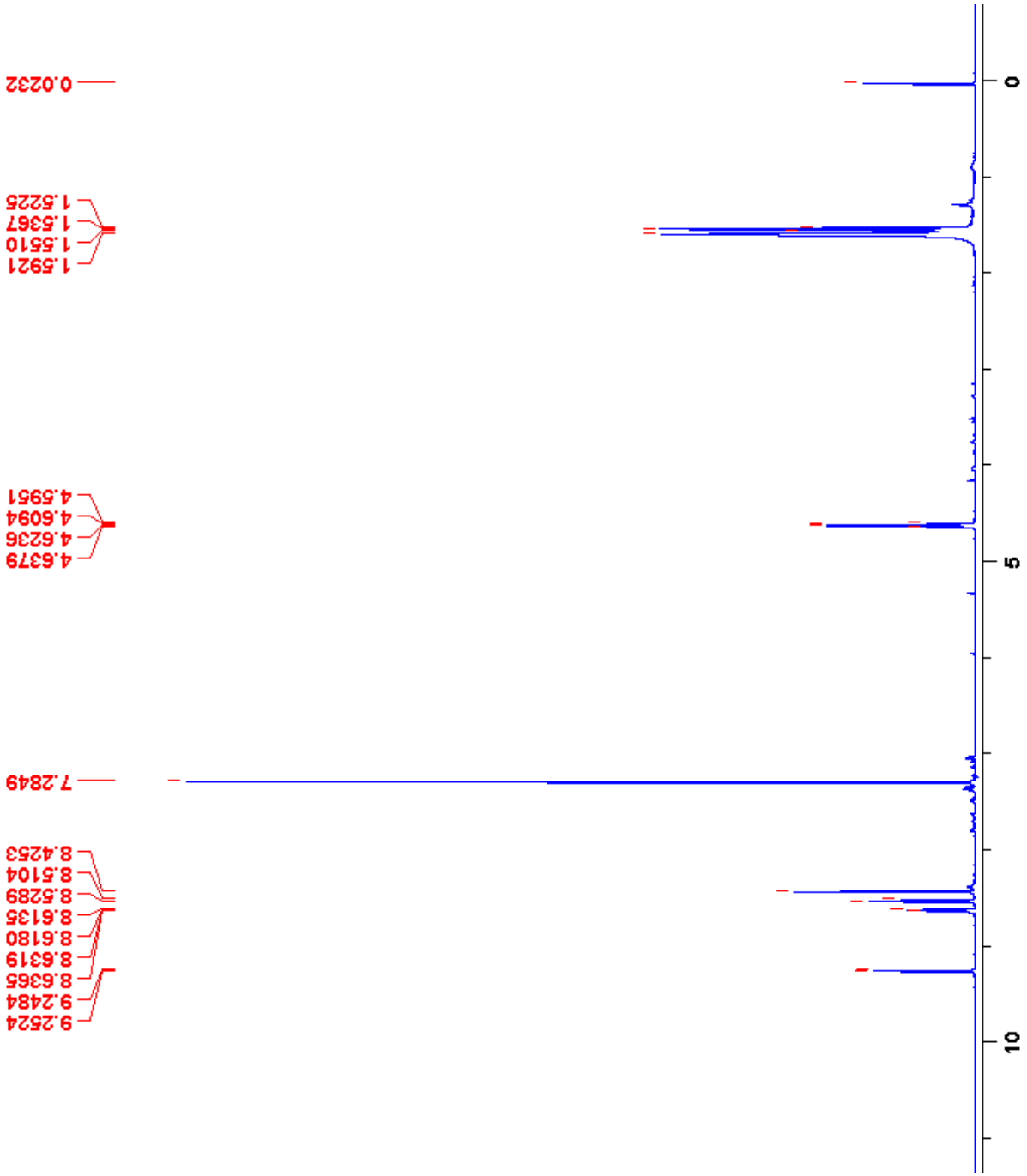

Spectrum 35: 19b 1H NMR (500 MHz, CDCl3)

[1]HNMR of Compound 19c

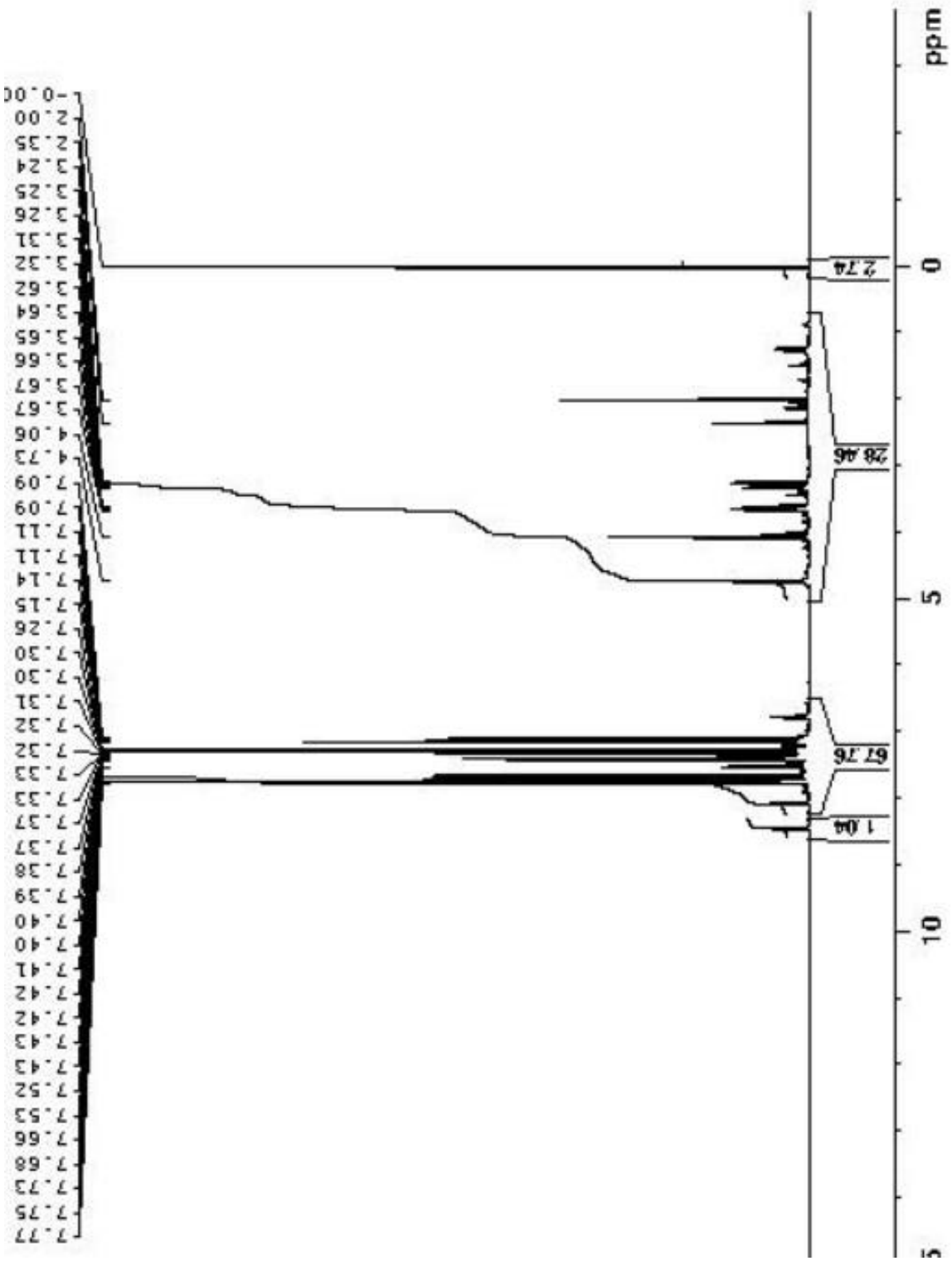

Spectrum 36: 19c 1H NMR (500 MHz, DMSO-d6)

^{1}HNMR of Compound 20a

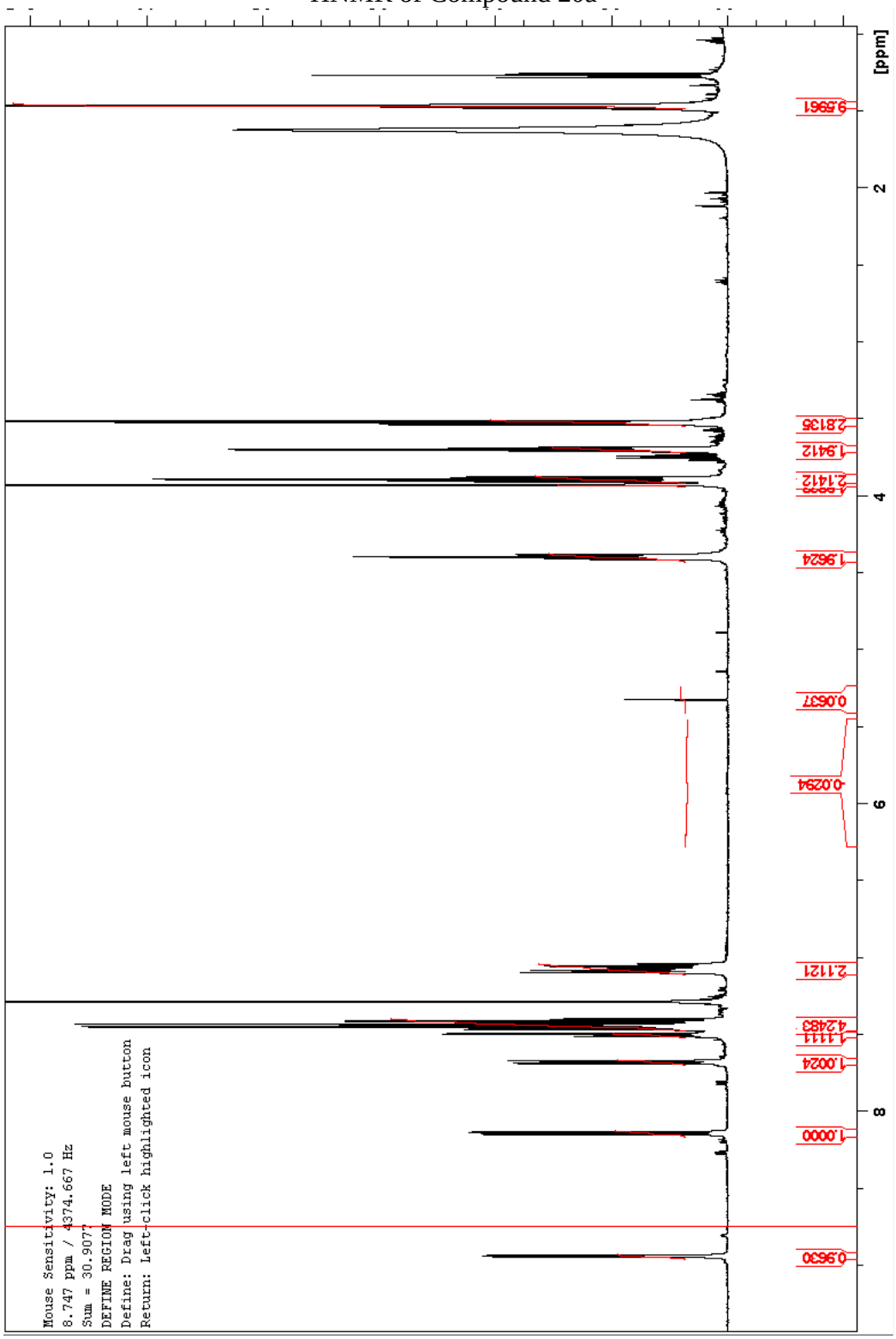

Spectrum 37: 20a 1H NMR (500 MHz, DMSO-d6)

^{1}HNMR of Compound 20b

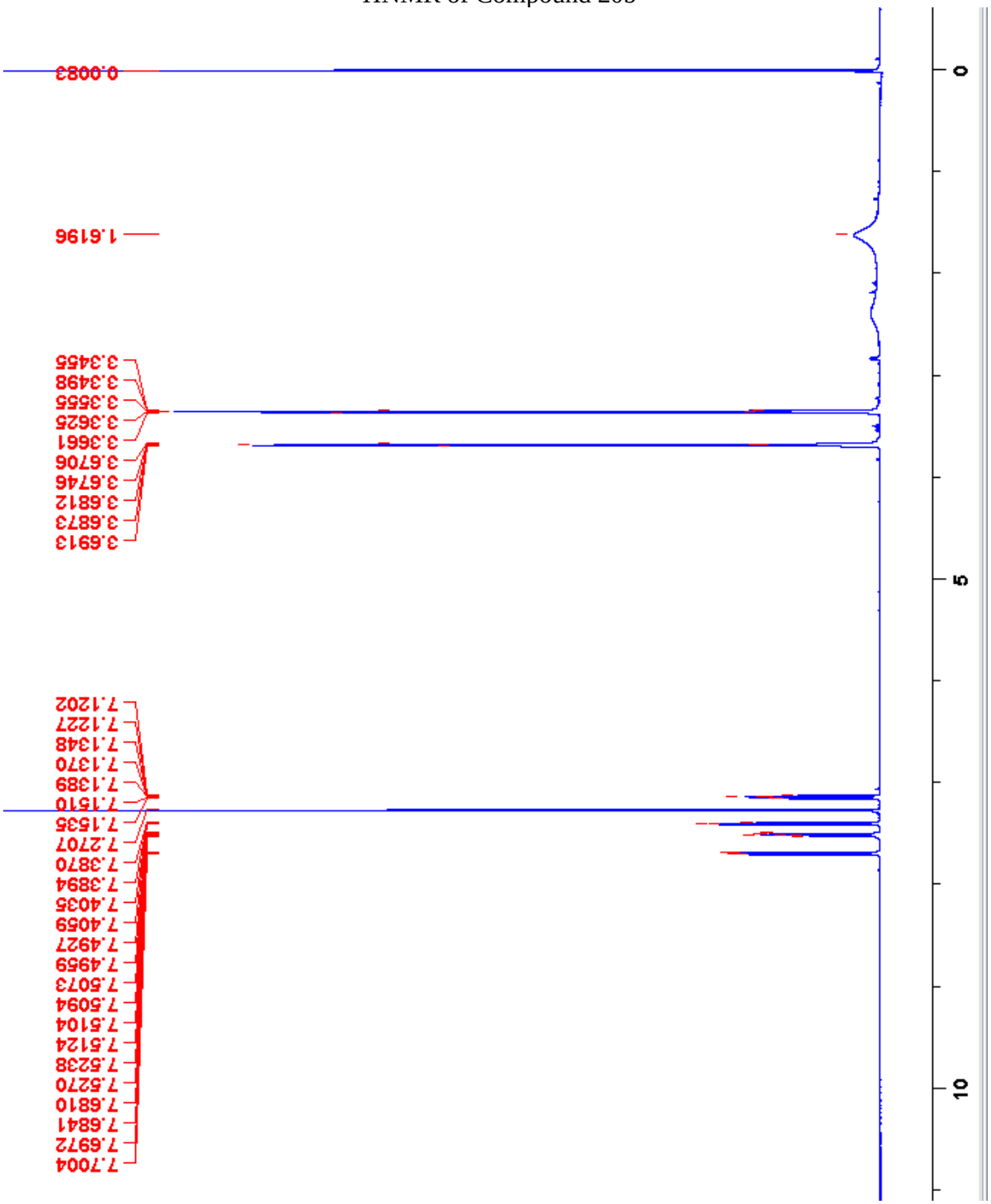

Spectrum 38: 20b 1H NMR (500 MHz, DMSO-d6)

[1]HNMR of Compound 21a

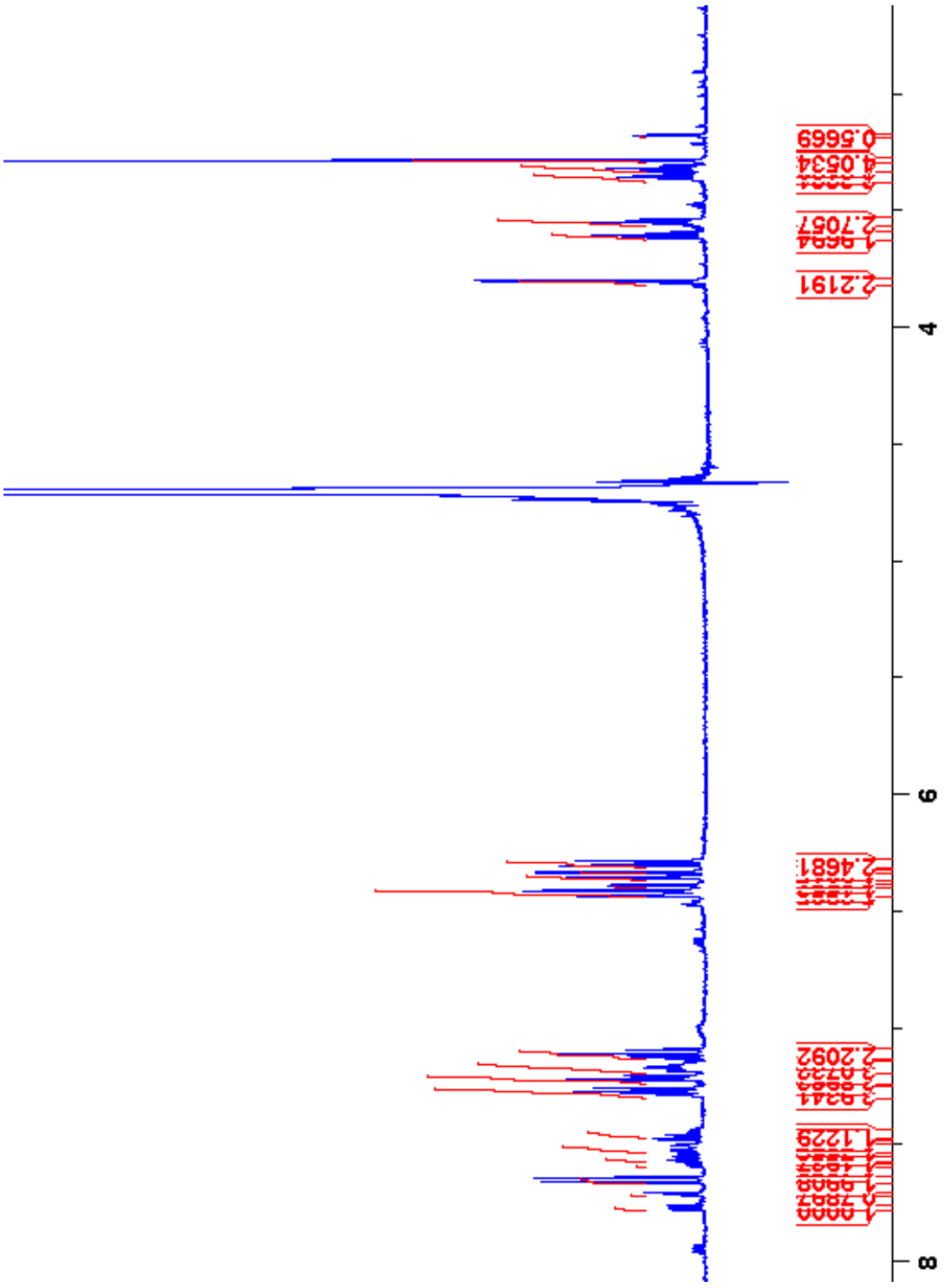

Spectrum 39: 21a 1H NMR (500 MHz, MeOD)

[1]HNMR of Compound 23

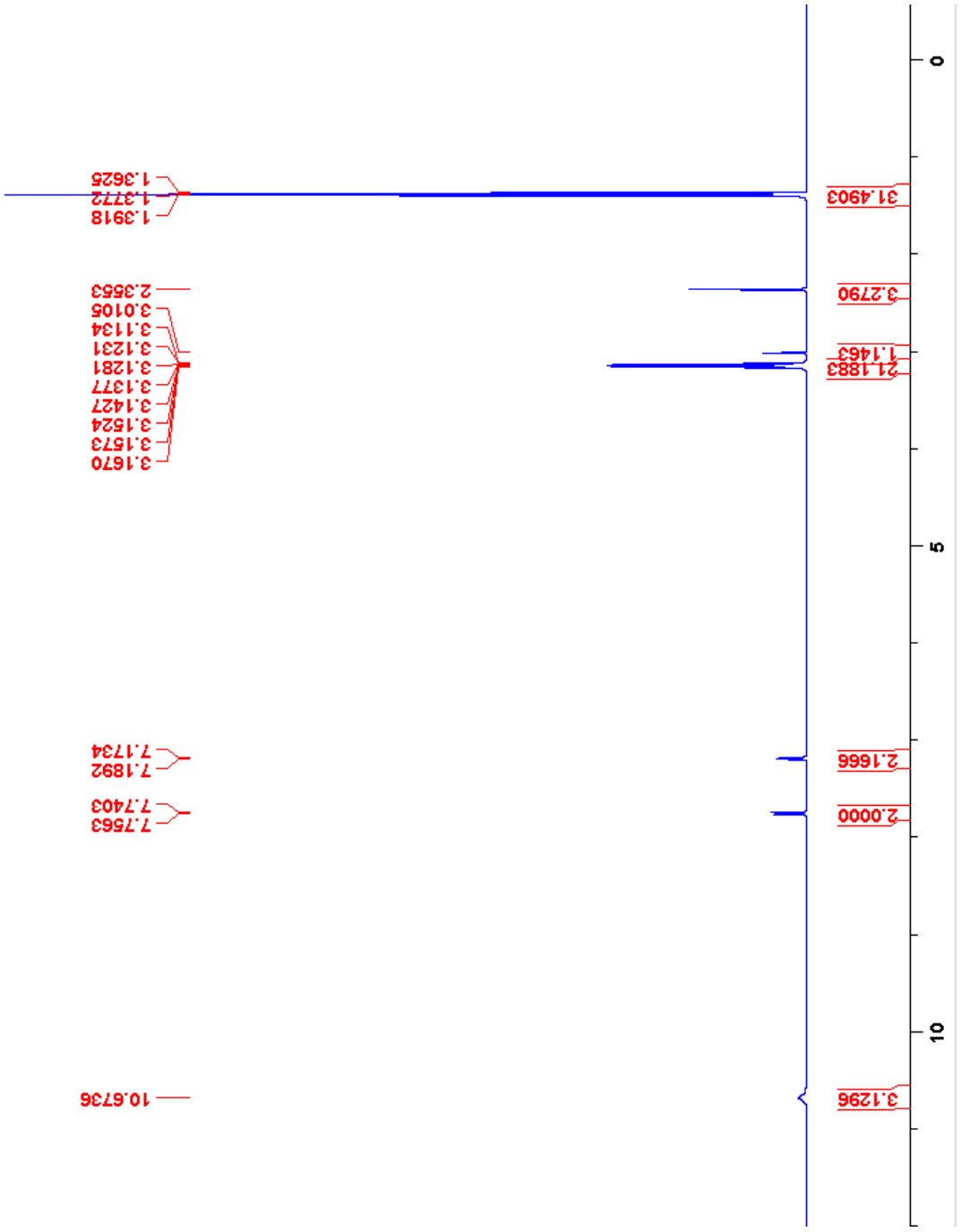

Spectrum 40: 23 1H NMR (500 MHz, CDCl3)

^{1}HNMR of Compound 24

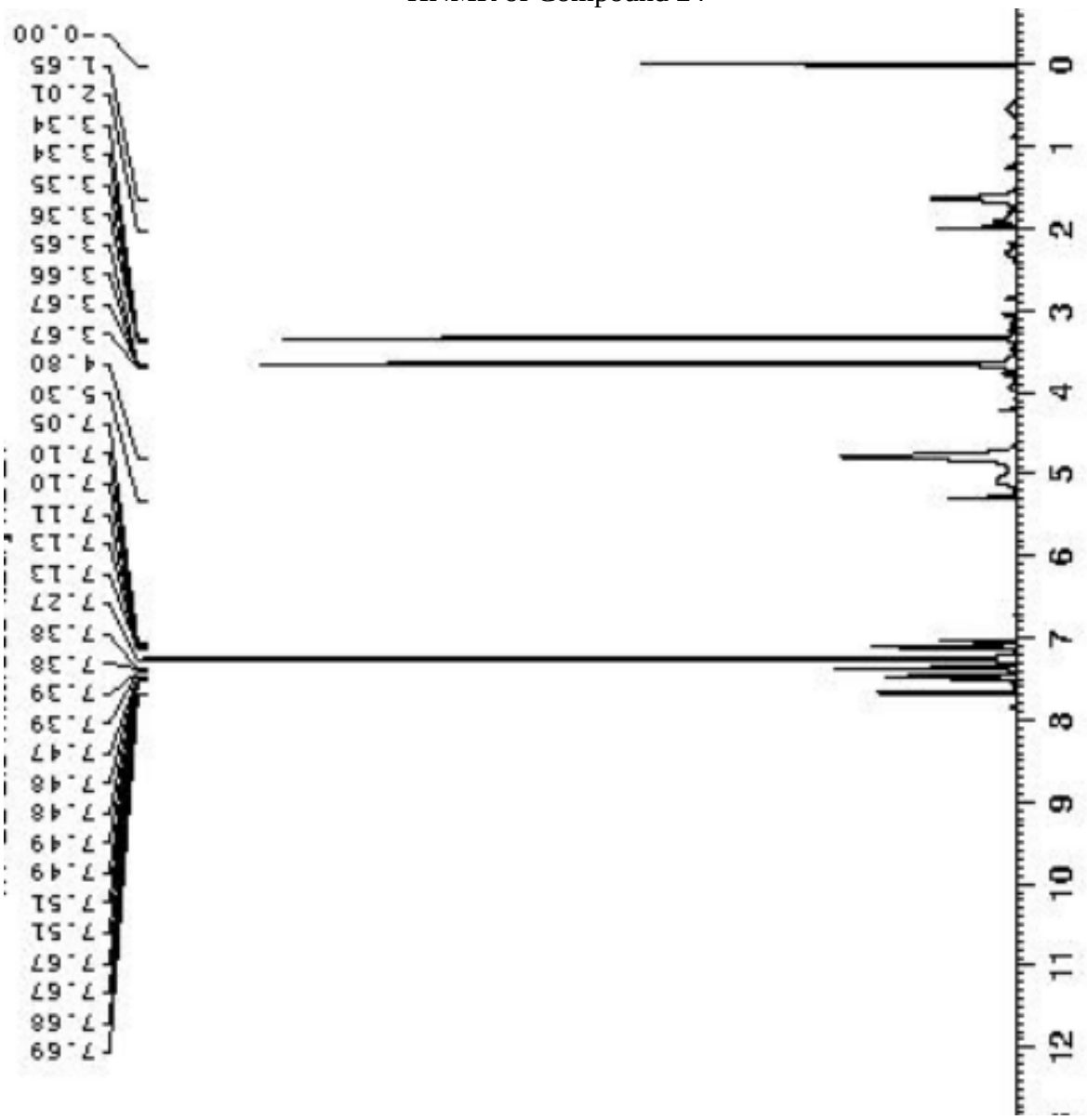

Spectrum 41: 24 1H NMR (500 MHz, CDCl3)

Titration of 18a, PbSF1-R right after synthesis, low ppm Pb pH 9

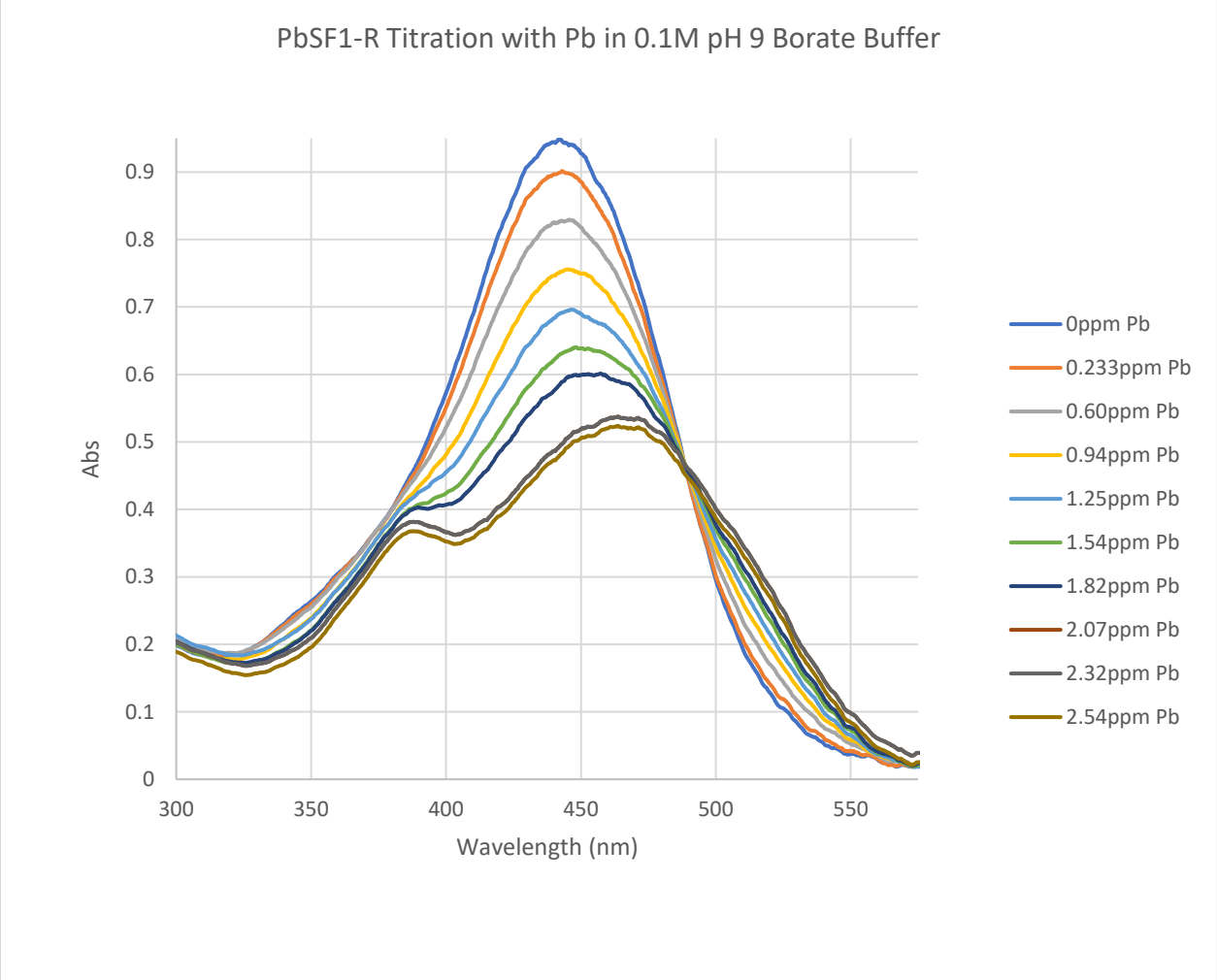

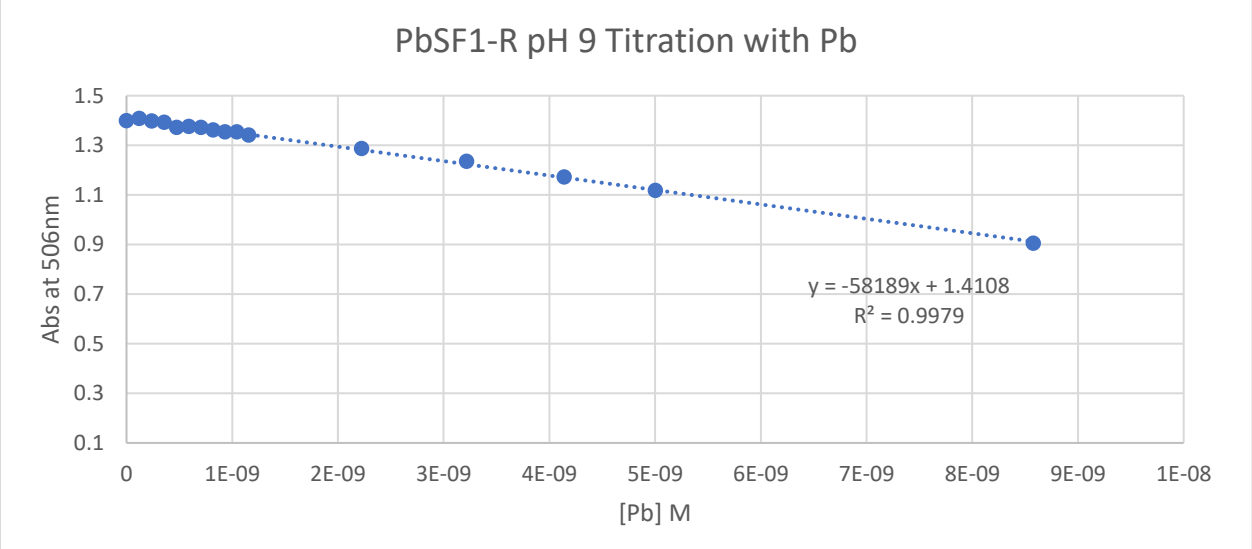

Spectrum 42: 18a Titration with Pb at pH 9, Week 0, low ppm; Abs vs [Pb]

Titration of 18a, PbSF1-R right after synthesis, ppm Pb and Zn

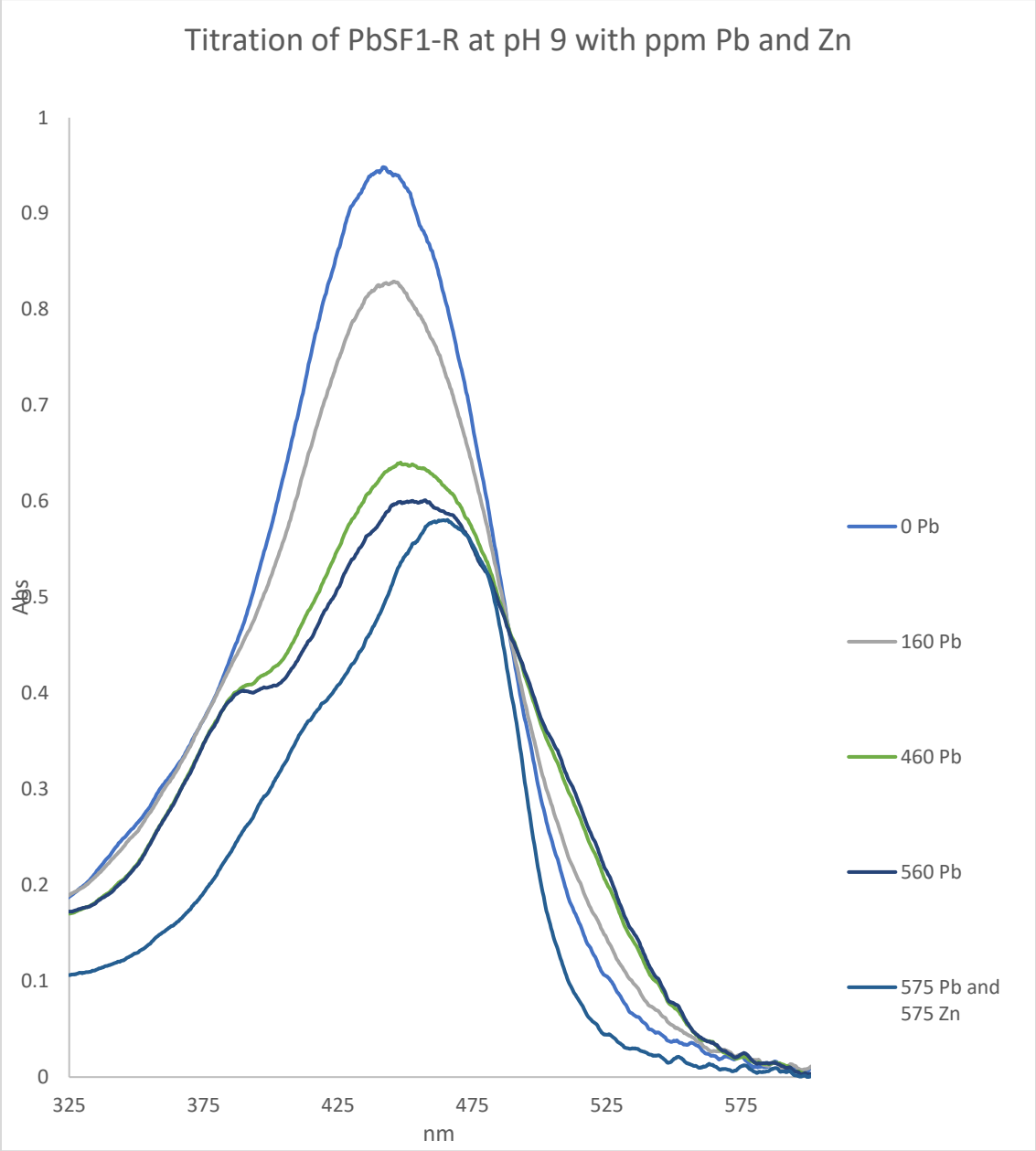

Spectrum 43: 18a Titration with Pb and Zn at pH 9, Week 0, ppm

Titration of 18a, PbSF1-R 3 weeks after synthesis, pH 9 low ppb Pb

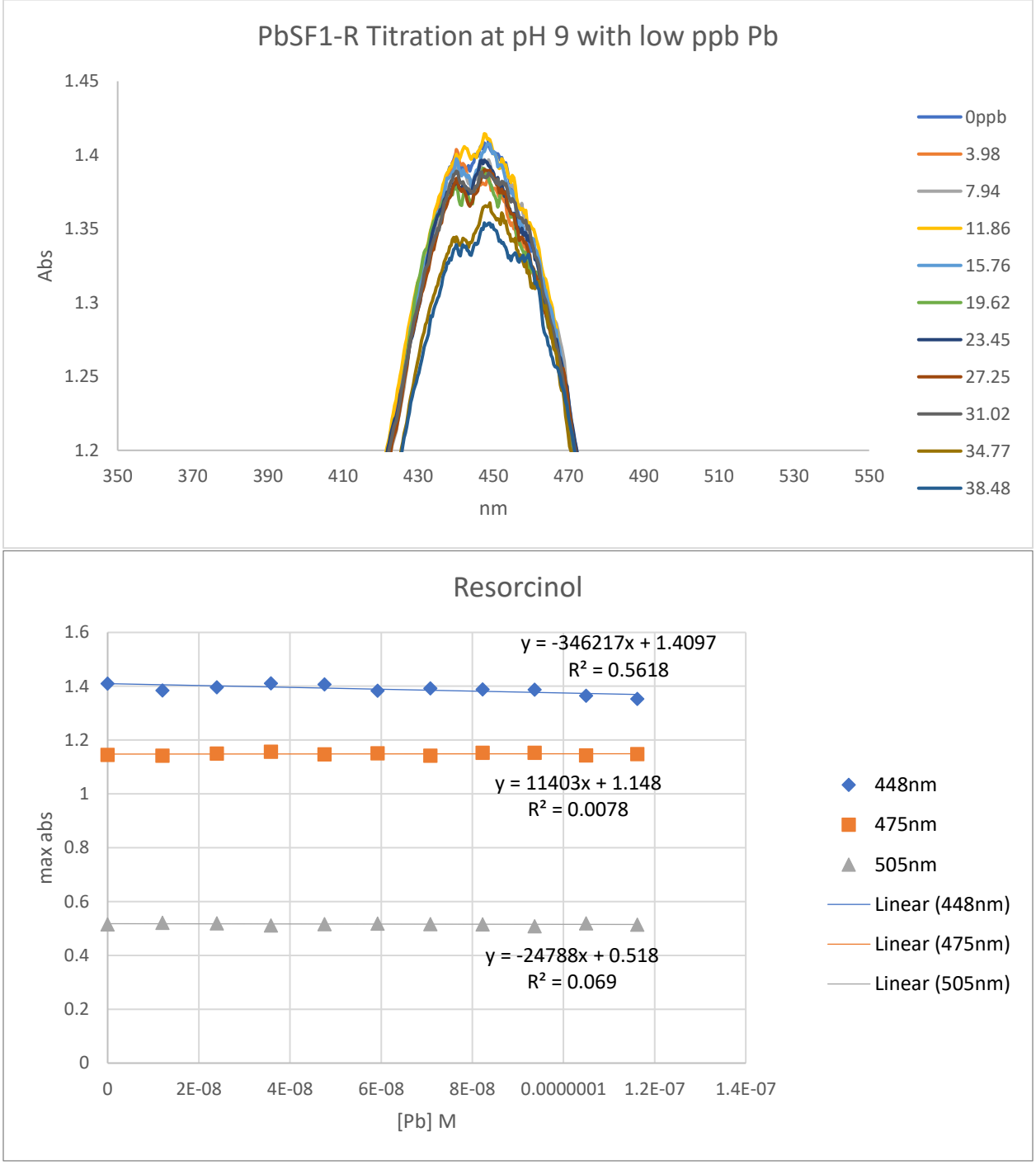

Spectrum 44: 18a Titration with Pb at pH 9, Week 3, low ppb; Abs vs [Pb]

Titration of 18a, PbSF1-R 2 weeks after synthesis at pH 7, varied metals

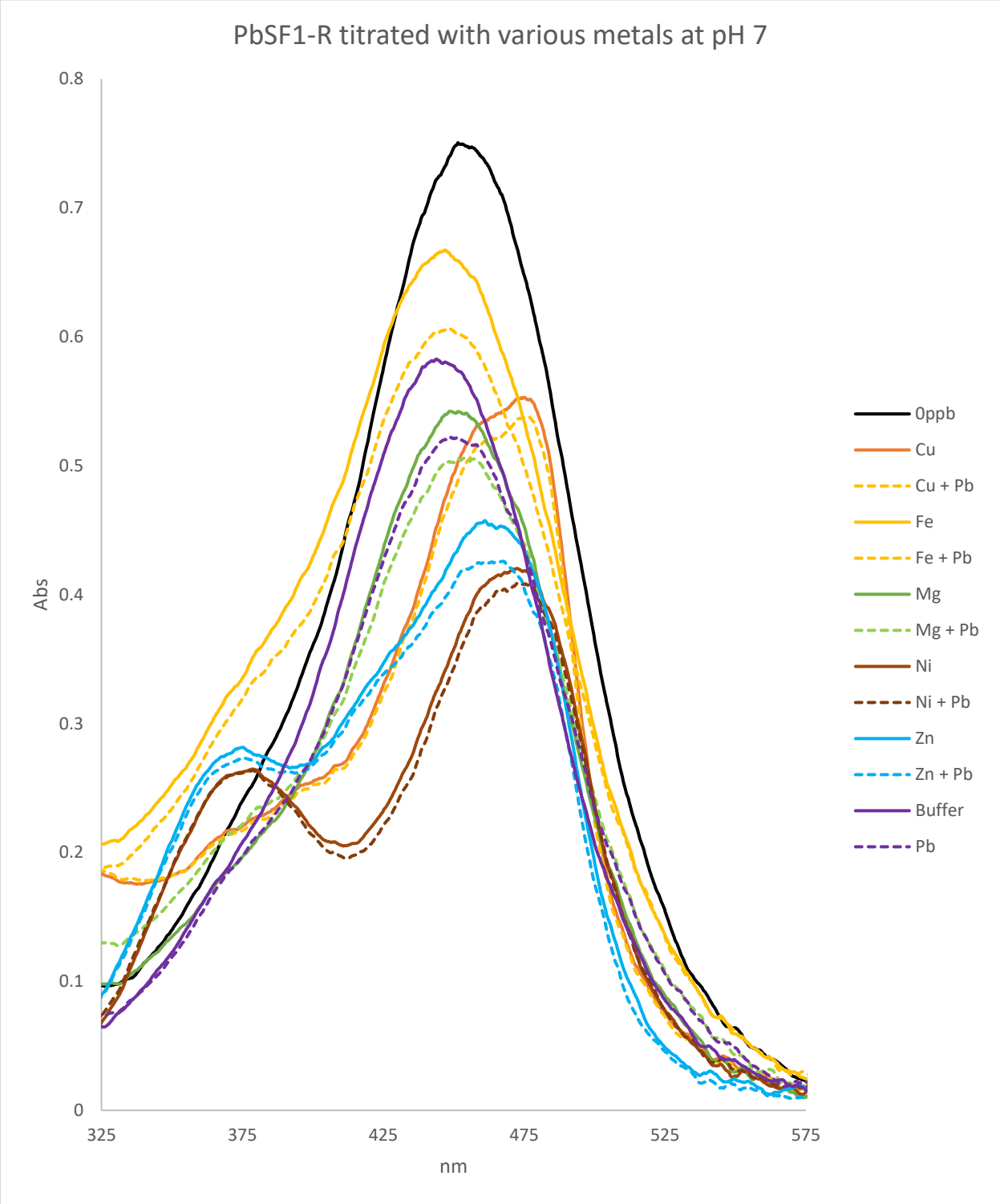

Spectrum 45: 18a Titration with varied metals, pH 7, Week 2, saturated

Titration of 18b, PbSF1-1n right after synthesis, low ppm Pb pH 9

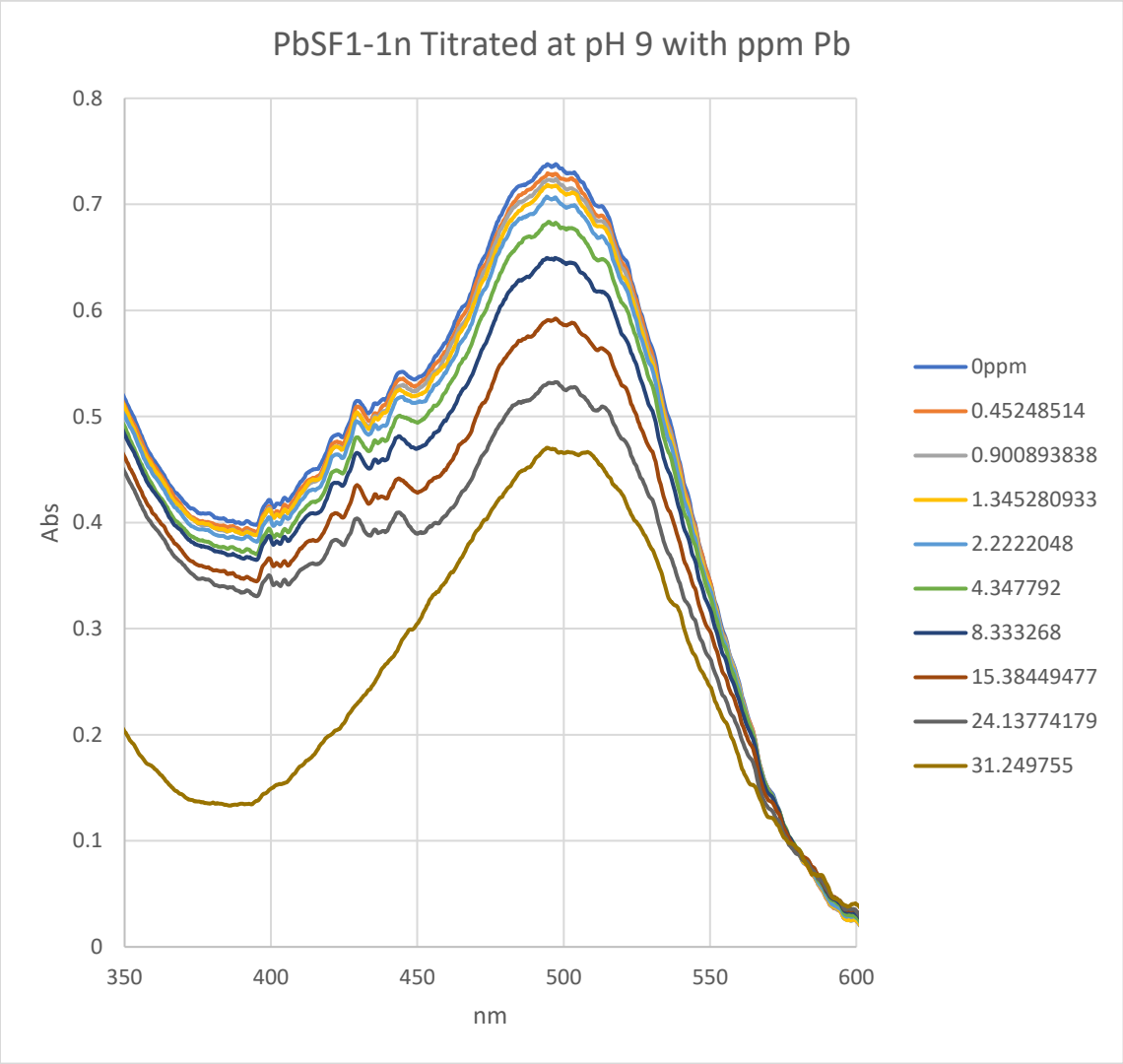

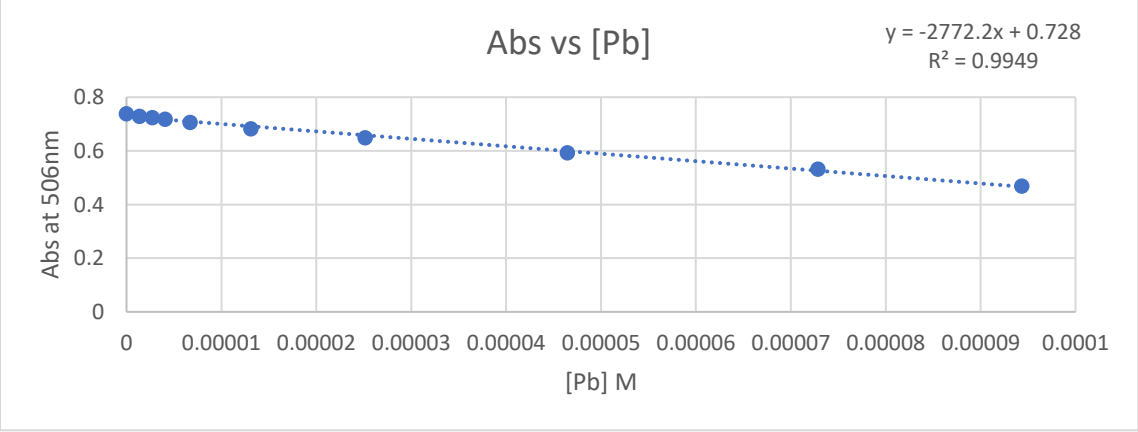

Spectrum 46: 18b Titration with Pb at pH 9, Week 0, ppm; Abs vs [Pb]

Titration of 18b, PbSF1-1n right after synthesis, low ppb Pb pH 9

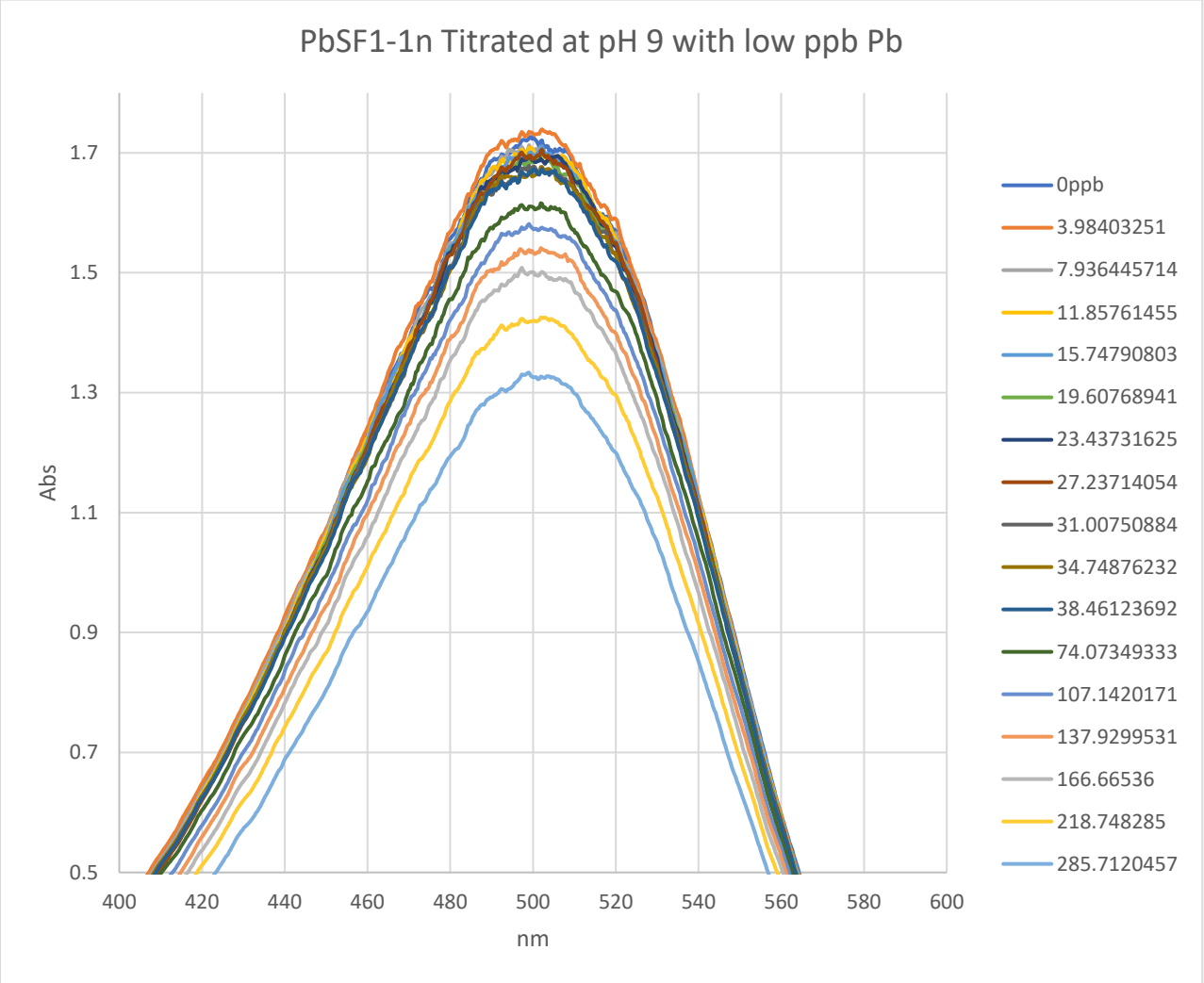

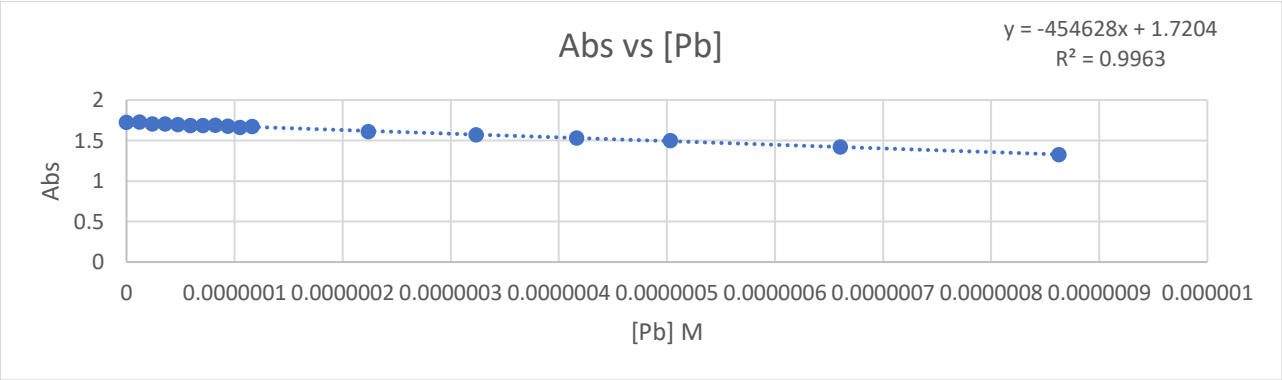

Spectrum 47: 18b Titration with Pb at pH 9, Week 0, low ppb; Abs vs [Pb]

Titration of 18b, PbSF1-1n three weeks after synthesis, ppb Pb pH 9

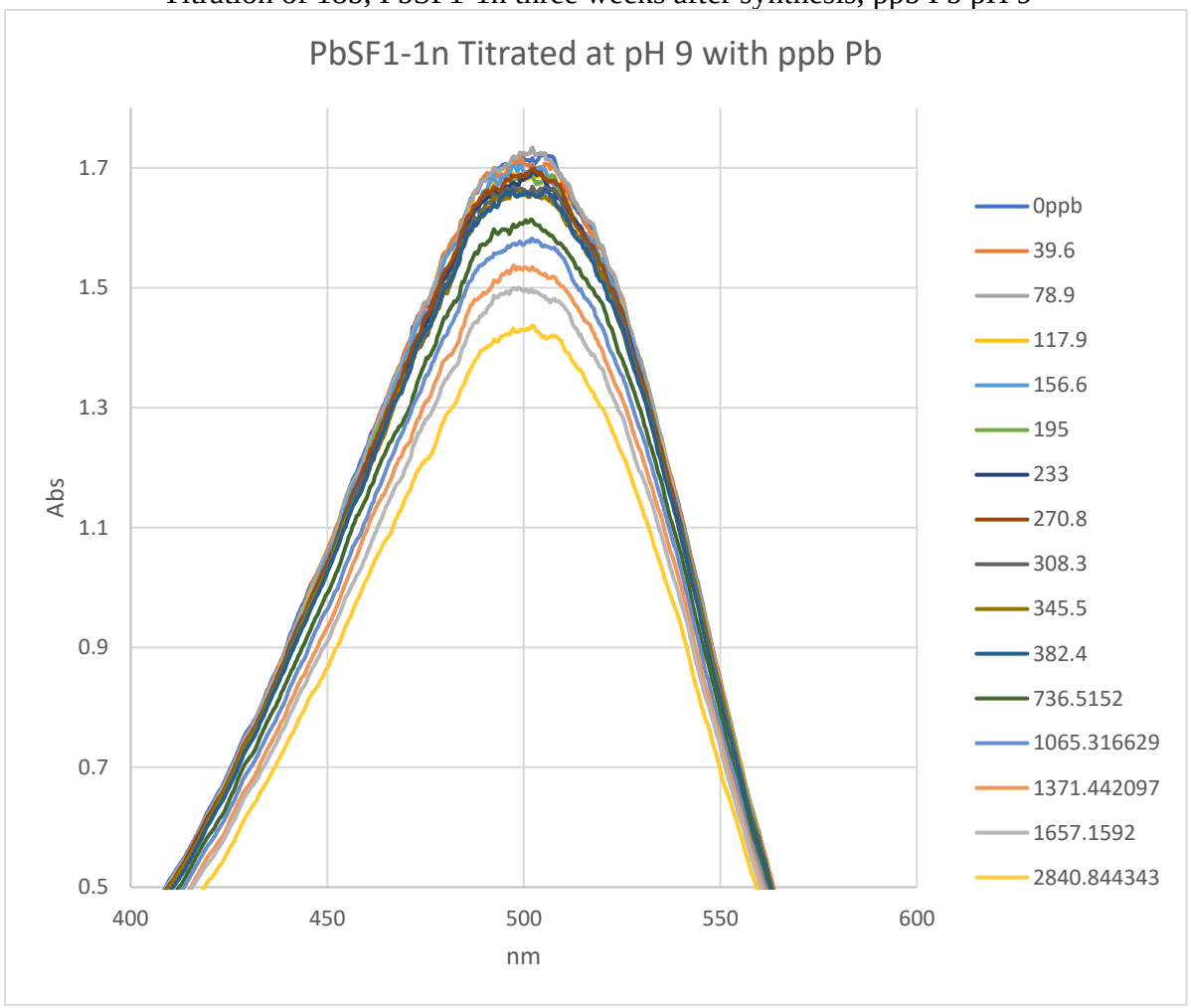

Spectrum 48: 18b Titration with Pb at pH 9, Week 3, low ppb; Abs vs [Pb]

Titration of 18b, PbSF1-1n immediately after synthesis, titrated with Cu, pH 9

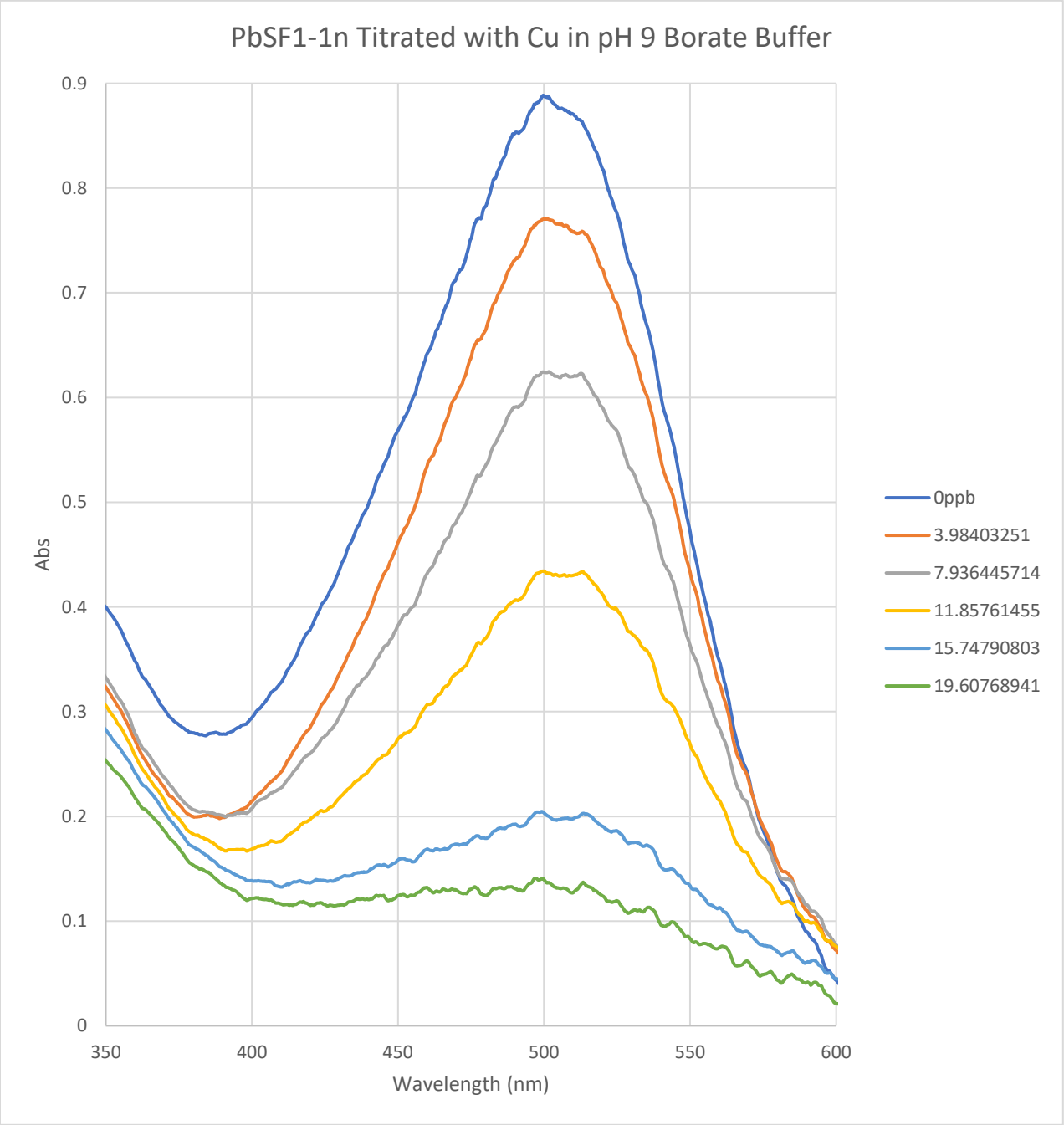

Spectrum 49: 18b Titration with Cu at pH 9, Week 0, low ppb

Titration of 18b, PbSF1-1n two weeks after synthesis, pH 7, varied metals

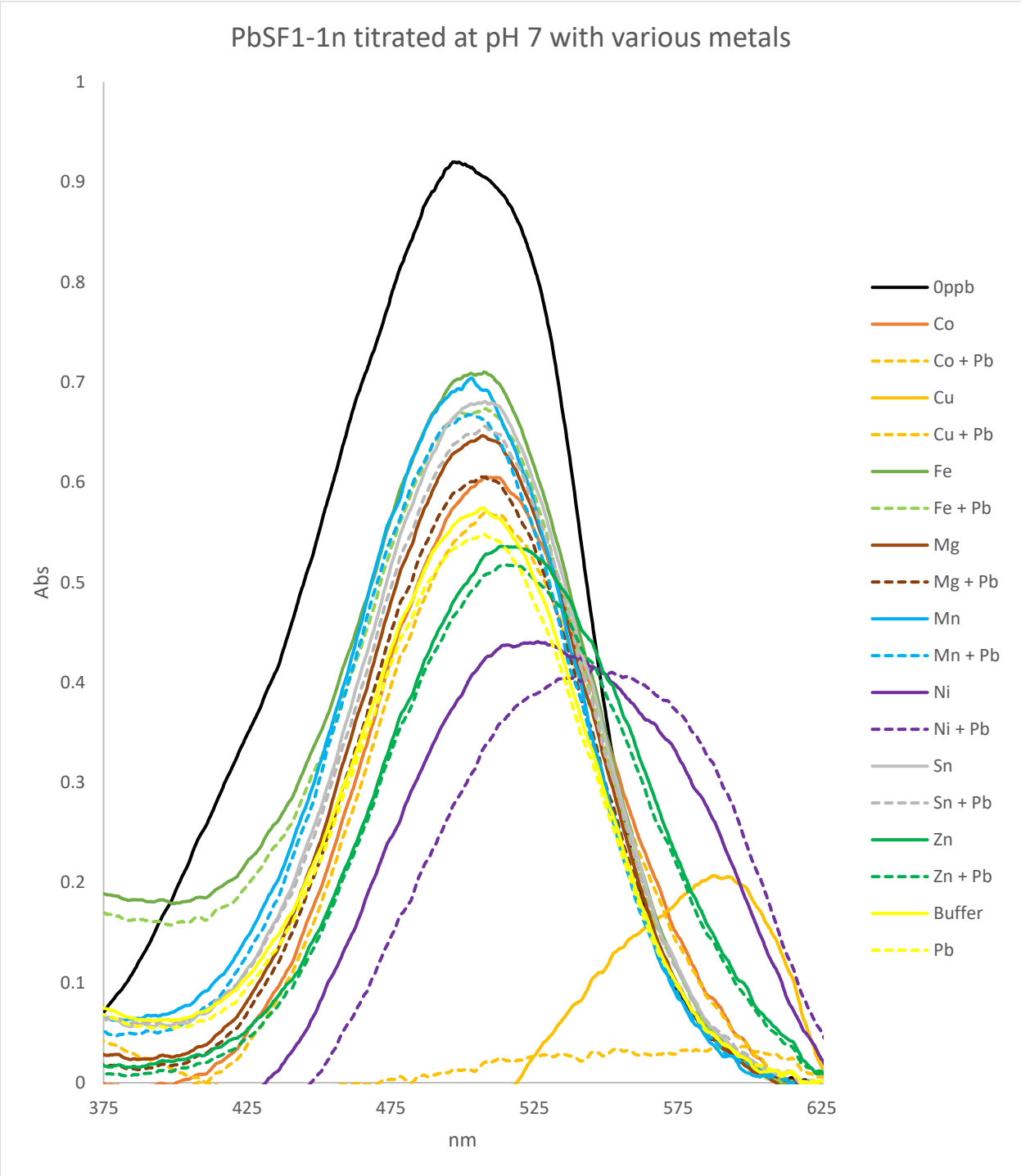

Spectrum 50: 18b Titration with varied metals at pH 7, Week 2, saturated

Titration of 18c, PbSF1-2n 3 days after synthesis at pH 9, low ppb Pb

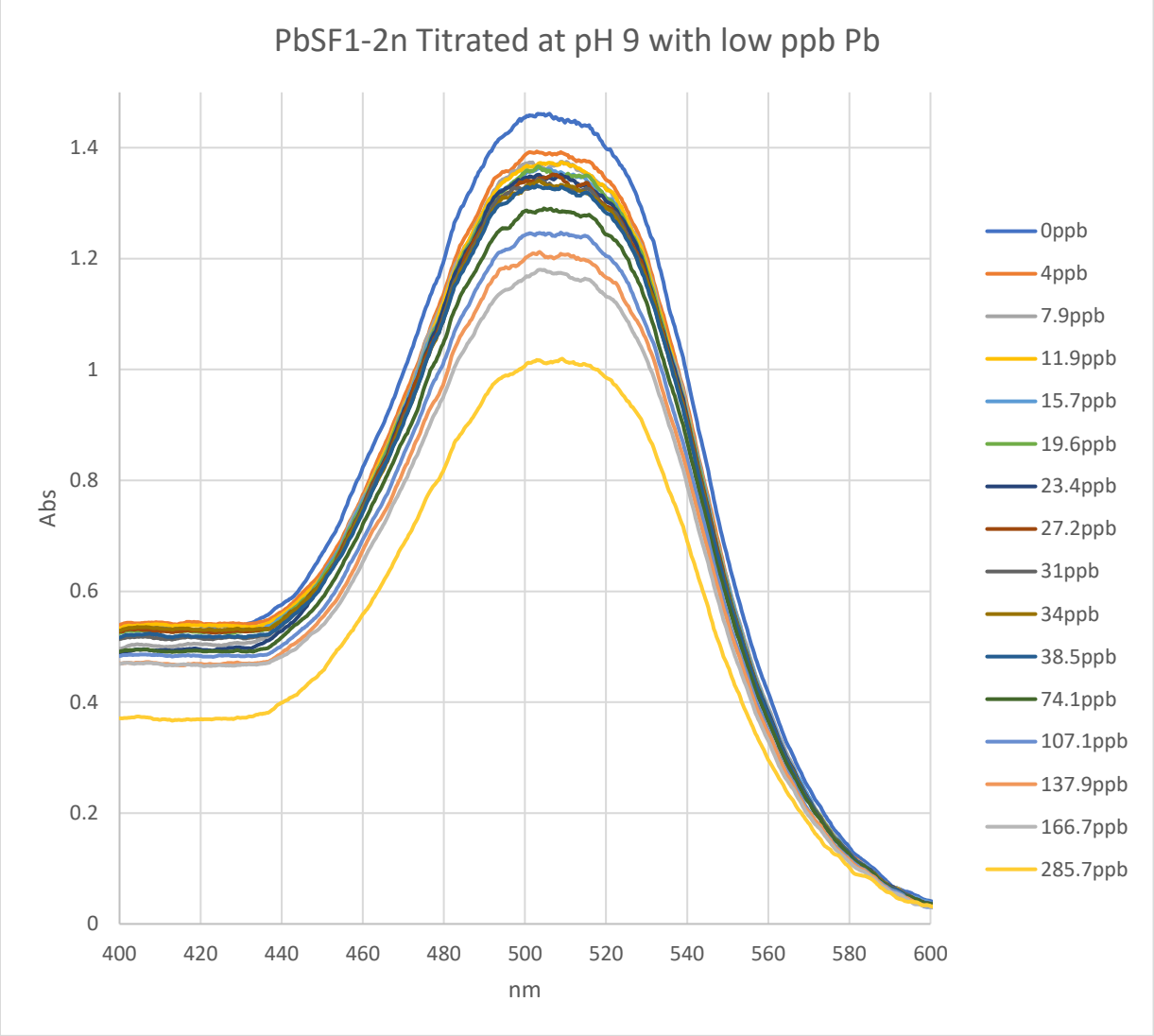

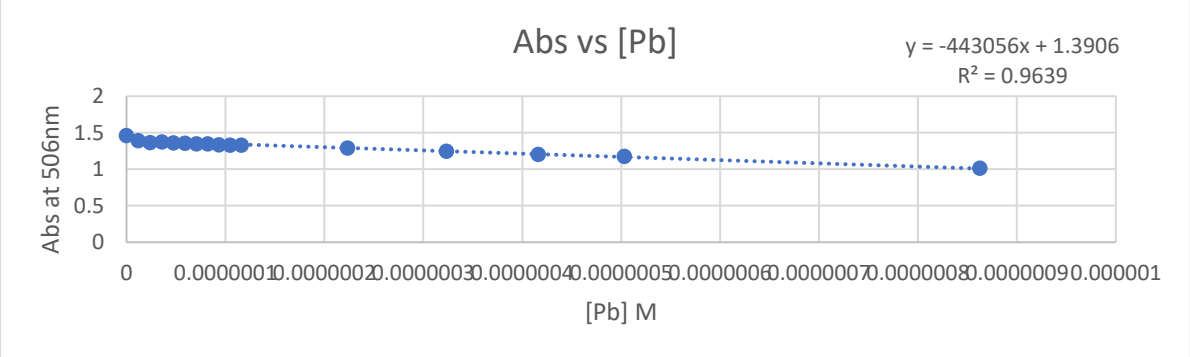

Spectrum 51: 18c Titration with Pb at pH 9, Day 3, low ppb; Abs vs [Pb]

Titration of 18c, PbSF1-2n, 8 days after synthesis at pH 9, low ppm Pb in tap water

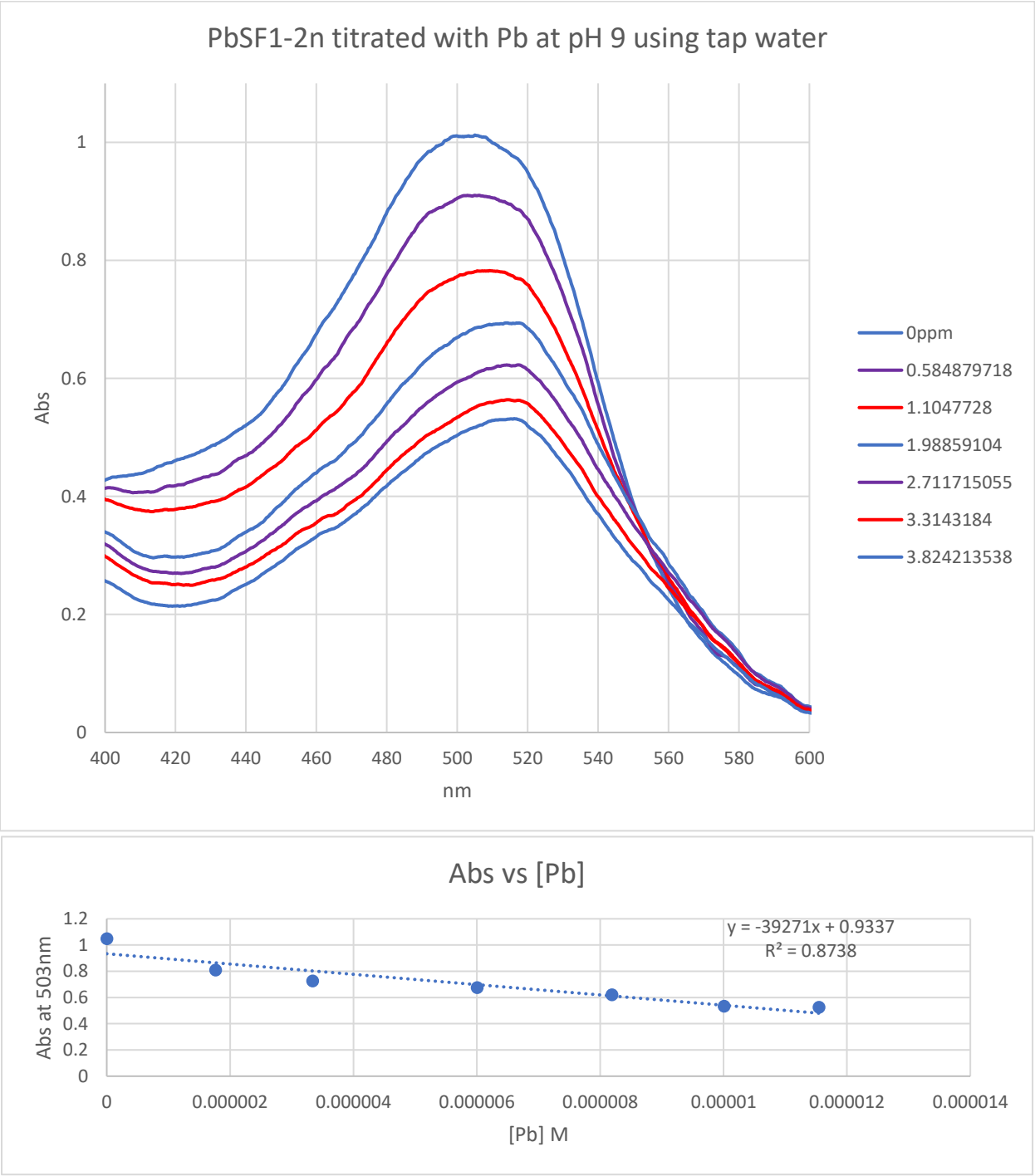

Spectrum 52: 18c Titration with Pb at pH 9, Day 8, low ppm, tap water; Abs vs [Pb]

Titration of 18c, PbSF1-2n, 8 days after synthesis at pH 9, low ppm Pb in DI water

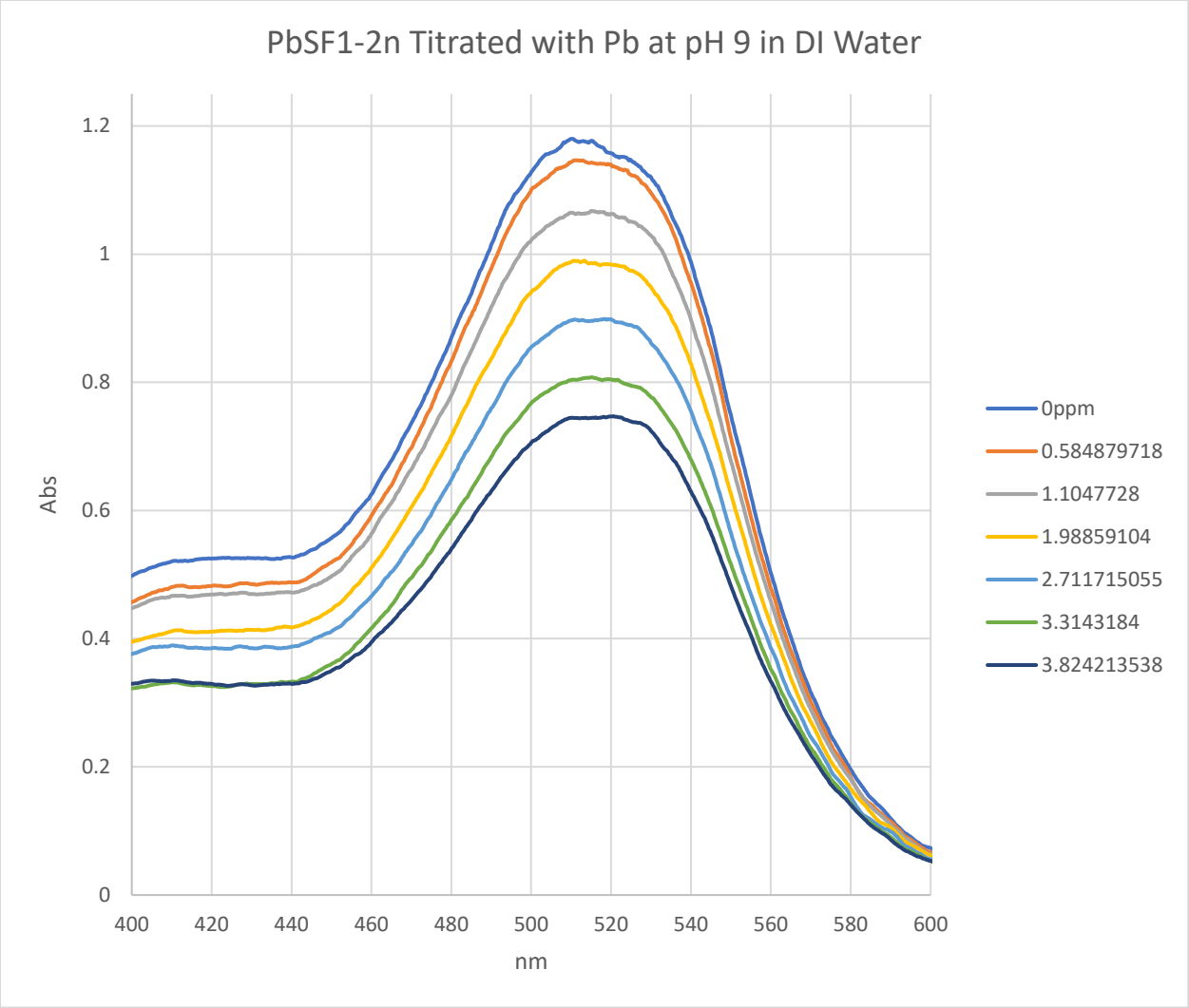

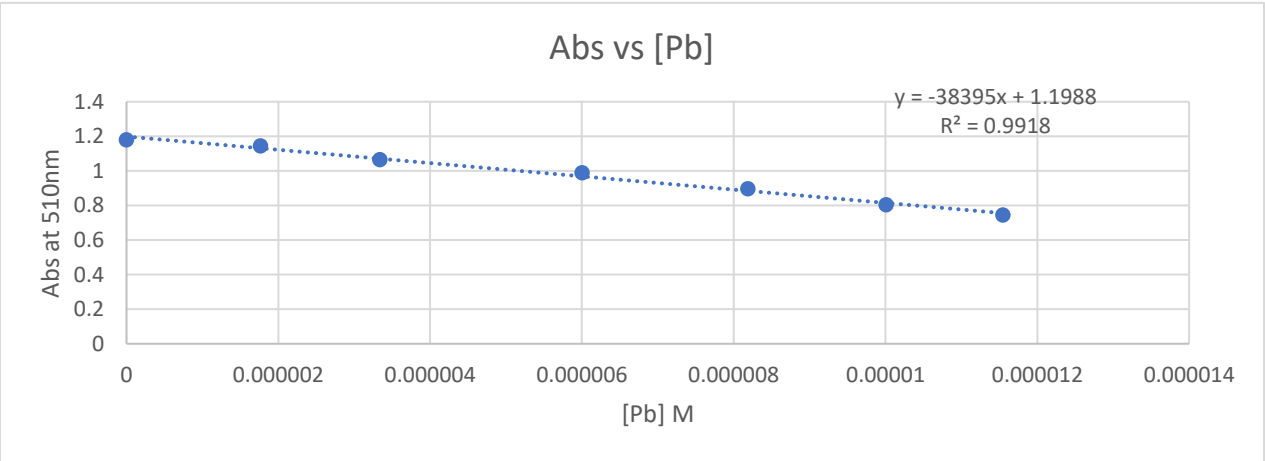

Spectrum 53: 18c Titration with Pb at pH 9, Day 8, low ppm, DI water; Abs vs [Pb]

Titration of 18c, PbSF1-2n, 4 weeks after synthesis at pH 9, low ppm Pb

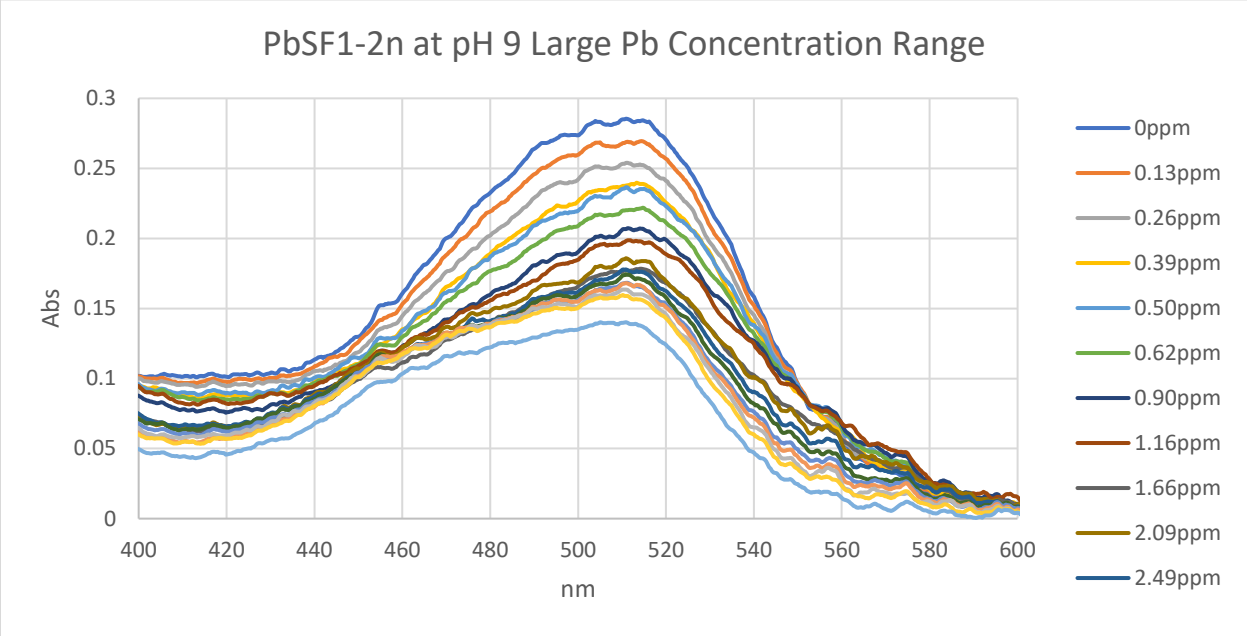

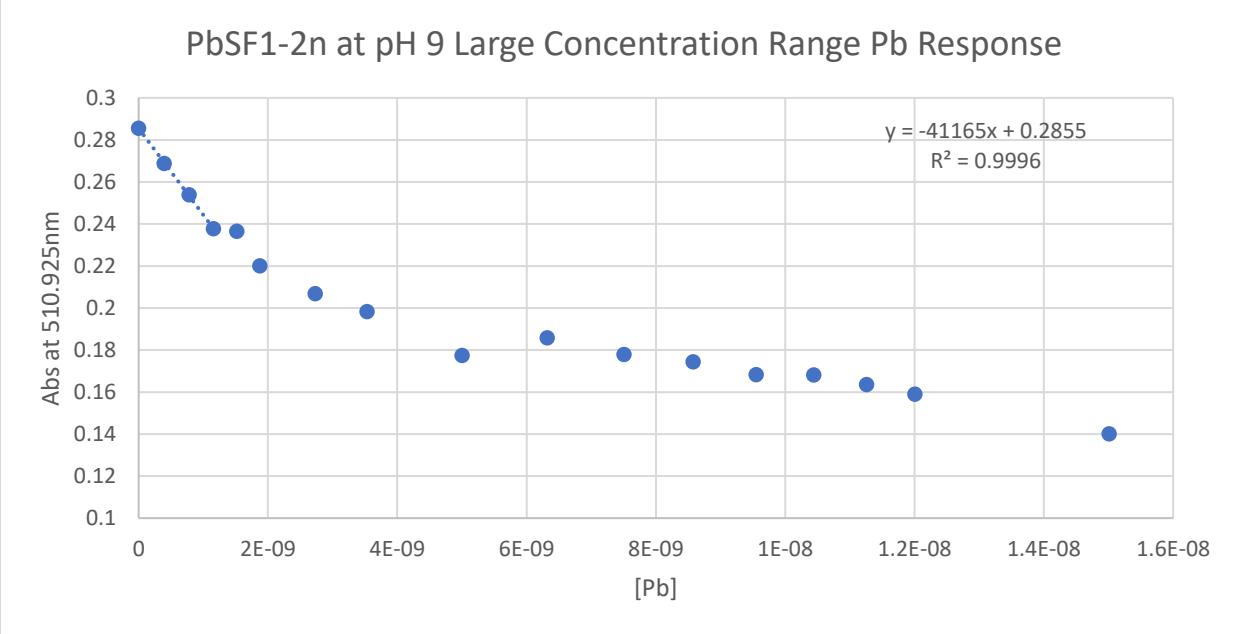

Spectrum 54: 18c Titration with Pb at pH 9, Week 4, low ppm to saturation

Linear until saturation

Titration of 18c, PbSF1-2n two weeks after synthesis, pH 5, varied metals

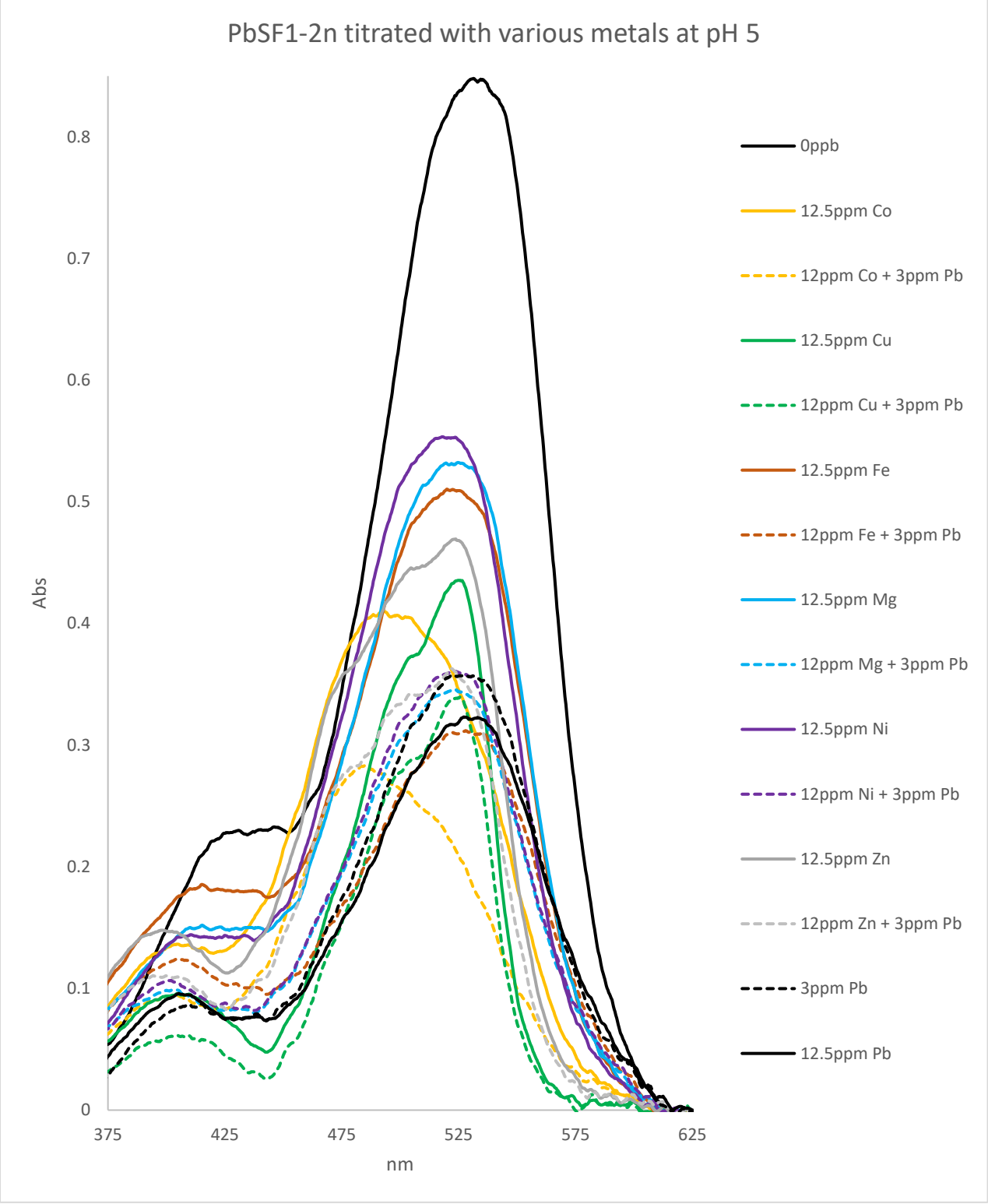

Spectrum 55: 18c Titration with varied metals at pH 5, Week 2, saturated

Titration of 18d, PbSF1-13 right after after synthesis, pH 9, ppm Pb

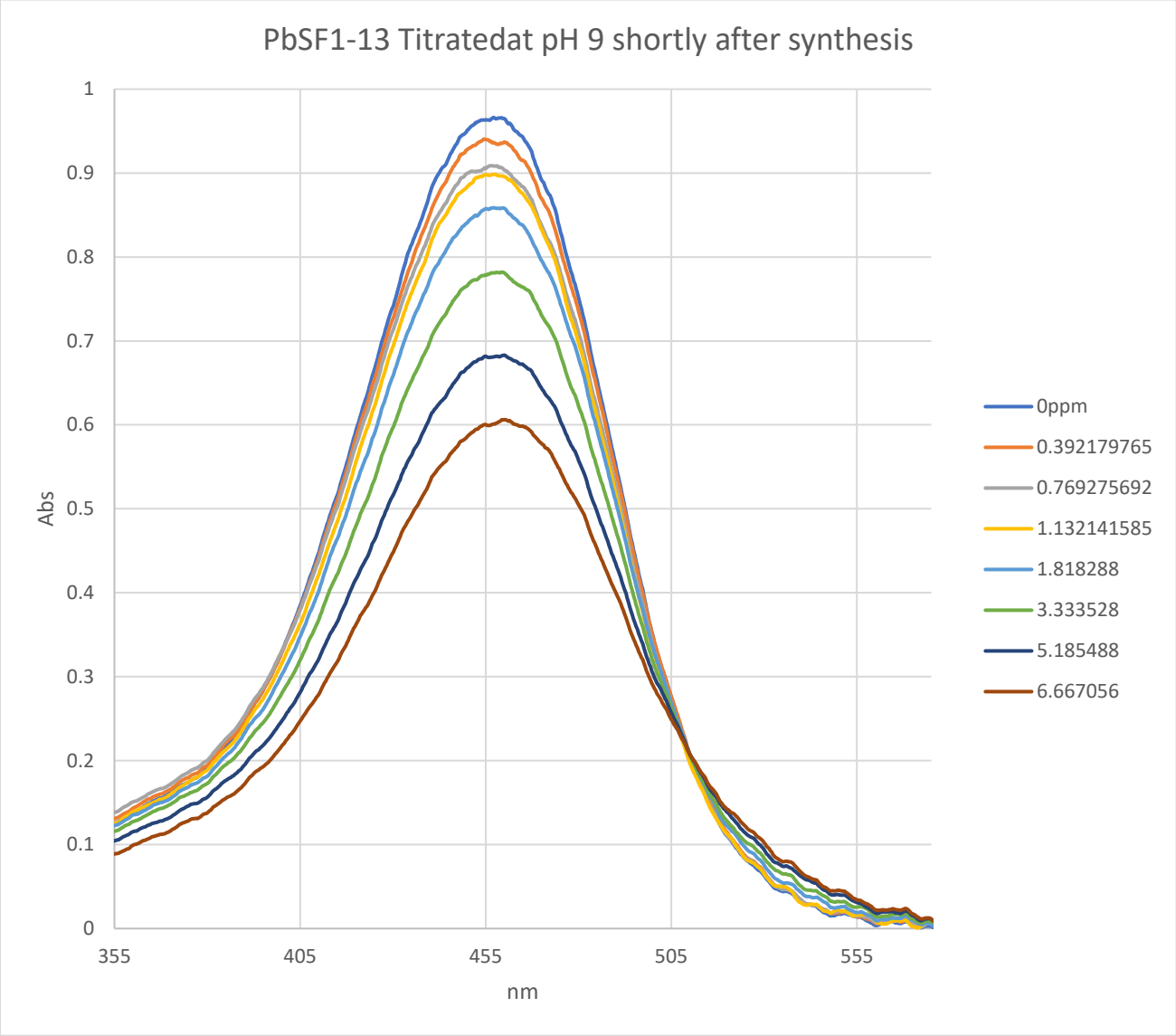

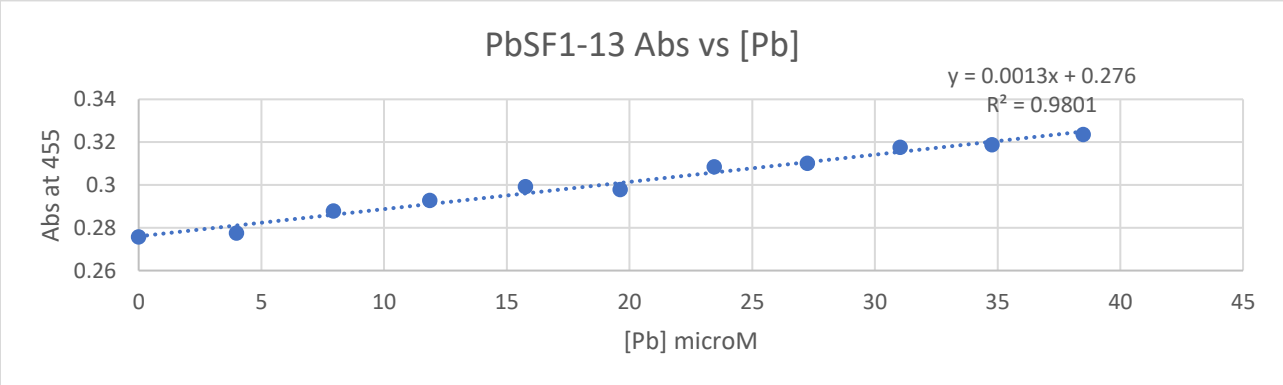

Spectrum 56: 18d Titration with Pb at pH 9, Day 1, low ppm; Abs vs [Pb]

Titration of 18d, PbSF1-13 two weeks after synthesis, pH 7, ppb Pb

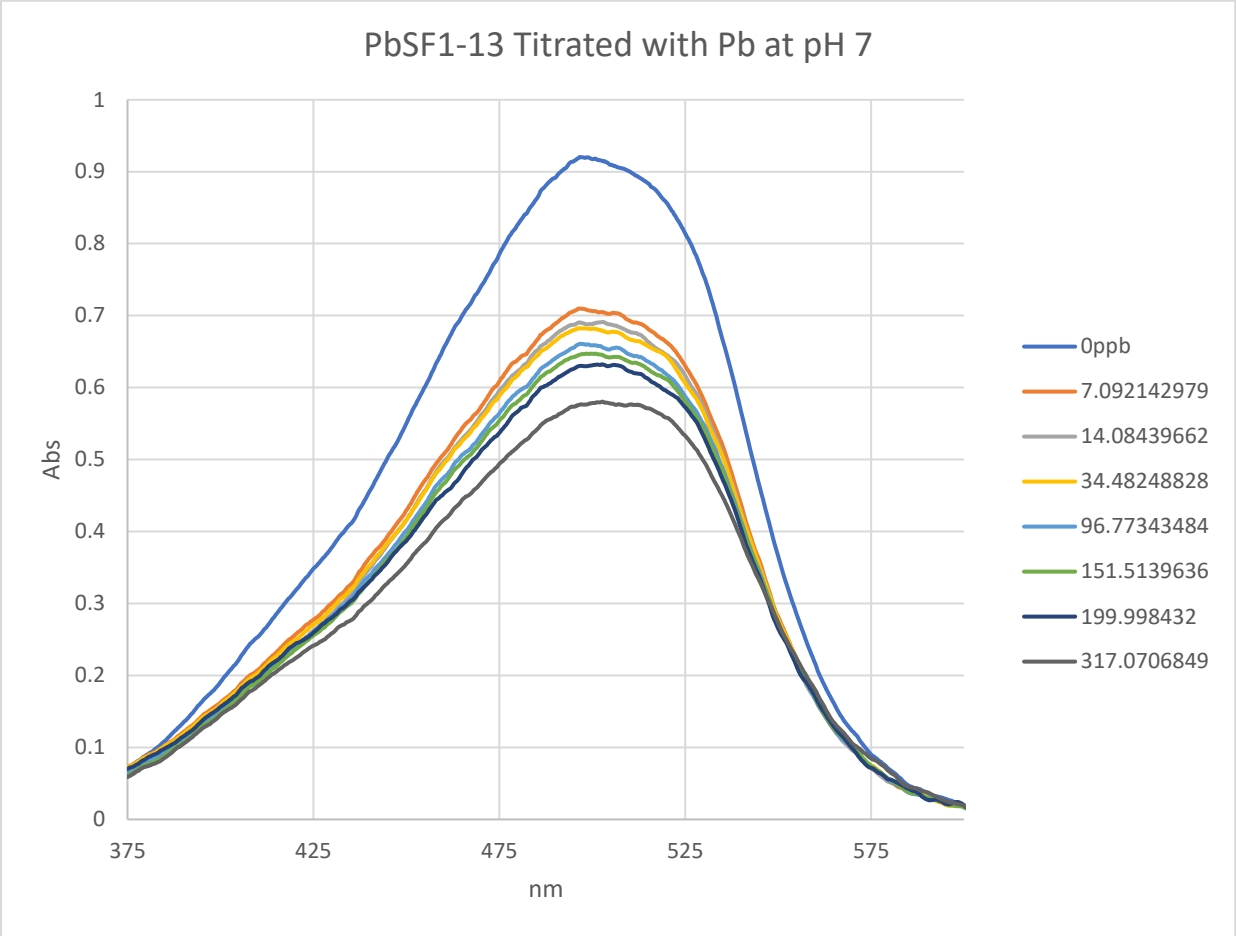

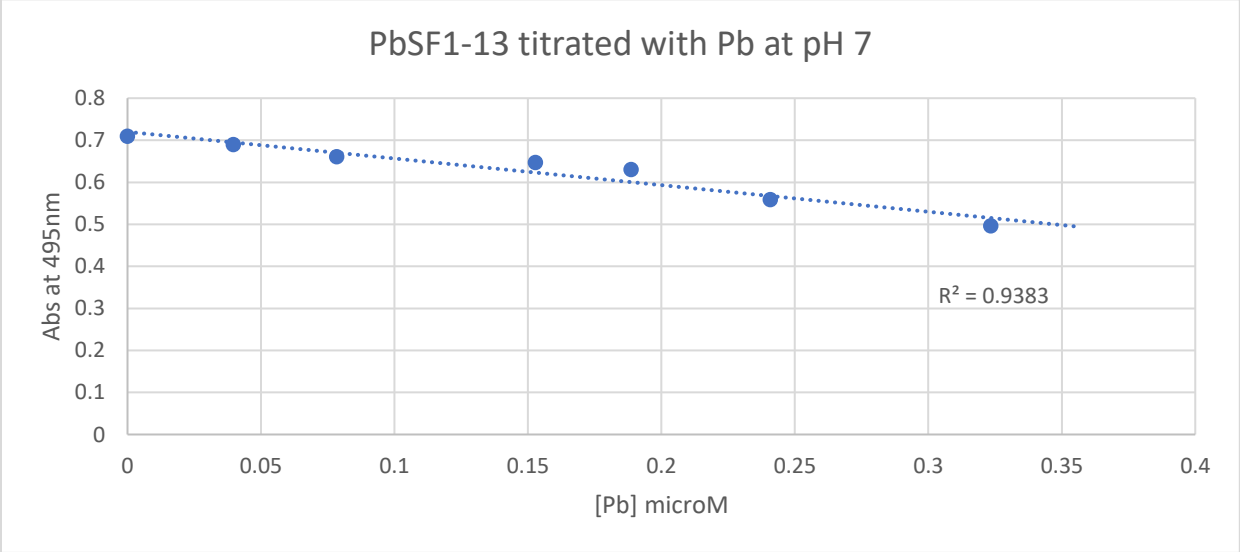

Spectrum 57: 18d Titration with Pb at pH 7, week 2, low ppb; Abs vs [Pb]

Titration of 18d, PbSF1-13 one week after synthesis, pH 7, varied metals

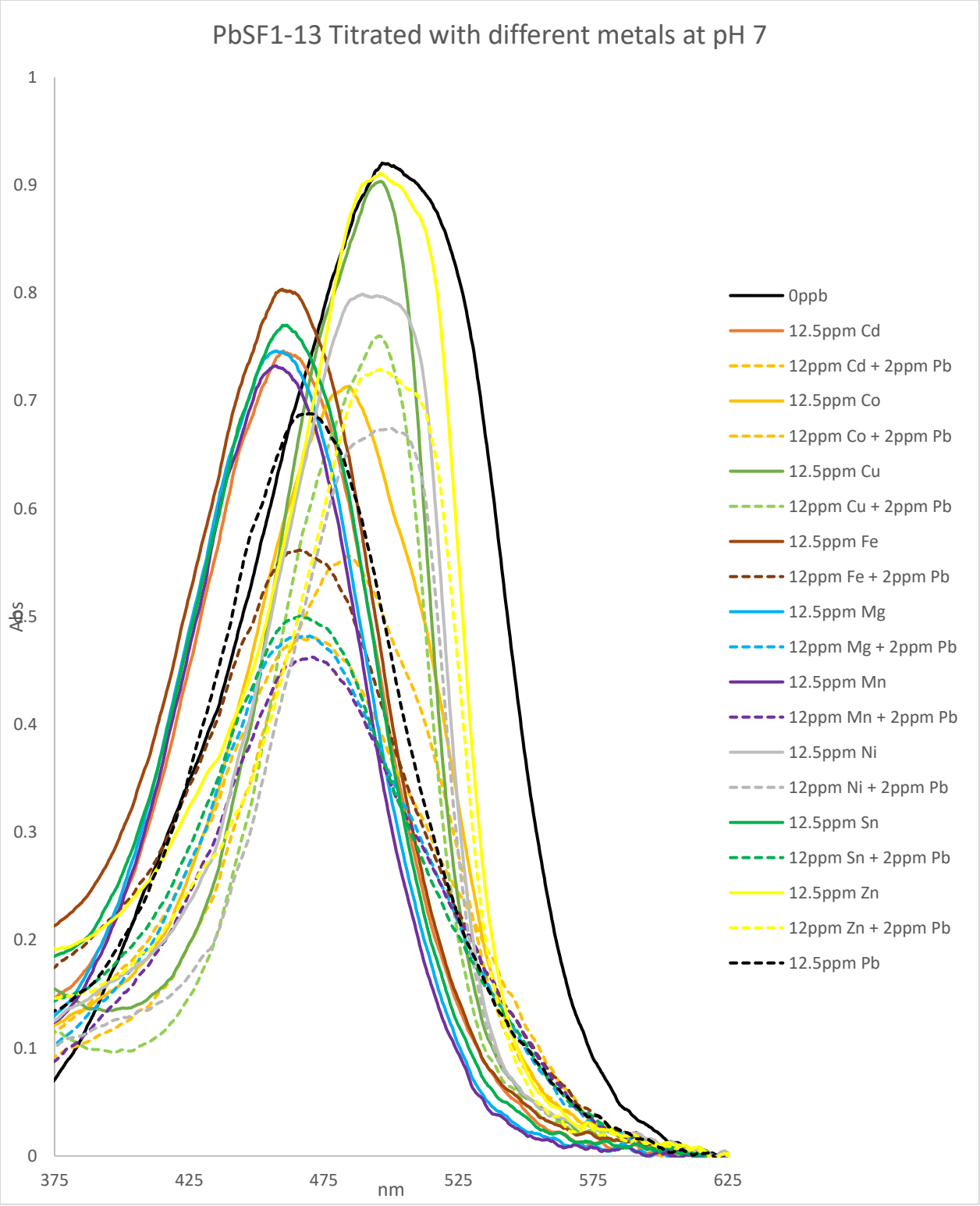

Spectrum 58: 18d Titration with varied metals at pH 7, Week 1, saturated

Titration of 18d, PbSF1-13 one week after synthesis, pH 7, Zn added first then Pb titration; low concentration then higher concentration

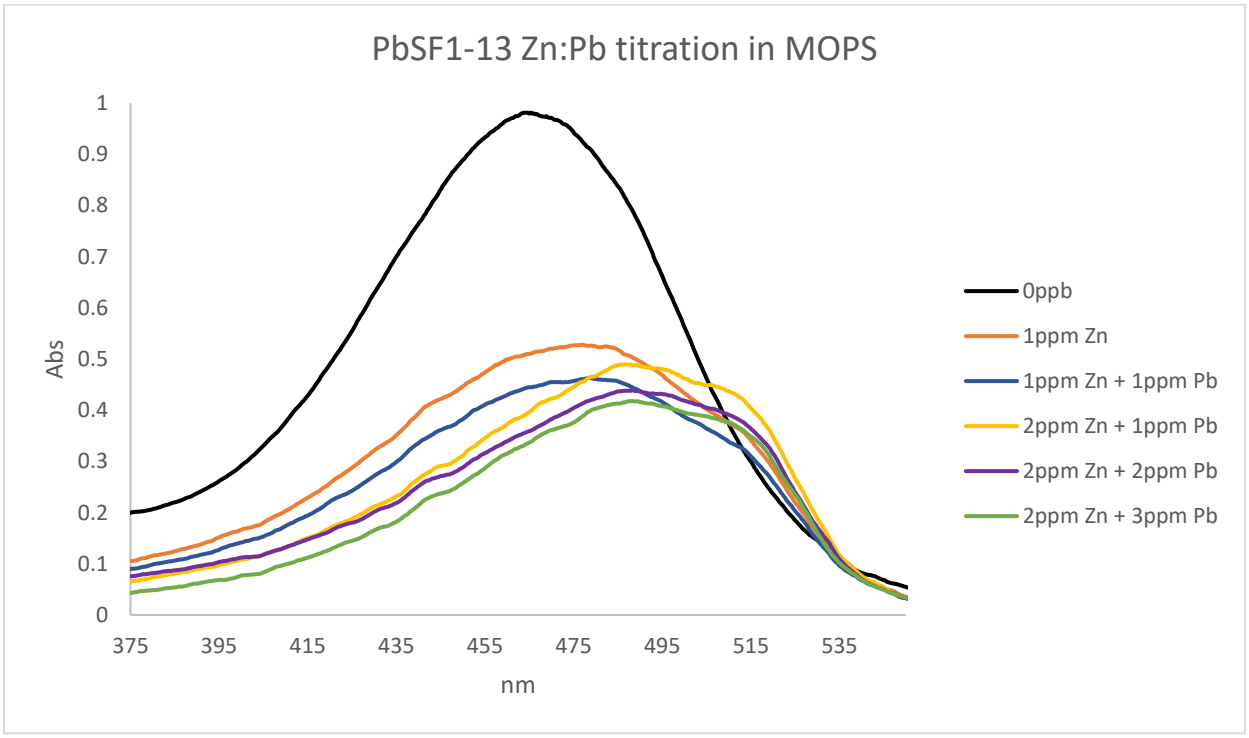

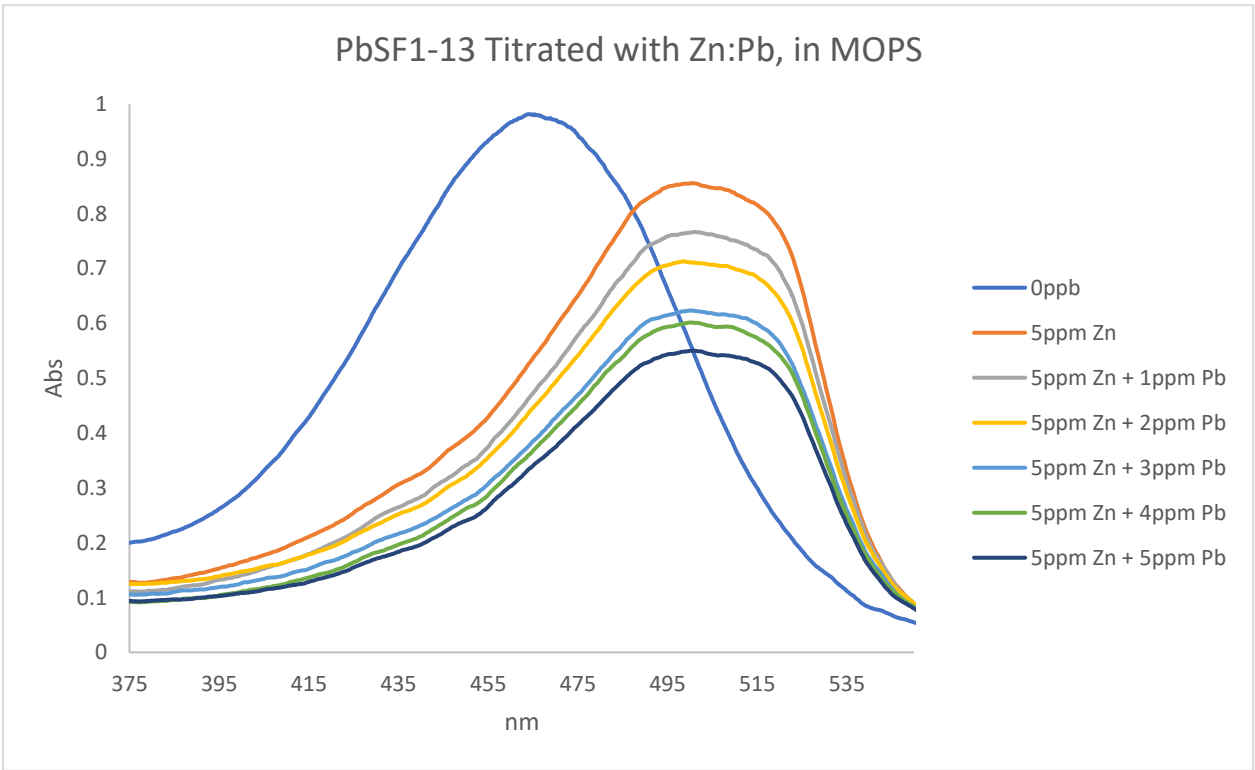

Spectrum 59: 18d Titration with Zn and Pb at pH 7, Week 1, low ppm; 18d Titration with Zn and Pb at pH 7, Week 1, ppm

Titration of 18d, PbSF1-13 three weeks after synthesis, pH 9 titration Zn, Fe, Ni

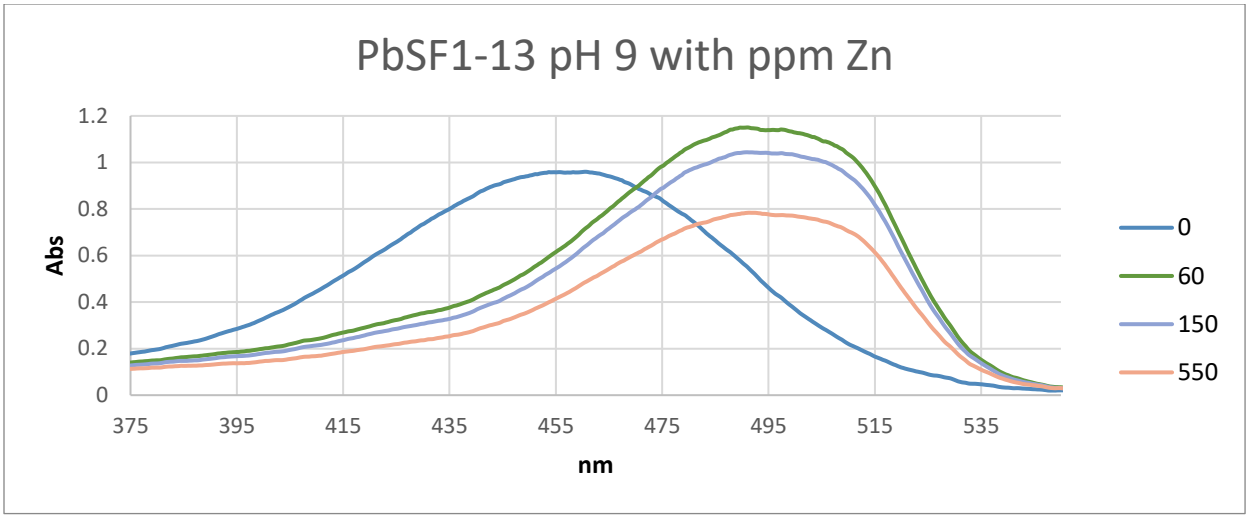

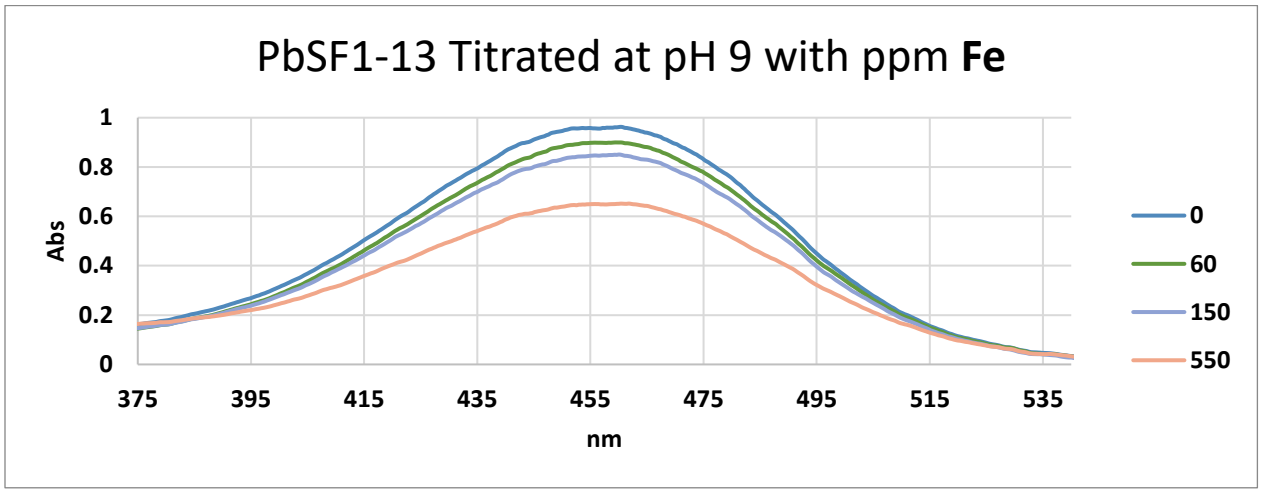

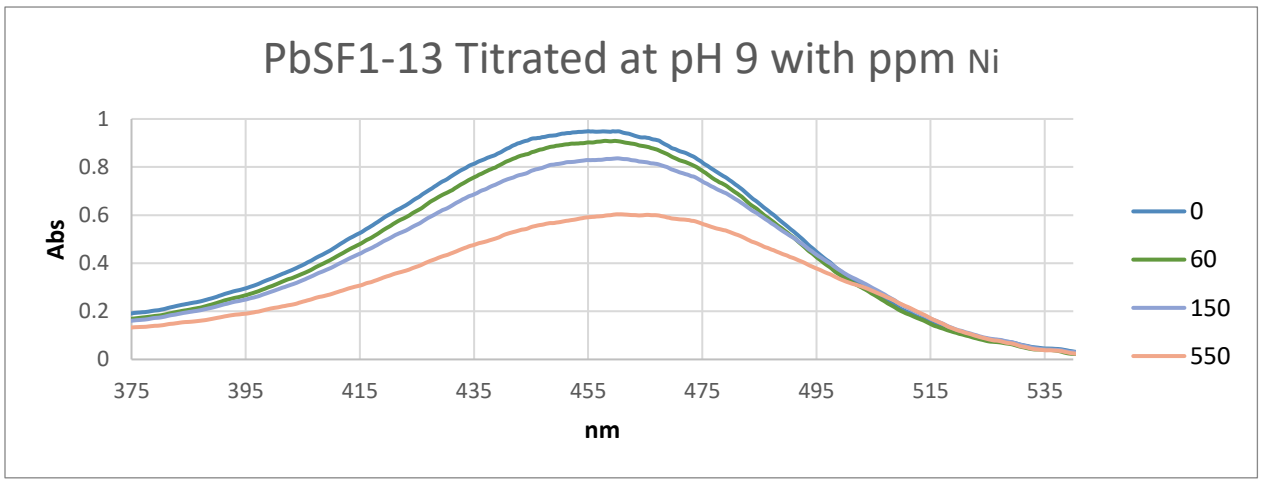

Spectrum 60: 18d Titration with Zn at pH 9, Week 3, ppm; 18d Titration with Fe at pH 9, Week 3, ppm; 18d Titration with Ni at pH 9, Week 3, ppm

Titration of 18d, PbSF1-13 three weeks after synthesis, pH 9 titration with Cu

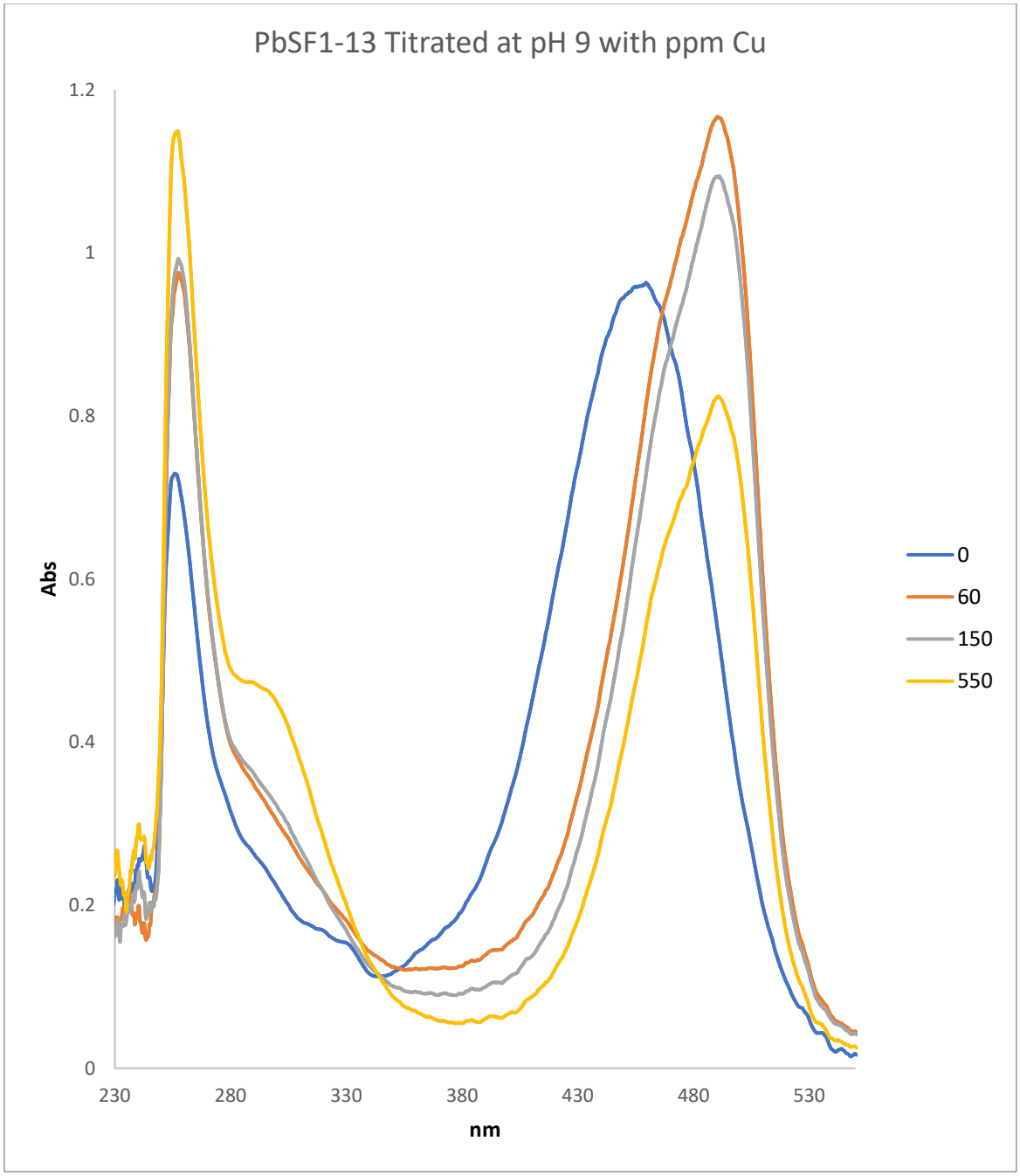

Spectrum 61: 18d Titration with Cu at pH 9, Week 3, ppm

Titration of 18d, PbSF1-13 six weeks after synthesis titrated with ppb Pb in tap water

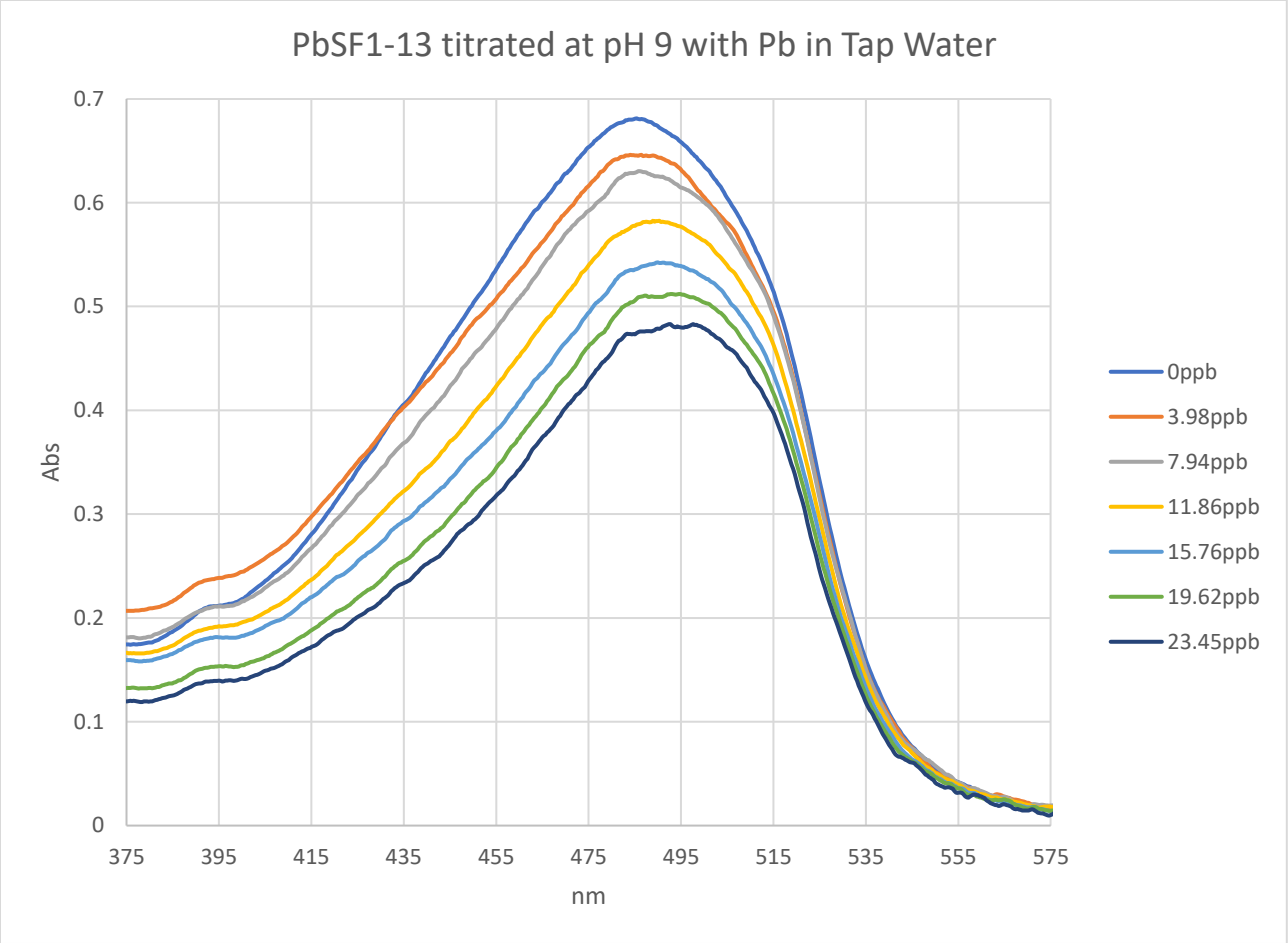

Spectrum 62: 18d Titration with Pb at pH 9, Week 6, low ppb, tap water; Abs vs [Pb]

Titration of 18d, PbSF1-13 three weeks after synthesis, pH 9 titration ppm Pb in DI water

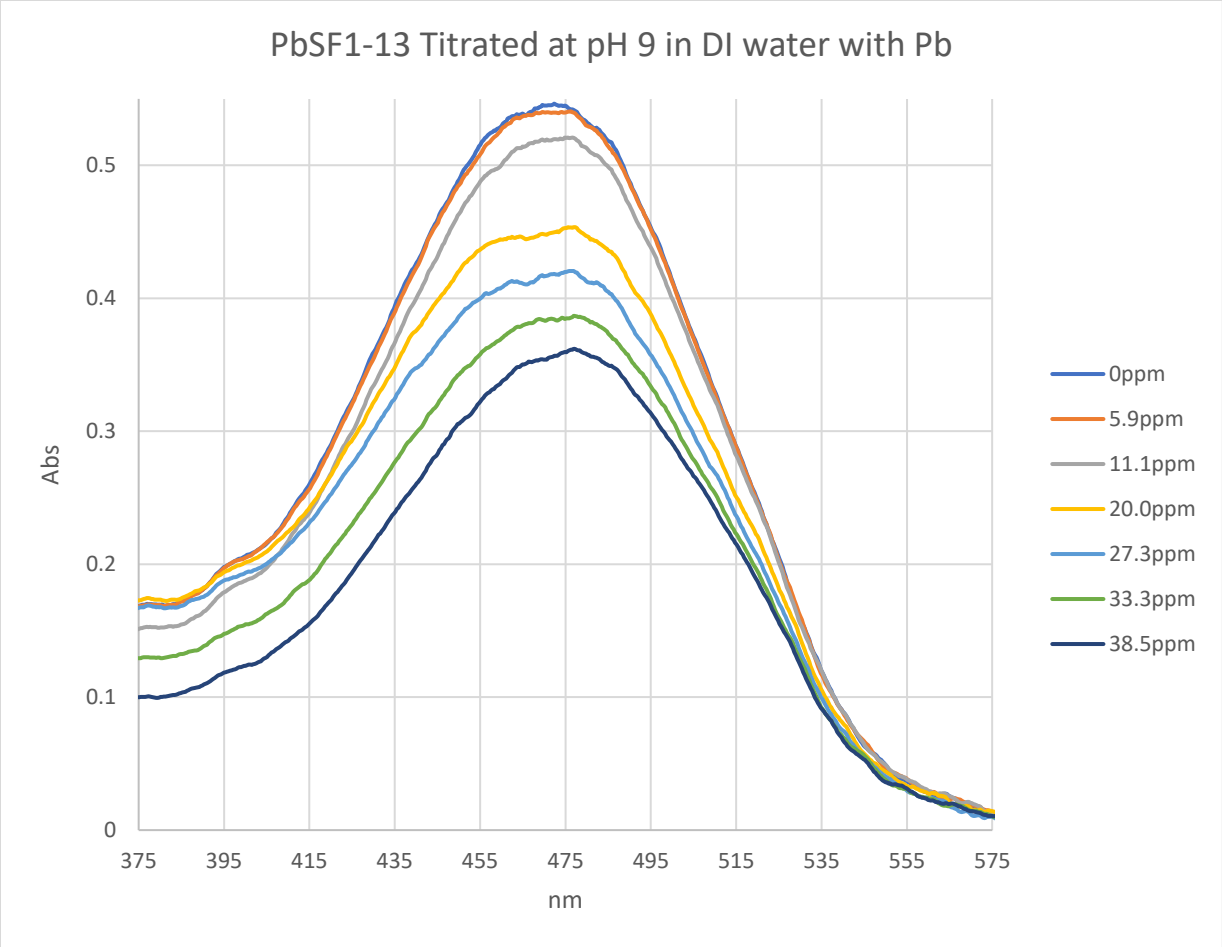

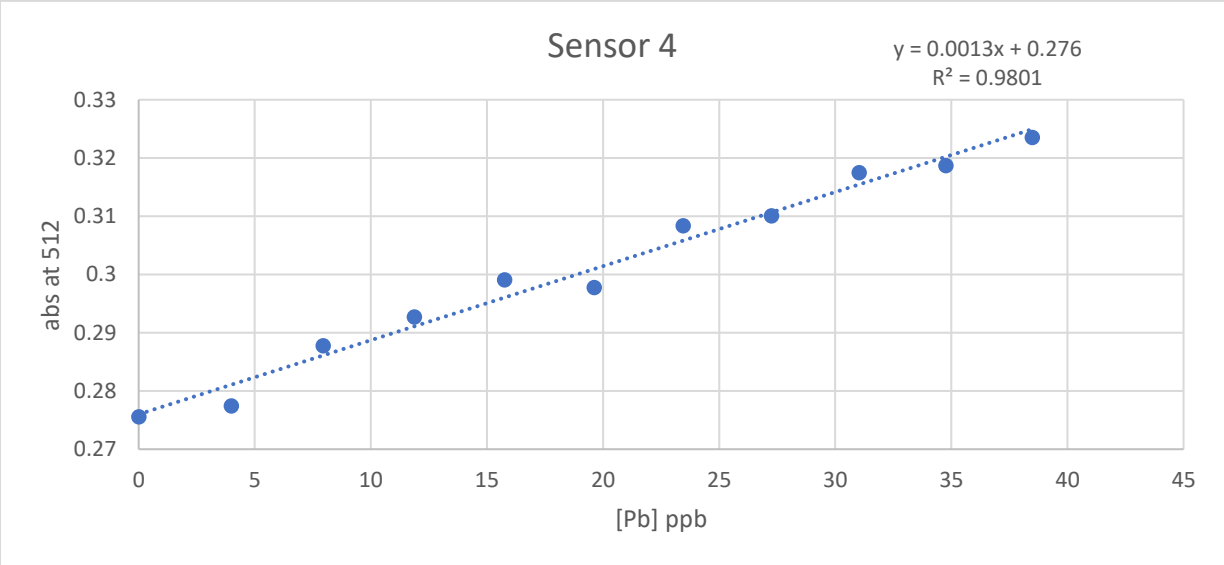

Spectrum 63: 18d Titration with Pb at pH 9, Week 6, low ppm, DI water; Abs vs [Pb]

Titration of 18d, PbSF1-13 9 days after synthesis, pH 9 titration low ppb Pb

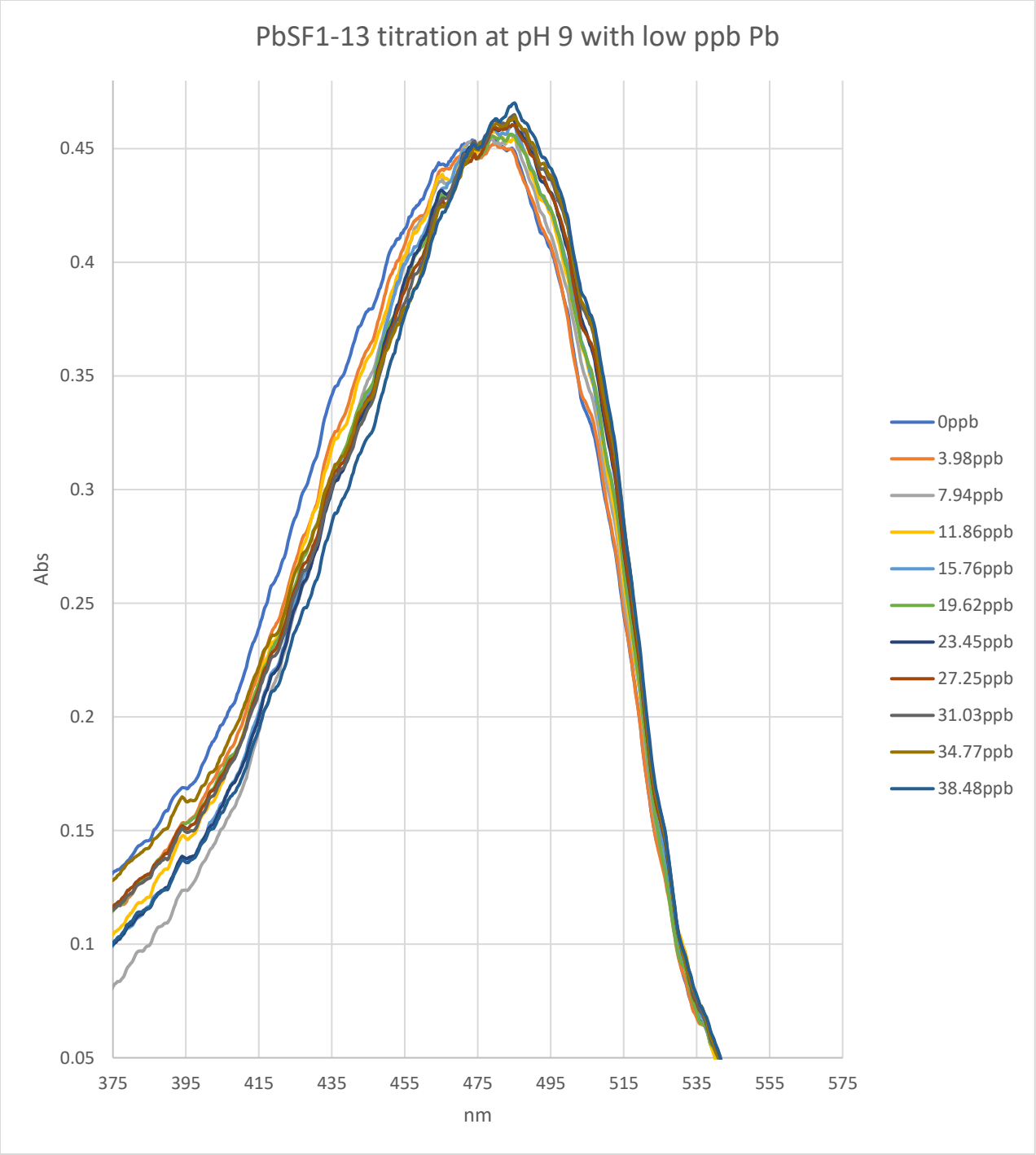

Spectrum 64: 18d Titration with Pb at pH 9, Day 9, low ppb

Titration of 18d, PbSF1-13 3 weeks after synthesis, titrated pH 9 with Pb and Cu; Titrated with Ca and Pb

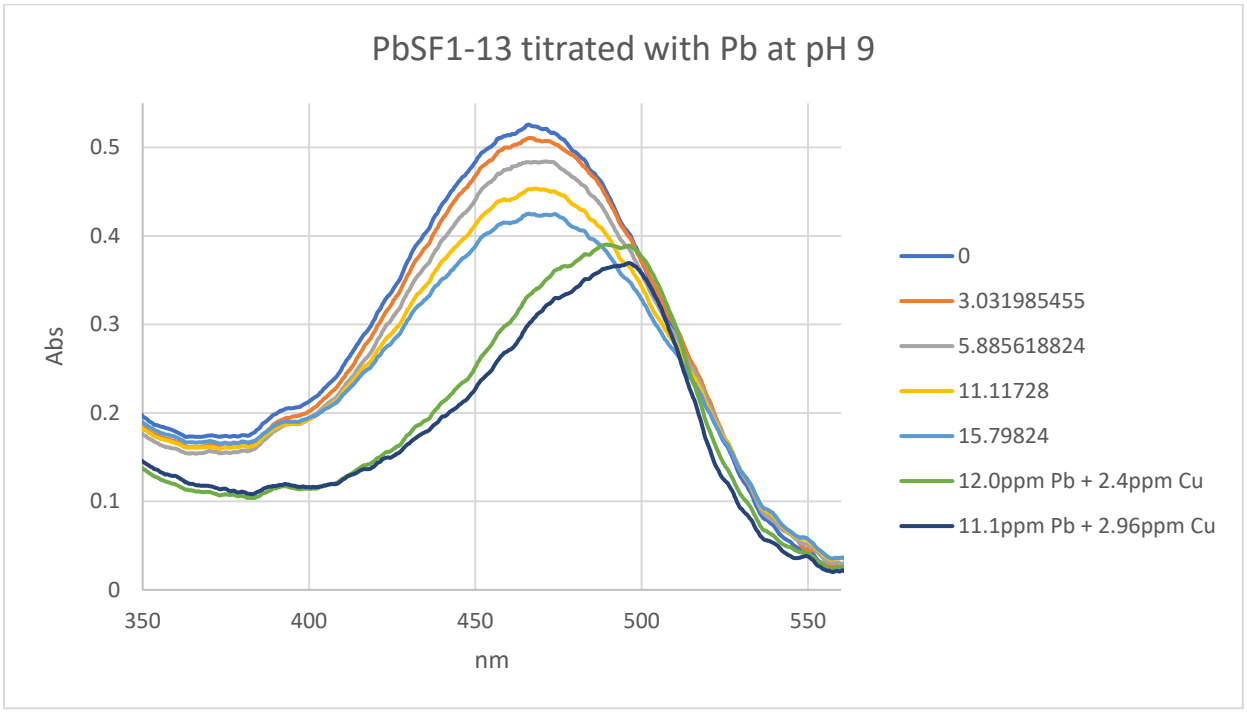

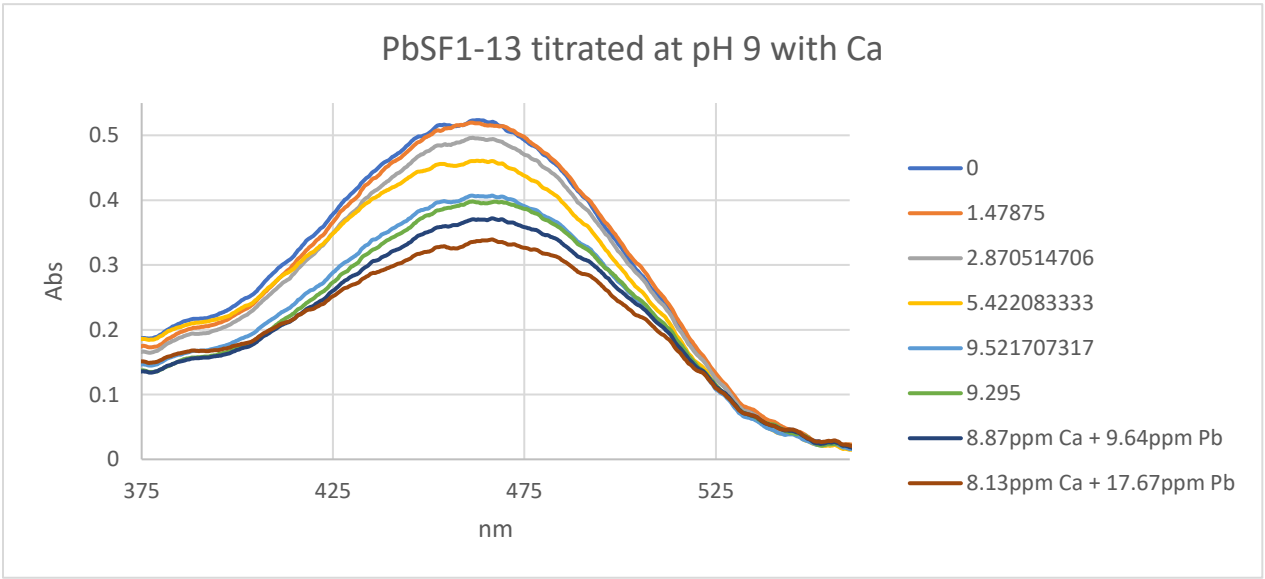

Spectrum 65: 18d Titration with Pb with Cu with Pb addition at pH 9, Week 3, ppm; 18d titration with Ca with Pb addition at pH 9, Week 3, low ppm

Titration of 18d, PbSF1-13 3 weeks after synthesis, titrated pH 9 with Mg and Pb

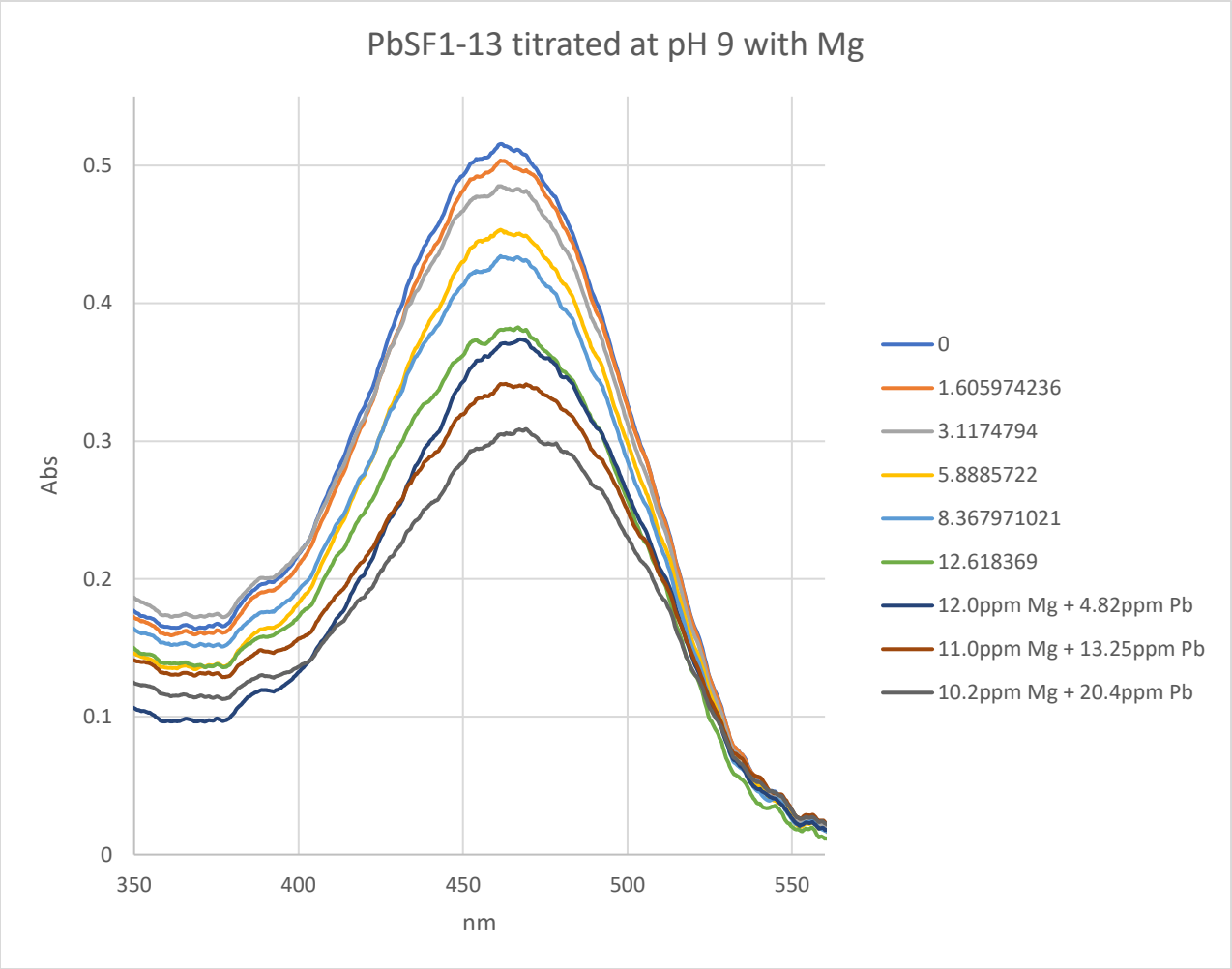

Spectrum 66: 18d Titration with Mg with Pb addition at pH 9, Week 3, low ppm

Titration of 18d, PbSF1-13 3 weeks after synthesis, titrated pH 9 with Zn and Pb

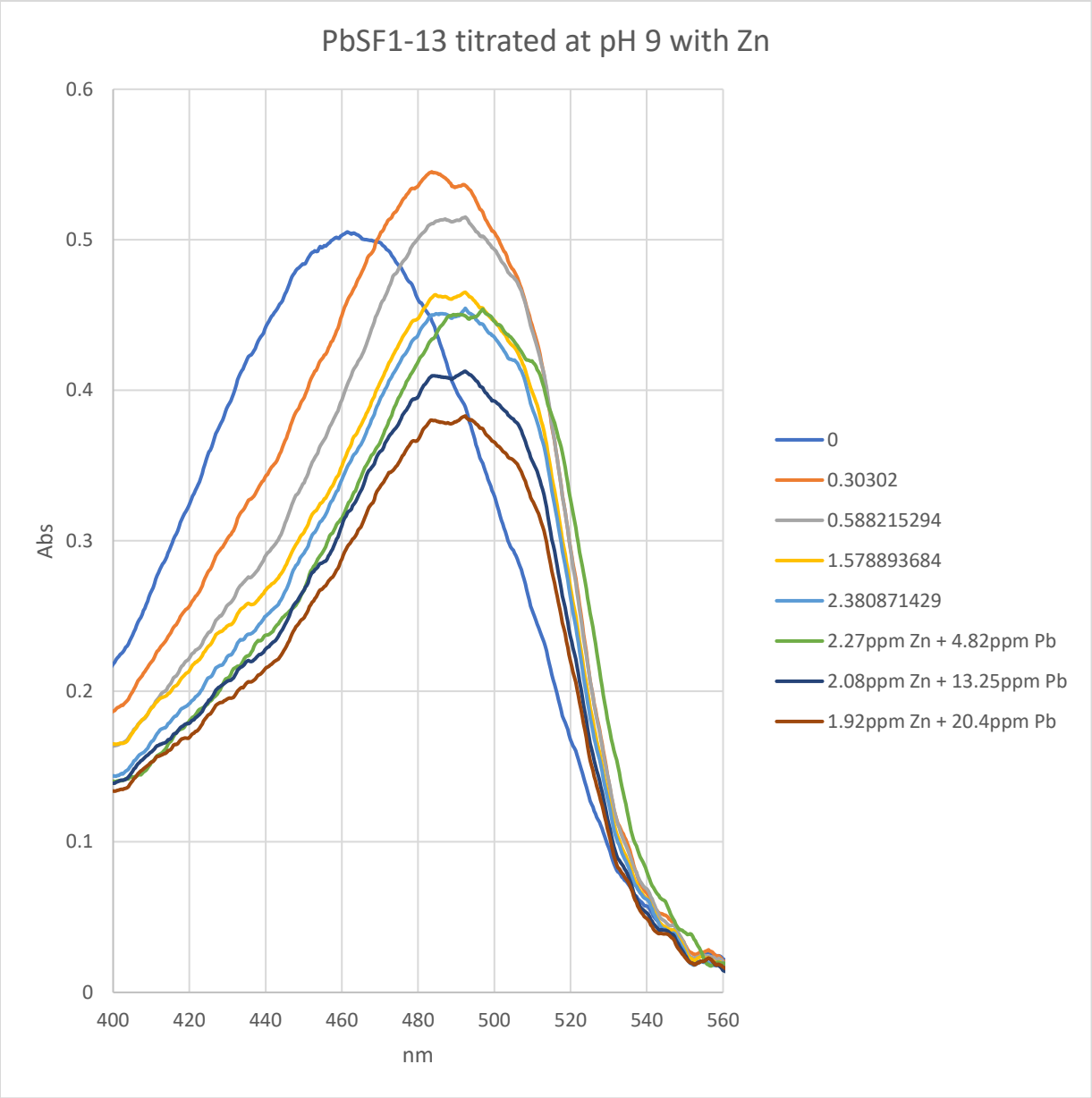

Spectrum 67: 18d Titration with Zn with Pb addition at pH 9, Week 3, low ppm

Titration of 18d, PbSF1-13 5 weeks after synthesis, titrated pH 9 with ppb Pb

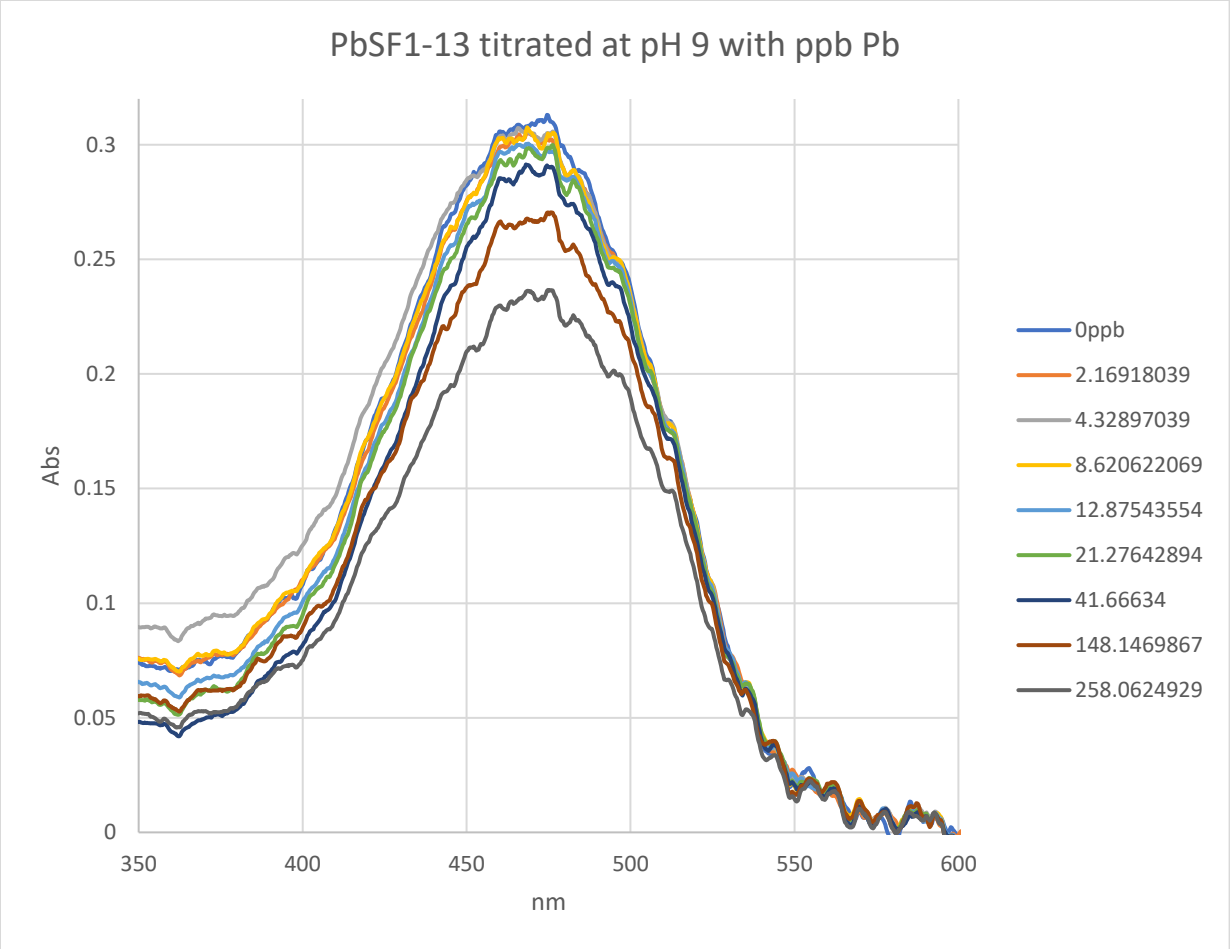

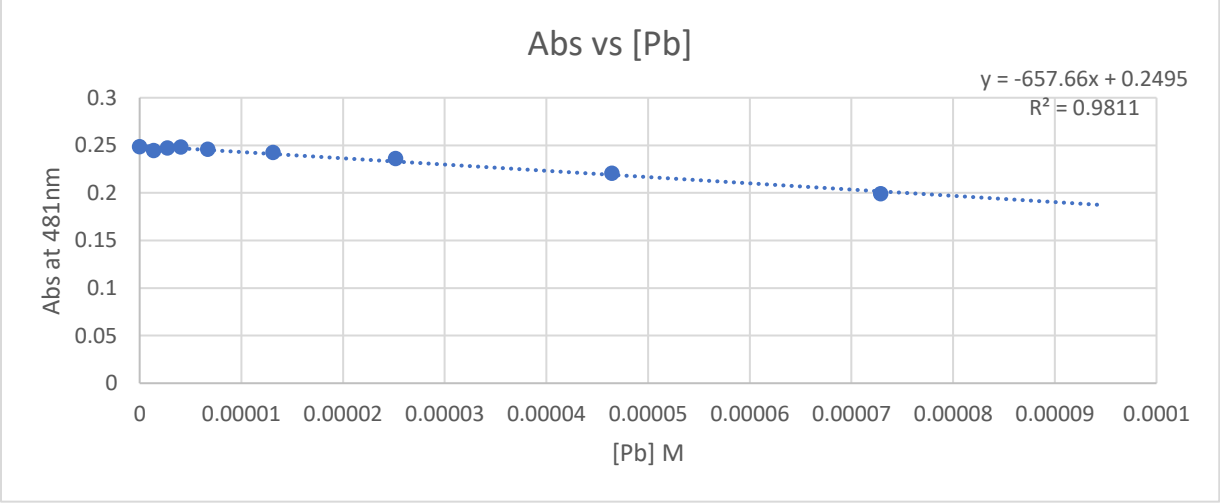

Spectrum 68: 18d Titration with Pb at pH 9, Week 5, ppb; Abs vs [Pb]

Titration of 18d, PbSF1-13 5 weeks after synthesis, titrated pH 9 with ppm Pb

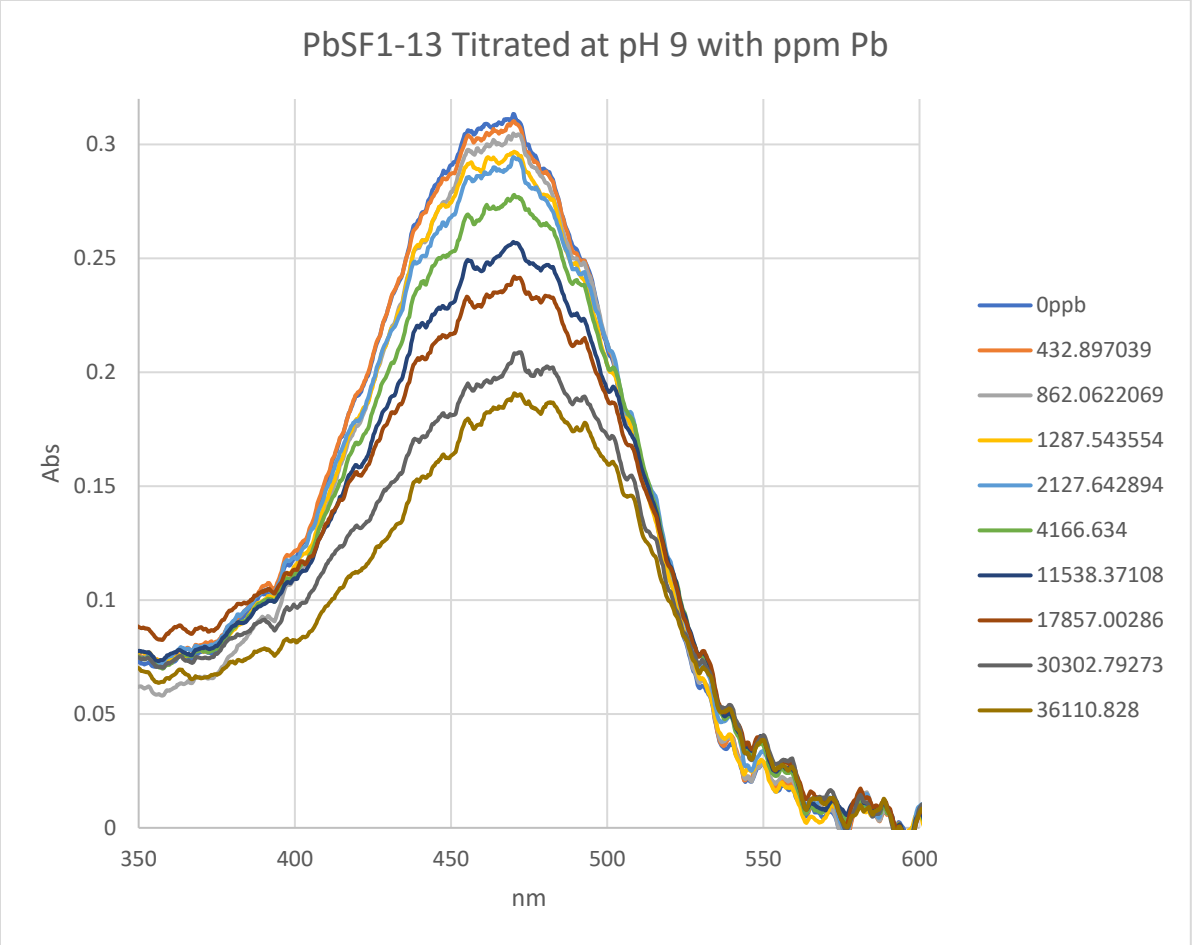

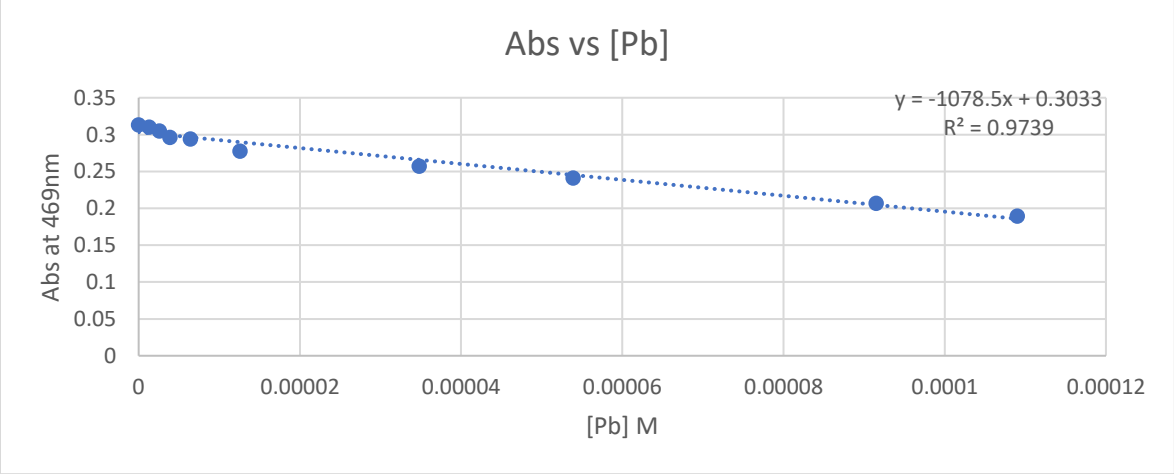

Spectrum 69: 18d Titration with Pb at pH 9, Week 5, ppm; Abs vs [Pb]

Titration of 18e, PbSF1-27 directly after synthesis, titrated pH 9 with ppm Pb

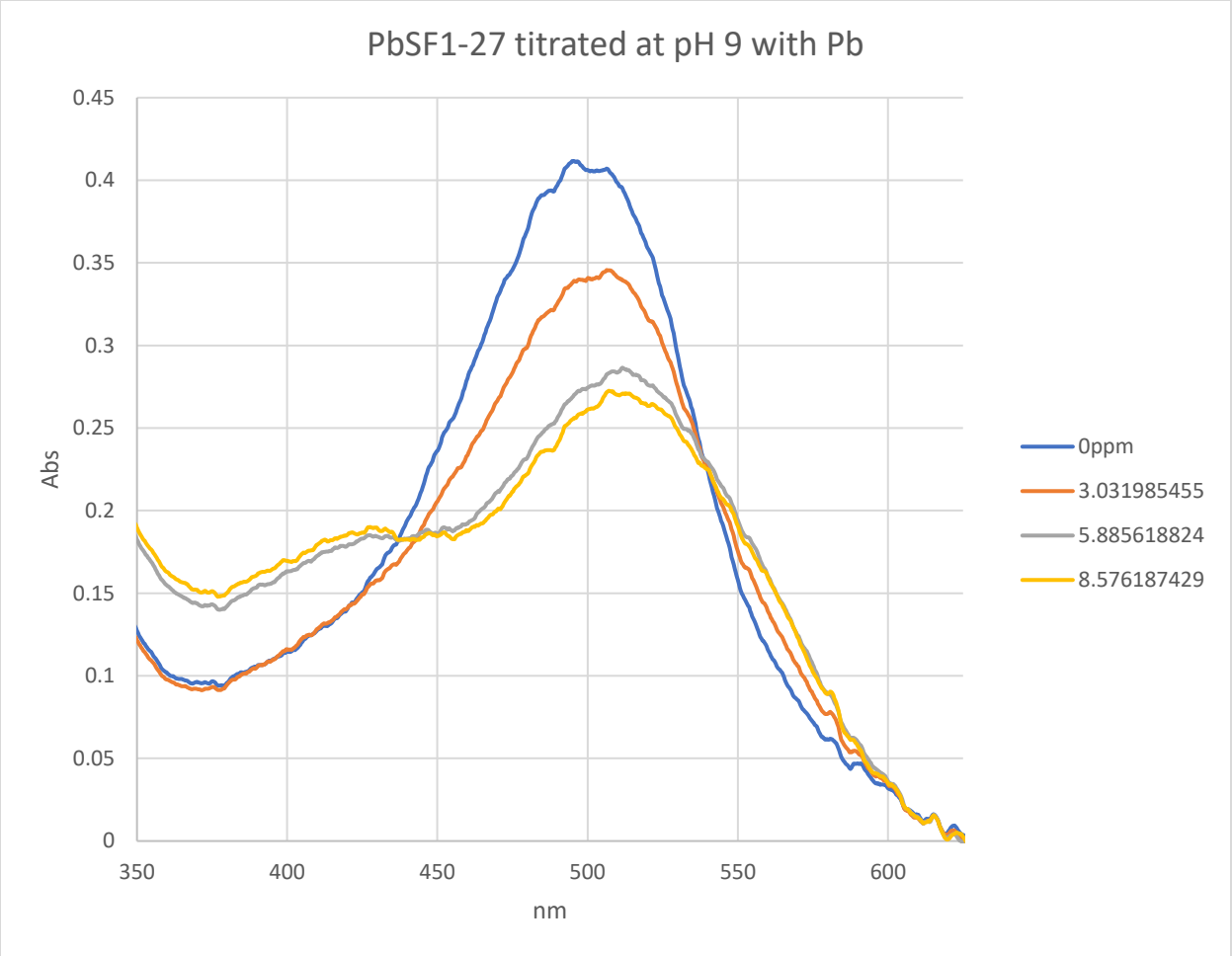

Spectrum 70: 18e Titration with Pb at pH 9, Day 0, low ppm; Abs vs [Pb]

Titration of 18e, PbSF1-27 directly after synthesis, titrated pH 9 with ppm Pb

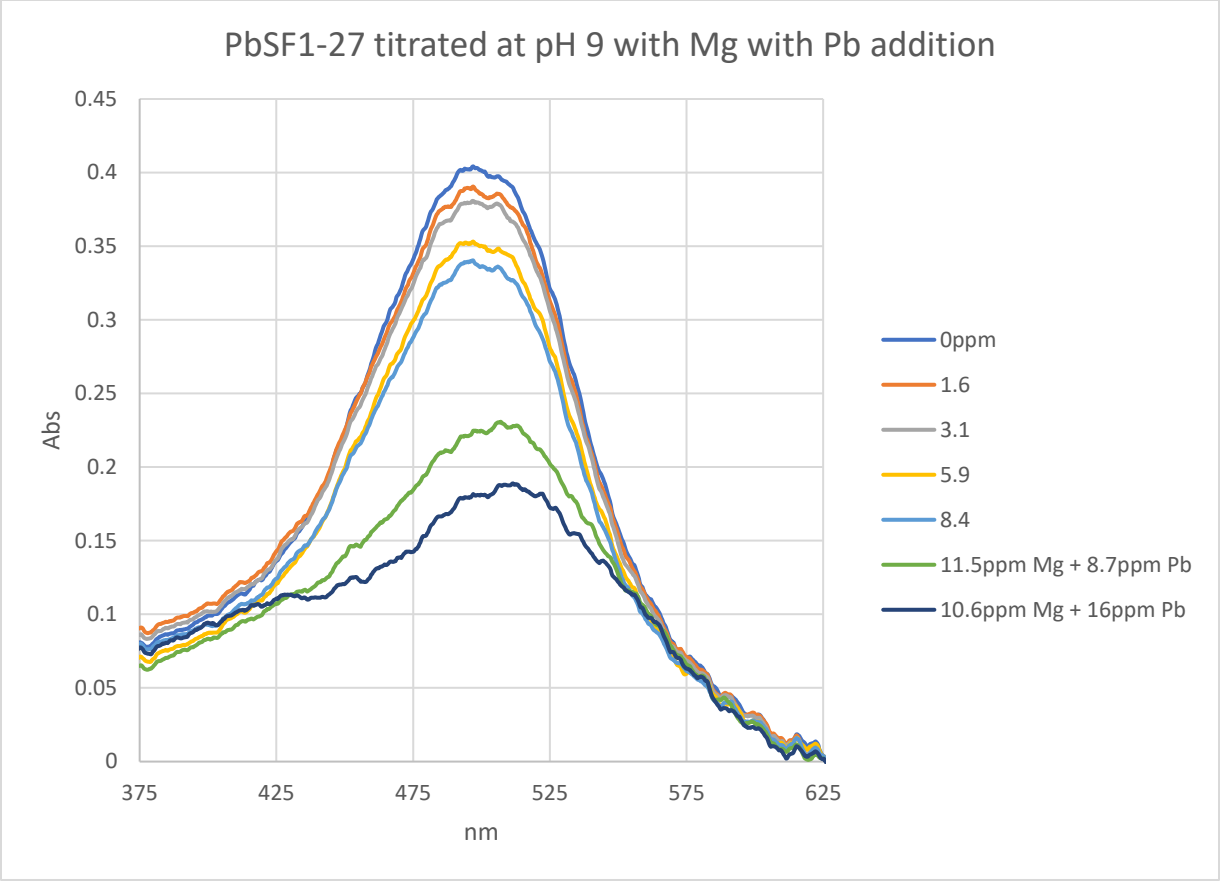

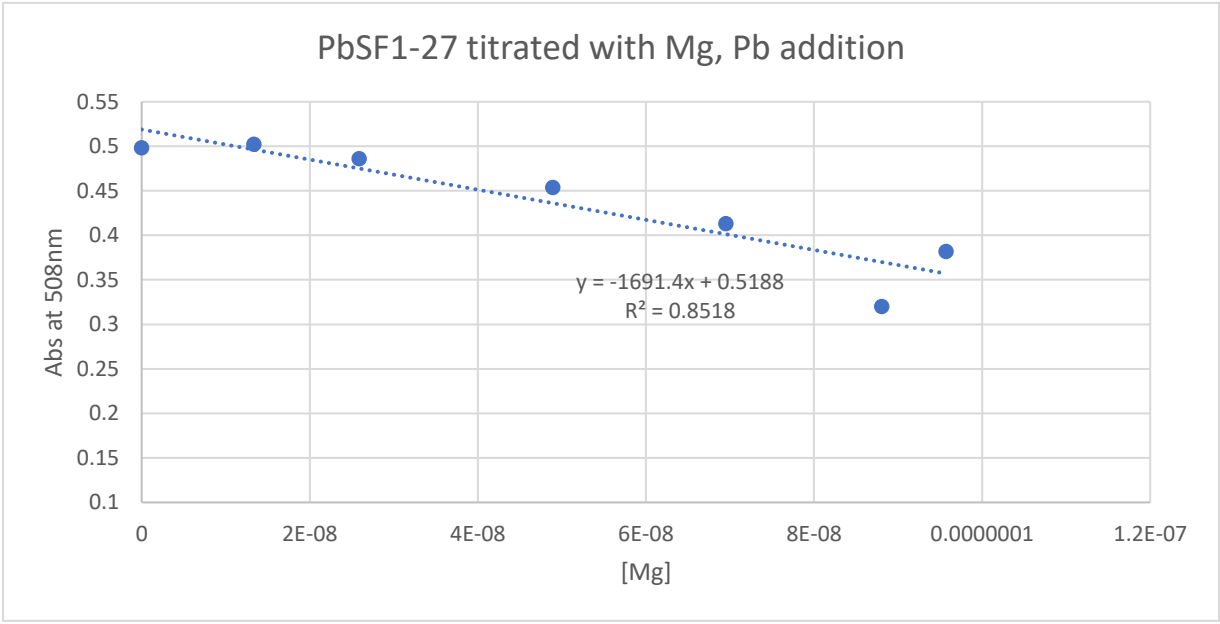

Spectrum 71: 18e Titration with Mg with Pb addition at pH 9, Day 0, ppm; Abs vs [Pb]

Titration of 18e, PbSF1-27 directly after synthesis, titrated with Ca and Pb

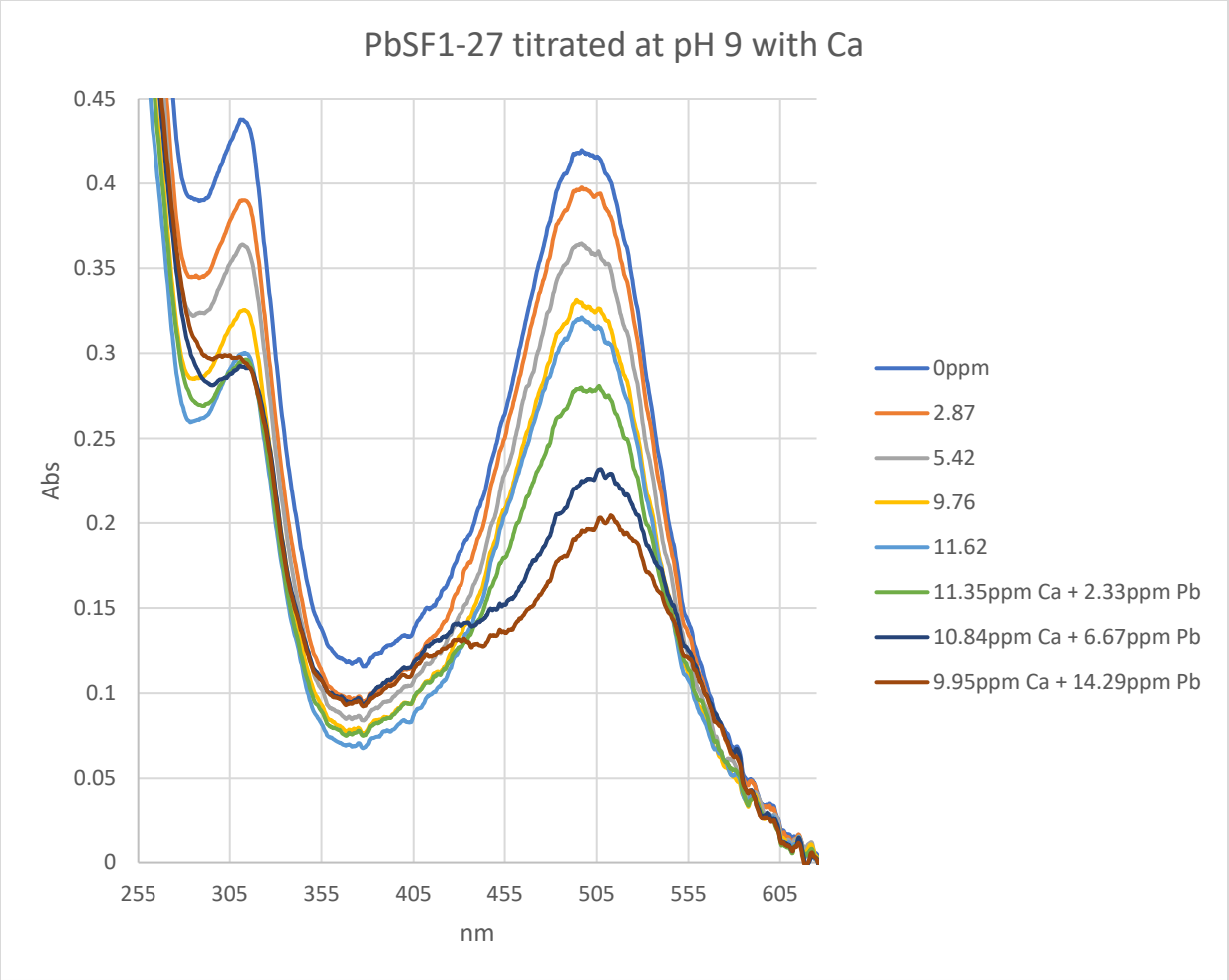

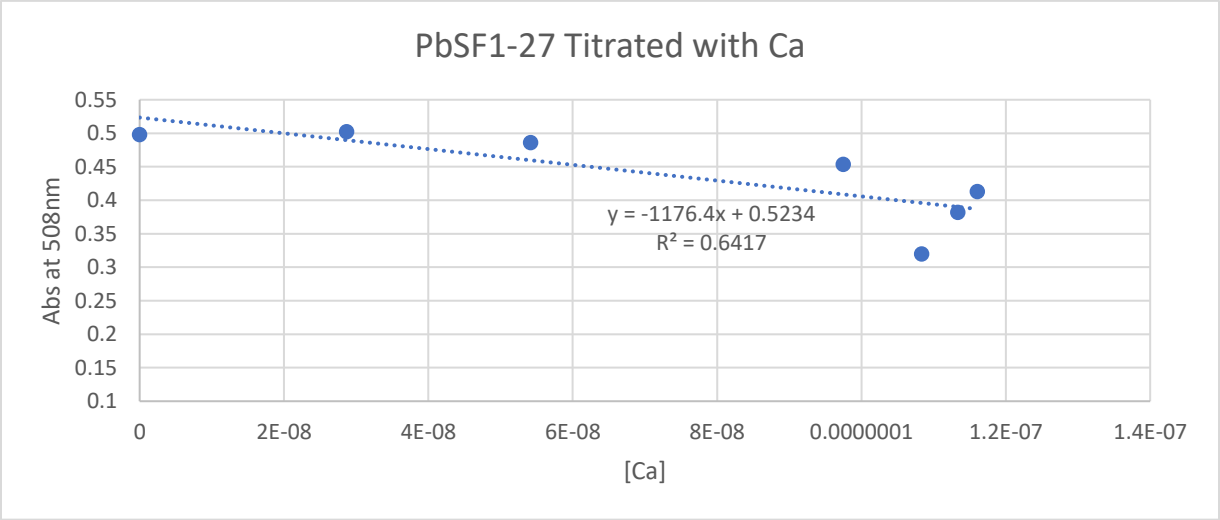

Spectrum 72: 18e Titration with Ca with Pb addition at pH 9, Day 0, low ppm Abs vs [Pb]

Titration of 18e, PbSF1-27 directly after synthesis, titrated pH 9 with ppm Zn, Pb added

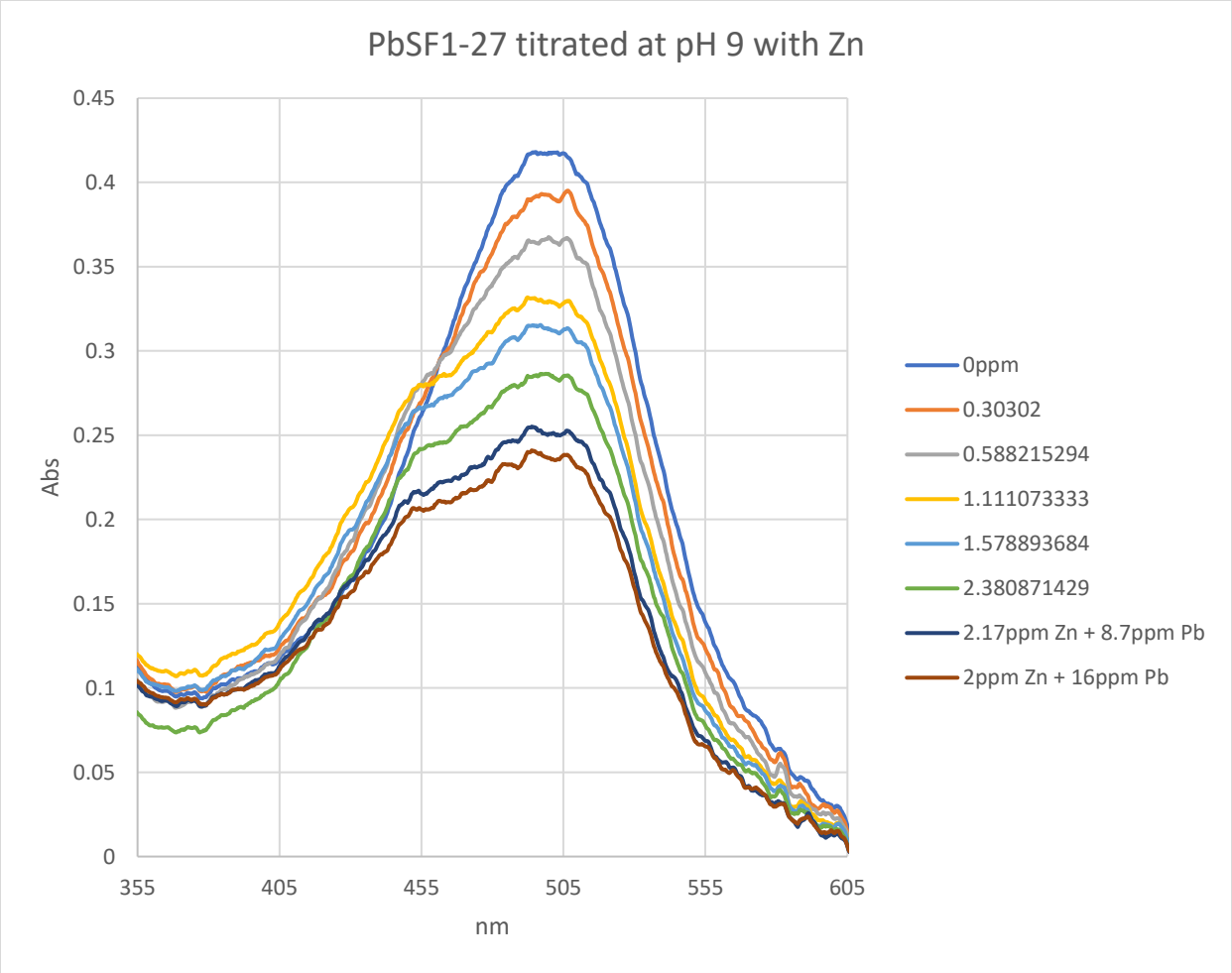

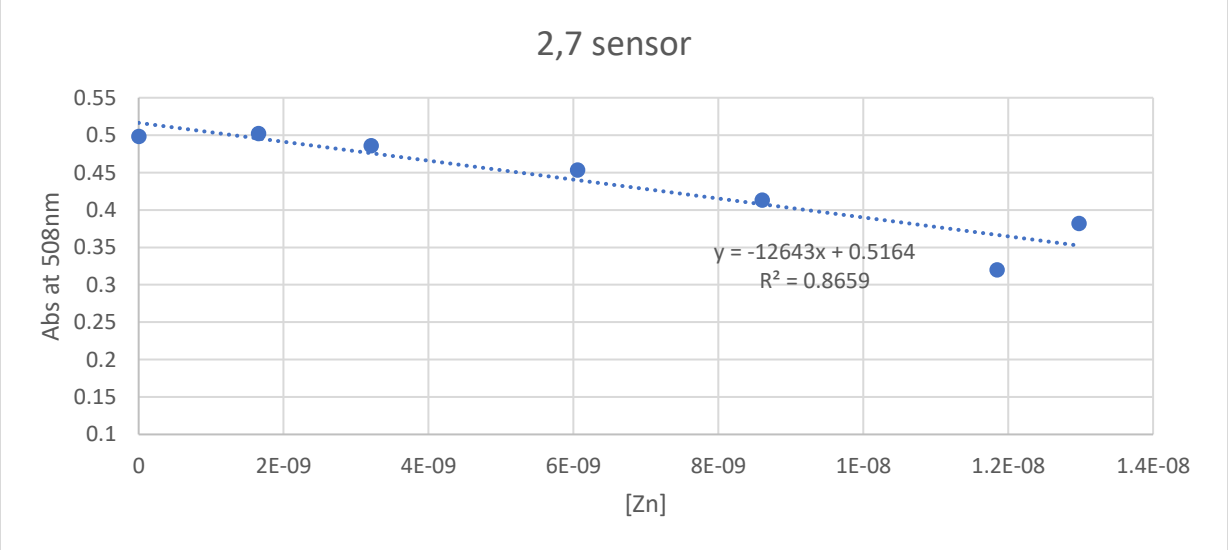

Spectrum 73: 18e Titration with Zn with Pb addition at pH 9, Day 0, low ppm; Abs vs [Pb]

Titration of 18e, PbSF1-27 one week after synthesis, titrated pH 9 with ppm Zn, Fe

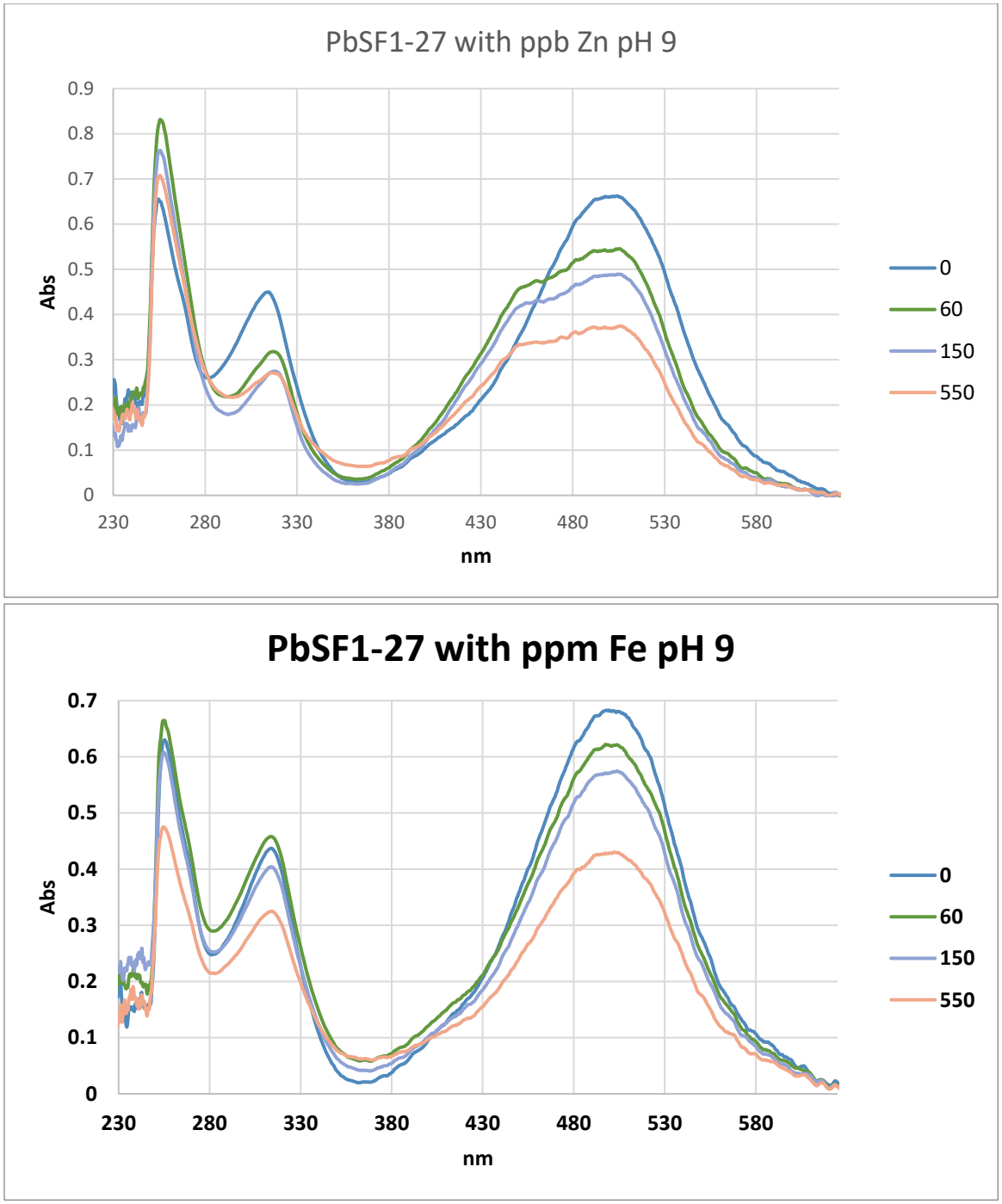

Spectrum 74: 18e Titration with Zn at pH 9, Week 1, ppm; 18e Titration with Fe at pH 9, Week 1, ppm

Titration of 18e, PbSF1-27 one week after synthesis, titrated pH 9 with ppm Ni, Cu

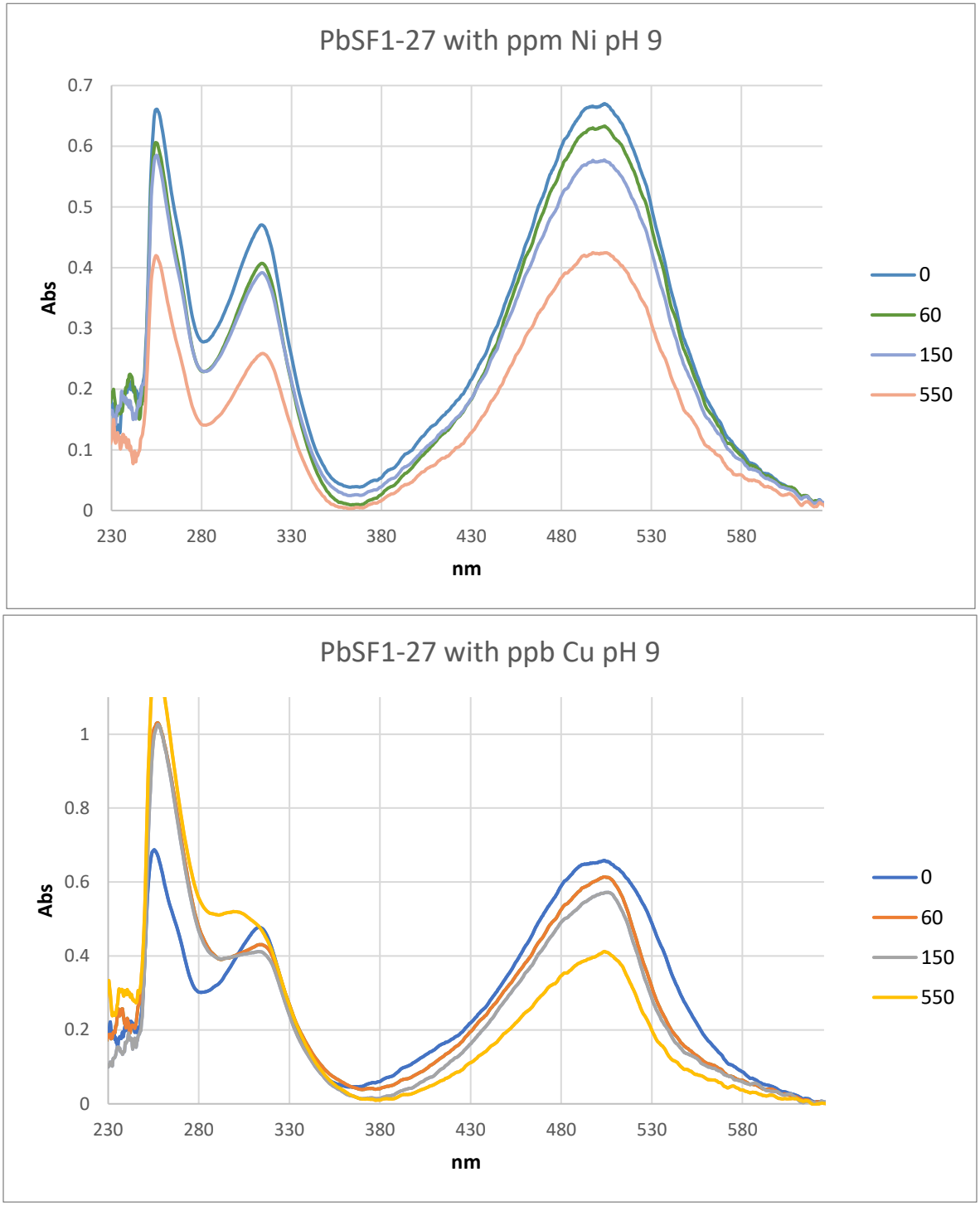

Spectrum 75: 18e Titration with Ni at pH 9, Week 1, ppm; 18e Titration with Cu at pH 9, Week 1, ppm

Titration of 18e, PbSF1-27 right after synthesis, titrated pH 9 with ppm Pb

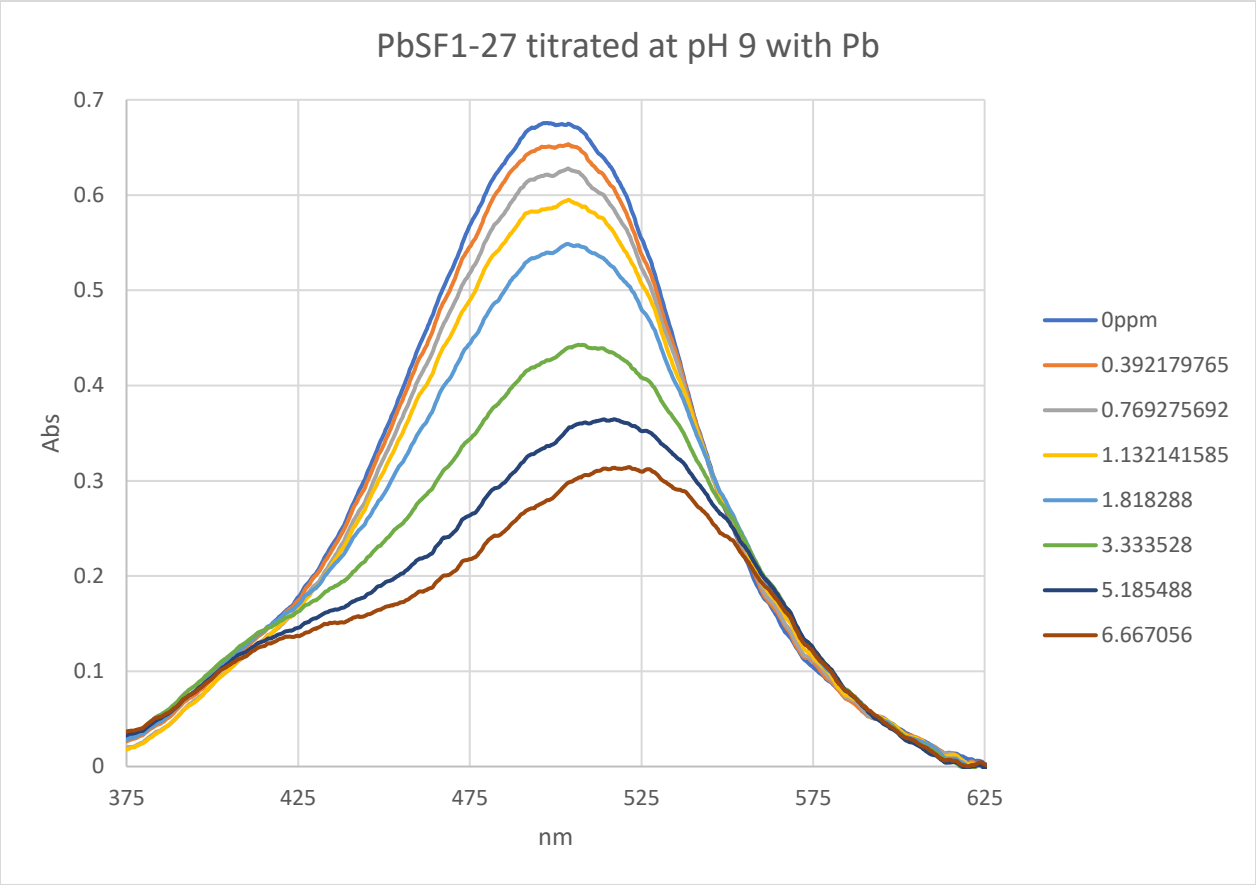

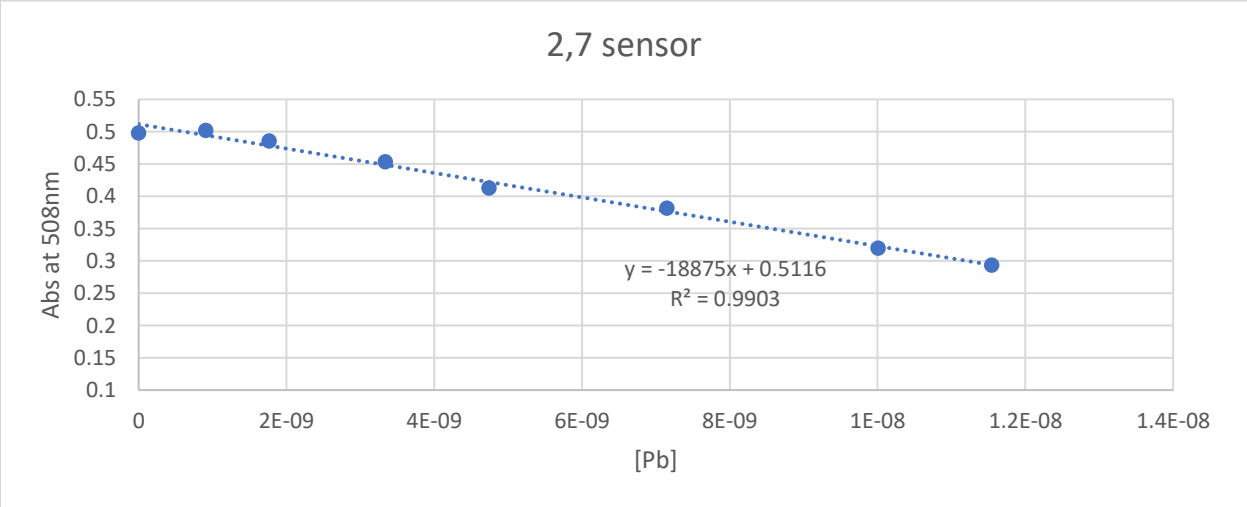

Spectrum 76: 18e Titration with Pb at pH 9, Day 0, low ppm; Abs vs [Pb]

Titration of 18e, PbSF1-27 right after synthesis, titrated pH 5 with ppm Pb

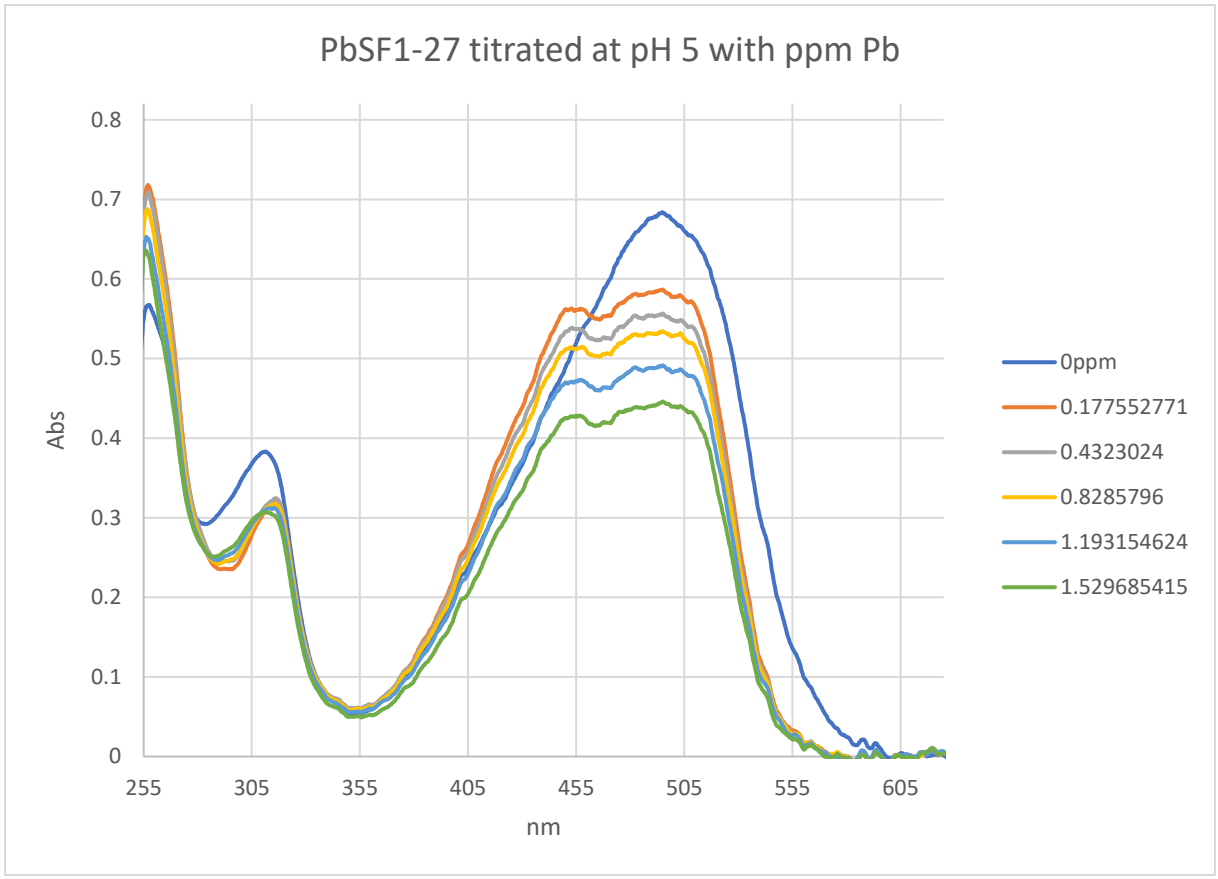

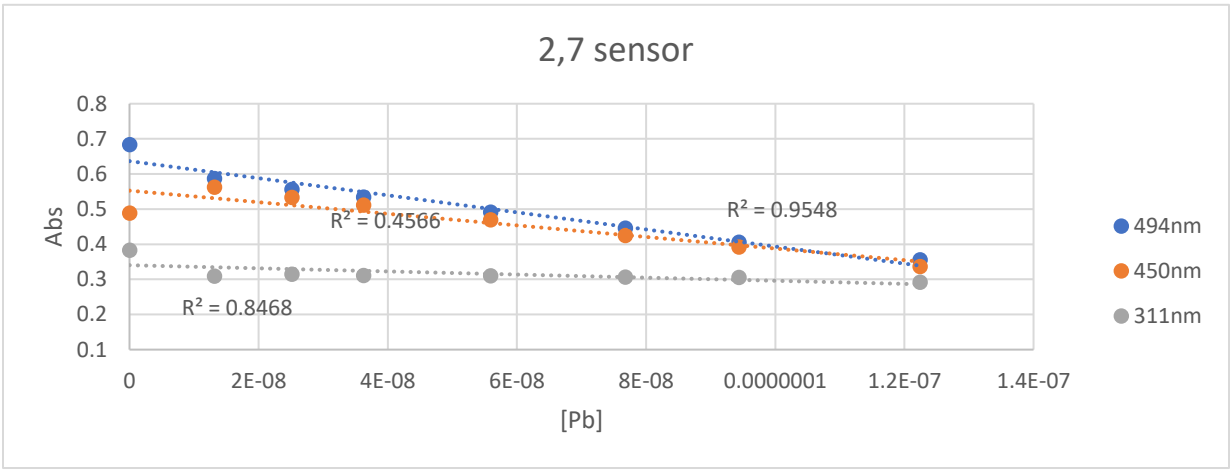

Spectrum 77: 18e Titration with Pb at pH 5, Day 0, low ppm; Abs vs [Pb]

Titration of 18e, PbSF1-27 two weeks after synthesis, titrated pH 5 with ppm Pb

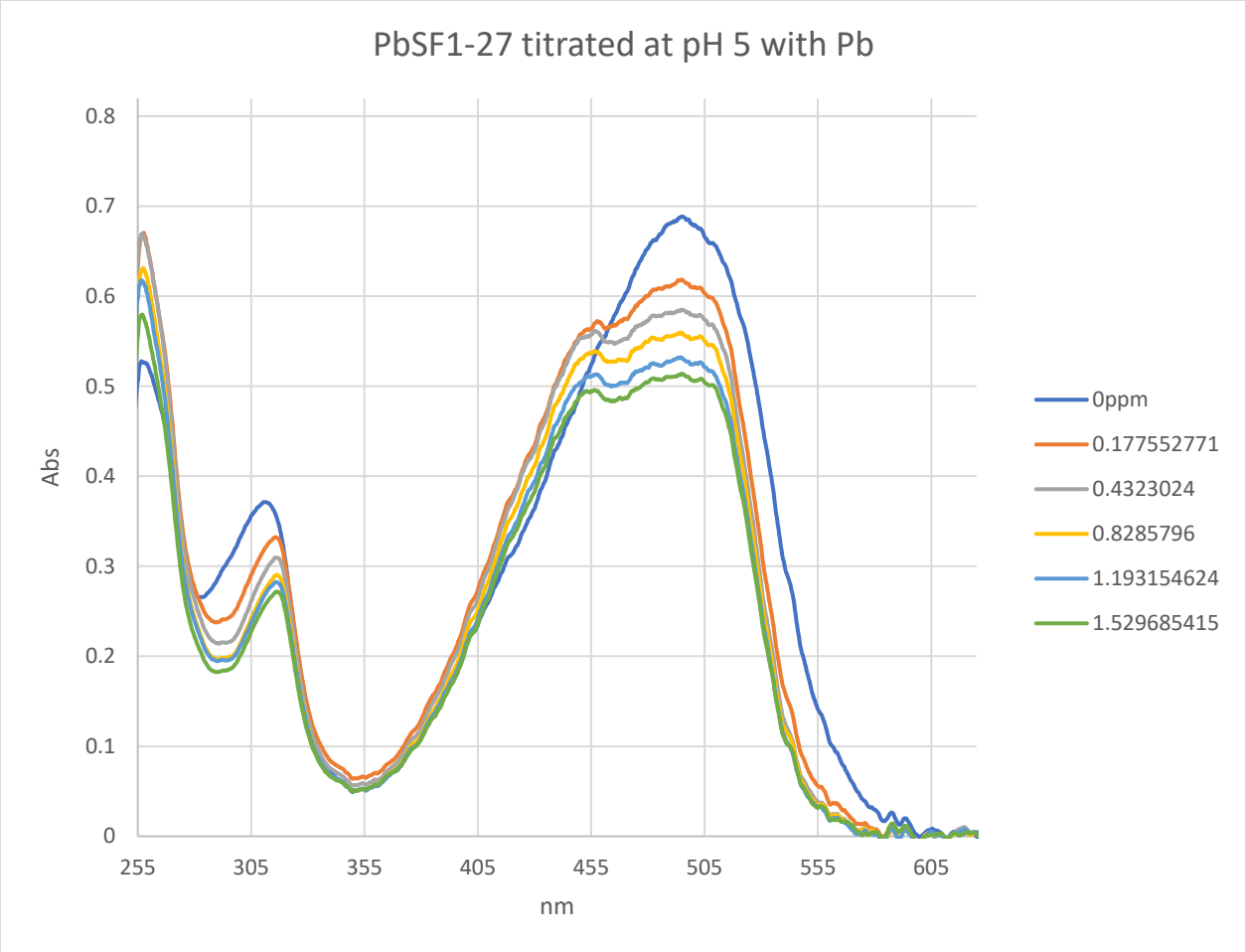

Spectrum 78: 18e Titration with Pb at pH 5, Week 2, low ppm; Abs vs [Pb]

Titration of 18e, PbSF1-27 two months after synthesis, titrated pH 9 with ppm Pb

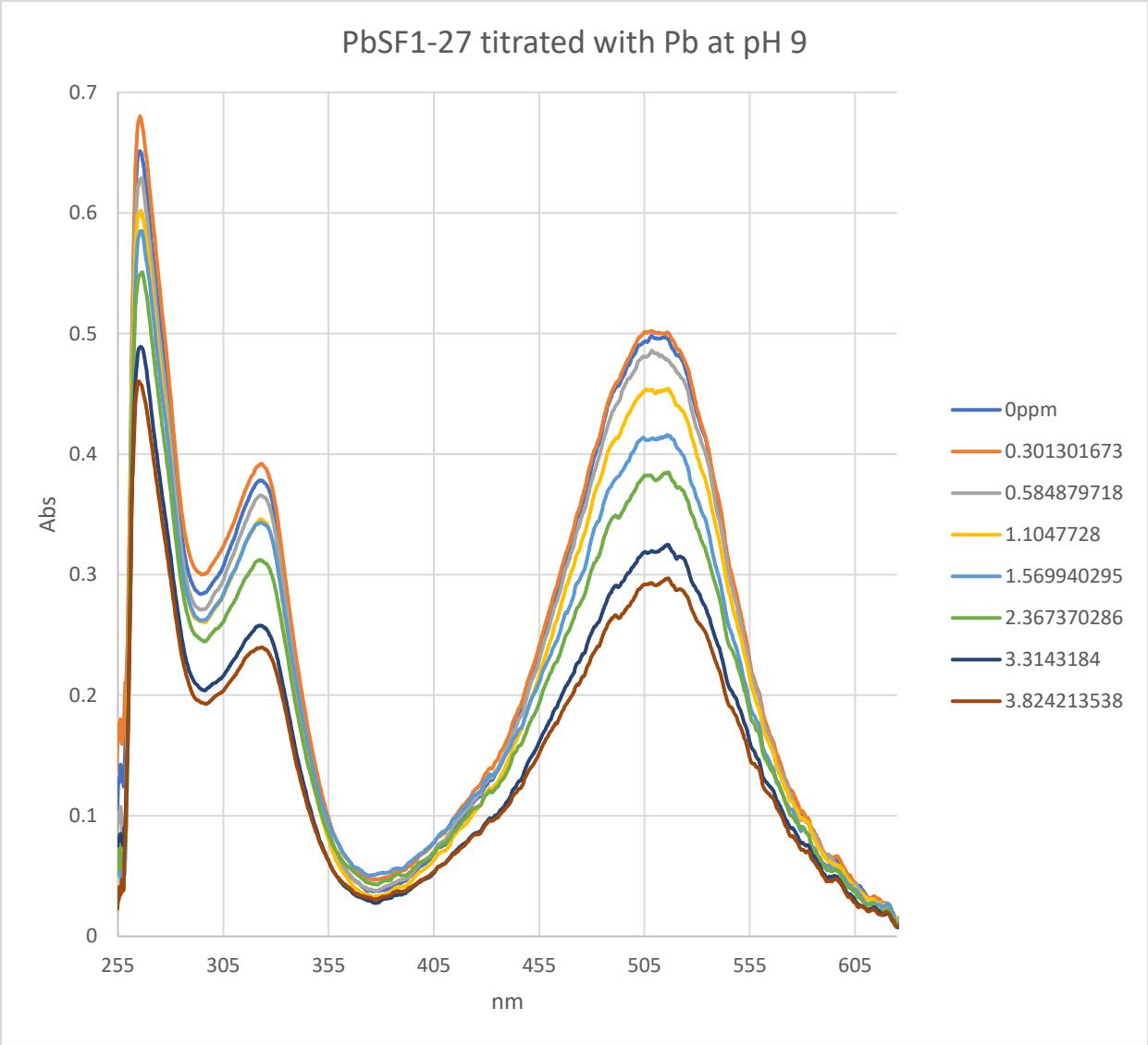

Spectrum 79: 18e Titration with Pb at pH 9, Month 2, low ppm

Titration of 18e, PbSF1-27 two weeks after synthesis, titrated pH 5 with ppm Pb

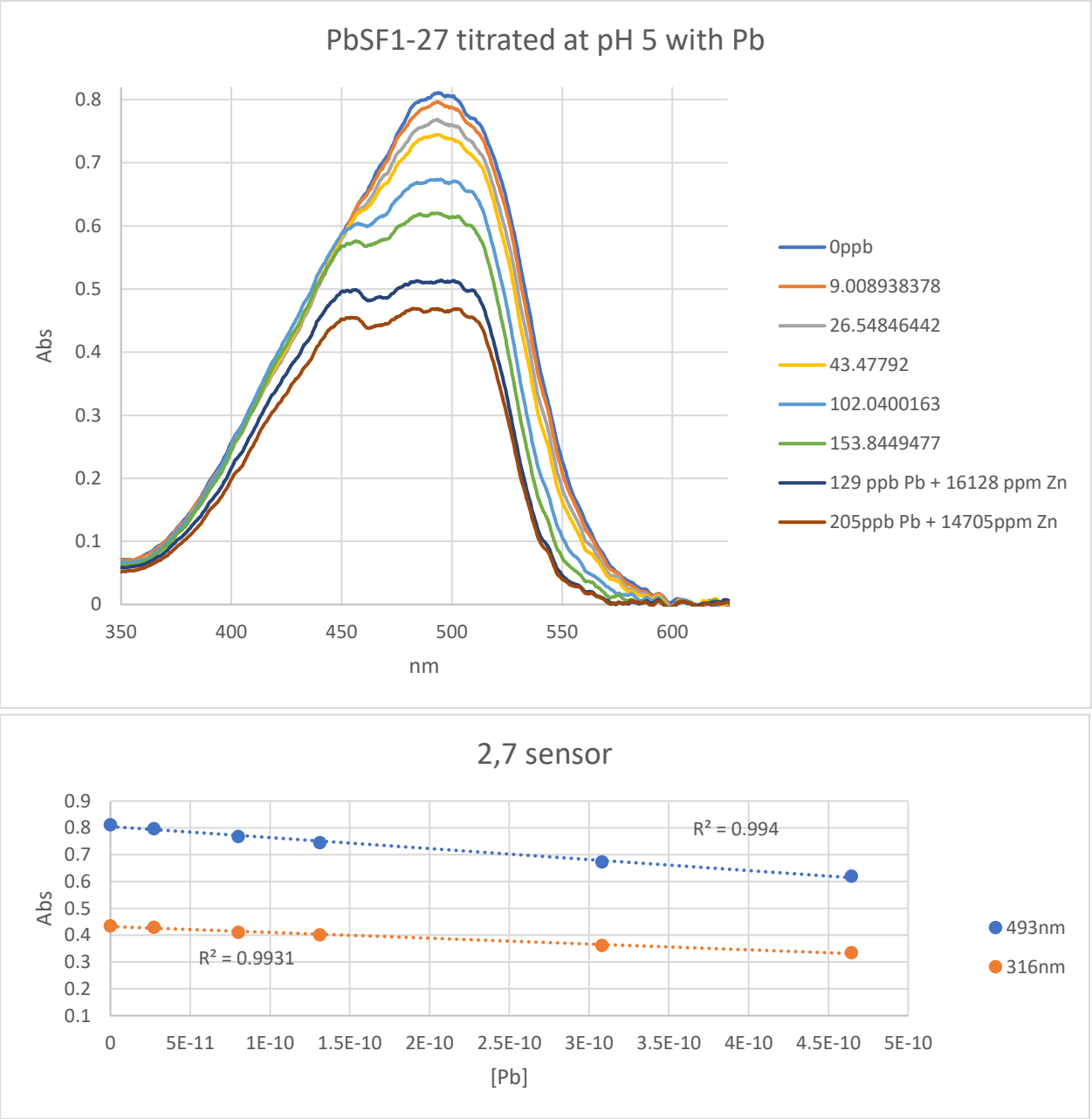

Spectrum 80: 18e Titration with Pb with addition of excess Zn at pH 5, Week 2, low ppb; Abs vs [Pb]

Titration of 18e, PbSF1-27 right after synthesis affinity tests pH 5,7,9 going from millimolar to nanomolar

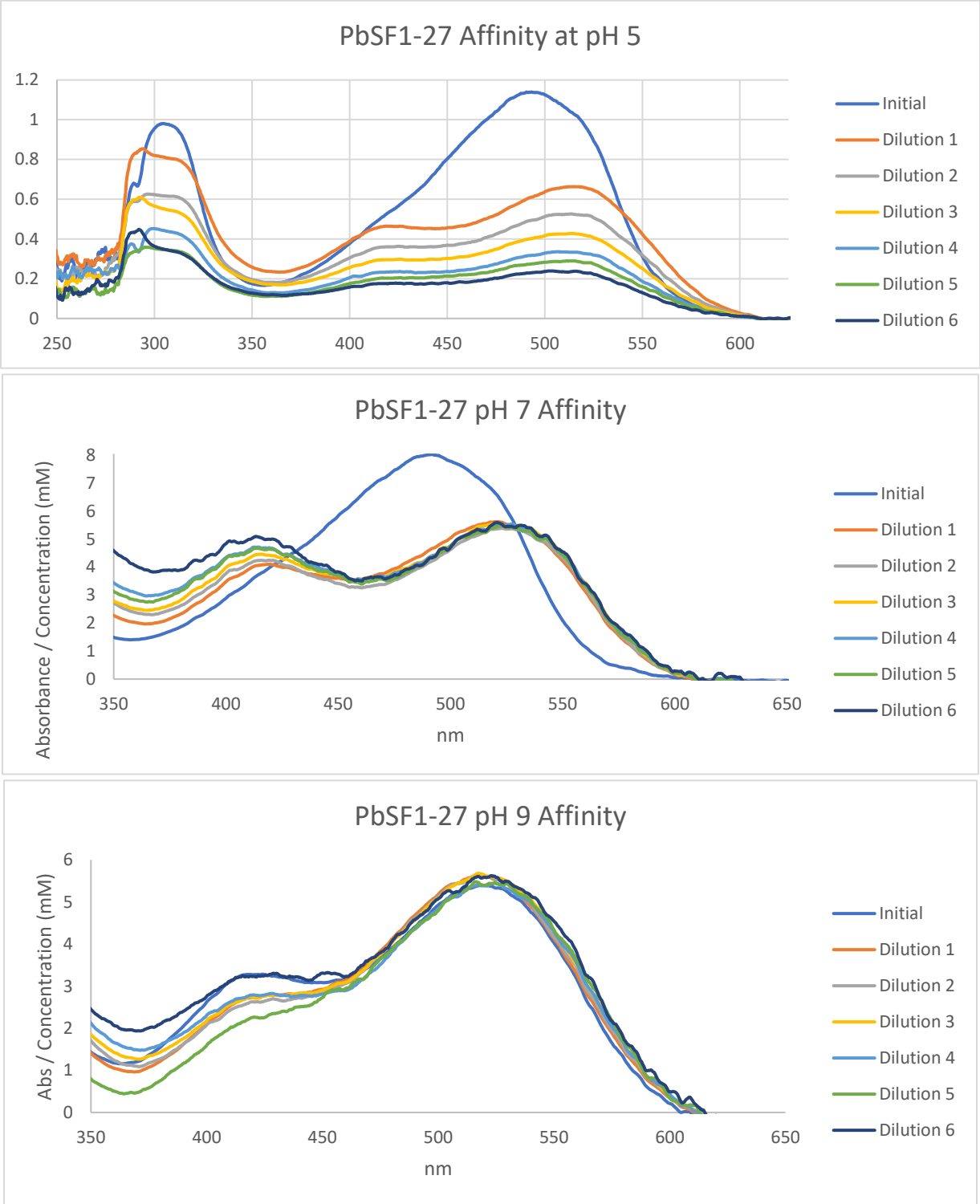

Spectrum 81: 18e Affinity tests at pH 5, 7, and 9 using Pb from millimolar to nanomolar

Titration of 18e, PbSF1-27 one week after synthesis, titrated pH 7 with varied metals

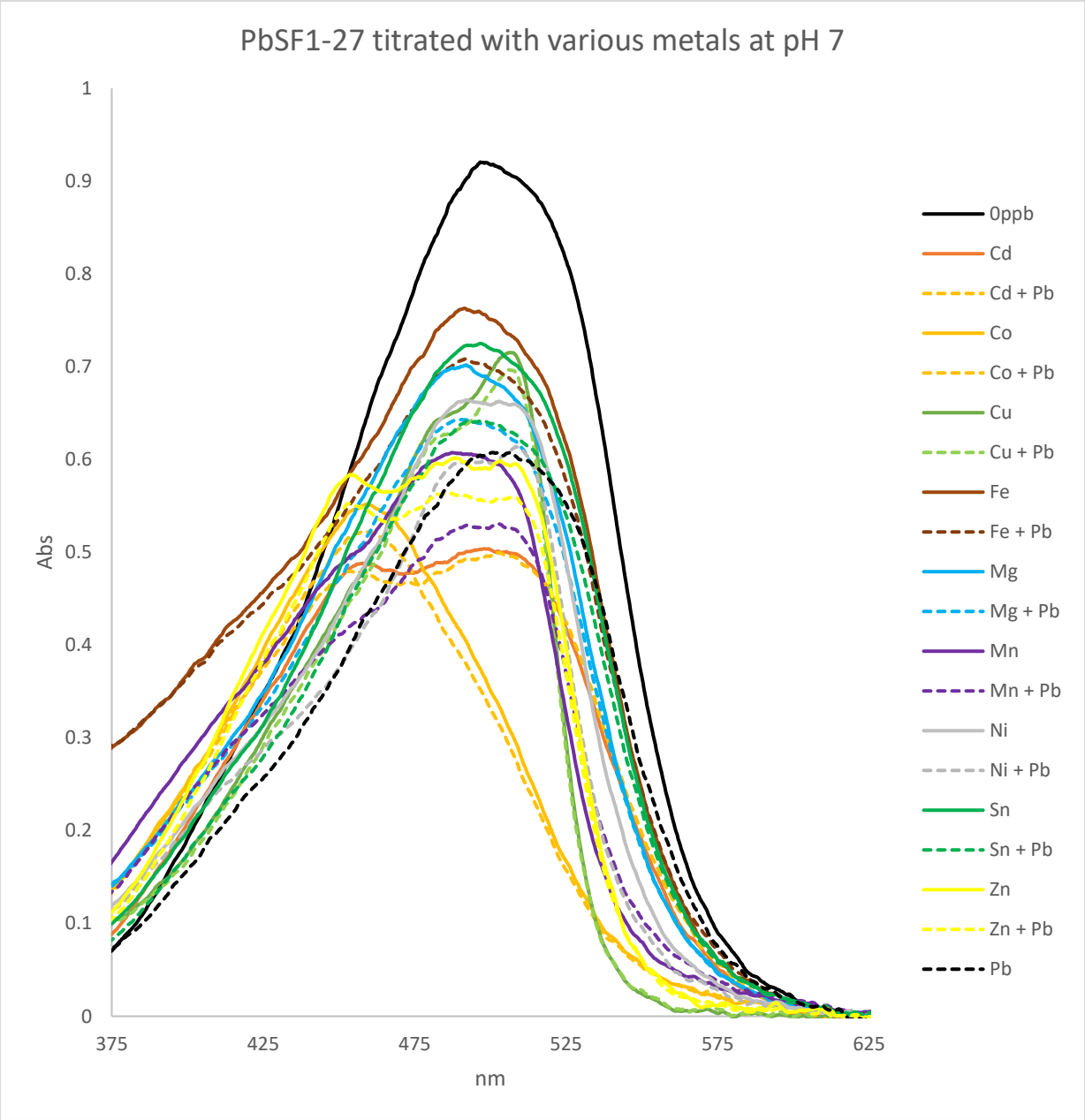

Spectrum 82: 18e Titration with varied metals at pH 7, Week 1, saturated

Titration of 18e, PbSF1-27 two months after synthesis titrated at pH 5 with ppb Pb

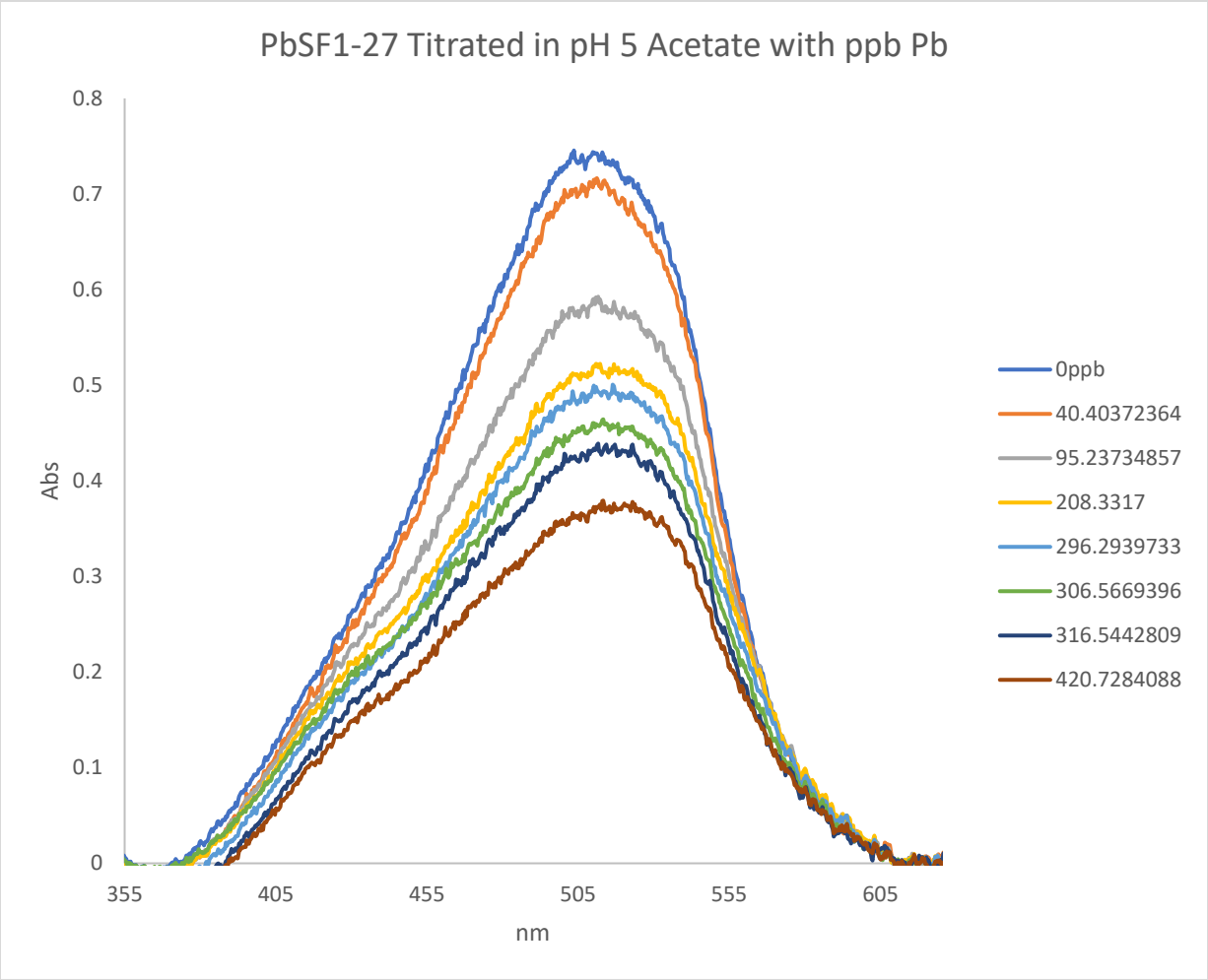

Spectrum 83: 18e Titration with Pb at pH 5, Month 2, ppb

Titration of 18e, PbSF1-27 one month after synthesis titrated at pH 5 with ppb going to ppm Pb and ppm Zn

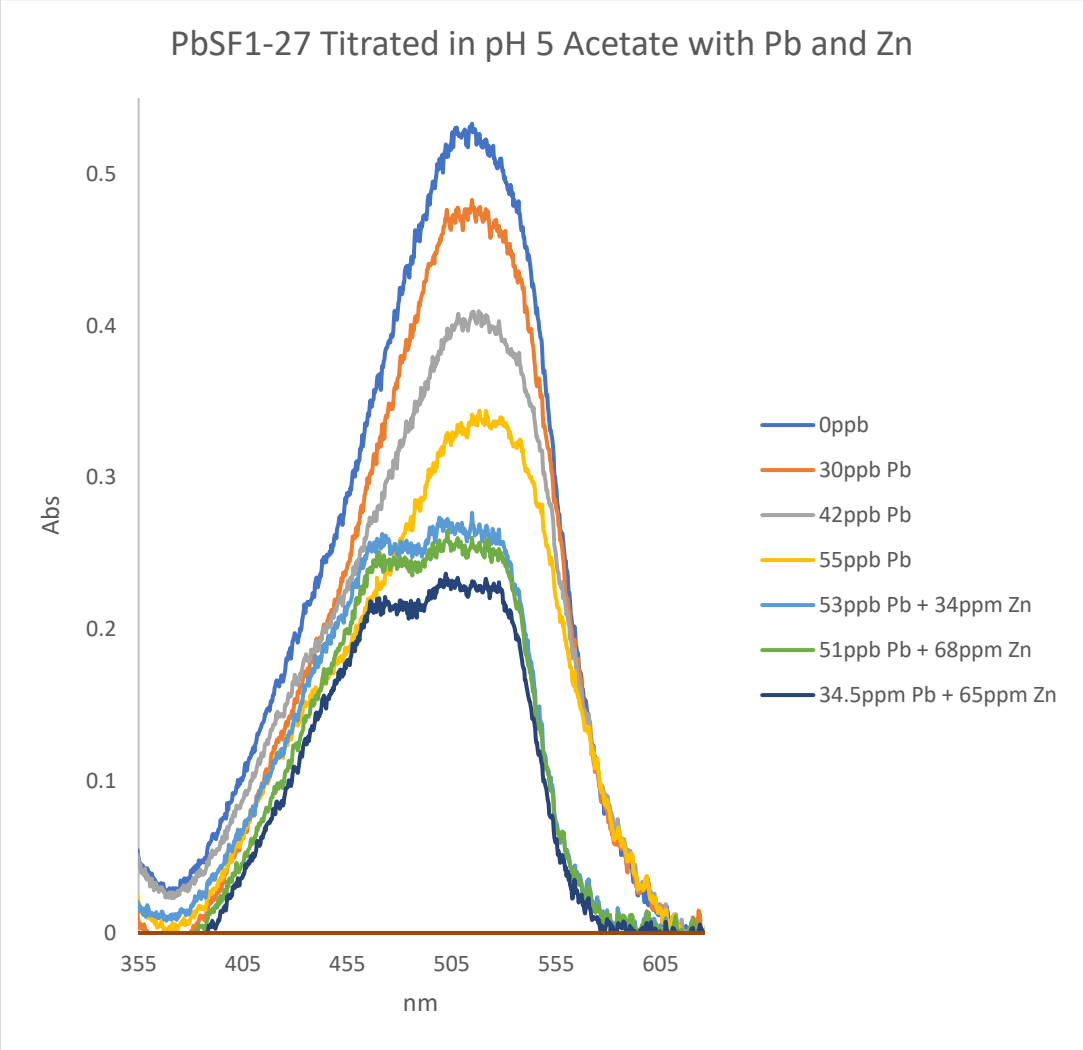

Spectrum 84: 18e Titration with Pb with Zn addition at pH 5, Month 1, ppb to saturation

Titration of 18e, PbSF1-27 one month after synthesis titrated at pH 5 with equal amounts of Zn and Pb in excess over sensor

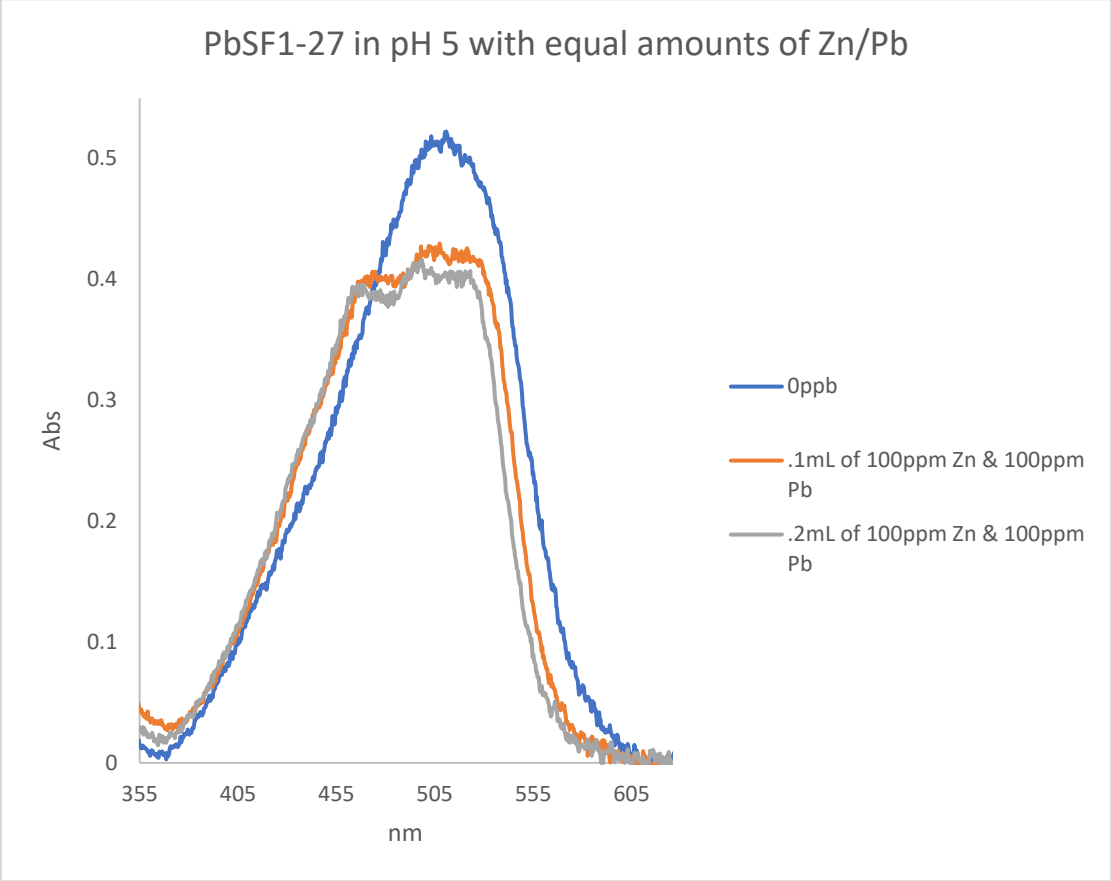

Spectrum 85: 18e Titration with equal Pb and Zn at pH 5, Month 1

18e, PbSF1-27, saturated Pb bound sensor titrated with saturated Zn bound sensor at pH 5

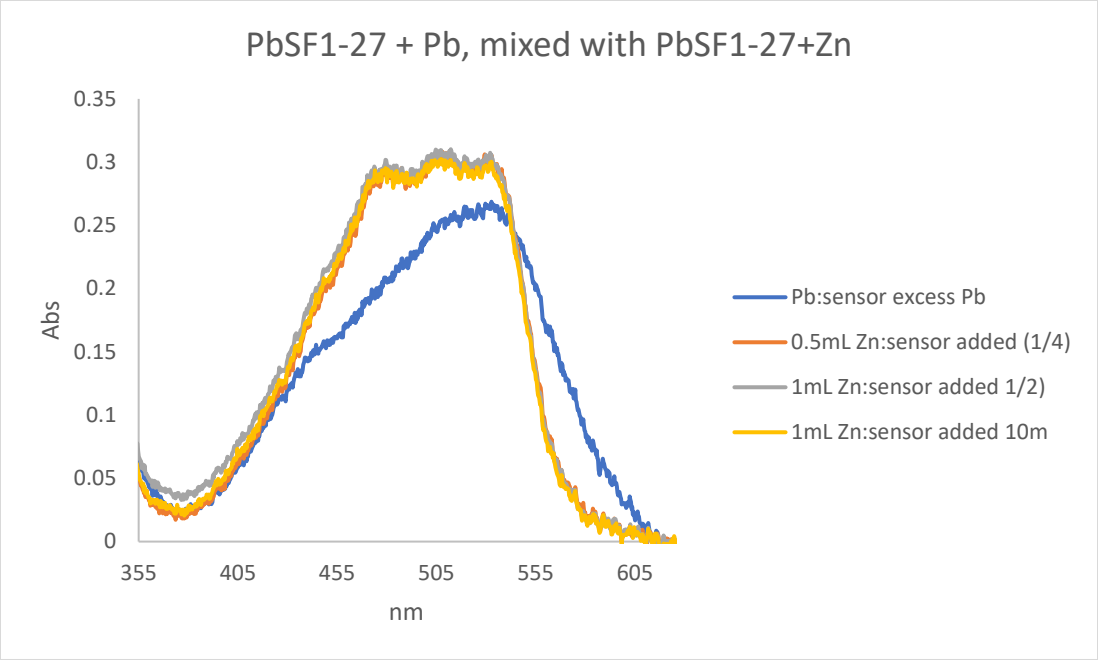

Spectrum 86: 18e Titration of saturated Pb bound sensor with saturated Zn bound sensor at pH 5, Month 1

Titration of 18e, PbSF1-27 three weeks at pH 5 with ppb Pb going to excess Pb with minor Cu and Zn additions

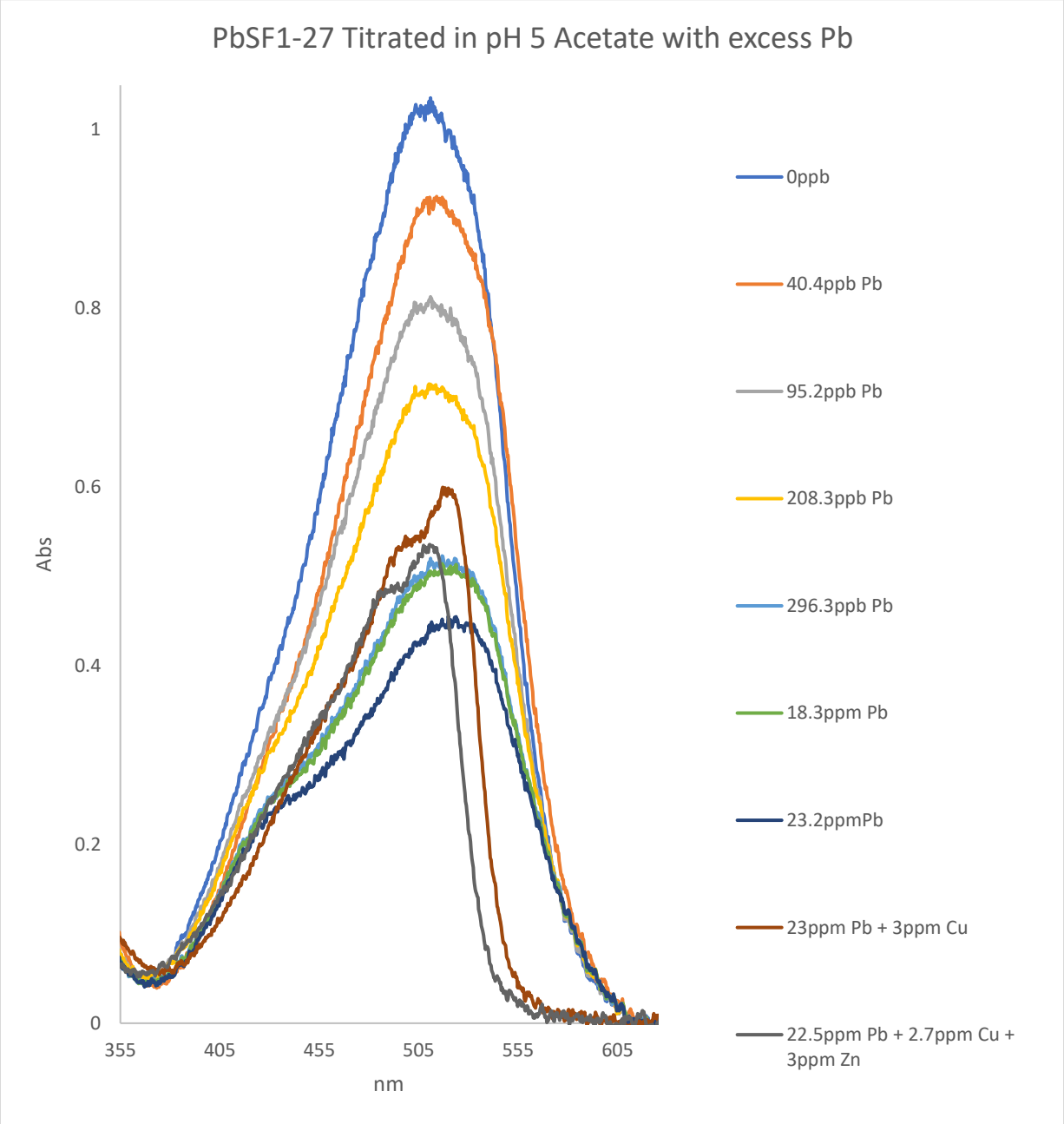

Spectrum 87: 18e Titration with Pb at pH 5 with Zn and Cu additions, Week 3, low ppb to saturation

Titration of 18e, PbSF1-27 one week after synthesis titrated at pH 5 with Pb with excess Zn present

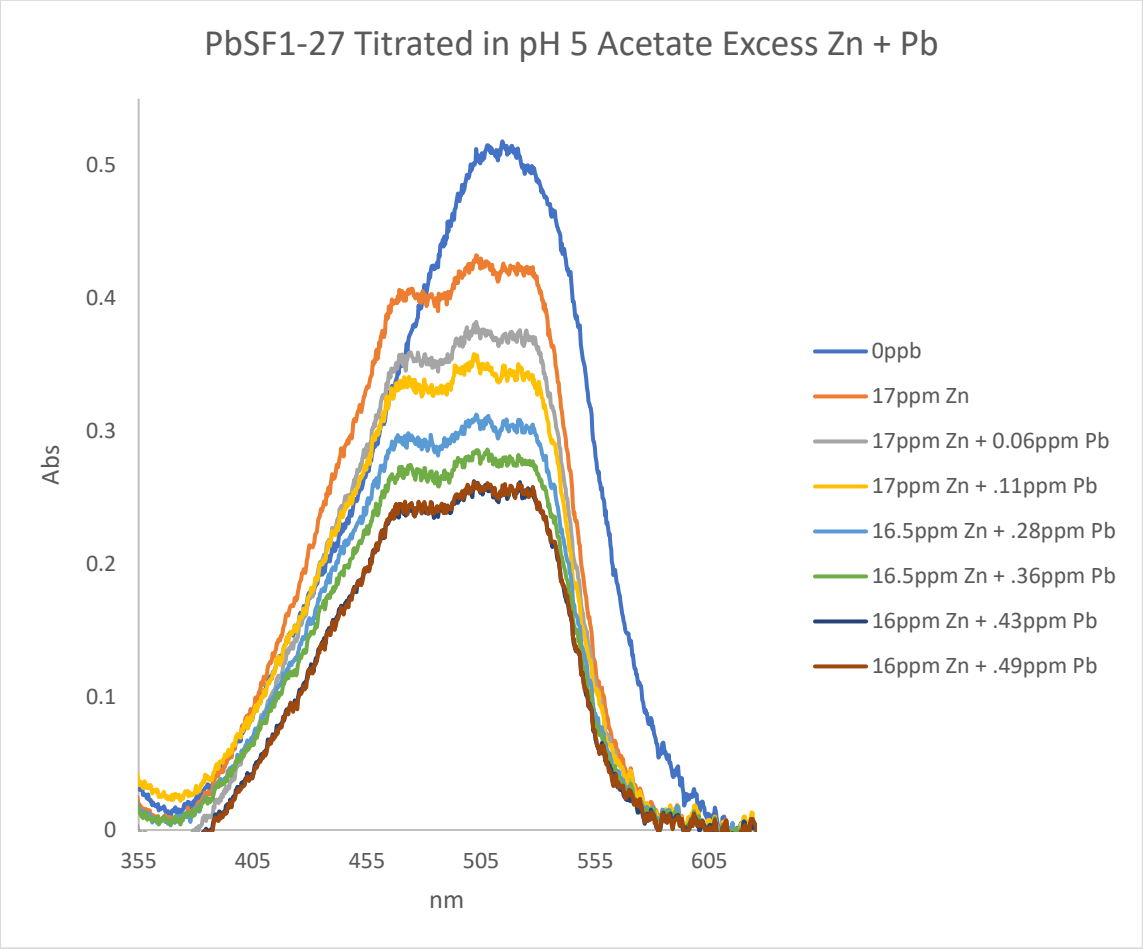

Spectrum 88: 18e Titration with Pb at pH 5, week 1, excess Zn in solution; Abs vs [Pb]

Titration of 18e, PbSF1-27 one week after synthesis titrated at pH 5 with excess Pb and then titrated with Zn

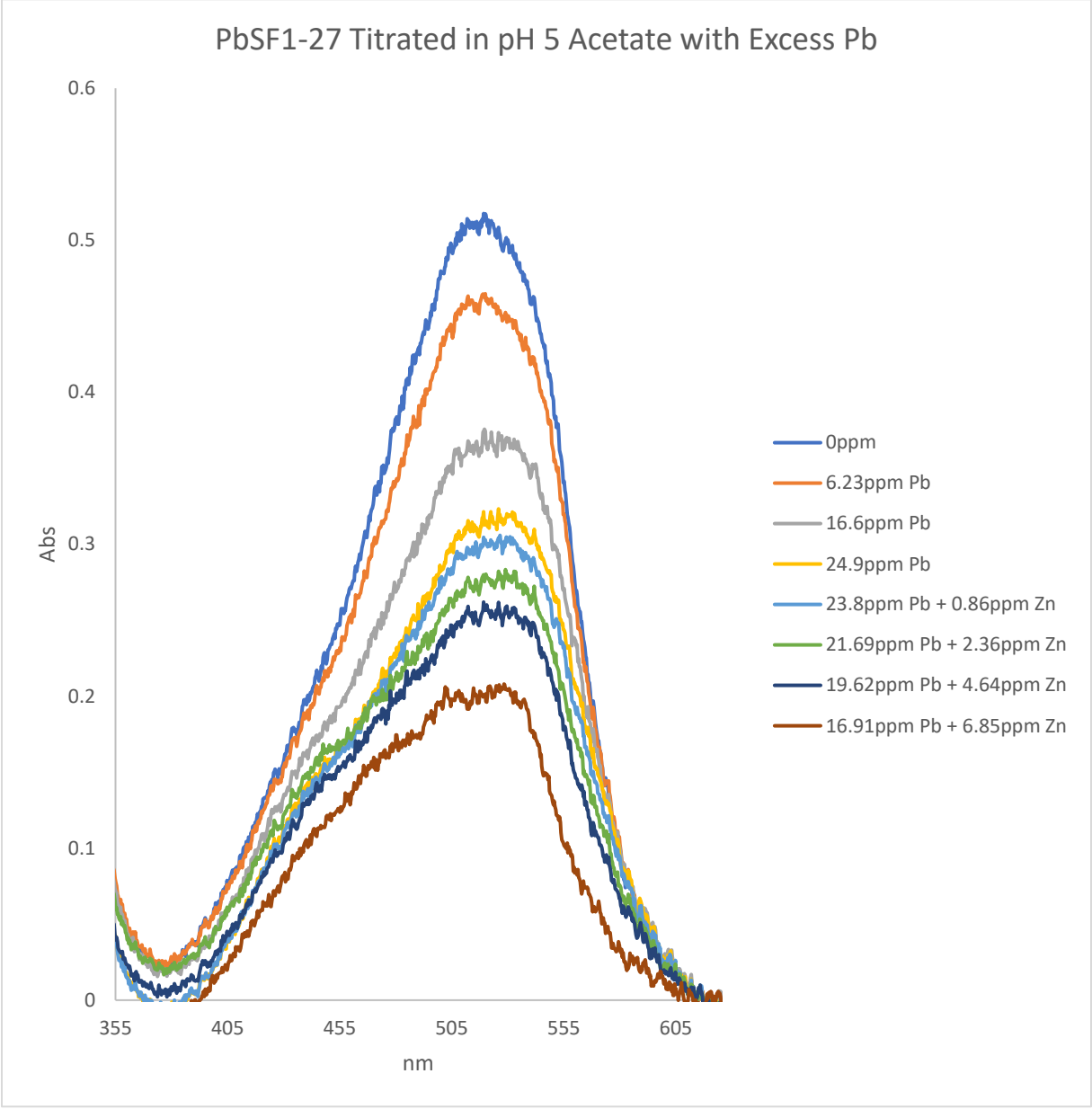

Spectrum 89: 18e Titration with Pb with Zn additions at pH 5, Week 1, ppm

Titration of 18f, PbSF1-15 right after synthesis titrated with Pb

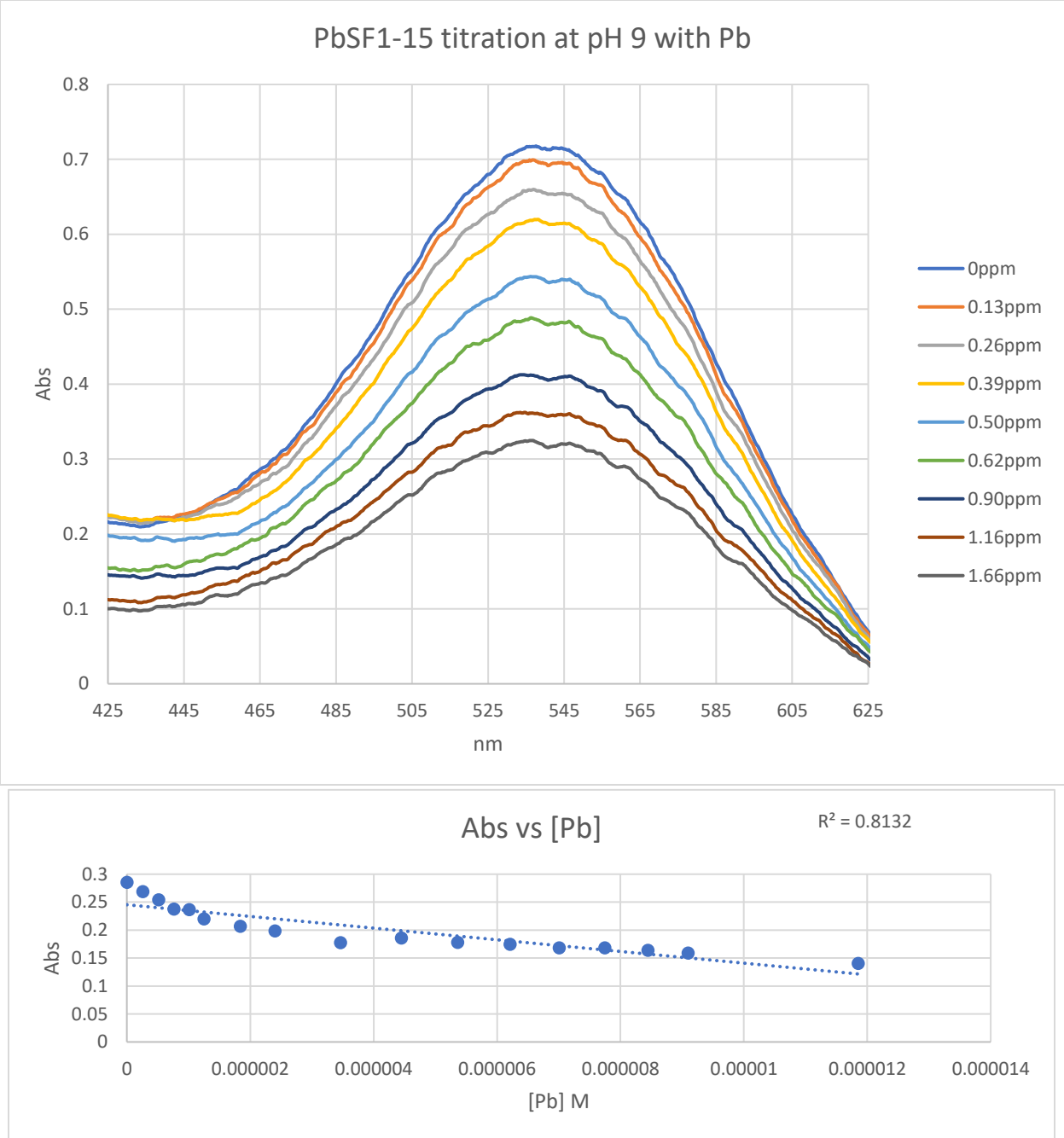

Spectrum 90: 18f Titration with Pb at pH 9, Day 0, low ppm; Abs vs [Pb]

Titration of 18f, PbSF1-15 right after synthesis titrated with various metals at pH 5

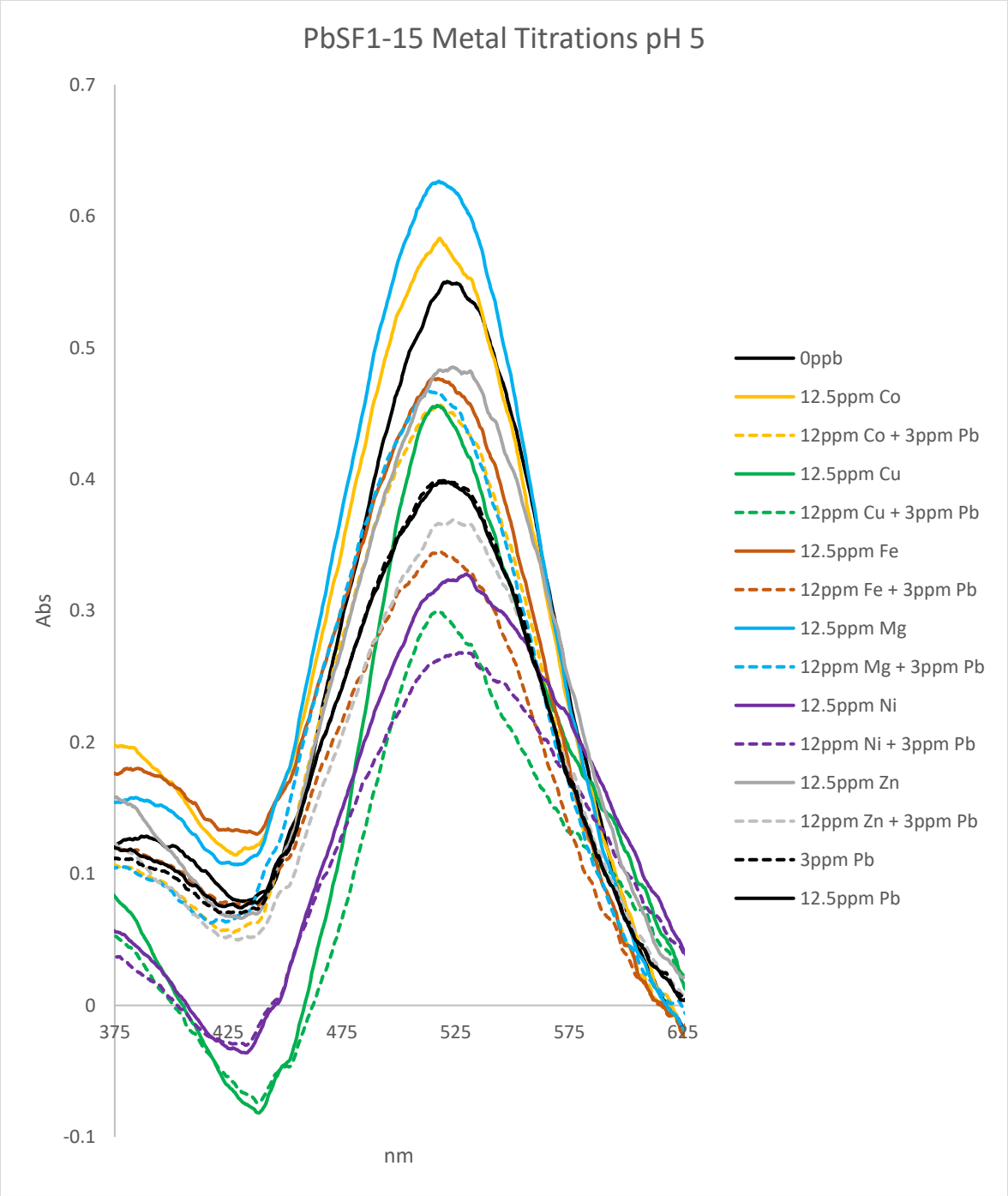

Spectrum 91: 18f Titration with varied metals at pH 5, Week 2, saturated

Titration of 18g, PbSF1-cR right after synthesis titrated with various metals at pH 5

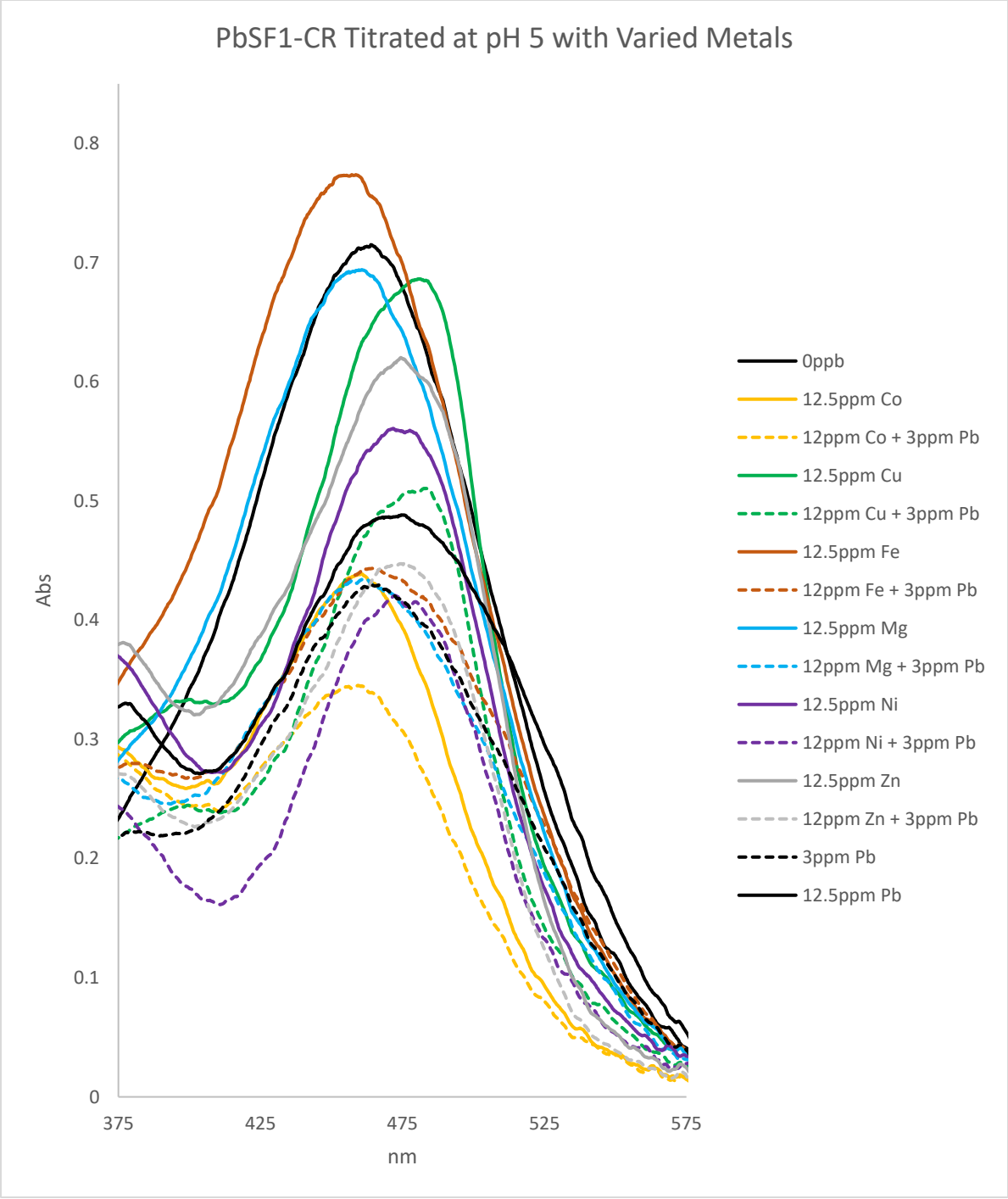

Spectrum 92: 18g Titration with varied metals at pH 5, Day 0, saturated

Titration of 19a, PbSF2-R right after synthesis titrated with Pb at pH 5

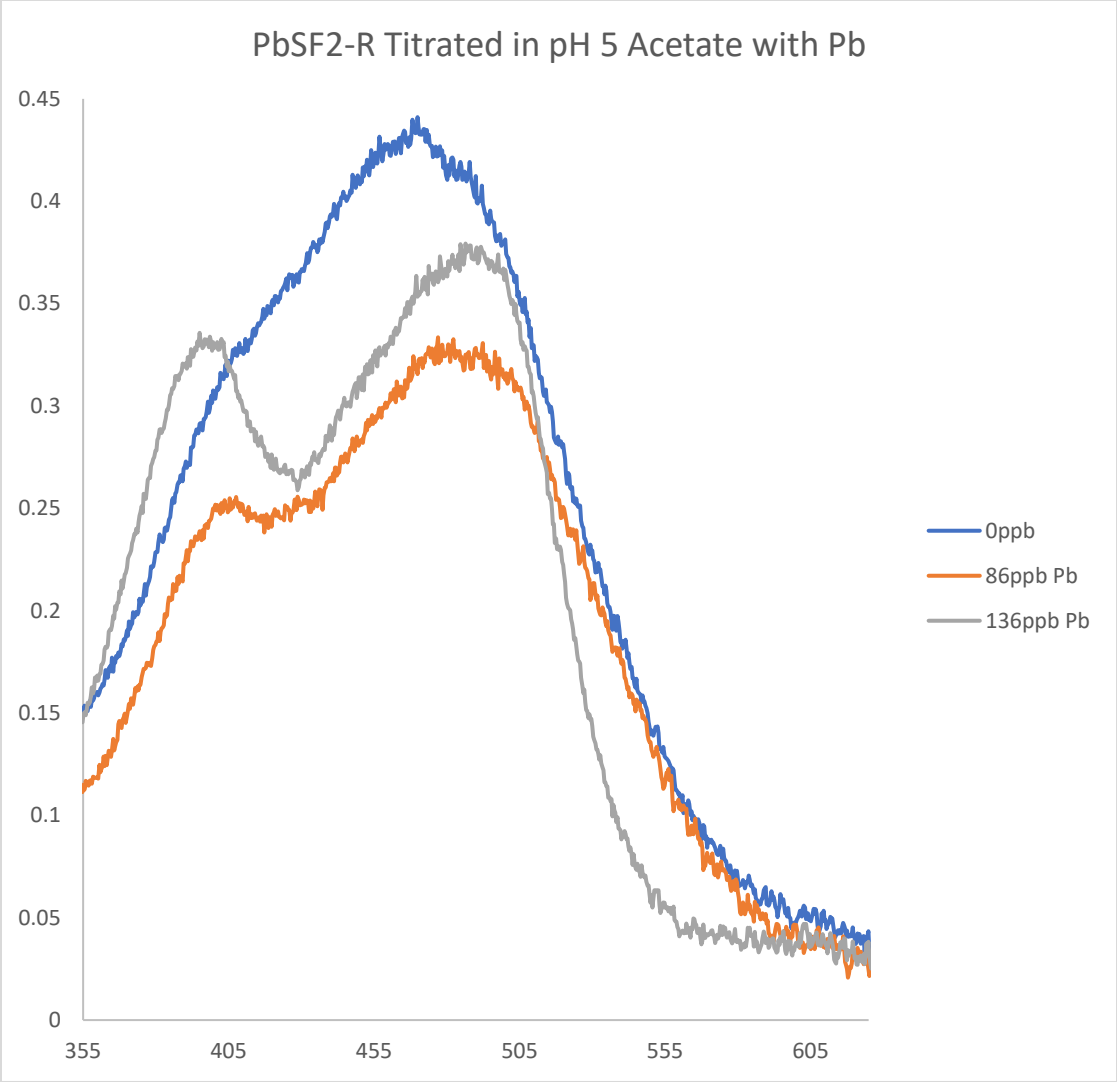

Spectrum 93: 19a Titration with Pb at pH 5, Day 0, ppb

Titration of 19e, PbSF2-15 right after synthesis titrated with ppb Pb at pH 5

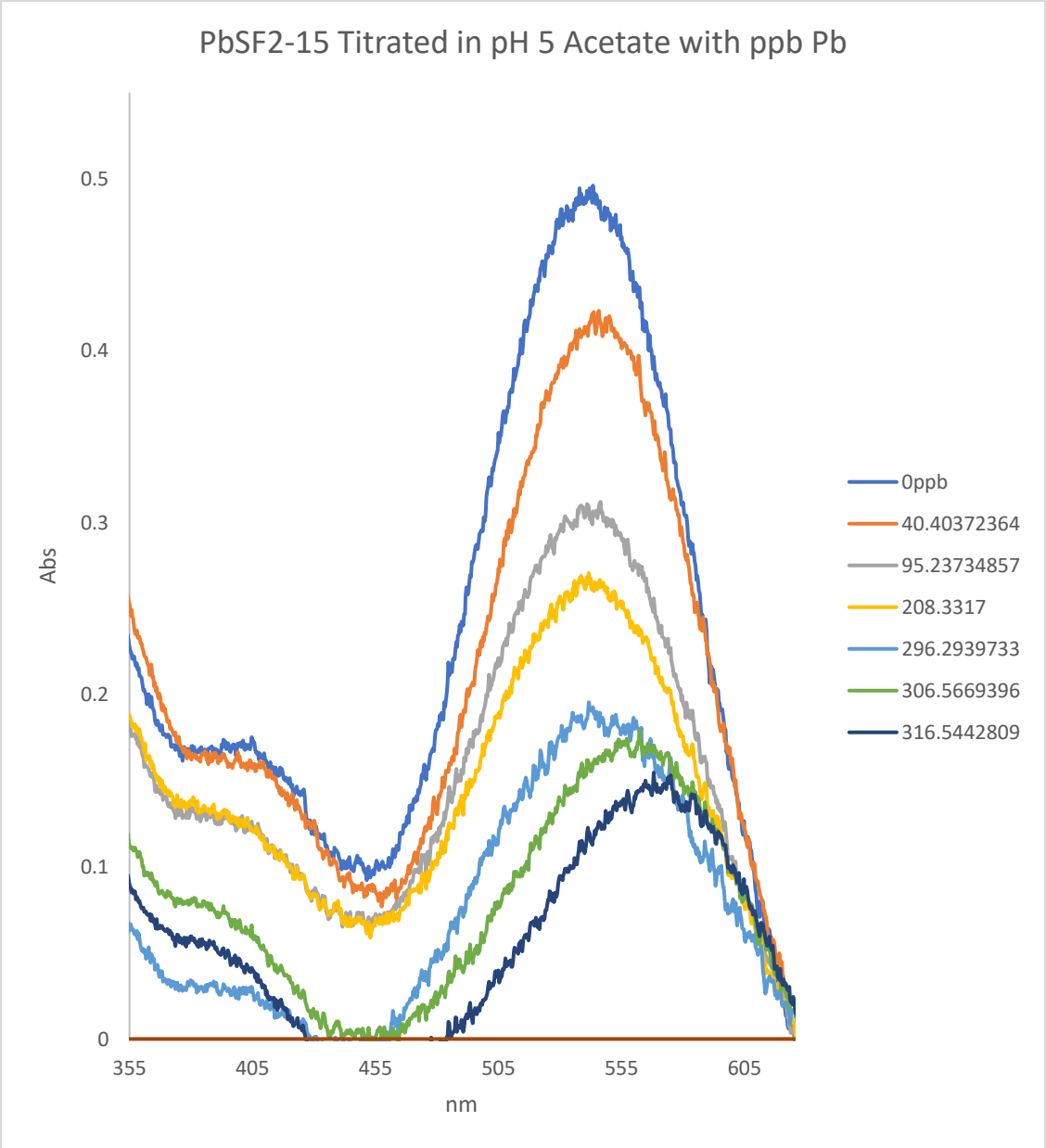

Spectrum 94: 19e Titration with Pb at pH 5, Day 0, ppb

Titration of 19d, PbSF2-27 right after synthesis titrated with Pb at pH 5 with Zn added

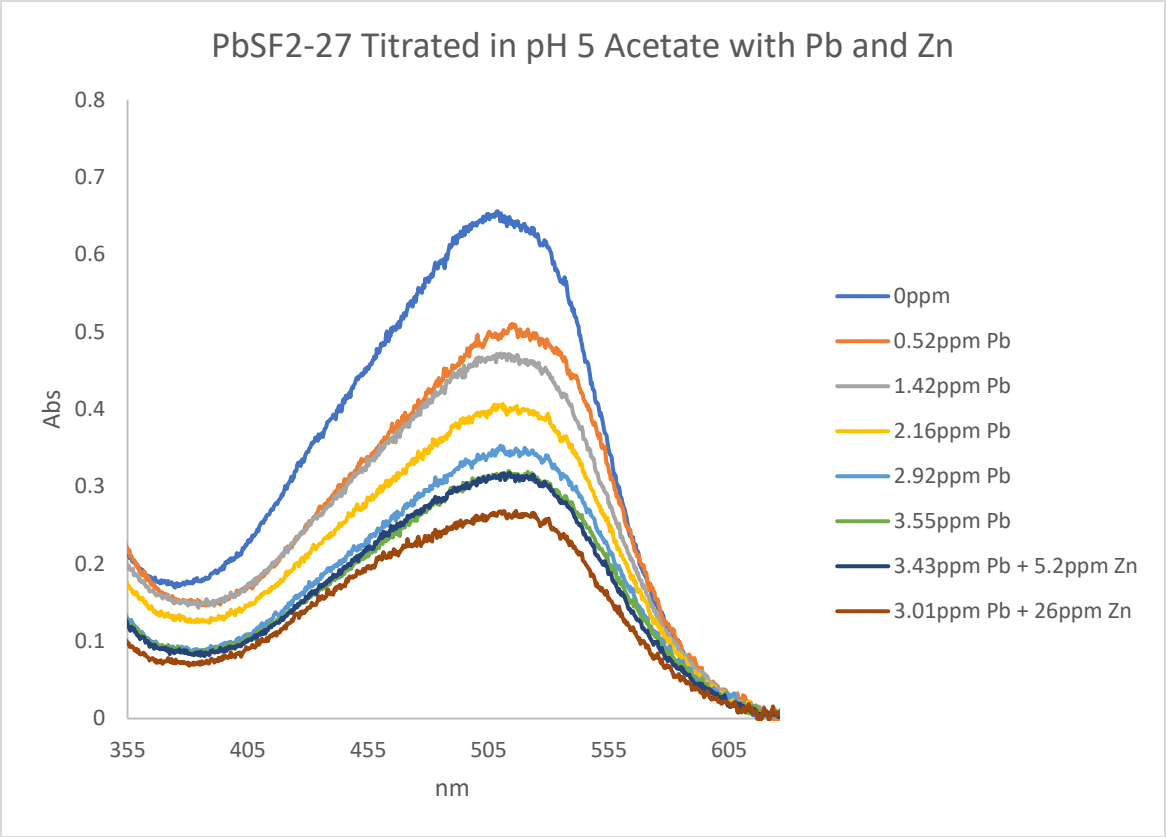

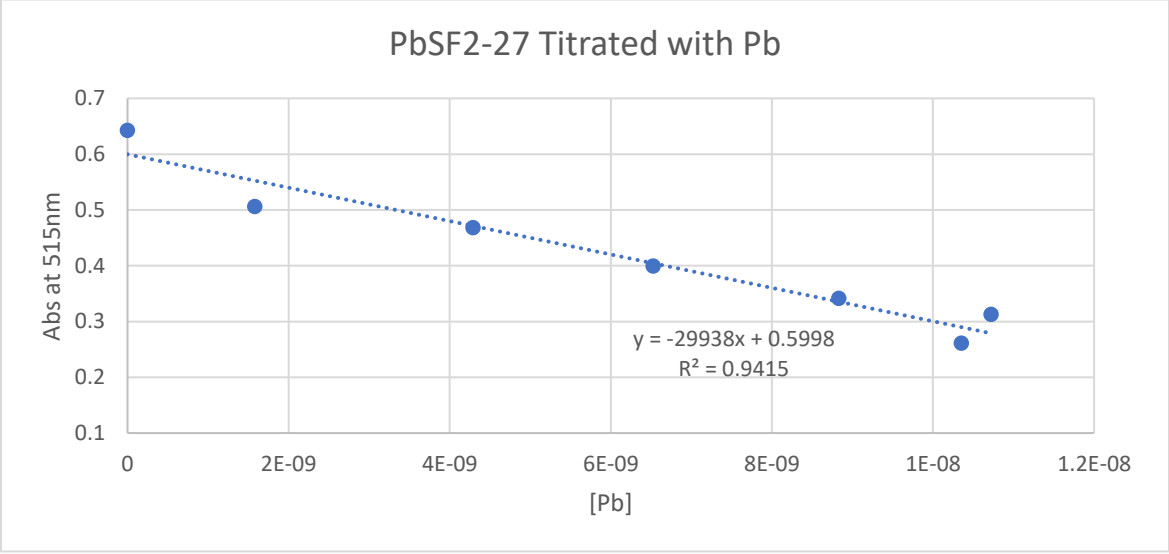

Spectrum 95: 19d Titration with Pb with Zn addition at pH 5, Day 0, ppm; Abs vs [Pb]

Titration of 19c, PbSF2-2n right after synthesis titrated with Pb at pH 5 with Zn added

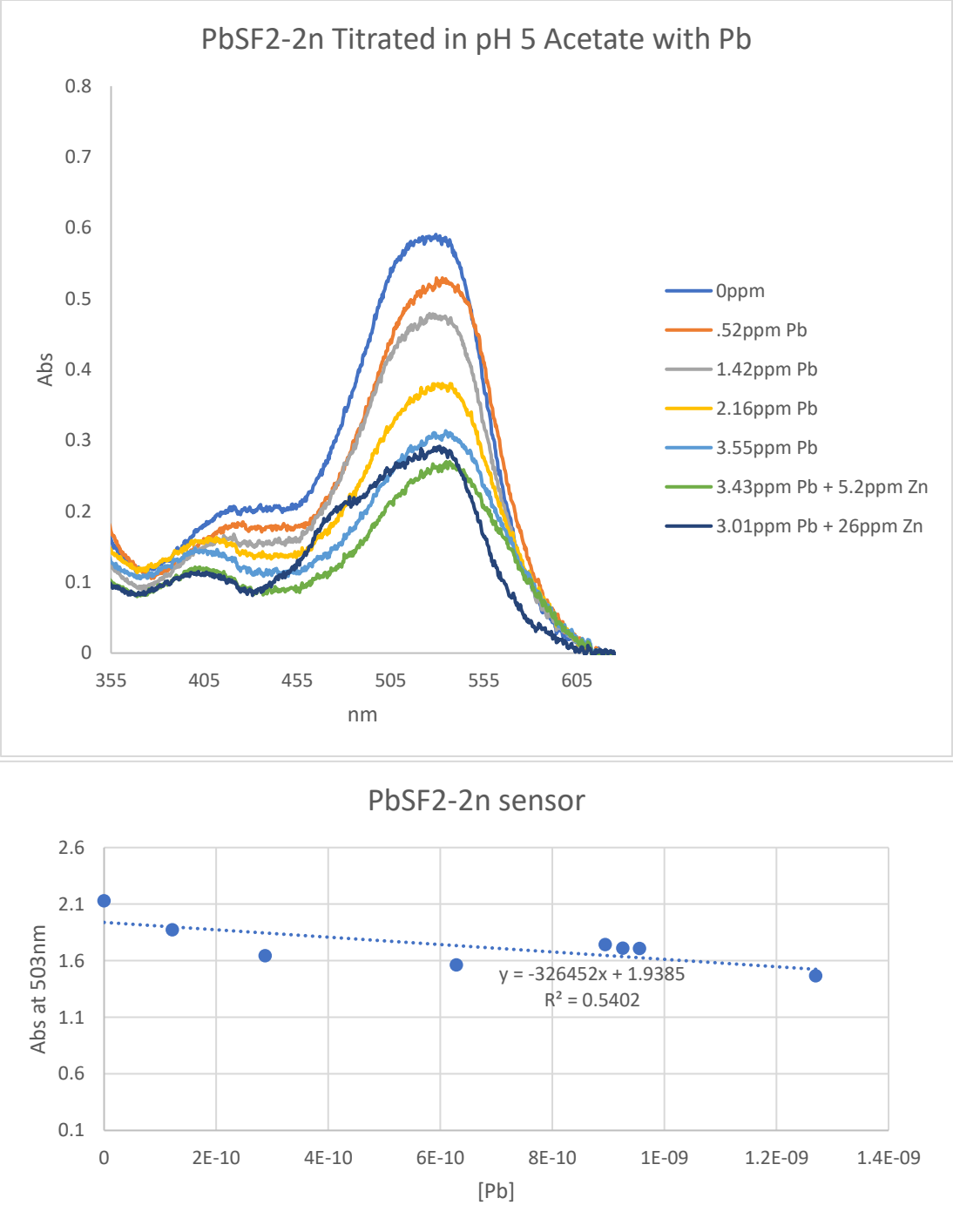

Spectrum 96: 19c Titration with Pb with Zn addition at pH 5, Day 0, ppm; Abs vs [Pb]

Titration of 21b, PbSF3-27MAP two weeks after synthesis titrated with ppm Pb at pH 9 ;

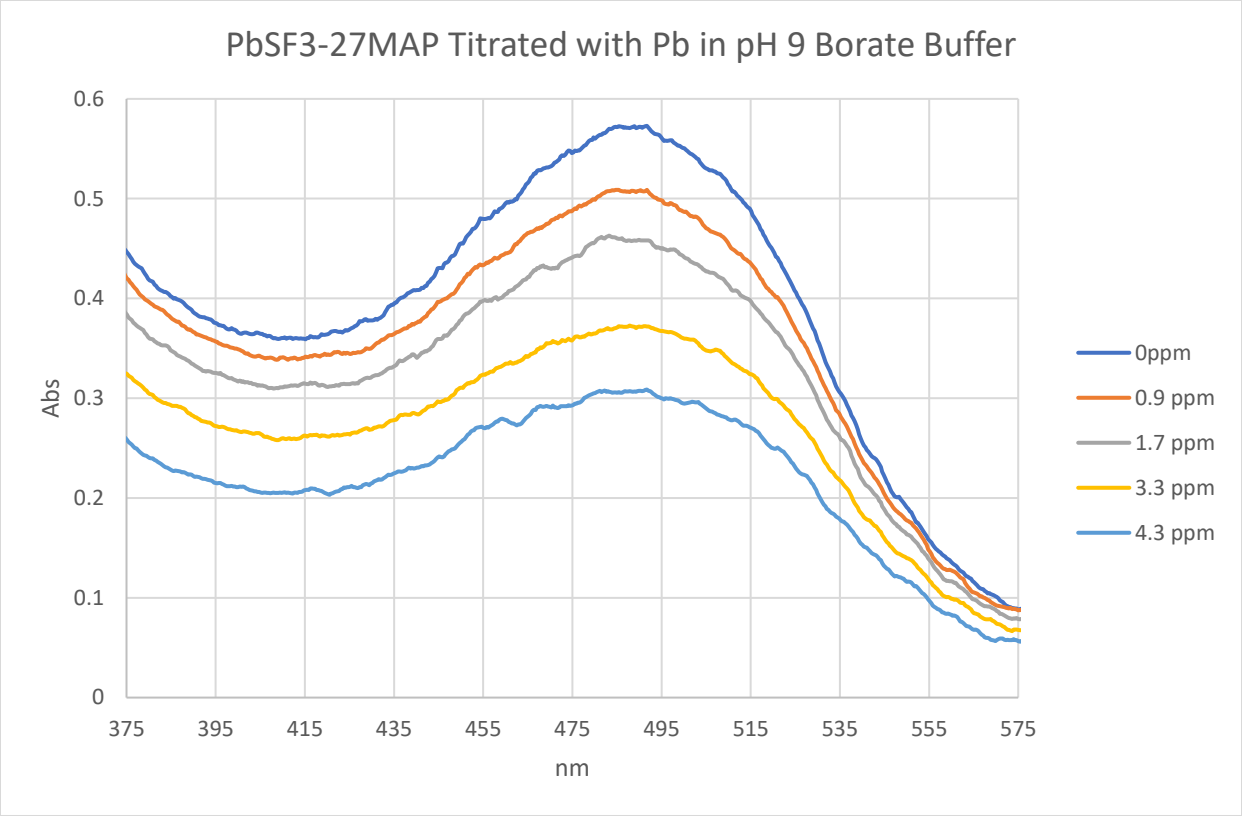

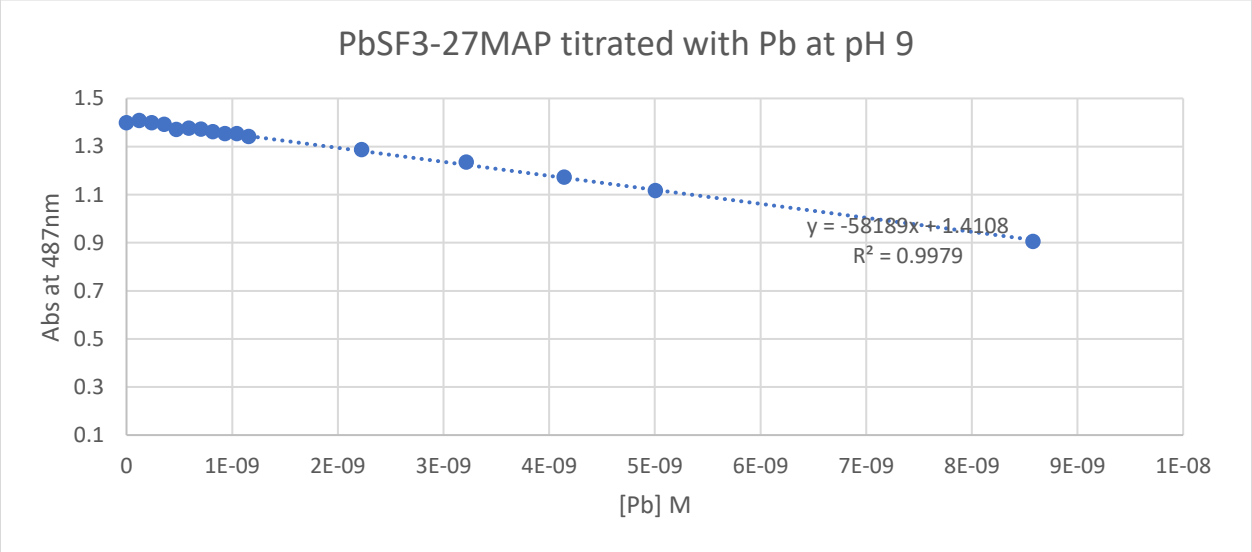

Spectrum 97: 21b Titration with Pb at pH 9, Week 2, ppm; Abs vs [Pb]

Titration of 21b, PbSF3-27MAP two weeks after synthesis titrated with ppm Cu pH 9; ppm Zn pH 9

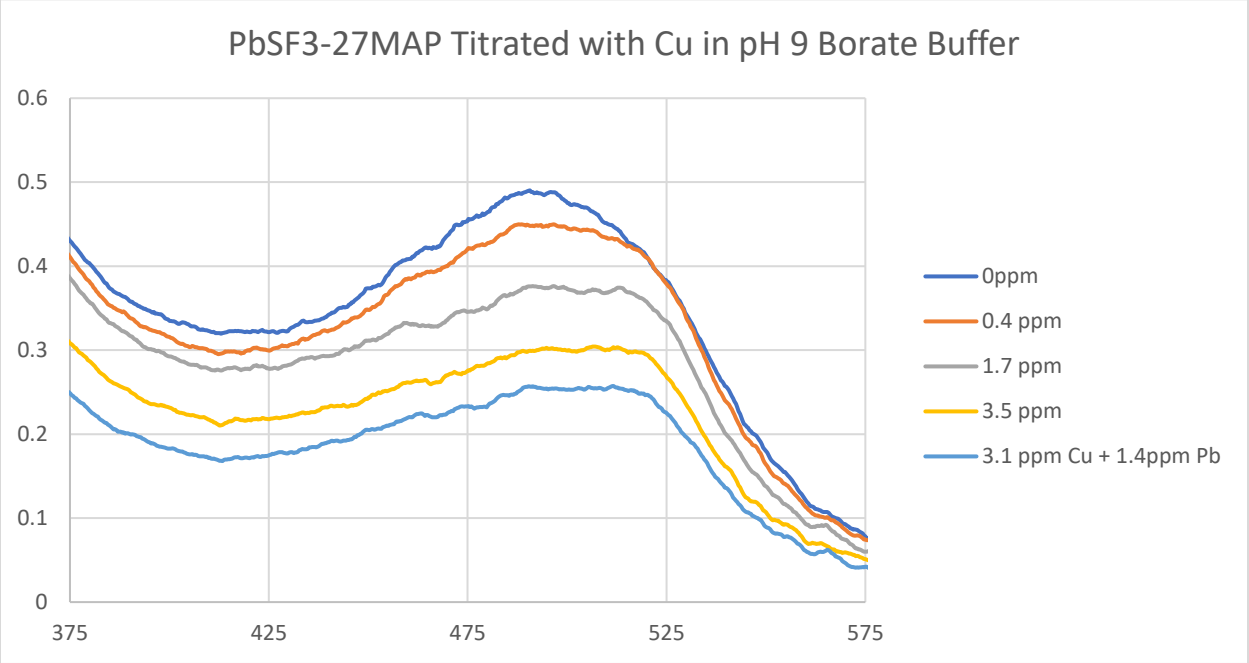

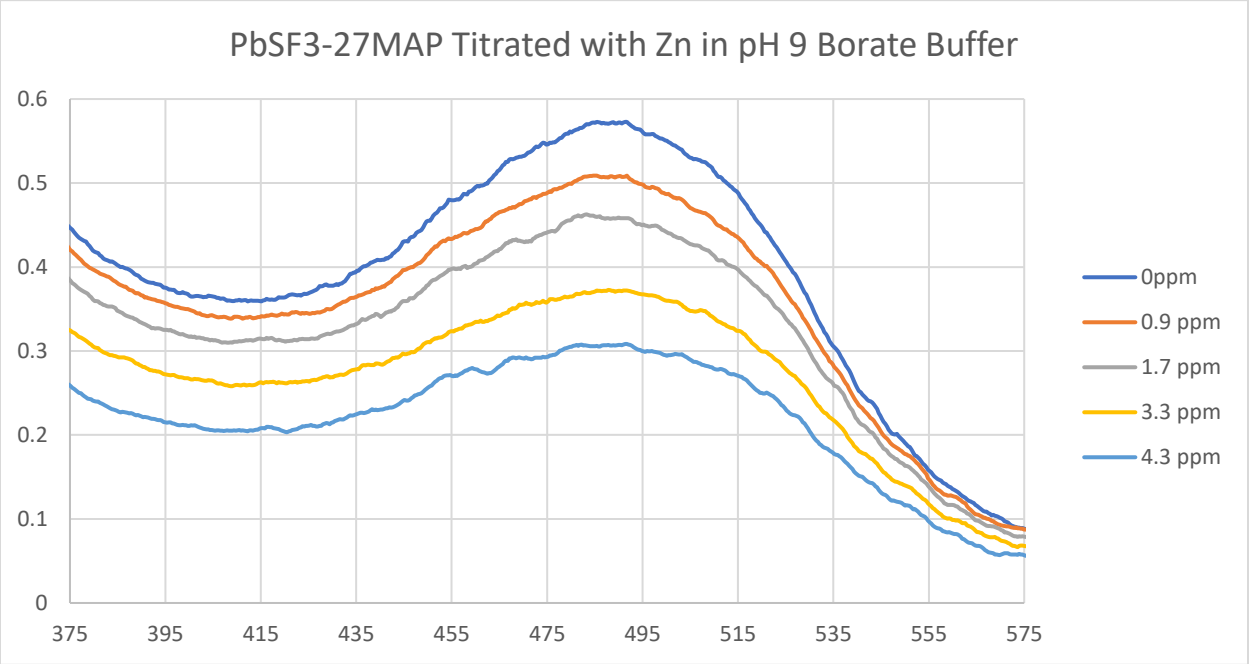

Spectrum 98: 21b Titration with Cu at pH 9, Week 2, ppm; 21b Titration with Zn at pH 9, Week 2, ppm

Titration of 21c, PbSF3-27Trp two weeks after synthesis titrated with ppm Cu pH 9

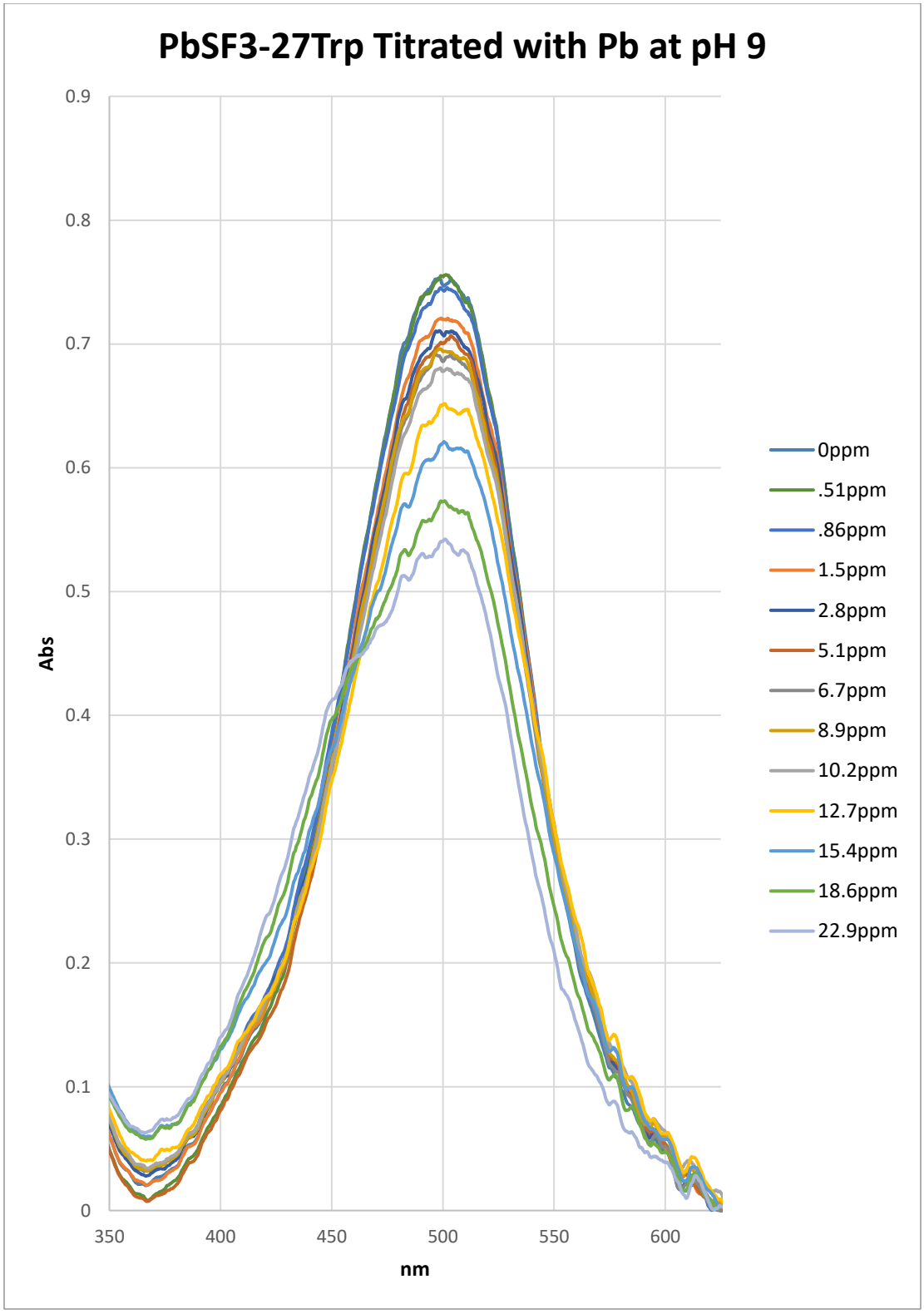

Spectrum 99: 21c Titration with Pb at pH 9, Week 2, ppm

Titration of 25a, PbSF1-27A at pH 9 with Zn 3 weeks after synthesis

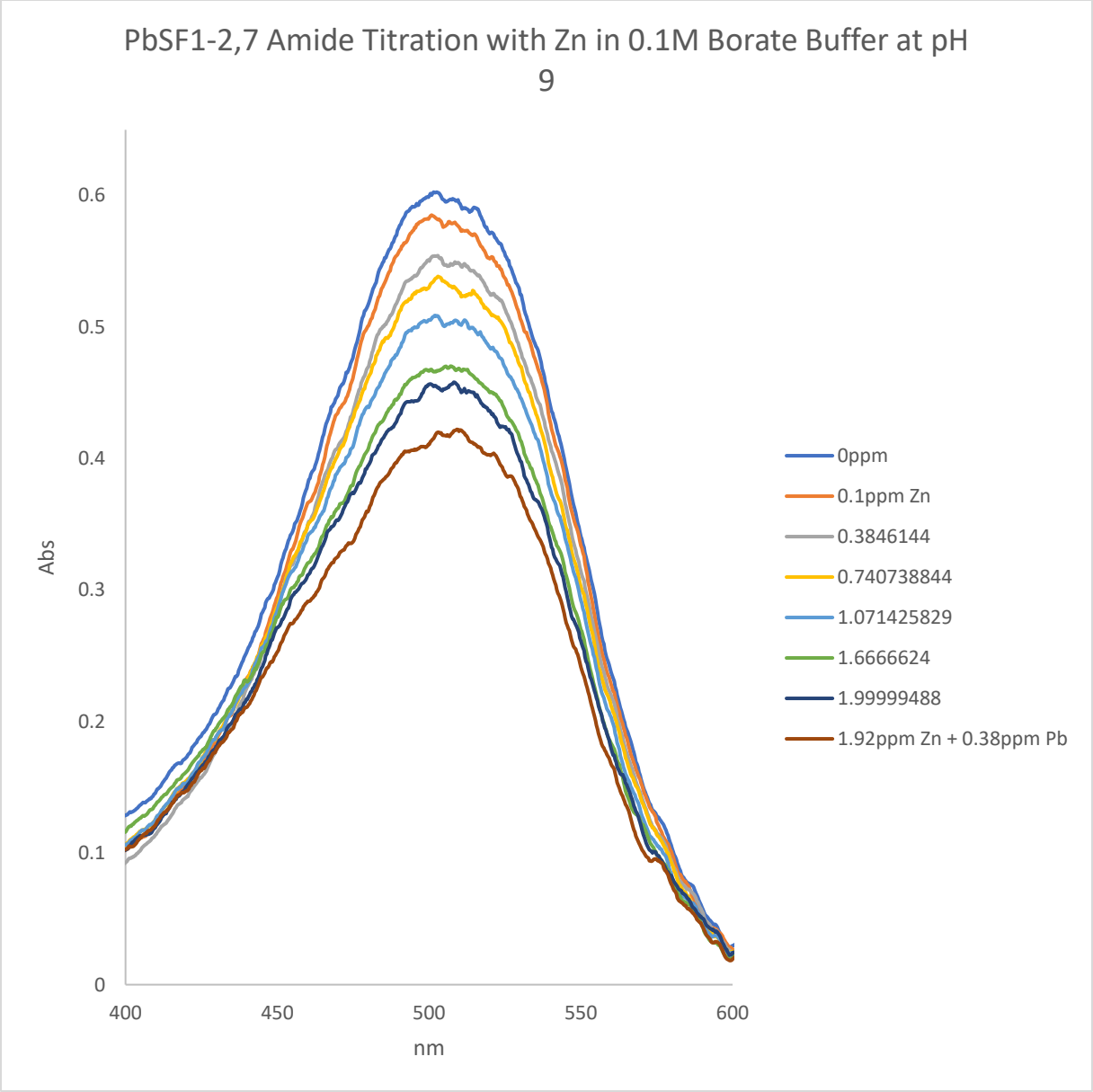

Spectrum 100: 25a Titration with Zn at pH 9, Week 3, ppm

Titration of 25a, PbSF1-27A at pH 9 with Cu 3 weeks after synthesis

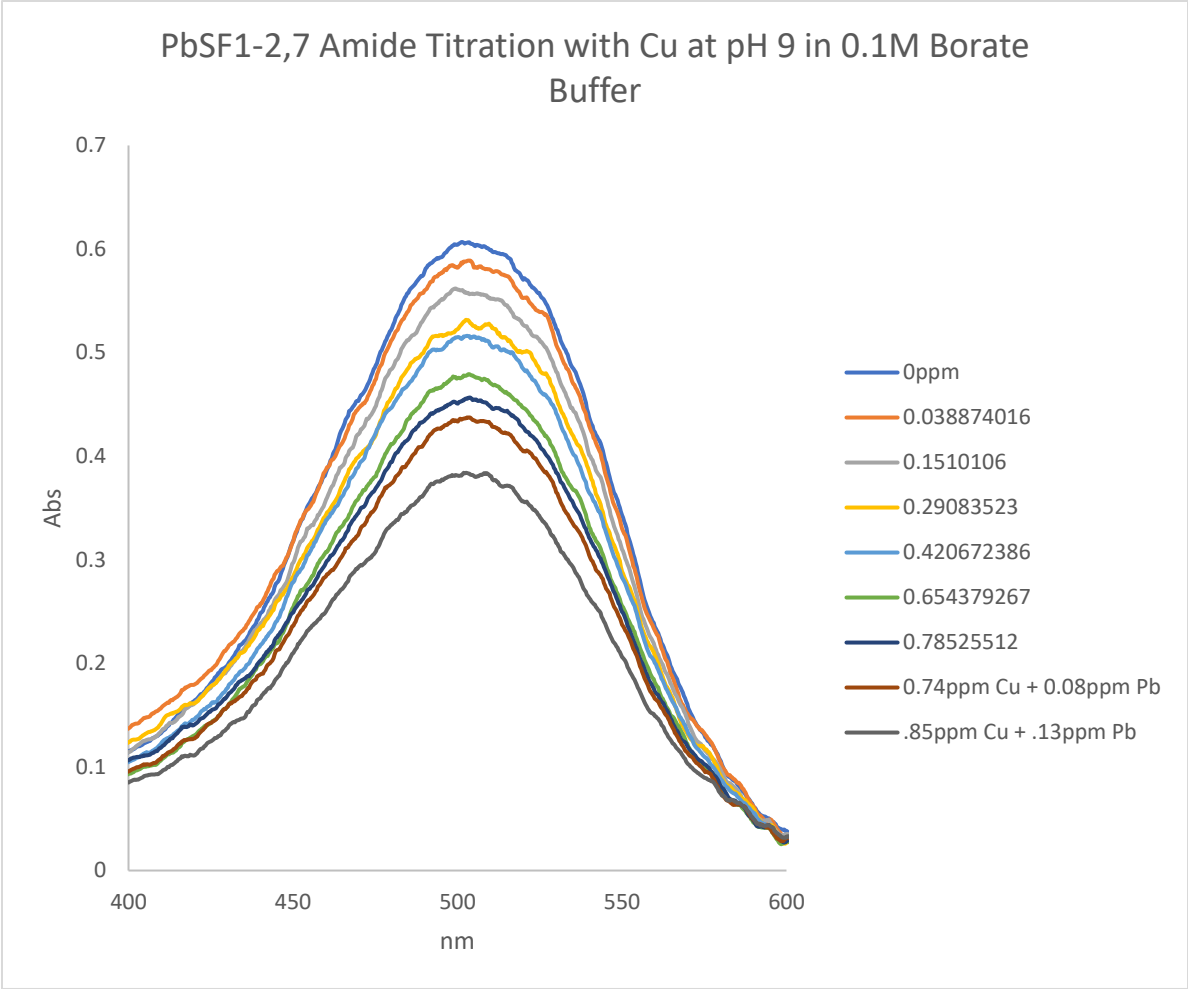

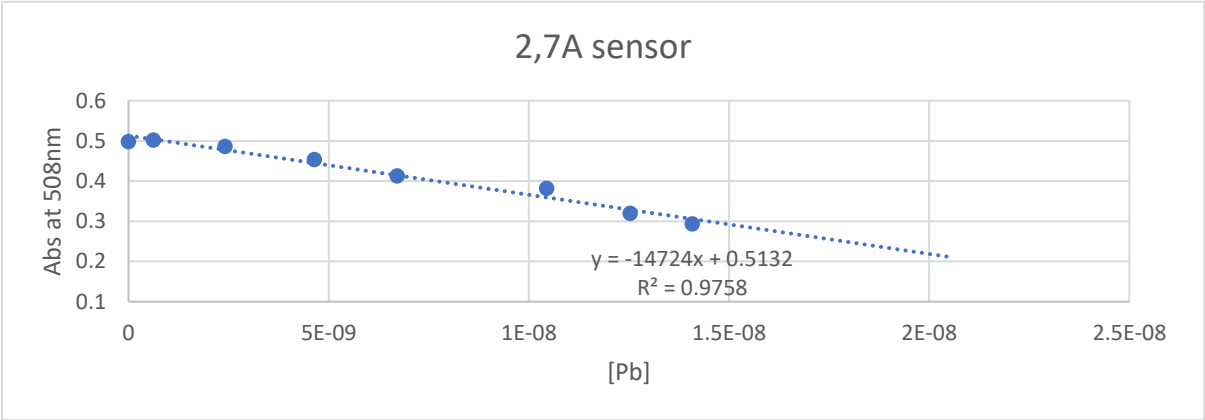

Spectrum 101: 25a Titration with Cu at pH 9, Week 3, ppm; Abs vs [Cu]

Titration of 25a, PbSF1-27A at pH 9 with Zn, Cu, Pb for comparison

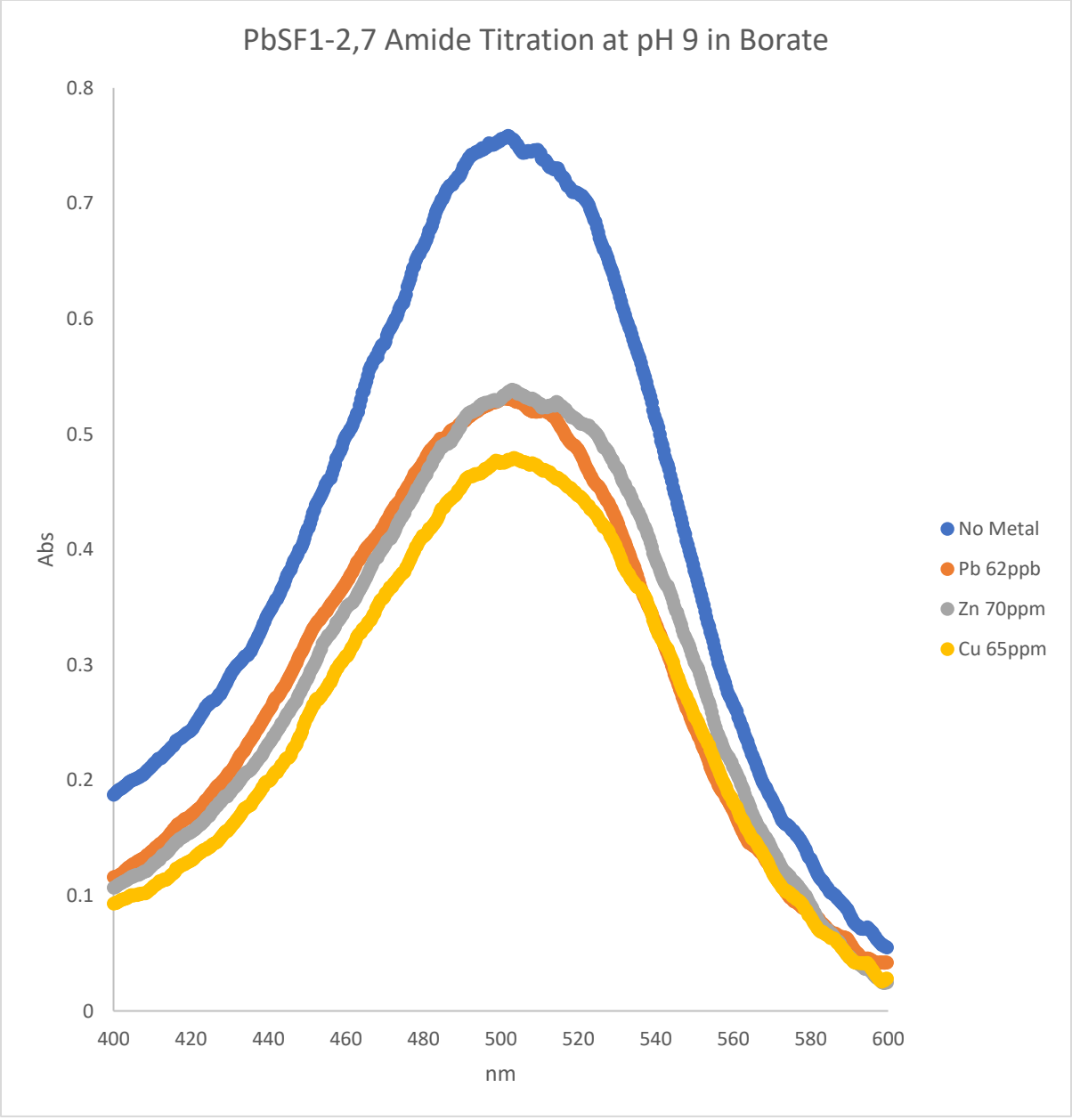

Spectrum 102: 25a Titration with Zn, Cu, Pb at pH 9, Week 3

Titration of 25a, PbSF1-27A at pH 9 with Pb two months after synthesis on benchtop

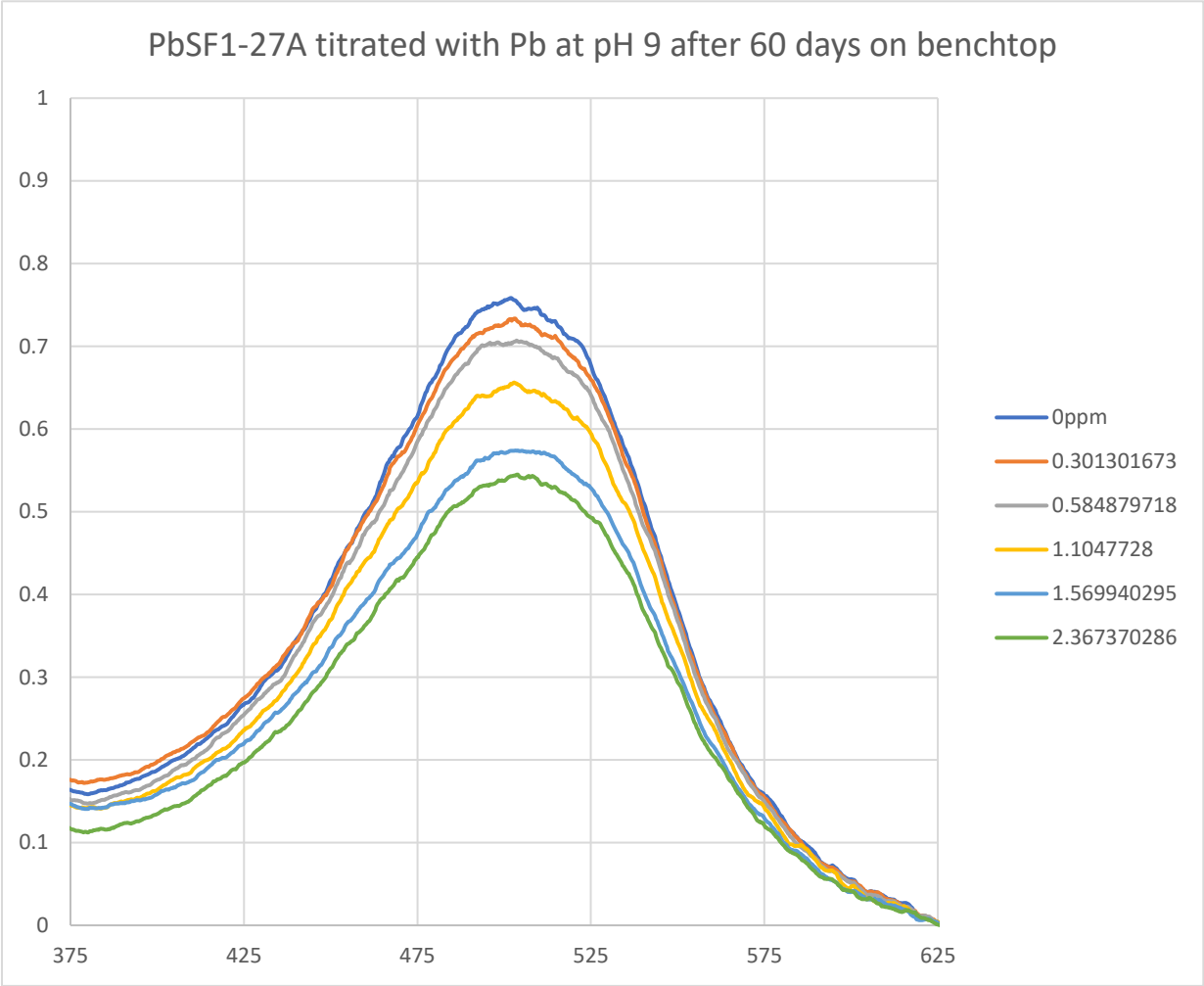

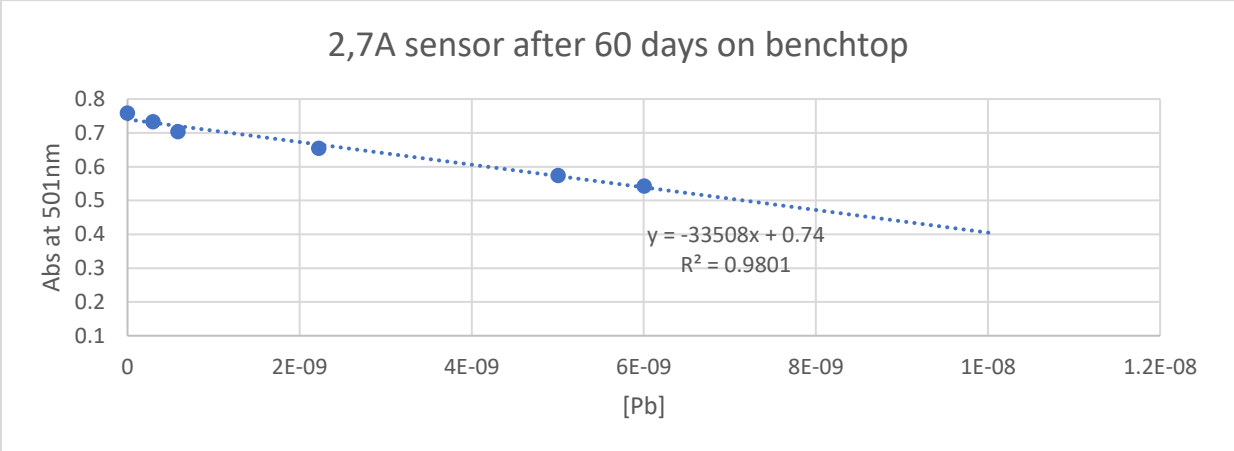

Spectrum 103: 25a Titration with Pb at pH 9, Month 2 after sitting on benchtop, ppm; Abs vs [Pb]

1H NMR 10b

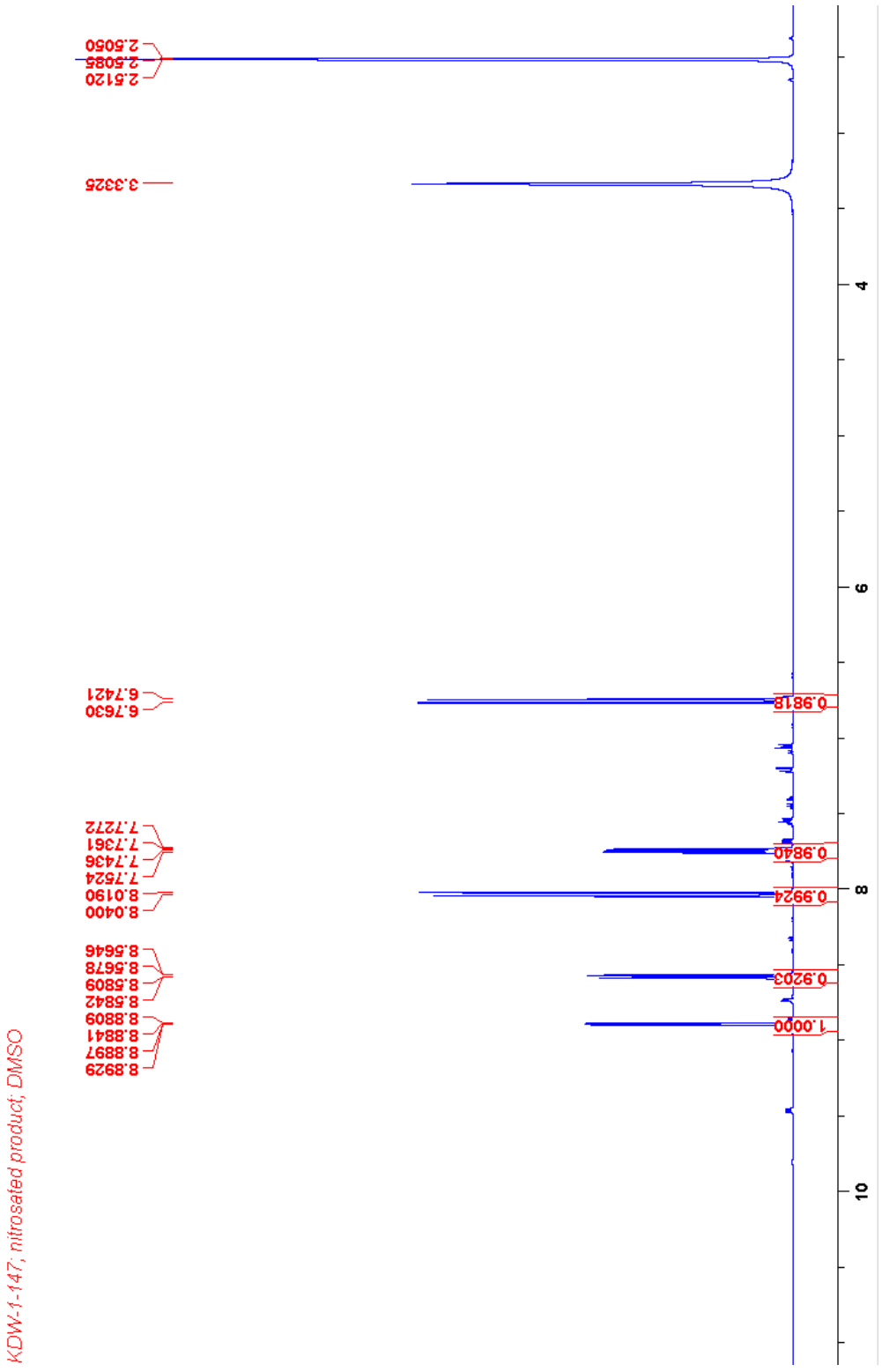

Spectrum 104: 10b 1H NMR (500 MHz, DMSO-d6

1H NMR 11b

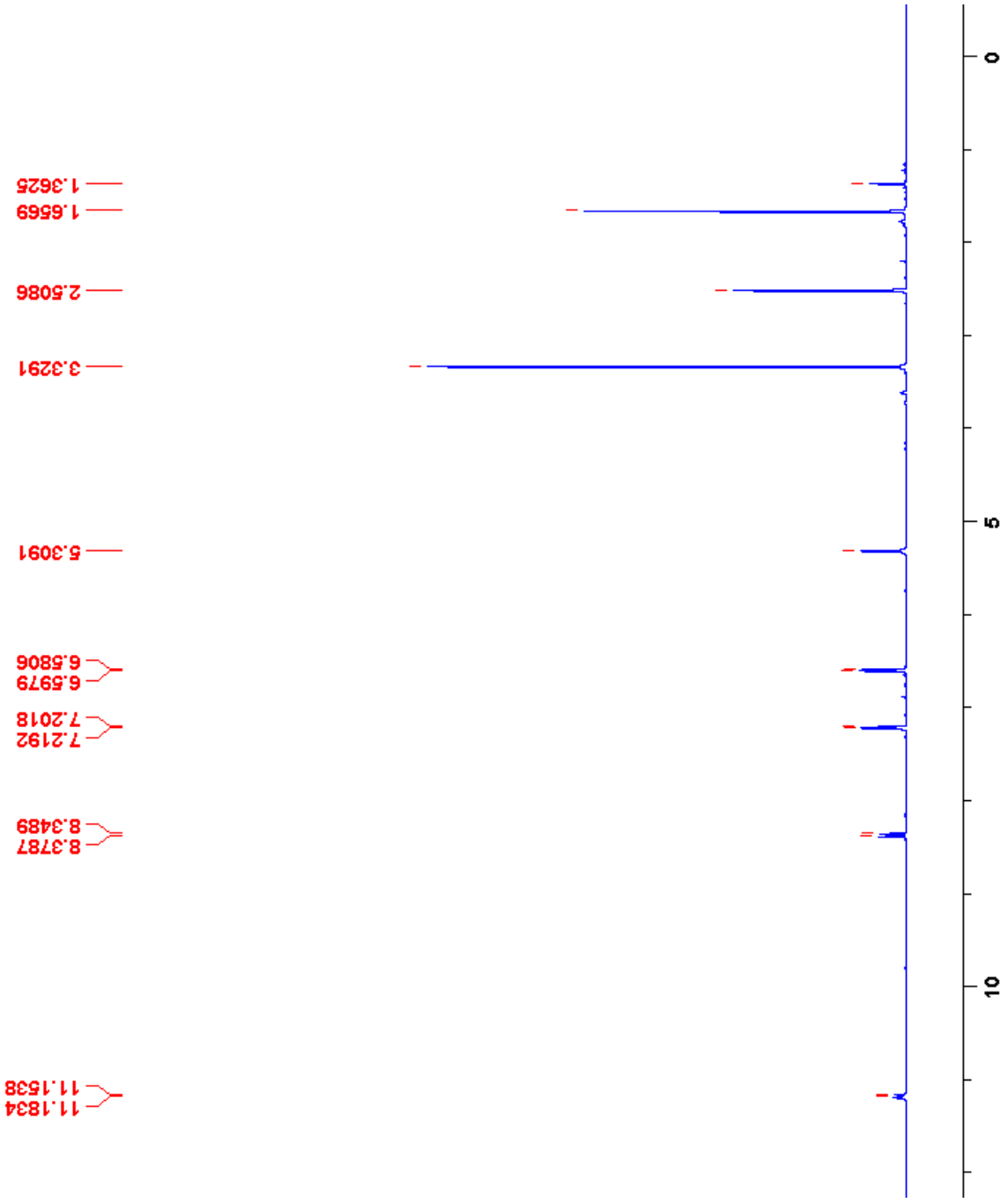

Spectrum 105: 11b 1H NMR (500 MHz, DMSO-d6

1H NMR compound **18**

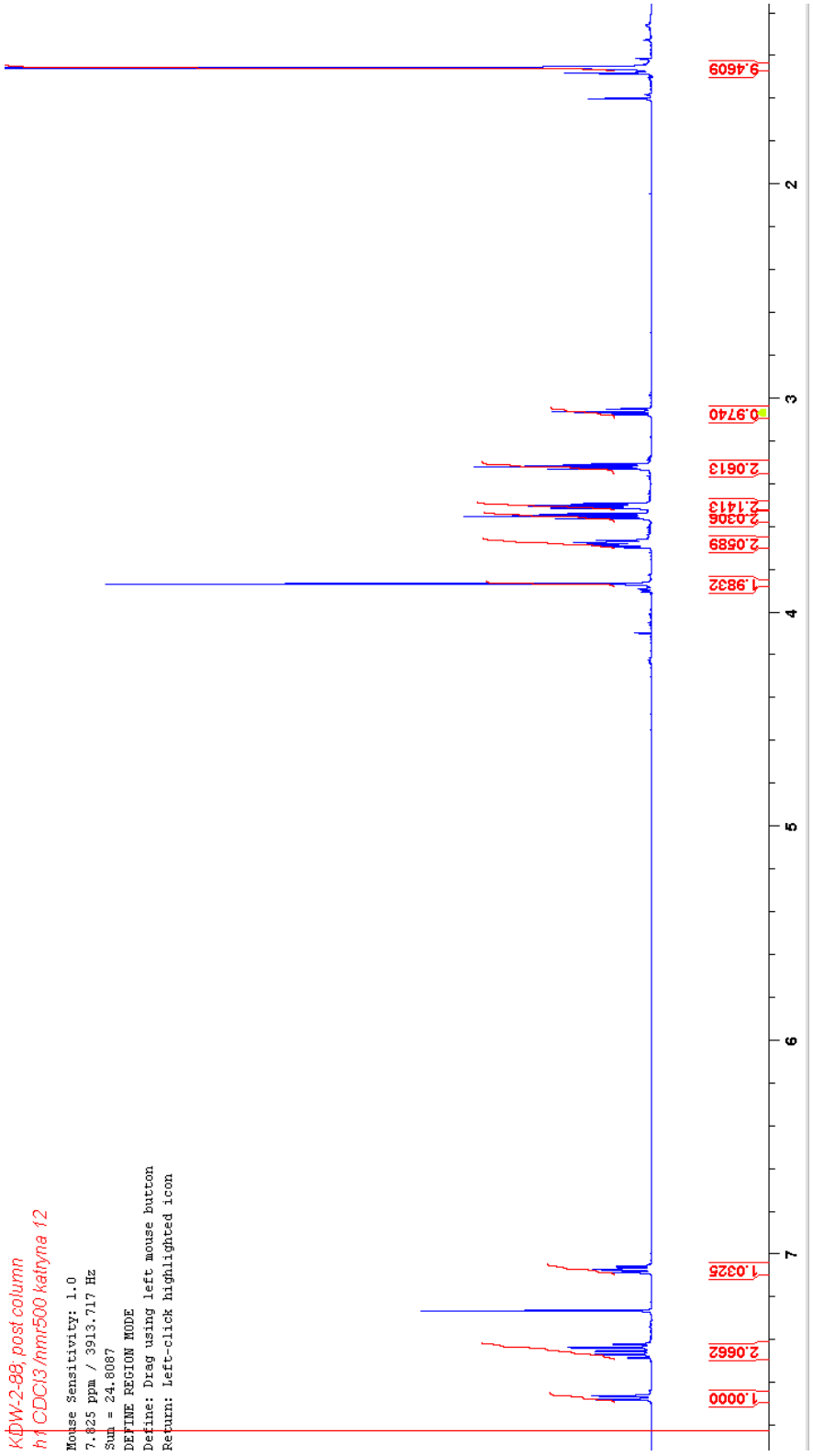

Spectrum 106: 18 1H NMR (500 MHz, CDCl3)

1H NMR compound **20**

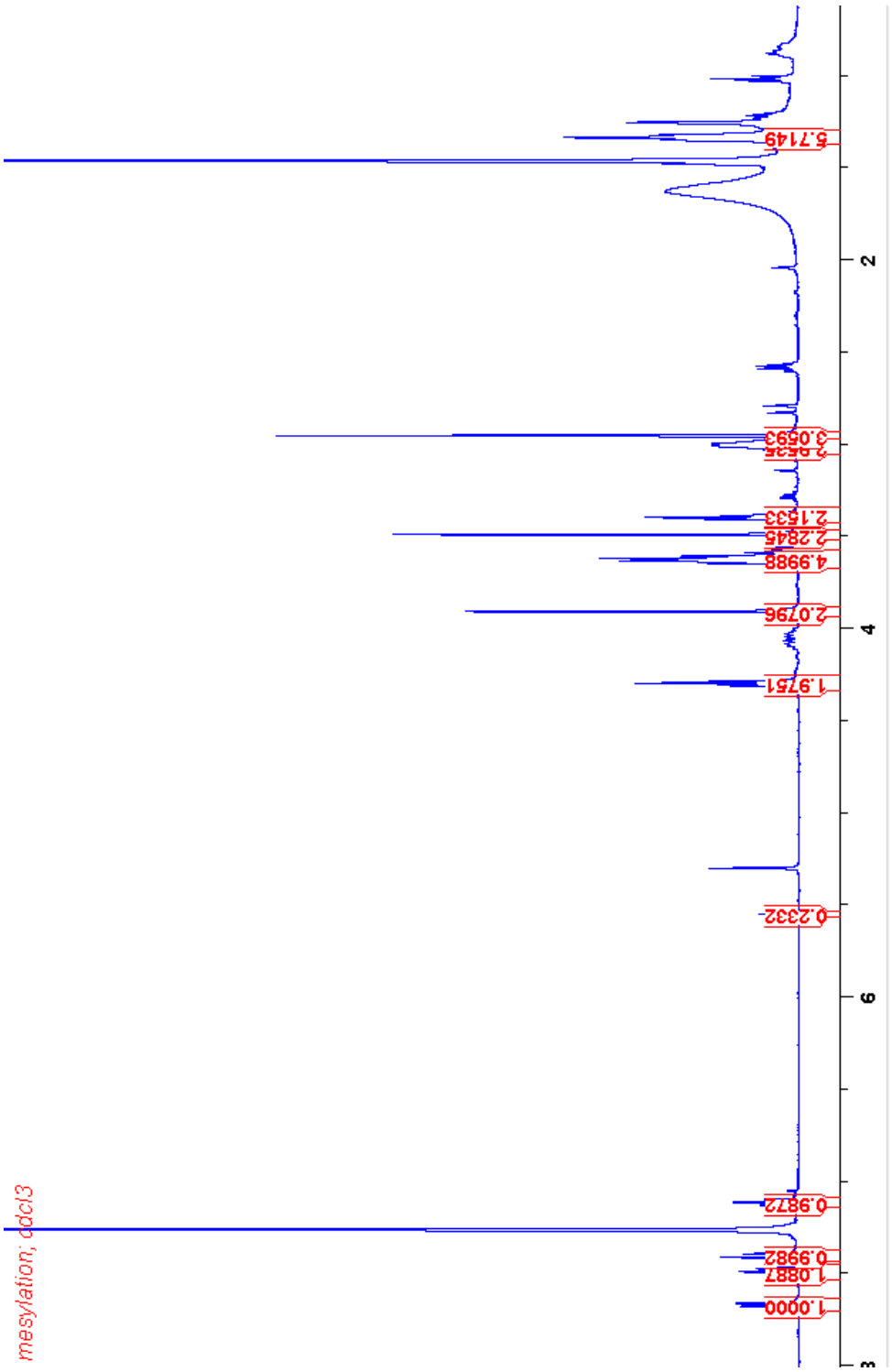

Spectrum 107: 20 1H NMR (500 MHz, D2O

1H NMR compound **20d**

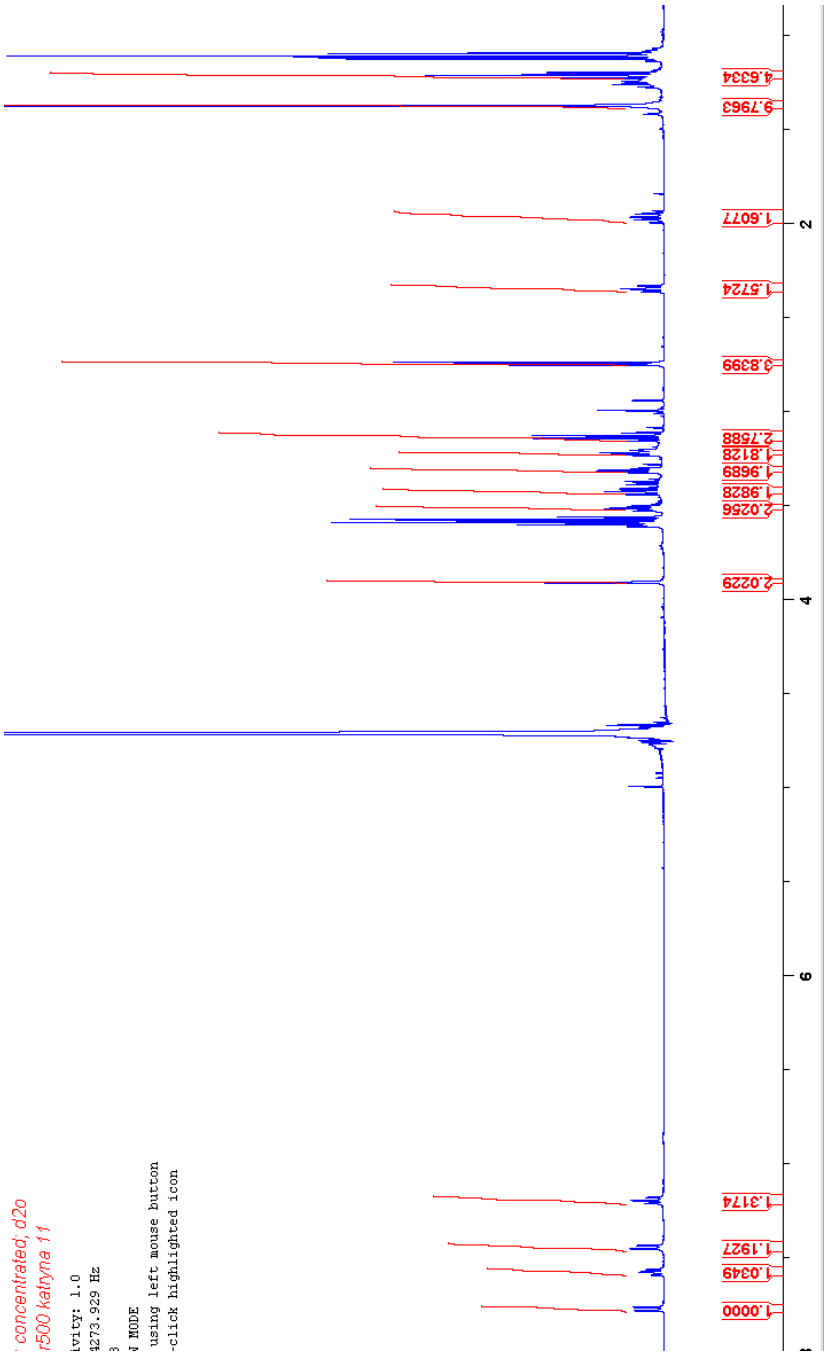

Spectrum 108: 20d 1H NMR (500 MHz, CDCl3)

1H NMR boc-diethanolamine

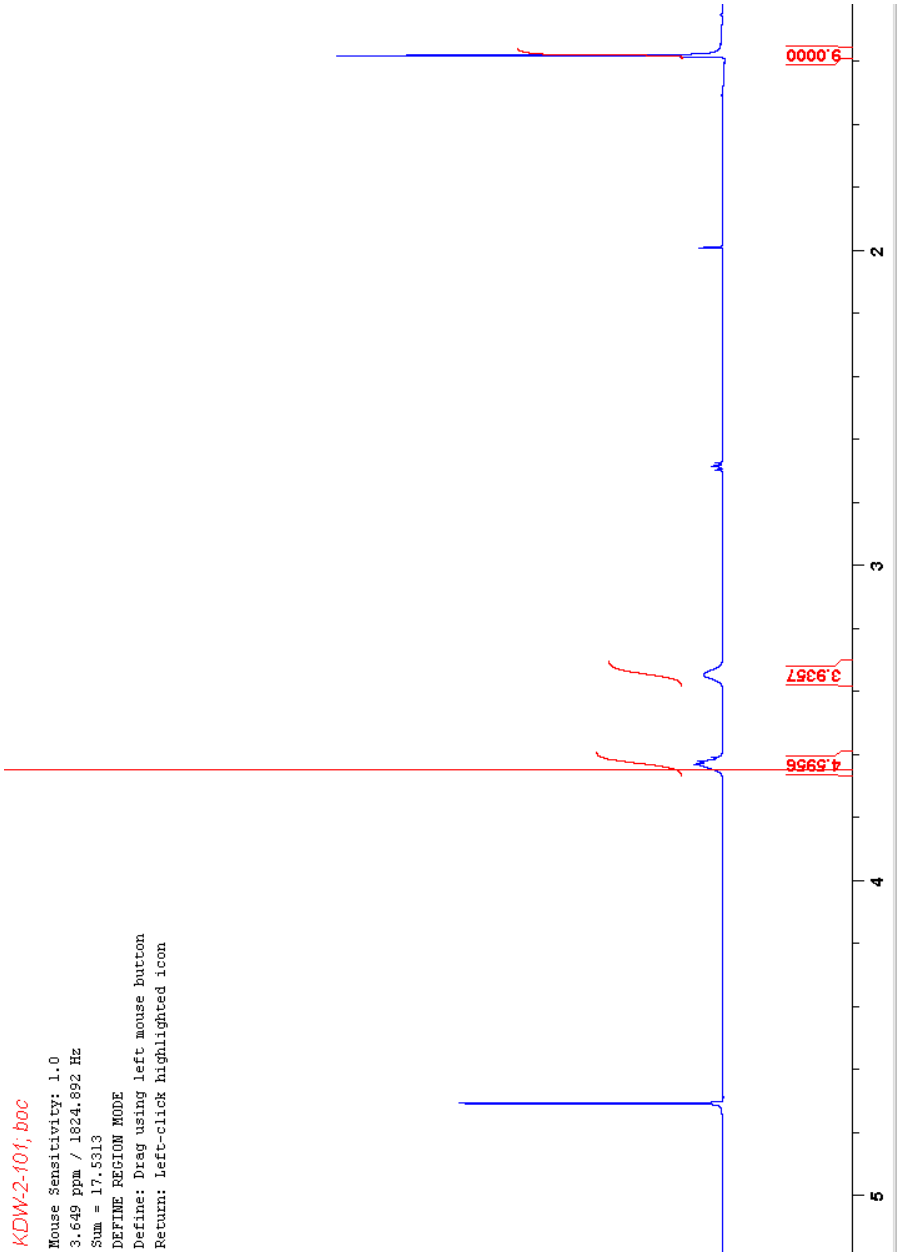

Spectrum 109: boc diethanolamine 1H NMR (500 MHz, CDCl3)

1H NMR of **14a (failed synthesis)**

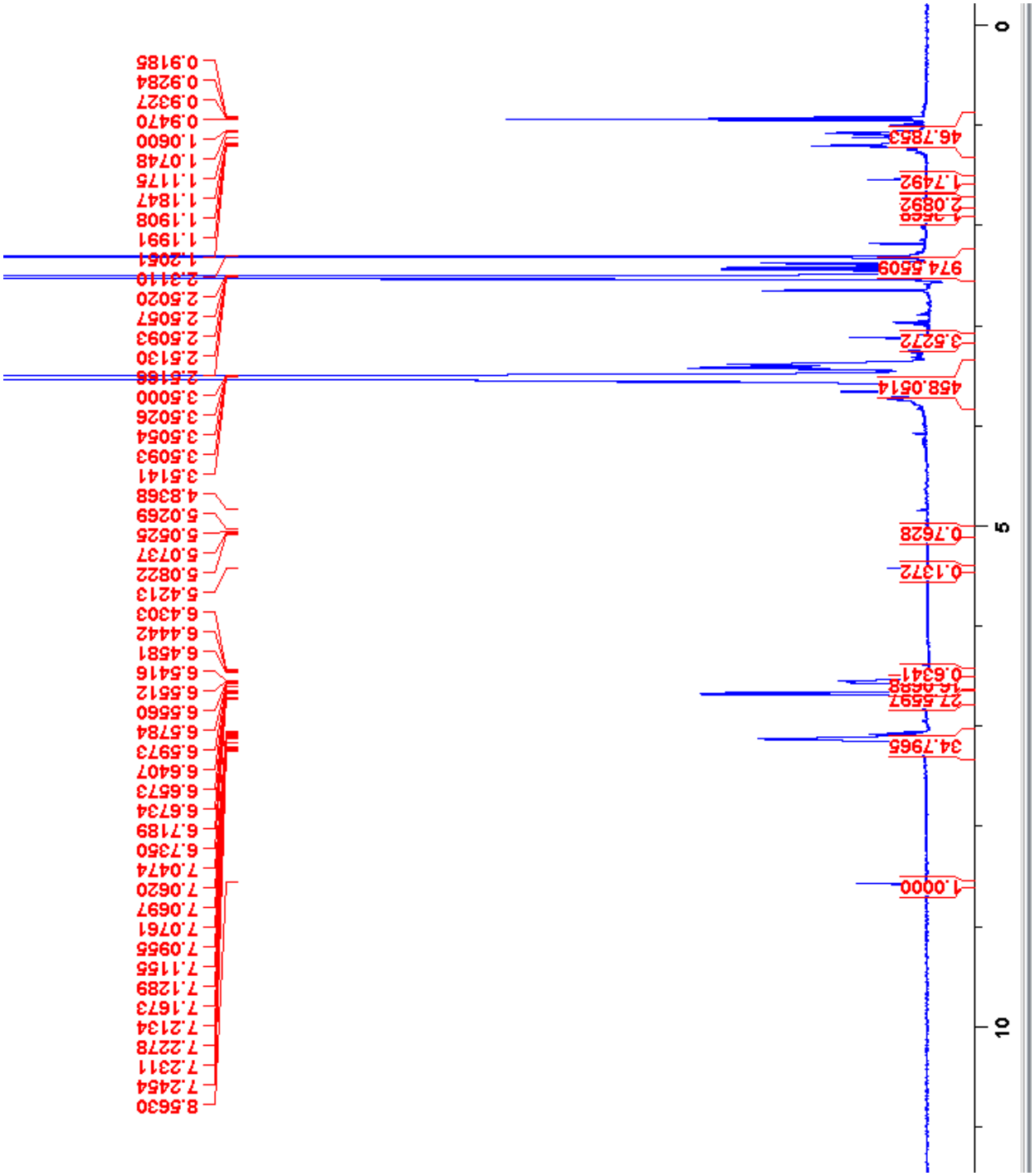

Spectrum 110: 14a 1H NMR (500 MHz, CDCl3) failed synthesis

13CNMR of **25a, PbSF1-27A**

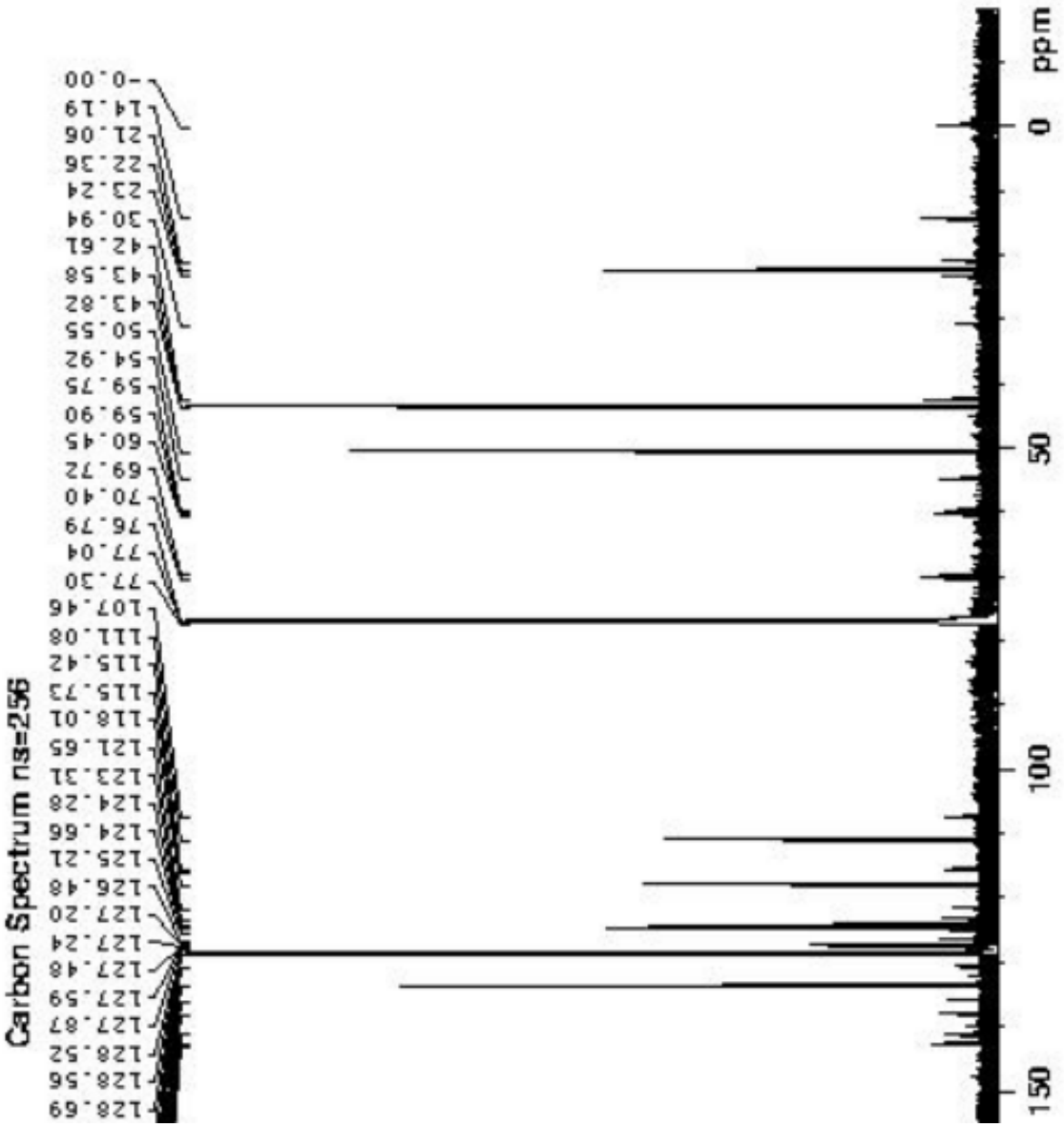

Spectrum 111: 25a 13CNMR (500MHz,DMSO-d6)

13CNMR of **25b** (PbSF1-13A)

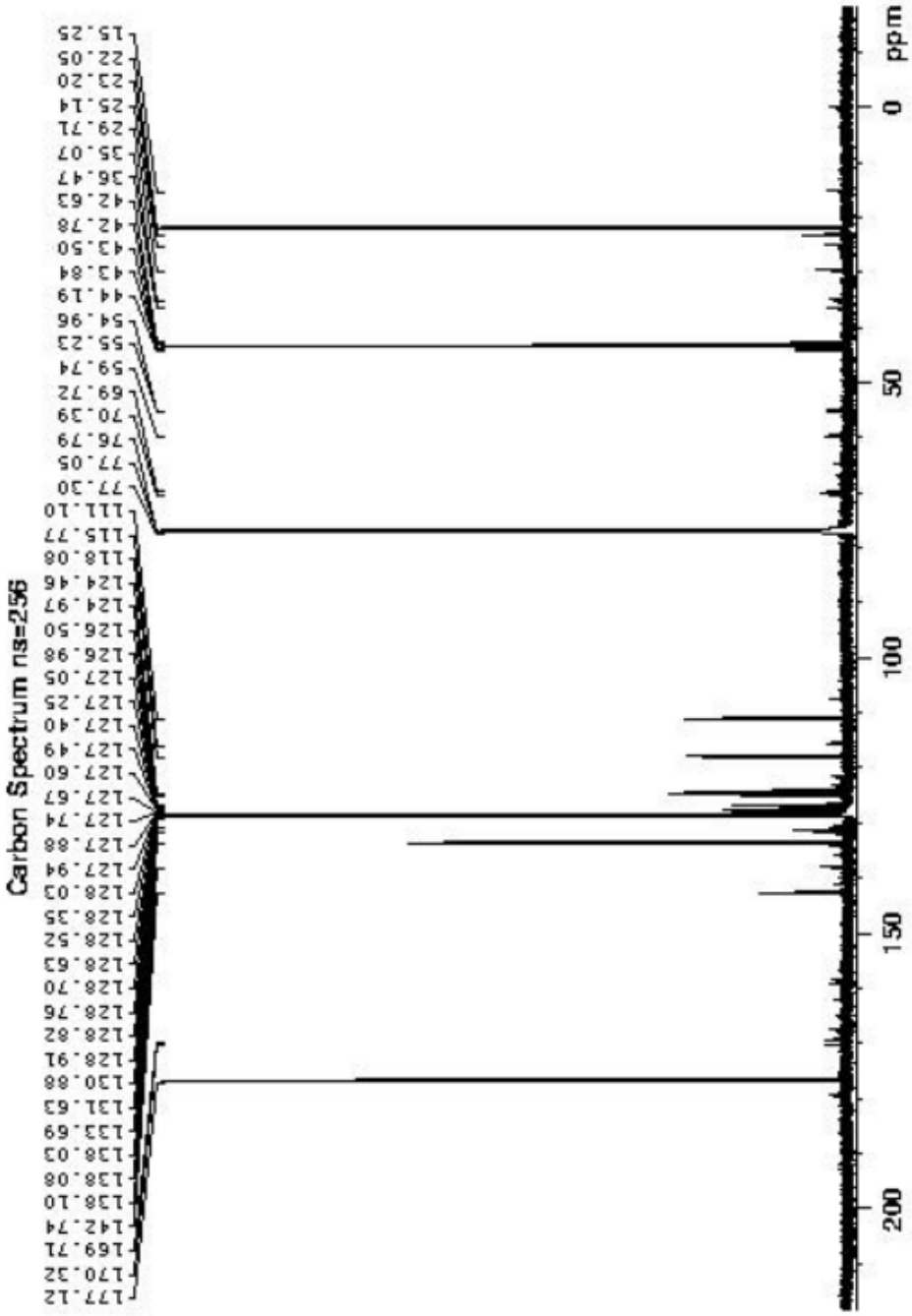

Spectrum 112: 25b 13CNMR (500MHz, DMSO-d6)

Curriculum Vitae

Katryna Williams

Place of birth: Greensburg, PA

Education:

B.A., Saint Vincent College, May 2018

Major: Biochemistry

Minor: Mathematics

PhD, University of Wisconsin-Milwaukee, May 2022

Major: Organic Chemistry

Dissertation Title:

PART I: SYNTHESIS OF QUINOLONES FOR INHIBITION OF THE B-BARREL ASSEMBLY MACHINE IN GRAM NEGATIVE BACTERIA

PART II: SYNTHESIS OF AZO DYE SENSORS FOR DETECTION OF METAL IONS IN AQUEOUS ENVIRONMENTS